Interferon Regulatory Factor 5: A Systematic Study of Macrophage Gene Regulation

Tariq Edward Khoyratty,

Exeter College

Michaelmas 2017

Thesis submitted for the degree of Doctor of Philosophy at the University of Oxford

Supervisors: Prof. Irina Udalova,

Prof. Nicholas Proudfoot

The Kennedy Institute of Rheumatology,

Nuffield Department of Orthopaedics, Rheumatology, and Musculoskeletal Sciences,

University of Oxford

Abstract

Macrophages are multifaceted innate immune cells, able to adapt their phenotype to respond to a myriad of conditions, engaging in tissue-specific functions and mediating either inflammatory or anti-inflammatory responses depending on the encountered stimuli. They conduct key roles in the orchestration of immune responses; from pathogen recognition through sterilising inflammation to resolution and repair. The Udalova laboratory has previously demonstrated that IRF5 promotes a pro-inflammatory macrophage phenotype, leading to the secretion of TNF, IL-12, and IL-23, enhancing Th1/Th17-mediated immune responses, and described the cooperation between IRF5 and the transcription factor RelA, which mediate the production of pro-inflammatory genes. The aim of this thesis is to further characterise the activity of IRF5 in macrophage inflammatory responses. I demonstrate that IRF5 not only regulates the transcription of cytokines and chemokines in response to bacterial stimuli, but also anti-microbial peptides, whilst simultaneously down-regulating homeostatic and resolving macrophage functions. My data also suggests that IRF5 plays a role in enforcing monocyte to macrophage differentiation by up-regulating the transcription of key macrophages markers and repressing dendritic cell identity genes. To further characterise the mechanisms of the inflammatory response mounted by macrophages I used an unbiased approach; combining twenty-three transcription factor ChIP-seq data sets with chromatin accessibility information from ATAC-seq, uncovering RUNX1 as a novel partner of IRF5 that binds co-operatively to clusters of enhancers, which control the transcription of pro-inflammatory genes in a signal-dependent manner. This is the first study demonstrating a critical role for RUNX1 in activity of inflammatory macrophages.

Declaration

I declare that the present thesis is the result of my own work. All experimental data described in this thesis are original and have been performed by myself, unless stated below or indicated in the text. Experiments and analyses described below were performed by or with help from others.

Dr. David Saliba (Udalova group, Kennedy Institute of Rheumatology, Oxford) performed IRF5 ChIP-seq and mRNA-seq in unstimulated and LPS stimulated GM-BMDMs from WT and $IRF5^{-/-}$ mice. IRF5 mRNA-seq was analysed as described in Chapter 2.2.4 and utilised in Chapter 4 and Chapter 5. mRNA derived from LPS stimulated WT and $IRF5^{-/-}$ GM-BMDMs for validation of mRNA-seq targets in Chapter 4 (Figure 4.9) was also prepared by Dr. David Saliba. IRF5 ChIP-seq has previously been published (Saliba et al., 2014), and was analysed as described in Chapter 2.2.2 and utilised in Chapter 5. IRF5 immunoprecipitation and RUNX1 Western blot in HEK293-TLR4-CD14/Md2 cells was conducted by Dr. Haley Eames (Udalova group, Kennedy Institute of Rheumatology, Oxford) (Figure 5.18). ATAC-seq in M-BMDMs was carried out by Laurienne Edgar (Choudhury group, Radcliffe Department of Medicine, Oxford), following the protocol outlined in Chapter 2.1.6 and analysed as described in Chapter 2.2.1. Dr. Stephen Sansom (Sansom group, Kennedy Institute of Rheumatology, Oxford) conducted the differential gene expression analysis of the chrRNA-seq data and comparison with mRNA-seq data (Figure 4.3). Dr. Stephen Sansom also contributed help and advice with bioinformatic analyses. Additionally, publically available ChIP-seq data sets were used in this thesis, full details of the data used and accession numbers are documented in

Chapter 2.2.2.

This work has been carried out at the Kennedy Institute of Rheumatology and was funded by the Kennedy Institute trustees, the American Asthma Foundation and the Medical Research Council.

Tariq Edward Khoyratty

(October 2017)

Acknowledgements

I would like to express my thanks to my supervisor Irina Udalova, whom has been a vital source of help and support throughout my DPhil, frequently offering new ideas, suggesting avenues of exploration, and providing guidance on experimental and computational results and approaches; whilst providing me with the flexibility to learn and develop my bioinformatic skills. I would also like to thank my co-supervisor Nicholas Proudfoot, for assistance and advice during the early stages of my DPhil and for his continued interest and support after our "scientific divorce", with the switching of my research focus from 3' to 5' mechanisms of gene regulation. Additionally, I am indebted to Stephen Sansom for promoting my interest in bioinformatics and facilitating my learning, and subsequently, his help and patience in troubleshooting the many errors I have encountered. I would also like to thank my former GSK supervisor Valentino Parravicini for fostering my interests in immunology and epigenetics and suggesting I study for a PhD.

I am grateful to all members of the Udalova lab for providing a fun and stimulating environment for work and for all of the advice garnered from our informal lab meetings, and personal conversations, which have contributed to the completion of this thesis. Firstly, I'd like to thank David Saliba, who first taught me ChIP and provided early support and guidance, in addition to generating a wealth of sequencing data, which has proved invaluable. I'd like to say thank you to Hayley Eames for teaching me various techniques, from IPs and Western blots to qPCR and virus work, and for her day-to-day help in organising the lab, and companionship. I'd also like to thank: Miriam for your positive encouragement, Corbin for your cheery disposition, Grisha for your wealth of information, Hannah for your baking, and Sara for sharing the frustrations of neutrophil genomics.

A special thank you to Nikki and my family, for providing me with much encouragement and support.

Table of Contents

List of Figures

List of Tables

List of Abbreviations

A adenine
AGM aorta-gonad-mesenephros
ATAC-seq assay for transposase-accessible chromatin and sequencing
ATP adenosine tri-phosphate
b.p. base pairs
BET bromodomain and extra-terminal
BM bone marrow
BMDM bone marrow derived macrophage
BRCA1 breast cancer 1
C cytosine
C/EBPα CCAAT/enhancer-binding protein α
CBFβ core binding factor β
cDC common dendritic cell
CDK cyclin-dependent kinase
CDP common dendritic cell progenitor
ChIP chromatin immunoprecipitation
ChIP-seq chromatin immunoprecipitation and sequencing
chrRNA chromatin-associated RNA
chrRNA-seq chromatin-associated RNA sequencing
CLR C-type lectin receptor
cMoP common monocyte progenitor
CMP common myeloid multipotent progenitor
CoTC co-transcriptional cleavage
CPA cleavage and polyadenylation complex
CPSF73 cleavage and polyadenylation specificity factor-73
CSF colony stimulating factor
Cstf cleavage stimulatory factor
CTCF CCCTC-binding factor
CTD C-terminal domain
DAMP danger associated molecular pattern
DBD DNA-binding domain
DC dendritic cell
DNA deoxyribonucleic acid
DSIF DRB sensitivity-inducing factor
EGR early growth response protein
eQTL expression quantitative trait loci
ETS E-twenty-six
FPKM fragments per kilobase per million
FRIP fraction reads in peaks
G guanosine
GAS gamma activated sequences
GM-CSF granulocyte macrophage colony-stimulating factor
GMP granulocyte myeloid progenitors
HAT histone acetyltransferase
HDAC histone deacetylase
HMT histone methyltransferase
HSC haematopoietic stem cell
IFN type I interferons
IFNAR interferon-α/β receptor
IFNGR interferon-γ receptor
IKK IκB kinase
IL4Rα IL-4 receptor α

IRF	interferon regulatory factor
ISG	interferon response gene
ISGF3	interferon-stimulated gene factor 3
ISRE	interferon stimulated response elements
k.b.	kilobase
LMPP	lymphoid multipotent progenitor
lncRNA	long non-coding RNA
LPS	lipopolysaccharide
LXR	liver X receptor
M-CSF	macrophage colony stimulating factor
mDDC	monocyte-derived dendritic cell
MDP	monocyte/macrophage and dendritic cell progenitor
miRNA	micro-RNA
MPS	mononuclear phagocyte system
mRNA	messenger RNA
NELF	negative elongation factor
NET	neutrophil extracellular trap
NGS	next generation sequencing
NLR	NOD-like receptor
NLS	nuclear localisation signal
NO	nitric oxide
NR	nuclear receptor
P-TEFb	positive transcription elongation factor-b
pA	poly-adenylate
PAF1C	polymerase associated factor 1
PAMP	pathogen associated molecular pattern
pAS	poly-adenylate sequence
PCA	principle component analysis
PIC	pre-initiation complex
PMA	phorbol 12-myristate 23-acetate
Pol II	RNA polymerase II
PPARγ	peroxisome proliferator- activated receptor γ
PRG	primary response gene
pri-miRNA	primary micro RNA transcript
PRR	pathogen recognition receptor
RIG1	retinoic acid-inducible gene 1
RLR	retinoic acid-inducible gene 1 - like helicase receptor
RNA	ribonucleic acid
RNA-seq	RNA sequencing
ROS	reactive oxygen species
RPB1	RNA polymerase B1
RPM	reads per million
RUNX1	Runt-related transcription factor 1
SDTF	signal dependent transcription factor
SETX	senataxin
snoRNA	small nucleolar RNA
snRNA	small nuclear RNA
SRG	secondary response gene
T	thymine
t-SNE	t-distributed stochastic neighbour embedding
TAD	topologically associated domains
TES	transcription end site
TLR	toll like receptor
TNF	tumour necrosis factor α
TPM	transcripts per million

Treg	regulatory T cell
TSS	transcription start site
UTR	untranslated region
vs	versus
VST	variance stabilised
WT	wild type
YS	yolk sac

1. Introduction

1.1. The Immune System

The immune system offers a defence against invading pathogens such as viruses, bacteria, and parasites, preventing infection and dissemination and plays an additional role to maintain homeostasis, destroying dysregulated endogenous cells. The primary barrier between the tissues and the environment is the skin, acting as a physical defence against infection. When this is breached inflammation ensues, characterised by five cardinal signs: *calor* (heat), *rubor* (redness), *tumor* (swelling), *dolor* (pain), and *function laesa* (loss of function). This is the interface at which host cells and invading pathogens meet, it is therefore vital for cells of the immune system to distinguish the foreign infiltrators from self. The two arms of the immune system have different mechanisms of accomplishing this. The innate arm relies on the recognition of conserved pathogen-associated molecular patterns (PAMPs), which are alien to endogenous tissues. This allows the rapid recognition of any invading pathogen and an ensuing response, typically characterised by the influx of leukocytes and phagocytosis of the pathogens; as initially observed by Élie Metchnikoff, the father of cellular immunology (Gordon, 2016). The adaptive arm of the immune system is delayed in responding to infection, but is able to mount highly specific immune responses tailored to the invading pathogen, and maintain a long-lasting immunological memory, aiding against subsequent reinfection.

Metchnikoff was the first to appreciate the immunological role of phagocytosis, describing two populations of phagocytic cell: macrophages “the big eaters” in Greek, and neutrophils “the small eaters” or microphages (Gordon, 2016). Myeloid cells were further characterised by Paul Erlich who utilised coal tar dyes to classify leukocytes on the basis of their morphology and staining. He first described the presence of granular leukocytes in the connective tissue, which he named the mast cell, before progressing to characterise blood leukocytes. Erlich described monocytes as large mononuclear cells with indented nuclei and

the polymorphonuclear granulocytes were further characterised based on the staining of their granules with acidic, basic, and neutral dyes. Neutrophils possessed neutrophilic granules, eosinophils were preferentially stained with acidic dye (acidophilic), and basophils with basic dye (basophilic) (Ehrlich, 1880; Kay, 2016). However, it wasn't until 1973 that the dendritic cell (DC), the lynchpin between innate and adaptive immunity, was identified and shown to be distinct from macrophages (Steinman and Cohn, 1973; Nussenzweig and Steinman, 1980). Together, these cells constitute the myeloid lineage, key components of the innate immune response. This thesis will focus on the macrophage, perhaps the most diverse myeloid cell, and a crucial regulator of immune responses, from initial pathogen recognition to its clearance and the return to homeostasis.

1.1.1. Myelopoiesis

Haematopoiesis occurs predominantly in the bone marrow after birth. Long-term haematopoietic stem cells (HSCs) are pluripotent, able to reconstitute all haematopoietic lineages and can undergo self-renewal or progress onwards in a multi-step process of differentiation, in which each step is coupled with a loss of pluripotency restricting developmental potential resulting in lineage commitment (Figure 1.1). In steady-state conditions, the level of HSCs remains constant, and progeny are replaced continuously as they mature. However, in response to injury or infection, the balance between HSC differentiation and renewal is tipped in favour of differentiation. This is mediated by the transcription factor c-Myc, increased levels of which promotes the transition of long term HSCs to short term HSCs (Wilson et al., 2004), which yield either the common myeloid multipotent progenitor (CMP) or the lymphoid multipotent progenitor (LMPP), giving rise to the myeloid and lymphoid lineages, respectively. CMPs give rise to the granulocyte myeloid progenitors (GMPs), from which the granulocyte lineages are derived. Neutrophils are the most numerous leukocytes in the blood and are derived from GMPs via additional proliferating precursors (myeloblasts, promyelocytes, myelocytes) which progress into post-

mitotic precursors (metamyelocytes and band cells), before maturing into segmented neutrophils, which bolsters the circulating pool of short-lived blood neutrophils. This process takes ten to twelve days, and is paralleled by the formation of distinct granule proteins throughout neutrophil development (Borregaard, 2010). The monocyte/macrophage and DC progenitor (MDP) also arises from GMPs, losing granulocyte potential. Monocyte-derived macrophages have been demonstrated to originate from common monocyte progenitors (cMoPs) (Hettinger et al., 2013), and tissue-resident DCs are derived from common DC progenitors (CDP) (Onai et al., 2007; Naik et al., 2007). However, the branch point at which these progenitors divide is unclear, with some challenging the existence of committed monocyte-macrophage and dendritic cell precursors (Sathe et al., 2014). Mice possess two main classes of monocytes: classical (which have high levels of Ly6C - Ly6C^{hi}) and non-classical (Ly6C^{lo}) (Geissmann et al., 2003). Ly6C^{lo} monocytes are thought to derive from Ly6C^{hi} cells in the bone marrow and in the blood (Hettinger et al., 2013; Yona et al., 2013). The function of these monocyte subsets differ, with Ly6C^{hi} cells being required for tissue inflammation (Croxford et al., 2015) and Ly6C^{lo} cells having a more homeostatic role, patrolling the endothelium and maintaining its integrity (Ginhoux and Jung, 2014). Ly6C^{hi} monocytes are highly dependent on granulocyte macrophage colony-stimulating factor (GM-CSF) for their pro-inflammatory activity (Croxford et al., 2015) and yield inflammatory macrophages and DCs in the tissue (Ginhoux and Jung, 2014). The spleen is an additional site of adult haematopoiesis, possessing pool of monocytes and precursors, which are mobilised in conditions of inflammation (Swirski et al., 2009).

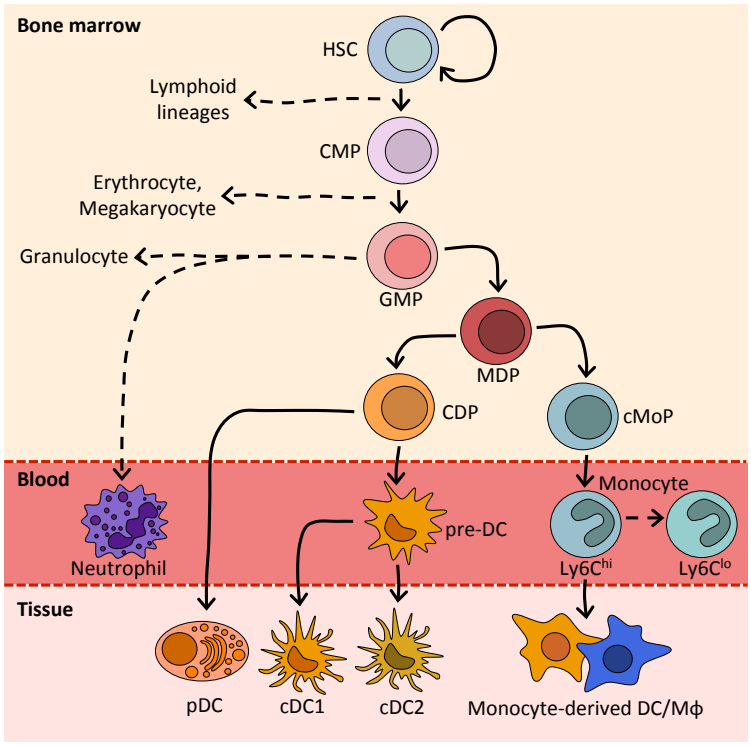

Figure 1.1. Myelopoiesis. Haematopoietic stem cells (HSCs) give rise to common myeloid progenitors (CMPs) and lymphoid multipotent progenitors (LMPPs), which give rise to the myeloid and lymphoid lineages respectively (lymphoid lineage not shown). CMPs differentiate into granulocyte myeloid progenitors (GMPs), losing potential for erythrocytes and megakaryocytes (dotted line). GMPs develop into granulocytes and neutrophils via additional precursors (not shown), neutrophils are the most abundant granulocytes and are released into the bloodstream from the bone marrow. The monocyte/macrophage dendritic cell (DC) precursor (MDP) splits into distinct DC and monocyte precursors: the common DC precursor (CDP) and common monocyte progenitor (cMoP). CDPs give rise to either plasmacytoid DCs (pDC) and pre-DCs, which further develop into common DCs (cDC1 and cDC2) in the tissue. cMoPs yield Ly6C^{hi} monocytes, from which Ly6C^{lo} monocytes are thought to derive (dotted line). Monocyte derived DCs and macrophages (mϕ) are derived from Ly6C^{hi} monocytes.

Lineage defining transcription factors

Lineage defining transcription factors are crucial for haematopoiesis and possess the rare ability of pioneering transcription factors to bind inaccessible cell-specific cis-regulatory elements in heterochromatin thus establishing cellular identities (Iwafuchi-Doi and Zaret, 2014) (further discussed in Chapter 1.3.1). The lineage defining transcription factor Runt-related transcription factor 1 (RUNX1) is notable as it is required for definitive haematopoiesis, occurring in the adult bone marrow (Okuda et al., 1996; Wang et al., 1996) (embryonic haematopoiesis is discussed in Chapter 1.1.2). RUNX1 promotes the expression of the E-twenty-six (ETS) family member and pioneering transcription factor PU.1 in HSCs (Imperato et al., 2015). PU.1 is required in the development of both myeloid and lymphoid

lineages (E.W. Scott et al., 1994), although its expression of PU.1 is ten-fold higher in macrophages than B cells (DeKoter and Singh, 2000), signifying its importance in the myeloid lineage. Critically, PU.1 controls the expression of the macrophage colony stimulating factor (M-CSF) and GM-CSF receptors, along with CCAAT/enhancer-binding protein α (C/EBPα), thus promoting myeloid commitment (Hohaus et al., 1995; Aikawa et al., 2010; Rieger et al., 2009). Granulocyte differentiation of GMPs is suppressed by the up-regulation of early growth response protein (EGR) 1 and EGR2 by PU.1, which act to activate macrophage genes and repress the neutrophil program (Laslo et al., 2006). IRF8 is expression is also induced in GMPs and also promotes monocyte/macrophage/DC differentiation over that of granulocytes (Tamura et al., 2000). Furthermore, in differentiated macrophages IRF8 cooperates with PU.1 to specify cell specific enhancers associated with core macrophage functions (Mancino et al., 2015).

1.1.2. Origins of tissue-resident macrophages

The mononuclear phagocyte system

Tissue-resident macrophages were initially categorised as the reticuloendothelial system, on the basis of their ability to accumulate vital dyes from the circulation by phagocytosis (Aschoff, 1924). *Reticulo* refers to the network formed by their cytoplasmic extensions and *endothelial* to their proximity to the vasculature in tissues. The origins of macrophages within this system were not investigated, but it was believed that they were derived locally (Yona and Gordon, 2015). A major change came with the introduction of the mononuclear phagocyte system (MPS), attributing monocytes as the precursors for all tissue-resident macrophages (Van Furth et al., 1972). The MPS was initially comprised of bone marrow monocyte precursors, blood monocytes, and tissue macrophages, and was later extended to include the newly discovered DCs (Van Furth, 1981). However, this broad classification system has been challenged in the light of the embryonic origins of many tissue-resident macrophages (Guilliams et al., 2014; Ginhoux and Guilliams, 2016).

Embryonic origins of tissue-resident macrophages

Embryonic myelopoiesis occurs in step-wise process, beginning on embryonic day 7 (E7) in mice with the generation myeloid progenitors in the ectoderm of the yolk sac (YS). These primitive progenitors are c-Myc independent and directly give rise to YS macrophages, without a monocytic intermediate. Definitive haematopoiesis is dependent upon the generation of HSCs, which first arise from the ventral wall of the aorta in the aorta-gonad-mesenephros (AGM) region at E10.5, these then seed the foetal liver (Ginhoux and Guilliams, 2016). In the foetal liver HSCs expand and give rise to mature, c-Myc dependent, myeloid cells (Kumaravelu et al., 2002; Kieusseian et al., 2012; Ginhoux and Guilliams, 2016). Elegant fate-mapping strategies have demonstrated the variable contributions of embryonic and adult precursors to tissue-resident macrophages. The majority of tissue-resident macrophages are derived almost entirely from foetal monocytes with the exception of microglia in the brain, which are entirely YS macrophage derived (Sheng et al., 2015) (Hoeffel et al., 2015). Contributions from both of these origins can lead to heterogeneity of ontogeny within tissues with relative contributions of both embryonic precursors constituting Langerhans cells in the epidermis (Sheng et al., 2015). A third category of tissues is re-populated by definitive haematopoietic monocyte derived macrophages after birth this includes: the gut (Bain et al., 2014), dermis (Tamoutounour et al., 2013), heart (Molawi et al., 2014; Epelman et al., 2014), and pancreas (Calderon et al., 2015). Notably the rate of re-population is dependent upon accessibility of these tissues to blood-borne monocytes in steady state, with tissues either being “closed” (brain, epidermis, lung, liver), or “open” (heart, pancreas, gut, dermis) after birth (Ginhoux and Guilliams, 2016). Furthermore, the half-life of resident macrophage populations determines the rate of replacement of embryonic derived resident macrophages. Tissue-resident macrophages in the heart for example have an estimated half-life of 8-12 weeks and are slowly replaced with adult monocyte-derived macrophages (Molawi et al., 2014; Epelman et al., 2014), whereas

resident populations in the gut have a half-life of 4-6 weeks and are not capable of self-maintenance (Bain et al., 2014), they are therefore rapidly replaced (Ginhoux and Guilliams, 2016) (Figure 1.2). The implications of this in terms of functional and transcriptional responses are explored in Chapter 1.3.1.

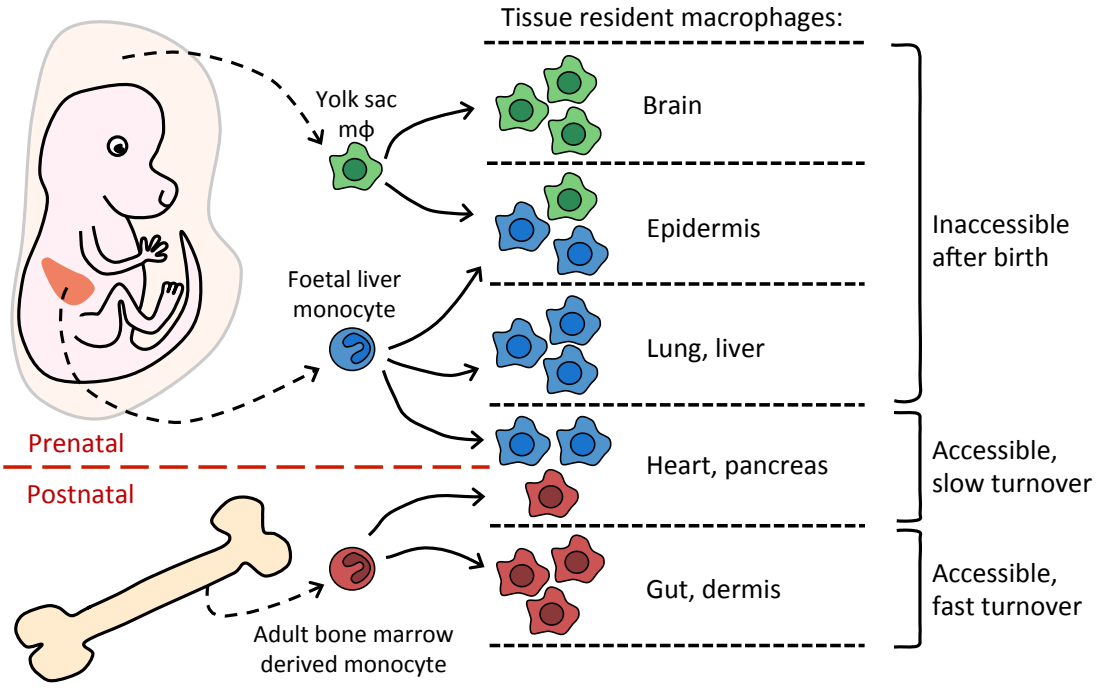

Figure 1.2. The origins of tissue-resident macrophages. Primitive myeloid progenitors form in the yolk sac at embryonic day 7 (E7), directly giving raise to yolk sac macrophages in a c-Myc independent manner. These early macrophages seed all of the foetal tissues. By E10.5 haematopoietic progenitor cells (HSCs) are formed, these seed the foetal liver where haematopoiesis takes place in a c-Myc dependent manner until birth. Foetal liver monocytes give rise to tissue-resident macrophages in all tissues, with the exception of the brain, and partially, the epidermis. Foetal liver monocytes out compete the early yolk sac derived macrophages and are the dominant populations until birth. After parturition the accessibility of tissues to monocytes is altered, with some tissues becoming inaccessible. Monocytes arising from definitive haematopoiesis, occurring in the bone marrow after birth, are therefore only able to contribute to tissue-resident macrophage populations in accessible tissues. Furthermore, the rate of turnover of tissues resident macrophages within these tissues determines the rate at which they are re-populated by bone marrow derived monocytes, leading to mixed contributions from foetal liver and bone marrow monocytes to the tissue-resident macrophages in tissues with a slow turnover such as the heart and pancreas, which alters with age.

1.1.3. Macrophage polarisation

In vitro macrophage polarisation

Macrophage polarisation has classically been described using the M1, M2 archetype to represent functionally opposing macrophage activation states, which were originally attributed to inflammatory and resolving macrophages on the basis of their nitric oxide (NO) and ornithine signalling (Murray et al., 2014; Murray, 2017). These are predominantly based on *in vitro* phenotypes exhibited by macrophages derived from bone marrow (BMDMs) though extended cultures with colony-stimulating factors (CSFs), namely GM-CSF, yielding GM-BMDMs, and M-CSF, yielding M-BMDMs. L-conditioned medium, containing M-CSF, is also commonly used to generate M-BMDMs (Murray et al., 2014; Murray, 2017). There is considerable heterogeneity between and within BMDM cultures even when the same CSFs are used, due to discrepancies in: culture times, selection protocols, and further laboratory-specific differences. Notably, GM-BMDMs contain a mixture of monocyte derived macrophages and cMoP derived DCs (Helft et al., 2015). Significant efforts have therefore been initiated to standardise practices and nomenclature (Murray et al., 2014).

To mimic *in vivo* stimuli BMDMs are often exposed to the Gram-negative bacterial outer membrane component lipopolysaccharide (LPS) and interferon-γ (IFN-γ) to recapitulate signals encountered in an inflammatory setting, from invading bacteria and Th1 cells, and IL-4 and IL-13 to represent Th2 mediated responses (Munder et al., 1999; Munder et al., 1998). Subsequent macrophage states are then termed classically activated (M1), and alternatively activated (M2), respectively. The M1-M2 dichotomy has also been applied to the products of BMDM cultures, with GM-BMDMs being described as “M1” and M-BMDMs as “M2” (Joshi et al., 2014) (Figure 1.3). These models have shown to be very useful in characterising key macrophage processes and the cellular machinery driving these processes, however, they fail to capture the full complexity of macrophage responses to signals indicative of environmental and immunological state, reducing the full spectrum of macrophage

activation to bipolar extremes. More focus is therefore now being placed on the *in vivo* heterogeneity of macrophages, utilising technologies such as single-cell RNA sequencing (RNA-seq) and taking a multidimensional view to explore variation in macrophage responses (Ginhoux et al., 2015).

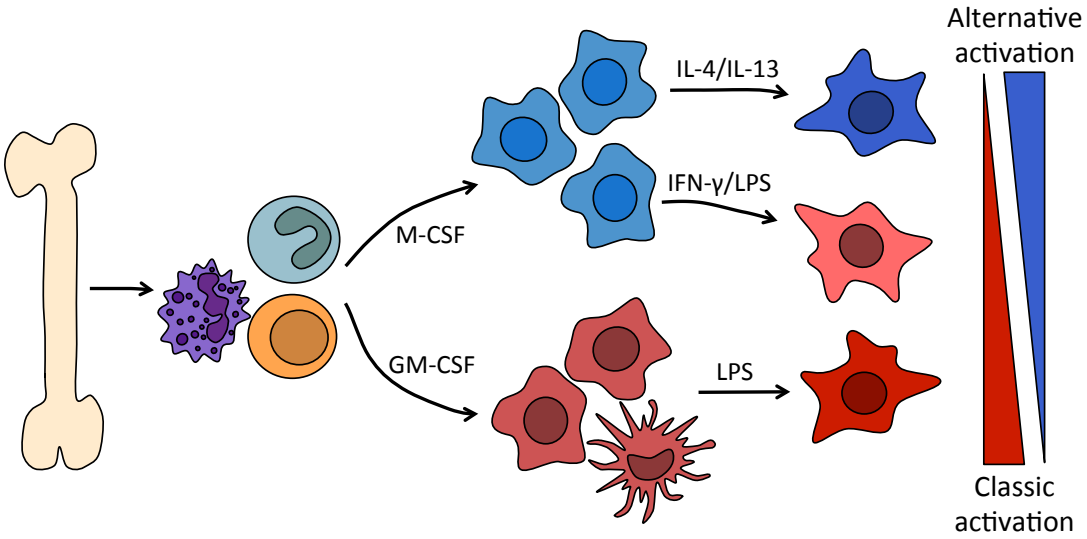

Figure 1.3. *In vitro* macrophage culture and polarisation. Cells from total bone marrow (predominantly consisting of progenitor cells, monocytes, and neutrophils) are cultured with either GM-CSF or M-CSF over a period of eight days to yield bone marrow derived macrophages (BMDMs). These can then by polarised to classic or alternatively activated states though treatment with LPS and/or IFN-γ, or IL-4 or IL-13.

In vivo macrophage functions

The dual nature of tissue-resident macrophage and inflammatory monocyte derived macrophage action coupled with the M1-M2 over simplification of macrophage heterogeneity has led to much confusion over the precise roles of macrophages in inflammation. Tissue-resident macrophages have complex roles *in vivo* and are integral for tissue function, acting to efficiently remove apoptotic cells in conditions of homeostasis and functioning as sentinels of infection, in addition to fulfilling a wide variety of tissue specific functions (discussed in Chapter 1.3.1). In the context of infection tissue-resident macrophages detect initial signs of microbes and respond through the release of chemokines and cytokines initiating the recruitment of neutrophils and monocytes from the blood (Cailhier et al., 2005; Maus et al., 2002; Ajuebor et al., 1999). However, tissue-resident

macrophages are not inflammatory in homeostatic conditions (Davies et al., 2013) and have been demonstrated to die upon infection (Di Paolo et al., 2013; Yatim et al., 2015). It has therefore been suggested that tissue-resident macrophages, with low microbicidal capacity, undergo programmed cell death upon infection as they are unable to efficiently destroy invading pathogens (Ginhoux et al., 2017). Pro-inflammatory mechanisms of cell death such as pyroptosis and necroptosis are strongly associated with the release of danger-associated molecular patterns (DAMPs), such as HMGB1, mitochondrial and nuclear deoxyribonucleic acid (DNA), ribonucleic acid (RNA), and adenosine triphosphate (ATP), coupled with extensive release of IL-1β in the case of inflammasome activation in pyroptosis (Kolb et al., 2017). These mechanisms of regulated necrosis are highly immunogenic (Yatim et al., 2015; Kolb et al., 2017; Ginhoux et al., 2017) acting to promote neutrophil and monocyte recruitment. The additional upshot of this localised destruction, which has been long observed as a by-product of acute inflammation, is the deprivation of a replication niche for intracellular pathogens such as viruses and bacteria. Furthermore, recent observations suggest that pyroptosis by macrophages encapsulates viable bacteria in the cellular debris aiding their destruction by neutrophils (Jorgensen et al., 2016). Indeed, it has been demonstrated that necroptosis of tissue-resident macrophages promotes anti-microbial Th1 responses via the recruitment of blood monocytes (Bleriot et al., 2015). The regulated processes of programmed cell death through immunogenic pyroptosis and necroptosis therefore likely represents an innate strategy of pathogen control and immune cell recruitment by tissue-resident macrophages (Ginhoux et al., 2017). It is therefore possible that in response to initial infections tissue-resident macrophages are able to progress down two potential routes: inflammatory polarisation and secretion of pro-inflammatory chemokines and cytokines, or inflammatory cell death. Both of these mechanisms result in the recruitment of monocytes and neutrophils from the circulation, however the propensity of tissue-resident macrophages to undergo either path is a relative unknown and is likely to vary on a contextual basis, given the inherent differences between macrophages resident in different tissues (Lavin et al., 2014).

Upon their recruitment incoming monocytes differentiate into inflammatory macrophages at the site of inflammation and mediate sterilising inflammation along with the remaining tissue-resident population. Once the threat has been overcome, a shift in the local milieu of cytokines (contributed to by the myriad of other immune cell at sites of infections), PAMPs, and DAMPs, favours resolution and repair over continued inflammatory activity, eliciting a shift in macrophage phenotype towards one favouring homeostasis. This process likely involves dynamic changes in macrophage gene expression profiles, from pro-inflammatory to favouring resolution and repair (Varga et al., 2016). Programmed cell death may also play a role in the resolution of inflammation with increased efferocytosis of apoptotic cells by macrophages initiating a transcriptional switch, acting through nuclear receptors (NRs) to mediate changes in gene expression, increasing phagocytic capacity and dampening inflammation (Elliott et al., 2017; Kolb et al., 2017). The effects of NRs on pro-inflammatory activity are discussed in Chapter 1.3.2. Once the tissue reaches homeostasis monocyte derived macrophages either join the resident population, egress back into the vasculature, or die *in situ*. Again, a question remains over the likelihood of each of these relative fates, with some suggesting the due to the magnitude of monocyte mobilisation during inflammation the majority of monocyte derived macrophages are likely to die upon the restoration of homeostasis (Murray, 2017). However, taking the liver as an example, many resident Kupffer cells have been shown to die in response to inflammation (Di Paolo et al., 2013; Bleriot et al., 2015), and separate studies indicate that the empty niche can be repopulated by monocyte derived macrophages (Bleriot et al., 2015; C.L. Scott et al., 2016), which are transcriptionally highly analogous to the original tissue-resident cells and, importantly, acquire their self renewal capacity (C.L. Scott et al., 2016). The potential for monocyte-derived macrophages to adapt to tissue-resident populations is further discussed in Chapter 1.3.1. However, it can be appreciated that the extraordinary plasticity exhibited by macrophages *in vivo* (Figure 1.4) requires careful coordination and is mediated by close transcriptional control.

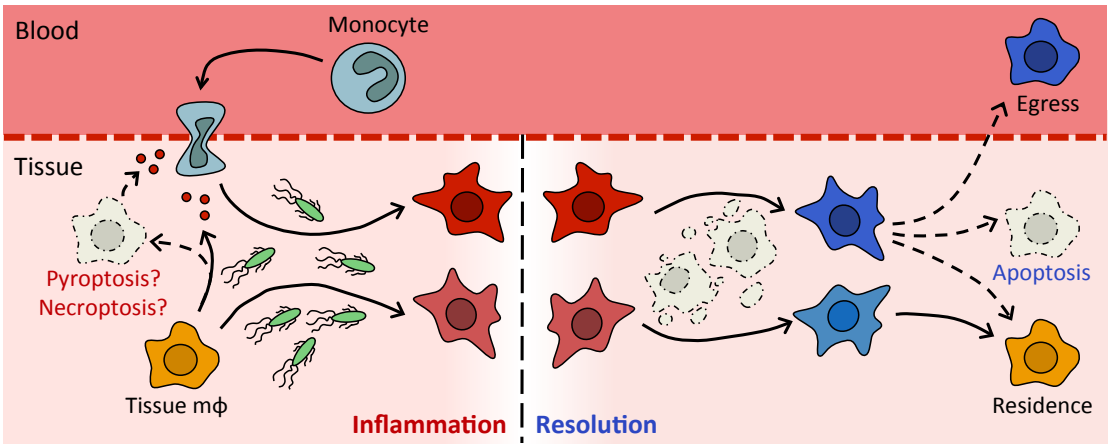

Figure 1.4. *In vivo* macrophage functions at sites of inflammation. Inflammatory stimuli (PAMPs) activate tissue-resident macrophages (mϕ), which release chemokines, initiating recruitment of Ly6C^{hi} monocytes from the blood (solid arrow). Tissue-resident macrophages may also die by pyroptosis and/or necroptosis promoting inflammation and monocyte recruitment through the release of DAMPs (dotted arrows). Recruited monocytes differentiate into inflammatory macrophages in the tissue (not shown) and are activated by pathogens. Inflammatory macrophages then contribute to the localised inflammation and clearance of the infection. As inflammation decreases localised signals, such as those associated with apoptosis, alter macrophage phenotypes to favour resolution and the return to homeostasis. Once tissue homeostasis is reached monocyte derived macrophages may either: replenish tissue resident populations, die *in situ* (by apoptosis), or egress back into the circulation.

1.2. Transcription

Genes are defined as single transcription units, initiating at the transcription start site (TSS) and ending at the transcription end site (TES). Cellular identity is mediated through the precise regulation of gene expression and complex co-transcriptional processing such as alternative splicing coupled with post-translational protein modifications to give rise to a vastly complex proteome. The advent of next generation sequencing (NGS) technology has allowed molecular interrogation of transcriptional processes, with the application of NGS to study transcription factor binding with ChIP sequencing (ChIP-seq) revealing the precise binding locations of transcription factors genome wide. Much study has therefore been devoted to the contribution of transcription factor binding to promoters and distal *cis*-regulatory elements to gene expression, which broadly act to influence the recruitment of RNA polymerase II (Pol II) to gene promoters and induce transcription. However, diverse

regulatory mechanisms exist to control the expression of genes, mediated by precise regulation of both the initiation and termination of transcription.

1.2.1. 5' regulation of transcription

Cis-regulatory elements

DNA has an inherent affinity for the core histone subunits (H1, H2a, H2b, H3, and H4) allowing the spontaneous assembly and packaging of DNA around nucleosomes in a highly ordered structure, with ~147 b.p. DNA wrapping around each nucleosome, sequestering it from damage and preventing the binding of other factors. *Cis*-regulatory regions involved in the regulation of gene expression have an altered affinity for nucleosomes. Promoters consist of a short DNA sequences ~100 base pairs (b.p.) in length located in very close proximity to TSSs. They regulate the recruitment of Pol II and assembly of the pre-initiation complex (PIC), controlling the directionality of transcription and coordinating the initiation of transcription at TSSs (Roeder, 1996). The assembly of transcriptional machinery at promoters is mediated, in part, by their increased guanosine (G) and cytosine (C) content, which increases the affinity of DNA to nucleosomes. However, in areas with very high CG dinucleotide enrichment (known as CpG islands) the ability of DNA to bind nucleosomes is constrained, resulting in nucleosome depletion (Fenouil et al., 2012; Ramirez-Carrozzi et al., 2009). Approximately seventy percent of mammalian gene promoters contain CpG islands, allowing dynamic turnover of histones and competition with transcriptional apparatus for binding. Despite this, promoters mediate only weak levels of gene expression on their own, requiring the activity of accessory enhancers to facilitate increased rates of transcription.

Enhancers are often located many kilobases (k.b.) away from promoters, their function not being affected by distance or orientation with respect to their target gene (Banerji et al., 1981). Enhancers consist of longer genomic sequences of several hundred base pairs, rich in transcription factor binding domains (motifs), which act to recruit transcription factors and

the associated activating or repressive co-factors, thereby exerting regulatory effects on their target promoters. Enhancers have an intrinsically high affinity for nucleosomes (Tillo et al., 2010), this increases the energetic barrier that must be overcome for transcription factors to be recruited; establishing a need for the recruitment of multiple transcription factors, thus favouring nucleosome displacement (Spitz and Furlong, 2012). This is thought to be mediated by direct protein interactions and the collaborative binding of transcription factors, or via competition for proximal motifs occupied by a single nucleosome (J.A. Miller and Widom, 2003; Long et al., 2016). A minority of transcription factors are endowed with the capacity to bind partially exposed DNA in heterochromatin, in a sequence-specific manner, facilitating nucleosome removal and allowing subsequent binding of additional transcription factors, these are known as pioneering factors (Zaret and Carroll, 2011; Barozzi et al., 2014; Soufi et al., 2015). Enhancer architecture is often characterised by two opposing models, which differ in their mechanisms of transcription factor binding. The first is the enhanceosome model, exemplified by the canonical *Ifnb1* enhancer (Thanos and Maniatis, 1995), which requires the cooperative binding of eight transcription factors to a highly conserved sequence of motifs for enhancer activation and initiation of *Ifnb1* transcription. The second is termed the "billboard" model in which transcription factors are recruited independently of one another with a cumulative effect on enhancer status and subsequent gene expression (Arnosti and Kulkarni, 2005). On the other hand, the collective model incorporates protein – protein interactions into enhancer function. Proposing that a core set of transcription factors is recruited to a many enhancers, which are diverse in their sequence composition, instead direct interactions between cooperating transcription factors, comprising a protein scaffold, increases the flexibility of recruitment, which has little reliance on precise enhancer structure (Junion et al., 2012). These models of enhancer activity are summarised in Figure 1.5.

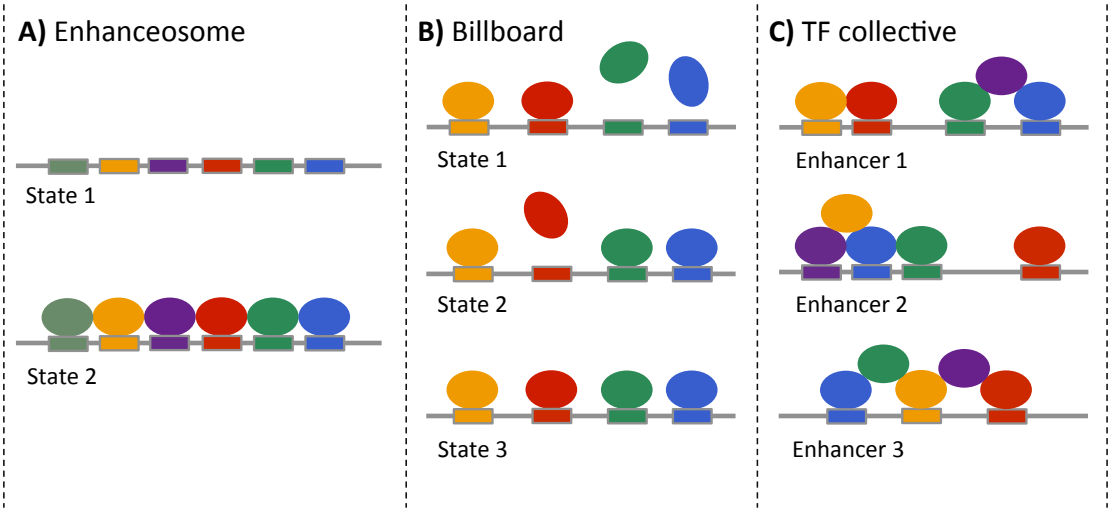

Figure 1.5. Models of enhancer activation. A) Enhanceosome model. Highly conserved DNA sequence contains precisely orientated motifs, which are bound cooperatively by transcription factors (TFs). Enhancers therefore have two states: unoccupied (state 1), and occupied (state 2). **B)** Billboard model. Sequence composition and orientation are more flexible but precise motifs are required for TF recruitment. Enhancers can exist in a range of states, with both cooperative and additive TF binding. **C)** TF collective model. A defined set of TFs is capable of cooperatively binding a range of enhancers, which are variable in their motif composition

Many questions exist over how such distal regulatory elements are able to target their cognate promoters in three-dimensional space. However, this remains largely unanswered, with hypothesis including: the tracking of Pol II from enhancers to target promoters, the looping out of intervening DNA bringing enhancers and promoters into close proximity, and chromatin modifications at enhancers and promoters acting as a link between these elements (Bulger and Groudine, 2011; Ong and Corces, 2011). The substantial development of chromatin conformation capture (3C) (Dekker et al., 2002) based techniques: 5-C (Dostie et al., 2006) and Hi-C (Lieberman-Aiden et al., 2009), have allowed greater interrogation of chromatin interactions, with many observations supporting the model of enhancer promoter looping. However, most looping detected by these methods is in the form of stable interactions, mediated by the insulator CCCTC-binding factor (CTCF). This factor delineates large regions of chromatin ranging from kilobases to megabases, termed topologically associated domains (TADs) (Matharu and Ahituv, 2015; Long et al., 2016). Most enhancer-promoter interactions occur within the confines of these TADs, and whilst enhancers are essentially directionless, those located close to CTCF binding sites

demonstrate directionality, which can be reversed by inverting the DNA sequence containing the enhancer and CTCF binding site (Guo et al., 2015). Interestingly, it has been observed that genes within TADs are often co-ordinately regulated (Nora et al., 2012) (Gómez-Marín et al., 2015), implying enhancers within TADs may cooperate in the regulation of shared target genes. However, closely proximal genes are often differentially expressed; diverse factors such as the biochemical affinity of enhancers for their cognate promoters and the accessibility of target promoters are therefore also likely to play a role in specifying enhancer targets (Figure 1.6) (Zabidi and Stark, 2016).

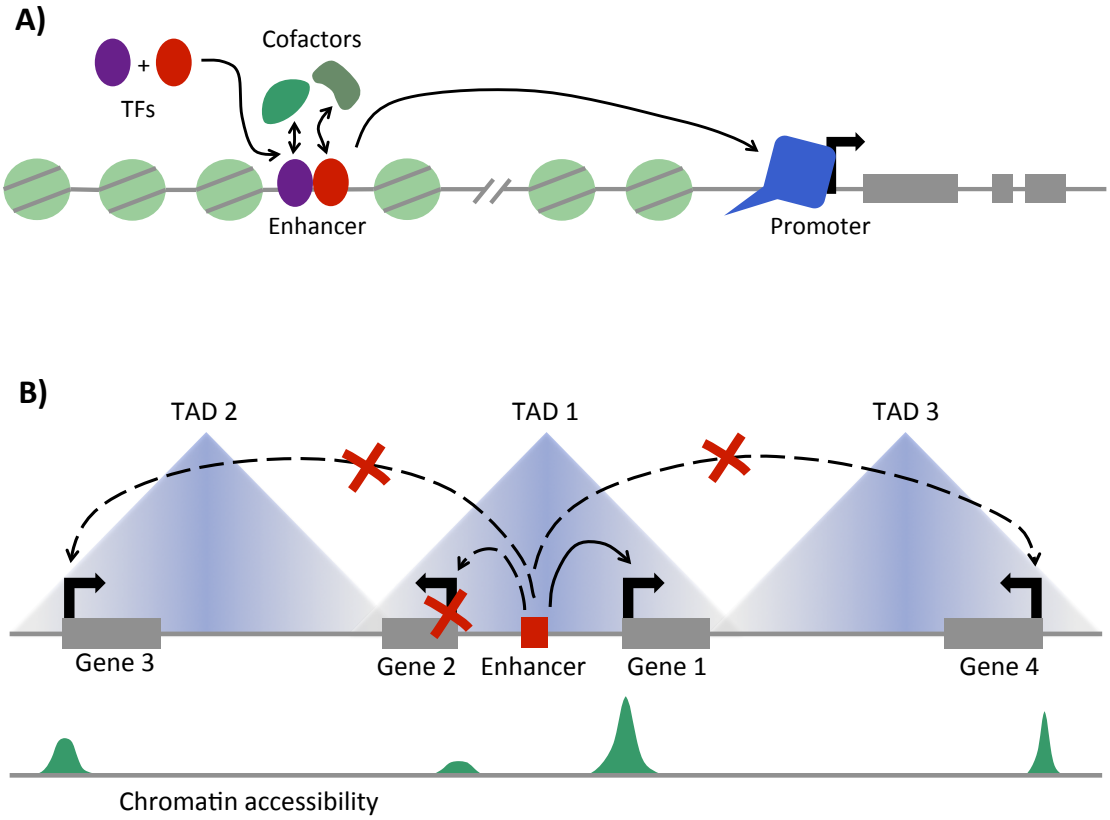

Figure 1.6. Enhancer function. A) Simple model of enhancer activity. Binding of specific transcription factors (TFs) to enhancers and recruitment of cofactors results in an association of enhancers with target promoters and regulation of Pol II recruitment. **B)** Topologically associated domains (TADs) restrict enhancer interactions. Within TADs enhancer targeting to genes is determined in part by the accessibility of promoters.

NGS techniques typically require large amounts of starting material, averaging out variability in gene expression and leading to the perception of transcription as a uniform process. The adoption of imaging techniques for the analysis of transcription in individual cells has revealed novel findings such as the phenomenon of transcriptional bursting (Zhao et al., 2016). Bursting implies a more stochastic mechanism for the initiation of transcription with irregular bursts of activity involving the release of consecutive Pol II complexes, leading to the generation of several transcripts, followed by a refractory period of reduced transcriptional activity. Recently it has been observed that linked reporter genes in *Drosophila* driven by a shared enhancer exhibit coordinated transcriptional bursting (Fukaya et al., 2016), challenging the paradigm in which a single enhancer targets a single promoter, and emphasising the complex spatial interactions likely occurring within TADs to exert coordinated gene regulation by enhancers (Hnisz et al., 2017).

5' transcription checkpoints

Pol II mediates the transcription of all protein coding genes, in addition to that of non-coding transcripts, such as: long non-coding RNA (lncRNA), small nuclear RNA (snRNA), and small nucleolar RNA (snoRNA). Pol II is a very large complex comprising multiple subunits, the largest of which, RNA polymerase B1 (RPB1) possesses a unique unstructured C-terminal domain (CTD), which consists of 52 tandem repeats of the consensus sequence: Tyr^{1}-Ser^{2}-Pro^{3}-Thr^{4}-Ser^{5}-Pro^{6}-Ser^{7}. This is subject to various post-translational modifications, acting as a platform for the dynamic recruitment of multiple factors involved in the key stages of transcriptional activity: initiation, elongation, and termination. As Pol II progresses from the 5' to the 3' end of the gene, the phosphorylation status of the CTD alters, along with the composition of these CTD-associated factors, which have varying affinities for Pol II CTD modifications. CTD post-translational modifications are thus collectively referred to as the CTD code and act to regulate diverse activities co-transcriptionally, such as splicing, pre-messenger RNA (mRNA) processing, and histone modification (Harlen and Churchman,

2017). Pol II is recruited to promoters with an unmodified CTD, where it interacts with general transcription factors (TFIIA, B, C, D, E, F, and H) to form the PIC (Lu et al., 1991) (Harlen and Churchman, 2017). The unmodified CTD of newly recruited Pol II is important for this process as it has a strong affinity for the Mediator complex (Robinson et al., 2016), which acts as an essential link between transcription factors at enhancers and Pol II at promoters, transducing biological information into transcriptional changes (Jeronimo and Robert, 2017). Transcription is initiated by phosphorylation of Ser^5 and Ser^7 by the TFIIH component cyclin-dependent kinase (CDK) 7, lowering the affinity of Pol II for Mediator and inducing its escape from the promoter (Wong et al., 2014; Jeronimo and Robert, 2014). Successful initiation is therefore dependent on promoter accessibility, ensuring Pol II recruitment, and on the cooperative activity of an enhancer. The second regulatory checkpoint occurs shortly after early initiation, which is a highly abortive process, with many polymerases undergoing early termination. Once Pol II has negotiated this erroneous phase of early transcription and progressed to ~25-50 base pairs downstream of the TSS, promoter proximal pausing occurs, restricting onwards travel (Kwak and Lis, 2013). This is a rate limiting step of transcription in ~40% of eukaryotic genes (Min et al., 2011). Promoter proximal pausing is initiated by the actions of negative elongation factor (NELF) and DRB sensitivity-inducing factor (DSIF) (Adelman and Lis, 2012; Kwak and Lis, 2013; Jonkers and Lis, 2015). The release of Pol II from promoter proximal pausing is mediated by recruitment of positive transcription elongation factor-b (P-TEFb), which is made up of CDK9 and cyclin T1. P-TEFb phosphorylation of NELF, DSIF, and Pol II Ser^2 results in the dissociation of NELF, conversion of DSIF to a positive elongation factor, and the recruitment of chromatin remodellers and additional positive elongation factors to the Pol II CTD enabling the transition to productive elongation (Jonkers and Lis, 2015; Harlen and Churchman, 2017), which, subject to appropriate processing at the 3' end of the gene (as discussed below), results in the transcription of functional mRNA.

1.1.2. 3' Regulation of transcription

Protein coding genes encoding mRNA are characterised by the presence of 5' and 3' untranslated regions (UTRs), which encode 5' terminal caps and 3' poly-adenylate (pA) tails, complex pre-mRNA processing is required for the assembly of these features which act to promote the stability of mRNA. This occurs co-transcriptionally, along with the splicing of intronic non-coding DNA, which is interspersed between coding exons. The accumulation of machinery to aid termination, in particular, the cleavage and polyadenylation complex (CPA), is associated with the phosphorylation of Ser^2 residues on the Pol II CTD, which predominates towards the 3' ends of genes (McCracken et al., 1997; Hsin and Manley, 2012; Heidemann et al., 2013).

The termination of transcription consists of two main steps: 1) the cleavage of the nascent RNA transcript and 2) dissociation of the elongating Pol II from the chromatin template. Cleavage of RNA transcripts is mediated by cleavage and polyadenylation specificity factor-73 (CPSF73) (Kolev et al., 2008), both cleavage and polyadenylation of their 3' ends to form mRNA occurs upon the recognition of the canonical pA sequence (AAUAAA) (pAS) following its transcription at the TES, by the CTD components CPSF, and cleavage stimulatory factor (Cstf) (Nick J Proudfoot, 2011). The pAS was originally identified as a signal both for mRNA polyadenylation and for the termination of transcription (N J Proudfoot and Brownlee, 1976), however, for termination to occur successfully the rapidly transcribing polymerase must first be slowed down in a process known as pausing. Various mechanisms exist for this (Figure 1.7) (Nick J Proudfoot, 2016). The first of these mechanisms occurs concurrently with mRNA cleavage. It has been observed that the recruitment of CPA itself can induce Pol II pausing, acting as an anchor and decreasing Pol II processivity (Figure 1.7.A). In line with this, recognition of pAS by CPSF73 and Cstf-64 is directly associated with Pol II pausing (Nojima et al., 2015). A second mechanism is dependent on the presence of GC-rich sequences downstream of the pAS (Gromak et al., 2006), which favour the occurrence of R-loops (Skourti-Stathaki et al., 2011). These are RNA-DNA hybrids, which commonly form in

the wake of Pol II, between nascent RNA and temporarily unwound template DNA. R-loops act to slow Pol II but also run the risk of inducing single- and double- DNA strand breaks. RNA-DNA interactions are more stable than the association between DNA-DNA, R-loops therefore persist, thus inducing the recruitment of helicase Senataxin (SETX) both directly, and via the DNA repair factor breast cancer 1 (BRCA1), promoting the resolution of R-loops, promotion of termination and the avoidance of DNA damage (Skourti-Stathaki and Nicholas J Proudfoot, 2014; Nick J Proudfoot, 2016) (Figure 1.7.B). The third and final mechanism for the induction of Pol II pausing is the presence of heterochromatin downstream of gene TESs, which negatively impacts on polymerase processivity (Figure 1.7.C). Notably, R-loops have also been linked to the recruitment of chromatin modifier G9a/GLP, which deposits repressive H3K9me3 histone marks, inducing HP1 recruitment forming localised regions of repressive chromatin and promoting Pol II pausing (Skourti-Stathaki et al., 2014). This indicates that these mechanisms are not mutually exclusive and instead represent generalised processes that are impacted by a myriad of factors.

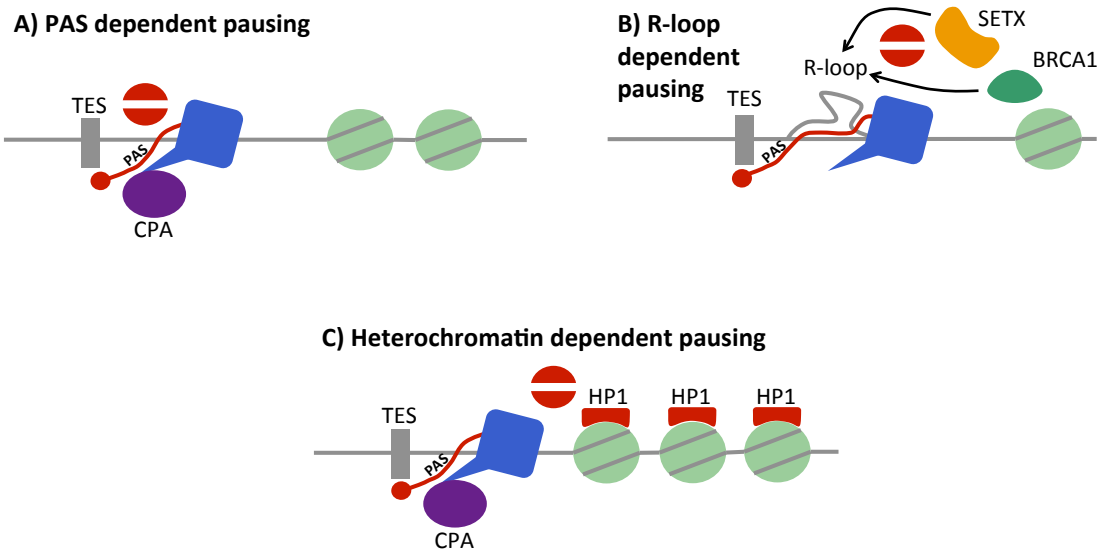

Figure 1.7. Models of RNA polymerase II pausing. A) Recruitment of cleavage and polyadenylation complex (CPA) acts to pause RNA Pol II. **B)** R-loops formed in the wake of Pol II decrease its forward momentum. BRCA1 and SETX are recruited to resolve stable R-loops preventing DNA damage. **C)** Pol II processivity is slowed by the presence of heterochromatin downstream of the transcription end site (TES).

Transcribing Pol II, nascent RNA, and the template DNA form a highly stable ternary complex (Wuarin and Schibler, 1994). Transcriptional termination is therefore reliant on the disruption of one or more of these elements to trigger release of Pol II from the DNA template. Two mechanisms have been suggested for Pol II termination. The allosteric model posits that conformational changes in Pol II subsequent to CPA recruitment are enough to promote termination. A second mechanism suggests that continued transcription past the pAS is halted by the 5' to 3' exonuclease Xrn2, which degrades uncapped nascent RNA transcripts following RNA cleavage at the pAS (Nick J Proudfoot, 2016). This mechanism is termed the torpedo model, as Xrn2 is in direct kinetic competition with the still transcribing polymerase, when Xrn2 reaches Pol II it induces a conformational change through degradation of the nascent RNA present in the active site promoting the dissociation of Pol II from the chromatin template (Nick J Proudfoot, 2016). Pausing therefore favours termination over on-going transcription, allowing Xrn2 to catch up with the elongating Pol II (Figure 1.8.A). A secondary mechanism for torpedo termination has also been observed, in which termination occurs co-transcriptionally, prior to pA cleavage (Figure 1.8.B). This is dependent on distal adenine (A) and thymine (T) rich co-transcriptional cleavage sequence (CoTC) (Dye and N J Proudfoot, 2001; Nojima et al., 2013), which once transcribed is cleaved rapidly, being highly unstable (West et al., 2008). Cleavage of CoTC elements allows rapid termination of transcription via degradation of very short stretches of nascent RNA by Xrn2, promoting prompt Pol II release from the chromatin. pAS cleavage and mRNA polyadenylation therefore occurs in the nucleoplasm, away from chromatin associated RNA exo-nucleases, thus enhancing gene expression (West and Nicholas J Proudfoot, 2009).

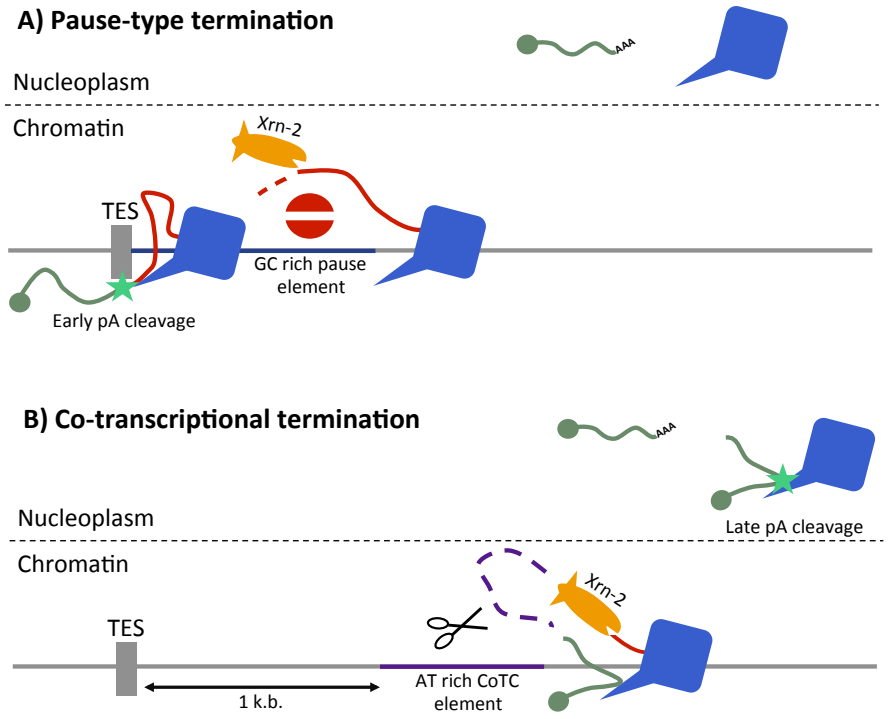

Figure 1.8. Models of the termination of transcription. A) TES proximal pausing of Pol II occurs at GC-rich elements, promoting degradation of nascent RNA by Xrn2 subsequent to pA cleavage. Once Xrn2 reaches Pol II removal of RNA from its active site promotes a conformational change and dissociation of the polymerase from the template DNA. **B)** AT-rich Co-transcription cleavage (CoTC) elements >1 k.b. downstream of the TES produce highly unstable RNA transcripts which are cleaved upon exit from Pol II. Xrn2 is therefore able to rapidly degrade the remaining nascent RNA promoting termination of transcription prior to pA cleavage, which occurs in the nucleoplasm. This protects mRNA from degradation by chromatin-associated RNA-degradation apparatus, enhancing gene expression.

1.3. Macrophage transcriptional regulation

1.3.1. The macrophage enhancer landscape

Closed chromatin regions are characterized by DNA methylation and the repressive H3K27me3 mark. These areas of heterochromatin are not accessible to low-order signal dependent transcription factors (SDTFs), which require exposed DNA to bind (Lone et al., 2013). The pioneer factor PU.1 is key to establishing macrophage identity. PU.1 is an ETS transcription factor family member and is well known as a lineage-determining transcription factor, induced early in hematopoiesis due to its requirement for both myeloid and lymphoid cell development (Olson et al., 1995; Back et al., 2005; Nutt et al., 2005). PU.1 binds partially exposed DNA in heterochromatin, in a sequence-specific manner, facilitating

nucleosome removal and maintaining nucleosome depletion at these sites (Barozzi et al., 2014; Soufi et al., 2015) and is crucial for the delineation of macrophage-specific enhancers with the H3K4me1 histone mark (Heinz et al., 2010; Ghisletti et al., 2010), which distinguishes them from promoters (Heintzman et al., 2007). PU.1 established enhancers subsequently act as platforms for the binding of inducible transcription factors (Schmidt et al., 2016; Ghisletti et al., 2010).

PU.1 designated enhancers encompass the core macrophage regulatory landscape, which is tailored in accordance with micro environmental signals to yield wide heterogeneity and specialisation dependent on tissue location, prior exposure to inflammatory signals, and the corresponding transcription factor expression profile. Tissue restricted SDTFs act in conjunction with PU.1 to establish *de novo* enhancers (Lavin et al., 2014; Ostuni et al., 2013; Gosselin et al., 2014). These changes in the enhancer landscape establish tissue-specific adaptions, for example: retinoic acid induces GATA-6 in peritoneal macrophages, altering their phenotype and enhancing proliferative renewal (Okabe and Medzhitov, 2014) (Rosas et al., 2014), haeme release by erythrocyte clearance promotes the Spi-C mediated generation of red-pulp macrophages (Haldar et al., 2014), GM-CSF in the lung promotes the specialisation of alveolar macrophages from perinatal monocytes via the induction of PPAR-γ (Schneider et al., 2014), and in the context of inflammatory responses, PU.1 has been shown to be crucial in the recruitment of chromatin remodelers BAF and PBAF (of the SWI/SNF family), to establish and maintain low nucleosome occupancy of enhancers corresponding to pro-inflammatory cytokines (McAndrew et al., 2016).

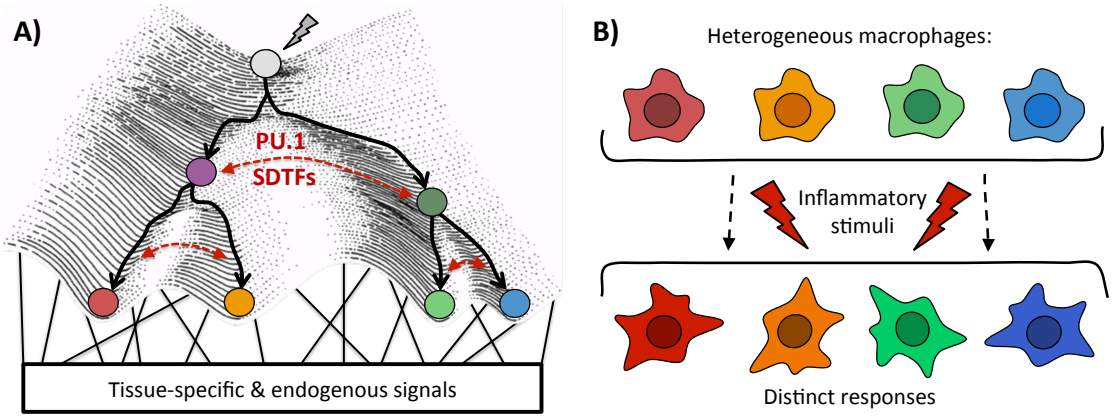

Figure 1.9. The macrophage enhancer landscape. A) Micro-environmental derived stimuli induce signal dependent transcription factors (SDTFs), which act alongside PU.1 to shape the macrophage enhancer landscape. Tissue specific adaptation of the enhancer landscape mediates cellular heterogeneity. **B)** Subsequent inflammatory stimuli activates SDTFs, which operate within the contours of the enhancer landscape mediating distinct transcriptional responses.

PU.1, along with tissue and environmental specific factors therefore designate and maintain the enhancers specific to the local milieu leading to a plethora of phenotypes demonstrable in tissue-resident macrophages (Gautier et al., 2012; Lavin et al., 2014). Resulting in the unique transcriptomes and patterns of enhancer utilisation exhibited by tissue-resident macrophages (Gautier et al., 2012; Lavin et al., 2014; Gosselin et al., 2014). This is reminiscent of C. H. Waddington's epigenetic landscape (Waddington, 1957) in which changes to the epigenome modulate the path of a differentiating cell promoting cellular heterogeneity (Figure 1.9.A). Interestingly, the ontogeny of tissue-resident macrophages isn't crucial for their function, with monocyte-derived macrophages able to recapitulate the phenotype of tissue-resident macrophages, demonstrating a dominant role for the environment in epigenetic reprogramming (Lavin et al., 2014). Furthermore, the macrophage enhancer landscape designates the stage on which SDTFs orchestrate transcriptional responses to inflammatory stimuli, supporting the specific initiation of gene expression programs tailored to the prior exposure of the cell in question and current microenvironment in which the stimuli is encountered (Glass and Natoli, 2015) (Figure 1.9.B).

1.3.2. Environmental sensing and transcriptional control

Pattern recognition receptors

Macrophages possess a wide array of receptors capable of recognising PAMPs and DAMPs. These pathogen recognition receptors (PRRs) are utilised to distinguish foreign pathogens from self, in addition to recognising damaged endogenous cells, and mounting appropriate responses. Their cellular distribution varies, from PRRs expressed on the cell surface and in endosomal compartment such as toll like receptors (TLRs), C-type lectin receptors (CLRs), and scavenger receptors, involved in the recognition of extracellular and phagocytosed signals; to the cytoplasmic receptors retinoic acid-inducible gene 1 (RIG1)-like helicase receptors (RLRs), and NOD-like receptors (NLRs), which survey the cytosol for ectopic PAMPs. This complex arsenal of PRRs allows for the effective sensing of pathogens and apoptotic cells and is further complemented by accessory sensors and receptors endowing macrophages with the capacity to respond to a wide array of metabolic and tissue microenvironmental signals (Okabe and Medzhitov, 2016). Perhaps the best-characterised PRRs are the TLRs. The TLR family is composed on twelve members in mice, all of which recognise specific PAMPs and are located either at the cell surface or intracellularly in endosomes. This diverse family of PRRs are widely expressed by macrophages. TLR4 was the first family member identified (Medzhitov et al., 1997), and is activated by LPS (Poltorak et al., 1998), and is a widely studied canonical form of *in vitro* macrophage activation.

Transcription factors mediating macrophage polarisation

Macrophage phenotypes are mediated in a large part by the activation of specific sets of SDTFs, which act dynamically to implement specific programs of gene expression, tailored to the activating stimuli. *In vitro* studies of macrophages often rely on polarising cells to opposing inflammatory and anti-inflammatory phenotypes, this is often implemented by treating cells with IFN-γ and LPS or IL-4/IL-13, respectively (see Chapter 1.1.3.). IFN-γ activates JAK-STAT signaling pathways through engagement of the interferon-α/β receptor

(IFNAR) and IFN-γ receptor (IFNGR), culminating in phosphorylation of STAT1, allowing its dimerisation and pro-inflammatory transcriptional activity through binding of gamma activated sequences (GAS) (Varinou et al., 2003). Phosphorylated STAT1 is also a component of the IFN-stimulated gene factor 3 (ISGF3) complex, along with STAT2 and IRF9, which mediates distinct antiviral responses down stream of IFN-γ signaling through the engagement of interferon stimulated response elements (ISRE) motifs at genomic targets (Ivashkiv and Donlin, 2014). On the other hand, treating macrophages with IL-4/IL-13 engages the IL-4 receptor α (IL4Rα) (Takeda et al., 1996), resulting in activation of JAK-STAT6 signaling promoting an alternatively activated phenotype (Martinez et al., 2009). IRF4 has also been shown to be integral for polarisation towards an M2 phenotype (Satoh et al., 2010), the transcription of which is dependent on the removal of repressive H3K9 methyl marks by Jmjd3.

Transcription factors mediating macrophage activation

Stimulation of macrophages with LPS activates TLR4 initiating a signalling cascade, which is mediated by two key adaptor molecules MyD88 and TRIF (Takeuchi and Akira, 2010). The MyD88 pathway induces the transcription of genes encoding inflammatory cytokines such as *Tnf* and *Il12b* via the activation of NFκB and AP-1. NFκB activation is mediated through activation of TRAF6 and subsequent degradation of the NFκB inhibiting protein (IκBα) via IκB kinase (IKK) activity, resulting in the translocation of NFκB constituents RelA and p50 to the nucleus, where they mediate changes in gene expression. AP-1 is activated via TAK1 mediated JNK signalling downstream of TRAF6 activation (Arthur and Ley, 2013). LPS also activates IRF5 in a MyD88 dependent manner, promoting inflammatory responses, this will be discussed more fully in Chapter 1.4.2. The MyD88 independent pathway results in activation of *Ifnb1* via activation and nuclear translocation of IRF3. Production of IFN-β promotes subsequent signalling through the IFNAR initiating a secondary wave of

transcription of antiviral genes (Doyle et al., 2002), which contributes significantly to the LPS response.

Phagocytosis of apoptotic cells, termed efferocytosis, has contrasting effects on macrophages. Promoting activation of the nuclear receptors peroxisome proliferator-activated receptor γ (PPARγ), and liver X receptor (LXR), which are important regulators of cellular lipid homeostasis and efferocytosis (Kolb et al., 2017). Activation of these receptors promotes efferocytosis (Mukundan et al., 2009; Roszer et al., 2011) and mediates increased production of TGF-β and IL-10, whilst counter-acting the pro-inflammatory effects of TLR-dependent SDTFs (Glass and Saijo, 2010; Kolb et al., 2017). Correspondingly agonists of PPARγ and LXR have been demonstrated to supress inflammatory responses (Mukundan et al., 2009; Poon et al., 2014).

Transcription factor mediated epigenetic reprogramming

In response to activation SDTFs are recruited to H3K4me1 defined enhancers, which undergo modification mediated by inducible recruitment of the histone acetyltransferases (HATs) p300/CBP (Ghisletti et al., 2010), and GCN5/PCAF (Schiltz et al., 1999). Resulting in acetylation of histones H3K27 (H3K27ac) and H3K9 (H3K9ac), by either p300/CBP or PCAF/GCN5, respectively (Jin et al., 2011). H3K27ac has further been shown to be associated with active enhancers in macrophages (Kaikkonen et al., 2013), and is commonly used as a marker for enhancer activation (Glass and Natoli, 2015; Zhu et al., 2013). H3K27ac is a crucial epigenetic mark, strongly associated with the induction of transcription. This is mediated by recognition of the mark by bromodomain and extra-terminal (BET) family protein BRD4. BRD4 binds p-TEFb, recruiting it to acetylated histones at sites of active transcription thus facilitating the transition from initiation to productive elongation (Yang et al., 2005). Additionally, all BET proteins interact with polymerase associated factor 1 (PAF1C), which contributes both to initiation and elongation (Dawson et al., 2011). Notably,

BRD4 augments NFκB RelA activity, binding acetylated RelA and acting as a co-factor to increase the expression of RelA target inflammatory genes (B. Huang et al., 2009). Macrophage enhancers are therefore categorized by their H3K27ac status, being described as being poised (H3K4me1 high, H3K27ac low) in naïve cells, and transitioning to active (H3K4me1 high, H3K27ac high) in response to stimuli.

Whilst the majority of SDTF binding is accounted for by open enhancers and promoters, a small proportion of such factors are capable of binding closed chromatin, in conjunction with pioneer factors, establishing *de novo* enhancers (Figure 1.10) (Kaikkonen et al., 2013) (Barish et al., 2010). These enhancers may represent a form of epigenetic memory of previous stimuli encountered, with re-stimulation leading to enhanced inflammatory responses (Kaikkonen et al., 2013; Netea et al., 2016). It has been observed that specific factors, such as IRF8, are particularly prone to this activity, binding a large proportion of PU.1 unmarked loci in response to stimulation (Mancino et al., 2015).

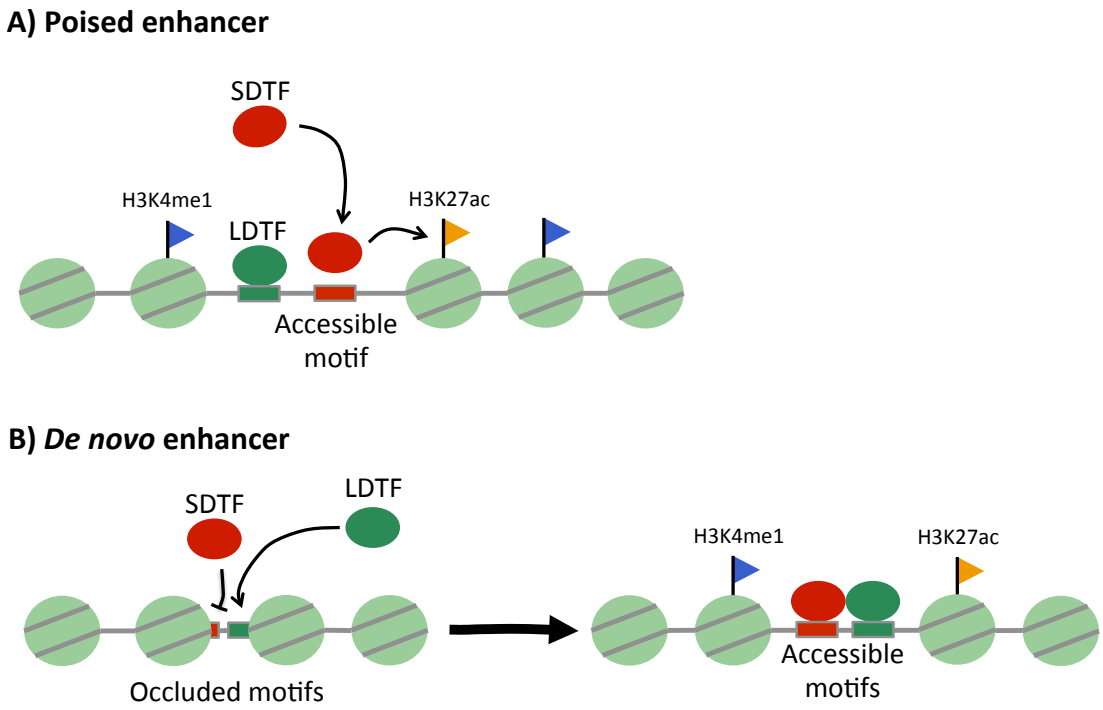

Figure 1.10. Inducible enhancer activation. **A)** Signal dependent transcription factors (SDTFs) commonly bind pre-specified enhancers, occupied by lineage determining transcription factors (LDTFs) and decorated with the H3K4me1 mark; termed poised enhancers. SDTF recruitment results in H3K27 acetylation and activation. **B)** Certain SDTFs are capable of cooperating with LDTFs to establish *de novo* enhancers in regions of heterochromatin. This is dependent on the ability of the LDTF to bind to partially occluded motifs. Transcription factor binding results in deposition of the H3K4me1 mark and H3K27 acetylation concurrent with activation.

1.4. Interferon Regulatory Factor 5

1.4.1. Interferon regulatory factors (IRFs)

The IRF transcription factor family comprises nine members in mammals (IRF1-9), which were originally described for their role in the induction of type I interferons (Miyamoto et al., 1988; Wathelet et al., 1998). IRFs bind to consensus ISRE motifs, consisting of two GAAA repeats, via their shared N-terminal DNA binding domain (DBD) (Tanaka et al., 1993). ISRE motifs are widely enriched at regulatory sites of immune genes, leading to the functional diversity of the IRFs and their key roles as master regulators of the innate immune responses (Honda and Taniguchi, 2006). The role of IRFs in the context of immune cell activation has been extensively studied. TLR and cytosolic PRR activation in response to PAMPs results in

specific inflammatory responses, tailored to the activating stimuli. IRF1, IRF3, IRF5, and IRF7 are phosphorylated in response virus detection, homo- and hetero-dimerizing and translocating to the nucleus, where they elicit expression of type I interferons (IFNs) (Honda and Taniguchi, 2006). However, Newcastle disease virus infection in $IRF1^{-/-}$ and $IRF5^{-/-}$ mice indicate that these factors aren't crucial for type I interferon induction as IFNβ & IFNα are still up-regulated in their absence (Matsuyama et al., 1993; Takaoka et al., 2005), thus implicating the highly homologous IRF3 and IRF7 as the core IRFs in mediating anti-viral responses. IRF5 on the other hand has much broader activity. It is widely expressed by immune cells, including macrophages, B cells, monocytes, and DCs (Heng et al., 2008), and can be used as a marker of inflammatory macrophages both *in vitro* and *in vivo* (Weiss et al., 2013).

1.4.2. IRF5

Studies in $IRF5^{-/-}$ mice highlight the importance of IRF5 to macrophage function. $IRF5^{-/-}$ mice are resistant to lethal endotoxic shock (Takaoka et al., 2005). This is due to a crucial role for IRF5 in promoting pro-inflammatory responses as a consequence of TLR activation. Stimulation of splenic macrophages with ligands for TLR3, TLR4, TLR7/8, and TLR9 all result in in IRF5 activation, via its direct interaction with the MyD88 and TRAF6 adaptors, which are required for IRF5 phosphorylation and ubiquitination (Takaoka et al., 2005). Interestingly, IRF4 binds to the same site on MyD88 as IRF5, competing with IRF5 for activation (Negishi et al., 2005). In addition, Lyn, a Src family kinase, was shown to physically interact with IRF5 and inhibit its activation via the TLR-MyD88 pathway (Ban et al., 2016). IRF5 contains two nuclear localisation signals (NLS), IRF5 phosphorylation results in the 5' NLS becoming exposed, mediating the nuclear translocation and retention of IRF5 in activated cells (Barnes et al., 2002). However, the precise mechanisms of IRF5 activation are not fully characterised (Ryzhakov et al., 2015). Once activated IRF5 reaches the nucleus where it mediates transcription of inflammatory cytokines such as TNF, IL-12, and IL-6, all of which are

drastically reduced in cells derived from the IRF5$^{-/-}$ (Takaoka et al., 2005). The transcriptional activity of IRF4 closely mirrors that of IRF5, downregulating IRF5 target genes (Negishi et al., 2005), the IRF4-IRF5 axis is therefore integral for the regulation of macrophage responses.

IRF5 has been shown to be a crucial mediator of inflammatory macrophages *in vivo* and classical macrophage activation *in vitro*. Its induction leads to TNF, IL-6, IL-12 and IL-23 secretion whilst simultaneously repressing IL-10 and TGF-β (Krausgruber et al., 2011) (Ouyang et al., 2007; Dalmas et al., 2015). IRF5 binds to promoters of both rapidly induced primary response genes (PRGs) (such as *Tnf* and *Il1a*) and to more slowly induced secondary response genes (SRGs) (*e.g. Il6*, *Il12b*) as a consequence of LPS stimulation, leading to large increases in Pol II recruitment (Krausgruber et al., 2011; Saliba et al., 2014). Intriguingly CBP and p300 interact directly with IRF5 (Feng et al., 2010), suggesting that IRF5 may contribute to the recruitment of epigenetic modulators to enhancers, eliciting histone acetylation, activation, and subsequent transcription of corresponding genes. Of the IRF5 up-regulated genes, those exhibiting the highest increases in expression with LPS stimulation are also targets of NF-kB RelA, the binding sites of which coincide with those of IRF5 and are centered on the promoters of these genes. Interestingly, RelA peaks not overlapping with IRF5 are more evenly distributed across both LPS up- and down- regulated genes (Saliba et al., 2014). This fits with other reports indicating that the majority of RelA binding sites are not associated with transcriptional changes (Lim et al., 2007). Similar IRF5-RelA interactions were observed at the *Tnf* loci in monocyte-derived dendritic cells (mDDCs), of note binding of IRF5 to both the promoter and to an enhancer downstream of the *Tnf* gene was demonstrated, mediating sustained high levels of TNF expression (Krausgruber et al., 2010). This raises the possibility that IRF5 3' activity at the *Tnf* loci augmenting gene expression via 5' to 3' gene looping or through promoting efficient termination and mRNA processing. Removal of RelA from this system results in a reduction in IRF5 binding and subsequent Pol II recruitment at *Il6*, *Il1a*, and *Tnf* promoters (Saliba et al., 2014), it is therefore likely that RelA aids in IRF5 recruitment to these regions. This poses an additional mechanism of regulation,

with IRF5 activation and binding to promoters being required for high levels of Pol II recruitment and gene expression.

Aside from its pro-inflammatory capacity, IRF5 is also able to as a negative regulator of transcription, particularly in instances in which IRF5 binding is observed in the absence of RelA (Saliba et al., 2014). This may be through the ability of IRF5 to recruit transcriptional repressors such as HDAC1 (Feng et al., 2010) and TRIM28 (Eames et al., 2012). TRIM28 is associated with the establishment of heterochromatin and resultant gene silencing via interactions with HP1 (Sripathy et al., 2006). TRIM28 is also associated with transient transcriptional changes, modifying histone tail residues, mediated by recruitment of SETDB1 (Schultz et al., 2002). SETDB1 is a histone methyltransferase, responsible for the establishment of the repressive H3K9me3 mark. In the context of *Tnf* it has been shown that IRF5 mediates fine-tuned regulation of this cytokine by a combination of binding *cis*-regulatory elements and the associated Pol II recruitment (Krausgruber et al., 2010), and epigenetic modulation of the underlying histones by SETDB1 recruitment and H3K9 methylation to limit aberrant over-production of TNF (Eames et al., 2012).

1.5. Hypothesis and Aims

Previous work at the Udalova laboratory has demonstrated that IRF5 contributes strongly to pro-inflammatory macrophage responses (Krausgruber et al., 2010; Krausgruber et al., 2011; Saliba et al., 2014). The aim of this thesis was to investigate the mechanisms by which the regulatory activity of IRF5 is achieved. To address this aim I have generated a number of hypotheses to test. My first hypothesis was that IRF5 affected the chromatin accessibility of macrophages in response to LPS, contributing to the formation of *de novo* enhancers, thus promoting the efficiency of transcription initiation. My second hypothesis was that the demonstrated 3' binding of IRF5 at the *Tnf* gene contributed to the efficient termination of transcription. Both of these ideas are investigated in Chapter 3. I also hypothesised that IRF5 has a wider role in regulating macrophage responses to inflammatory stimuli, not being restricted to the regulation of cytokines and chemokines, this is investigated in Chapter 4. My last hypothesis was that IRF5 interacts with novel partners to drive macrophage responses in inflammation. Chapter 5 describes our unbiased approach to investigate core SDTFs in the macrophage response to LPS stimulation and examines their cooperative action with IRF5 to promote transcriptional responses to inflammation.

2. Materials and Methods

2.1. Laboratory methods

2.1.1. Isolation and culture of bone marrow derived cells

IRF5$^{-/-}$ mice

IRF5$^{-/-}$ mouse generation was described previously (Takaoka et al., 2005), and were bred on a C57Bl/6 background. IRF5$^{-/-}$ mice don't express IRF5 protein due to the disruption of exon 2 of the *Irf5* gene. The mice develop normally and don't display overt differences in the proportions of haematopoietic cell populations, however, they are resistant to endotoxic shock and have reduced production of pro-inflammatory cytokines (Takaoka et al., 2005). Spontaneous mutation of the *Dock2* gene has been described in IRF5$^{-/-}$ mice (Purtha et al., 2012), all of the mice used in this thesis were determined to be free of this mutation by genotyping.

Isolation of bone marrow

Mice were sacrificed by the schedule 1 method using CO_2 inhalation followed by cervical dislocation. Hip joint and ankles were dislocated to allow the removal of femurs and tibias. Skin and tissue surrounding the bones were removed with scissors and remaining tissue was removed following dehydration of the bones in 70% ethanol (Sigma). The ends of the bones were removed by cutting with scissors and the bone marrow was flushed into a 50 mL tube (Falcon) through a 70 µM Easy Strainer (Greiner Bio One) with 10 mL sterile PBS (phosphate buffered saline, Gibco) using a 27G needle (BD) and 10 mL syringe (BD). Bone marrow exudate was topped up to 20 mL with PBS (Gibco) and centrifuged (Scanspeed 1580MGR, GRS-750-4 rotor) at 1,500 rpm for 5 min at room temperature. Pelleted cells were resuspended in 1 mL of bone marrow culture medium (BM medium) consisting of RPMI-1640 medium with L-glutamine (Lonza) supplemented with 10% FBS (foetal bovine serum, Labtech), 1% penicillin/streptomycin (P/S, Lonza), and 0.01% 2-mercaptoethanol (Gibco). All

cells subsequently derived from bone marrow were maintained at 37°C, with 5% CO_2 and 95% humidity.

GM-CSF macrophage differentiation

A 10 µL aliquot of the BM cell suspension isolated as described above was used for counting with a CASY cell counter (Roche Innovatis AG) before diluting the BM cells to $5x10^6$ cells/mL in BM medium. $5x10^6$ cells were plated into a bacterial petri dish (Greiner Bio One) in 10 mL of BM medium supplemented with 20 ng/mL recombinant murine GM-CSF (Peprotech). On day three of culture petri dishes were supplemented with an additional 10 mL BM media containing 20 ng/mL GM-CSF. On day six 10 mL of media were removed from each petri dish centrifuged at 1,500 rpm for 5 min at room temperature and the supernatant discarded. Cells were resuspended in 10 mL fresh BM medium containing 20 ng/mL GM-CSF and added back to the respective petri dishes. After eight days of differentiation cells in suspension were collected, in addition to adherent cells, which were washed in PBS and harvested after treatment with 4 mL Versene (EDTA; Lonza) for 10 min at 37 °C. Cells were resuspended in BM media at $1\text{-}2x10^6$ cells/mL and re-plated in tissue culture plates (BD). Cells were allowed to rest overnight before stimulation with 100 ng/mL LPS (Alexis Biochemicals).

Neutrophil isolation

Neutrophils were isolated by density gradient centrifugation using a discontinuous gradient of Percoll (GE Healthcare) and Hank's Balanced Salt Solution (HBSS; Lonza). Briefly, 1 mL of cells extracted from bone marrow (as above) were layered on top of a discontinuous 52%, 64%, 72% Percoll density gradient in a 15 mL tube (Falcon) and centrifuged at 1,500 g for 30 mins at 4 °C, with the brake turned off to avoid disturbing the gradient. Cells from the 64%/72% gradient interface were taken, diluted to 15 mL with BM media and centrifuged at 1,500 rpm at room temperature for 5 mins. The resultant pellet was resuspended in 1 mL BM medium and counted using the CASY cell counter (Omni Life Science). Cells were

resuspended in BM media at 1-2x10^6 cells/mL and re-plated in tissue culture plates (BD). Cells were allowed to rest overnight before stimulation with 100 ng/mL LPS (Alexis Biochemicals).

2.1.2. Chromatin associated RNA (chrRNA) studies

Subcellular fractionation

40x10^6 GM-BMDMs were collected in PBS and centrifuged at 1,500 rpm for 5 min at 4 °C, pellets were resuspended in 200 µL cytoplasmic lysis buffer (0.15% NP-40, 10 mM Tris pH 7.5, 150 mM NaCl; all from Sigma) and incubated on ice for 5 min, the lysate was layered on to 500 µL sucrose buffer (10 mM Tris pH 7.5, 150 mM NaCl, 24% sucrose w/v; Sigma) and centrifuged at 13,000 rpm for 10 min at 4 °C (Heraeus Biofuge Fresco). The top 200 µL of the supernatant was reserved as the cytoplasmic fraction and the rest of the supernatant was discarded. The nuclear pellet was then resuspended in 350 µL NUN1 (20 mM Tris pH 7.9, 75 mM NaCl, 0.5 mM EDTA, 0.1 mM DTT, 50% glycerol; Sigma) to which 350 µL NUN2 (20 mM HEPES pH 7.6, 7.5 mM MgCl2, 0.2 mM EDTA, 0.3 M NaCl, 0.1 mM DTT, 1 M urea, 1% NP-40; Sigma) was added and mixed by vortexing (Reax 2000, Heidolph) 2x 2 sec. Samples were then incubated on ice for 2 min before centrifuging at 13,000 rpm for 2 min at 4 °C, the supernatant was taken as the nucleoplasmic fraction and pellet as the chromatin fraction. The nucleoplasmic fraction was stored at -80 °C for protein analysis. The chromatin pellet was rinsed with 50 µL sterile PBS (Gibco) which was stored at -80 °C for protein analysis. For RNA analysis, chrRNA and mRNA were extracted from chromatin pellets and nucleoplasm, respectively, immediately after subcellular fractionation.

mRNA extraction

The nucleoplasmic fraction containing mRNA was mixed with 3.5x volumes of RLT lysis buffer (Qiagen) and mixed, prior to isolation by RNeasy Mini Kit (Qiagen) following the manufacturers instructions.

chrRNA extraction

Chromatin pellets were lysed in 1 mL TRIzol Reagent (Thermo Fisher Scientific), with repeated pipetting to break up the pellet. 200 µL chloroform (Sigma) was then added and samples were gently shaken for 15 s to mix before incubating 5 min at room temperature. Samples were then centrifuged at 13,000 rpm for 15 min at 4 °C, following this the aqueous phase was removed and RNA was precipitated by the addition of 1x volume isopropanol (Sigma), 1/10x volume Na acetate (Sigma), 1 µL GlycoBlue Coprecipitant (Thermo Fisher Scientific) and incubation overnight at -20 °C. RNA was pelleted by centrifugation at 13,000 rpm for 10 min at 4 °C, RNA pellet was washed once with absolute ethanol (Sigma) and twice with 70% ethanol (Sigma), prior to being air dried for 5 min and resuspended in 30 µL RNase/DNase free H_2O (Invitrogen). RNA was incubated with 2.5 µL DNase I and 10 µL Buffer RD (RNase-free DNase Set, Qiagen) for 10 min at room temperature. RNA extraction, as described above, was then repeated. RNA was quantified using a NanoDrop UV-Vis Spectrophotometer (Thermo Fisher Scientific). RNA samples for NGS were further tested for integrity using a RNA 6000 Nano Kit (Agilent Technologies) on the Bioanalyzer (Agilent Technologies).

Sequencing

chrRNA prepared as above from unstimulated and LPS stimulated wild type (WT) and $IRF5^{-/-}$ GM-BMDMs (0hr, 2hr, and 8hr time points), with two biological replicates for WT samples, and one biological replicate for $IRF5^{-/-}$. Samples were depleted of ribosomal RNA and strand-specific libraries were generated using the dUTP second-strand marking protocol (Parkhomchuk et al., 2009), followed by further library preparation and 100 b.p. paired end sequencing. Library preparation and sequencing was conducted by the High-Throughput Genomics Group at the Wellcome Trust Centre for Human Genetics, Oxford.

2.1.3. Western blots

SDS polyacrylamide gel electrophoresis (SDS-PAGE)

Protein was quantified using the Qubit Protein Assay Kit (Thermo Fisher Scientific) on a Qubit Fluorometer (Thermo Fischer Scientific). SDS-PAGE was used to resolve proteins by size. 10 µg of protein per sample was reduced by mixing with loading buffer (200mM Tris pH 6.8, 400 mM DTT, 8% w/v SDS, 0.4% w/v Bromophenol Blue, 40% w/v Glycerol; Sigma) and incubating at 95 °C for 5 min (Eppendorf Thermomixer). Gel electerophoresis was performed using NuPAGE Novex 4-12% Bis-Tris gels (Life Technologies) in NuPAGE MOPS SDS running buffer (Life Technologies) at 160 V, until proteins were fully separated (~120 min). Size estimation was conducted using Amersham ECL Full-Range Rainbow molecular weight markers (GE Healthcare).

Protein transfer

Following SDS-PAGE proteins were transferred onto PVDF membranes (GE Healthcare) for detection. Membranes were activated by treating with methanol (Sigma) for 1-2 mins prior to transfer. Transfer cassettes enclosed two sponges, two pieces of filter paper, the gel containing proteins to be transferred, the PVDF membrane, two more pieces of filter paper, and two more sponges. The sponges and filter paper were fully soaked in transfer buffer (25mM Tris-base, 192 mM Glycine, 15% v/v Methanol; Sigma) prior to assembly of the transfer cassette, which was inserted into a cooled tank of 4 °C transfer buffer. Proteins were transferred by applying 72 V for 120 min.

Immuno blotting

After transfer PVDF membranes were blocked with 5% milk in PBS-T (PBS + 0.1% Tween; Sigma) for 2 hours at room temperature on an orbital shaker. Membranes were washed in PBS-T three times and incubated with the primary antibodies, which were diluted in PBS-T containing 2% bovine serum albumin (BSA; Sigma). Primary antibodies used: H3 (1:5,000; ab1791, Abcam), SNRP70 (1:1,000; ab51266, Abcam), α-tubulin (1:5,000; ab7291, Abcam).

Membranes were incubated at 4 °C overnight on an orbital shaker. Following this the membranes were washed in PBS-T three times to remove the primary antibody and an appropriate secondary HRP-conjugated antibody was added (donkey α-rabbit, NA934, GE Healthcare or rabbit α-mouse, P0260, Dako), diluted 1:5,000 in PBS-T with 5% milk. The secondary antibody was incubated with the membrane for 2 hours at room temperature on an orbital shaker, and then removed by washing three times with PBS-T. Immunocomplexes were detected by addition of the chemiluminescent substrate ECL (Thermo Fisher Scientific), visualised with X-ray film RX NIF sheets (FujiFilm) and developed using an AGFA Cruis-60 automatic film processor (AGFA-Gaevert).

2.1.4. Chromatin immunoprecipitation (ChIP)

$10x10^6$ GM-BMDMs were fixed with 1% formaldehyde (Sigma) for 10 min at RT, then quenched with 150 mM Tris pH 7.5 (Sigma) and washed with PBS. Cells were pelleted by centrifugation at 1,350 g, 4 °C for 5 min and then lysed in 500 µL LB1 (50 mM Hepes-KOH pH 7.5, 140 mM NaCl, 1 mM EDTA, 10% glycerol, 0.5% NP-40, 0.25% Tx-100; Sigma). Nuclei were pelleted by centrifugation as previously, then washed with 500 µL LB2 (10 mM Tris-HCl, pH8.0, 200 mM NaCl, 1 mM EDTA, 0.5 mM EGTA; Sigma), prior to lysis with 500 µL LB3 (10 mM Tris-HCl, pH 8.0, 100 mM NaCl, 1 mM EDTA, 0.5 mM EGTA, 0.1 % Na-Deoxycholate, 0.5 % Na-Lauroylsarcosine; Sigma). Nuclear lysates were sonicated with a Bioruptor Pico (Diagenode) to yield chromatin fragments approximately 500 b.p. in size. Cellular debris were pelleted by the addition of 50 µL 10% Tx-100 and centrifugation at 13,000 rpm, 4 °C, for 10 min. 5 µg of H3 antibody (ab1791, Abcam) was conjugated to Protein G Dynabeads (Thermo Fisher Scientific), which were used for immunoprecipitation of cleared lysates overnight at 4 °C, aside for an aliquot which was reserved as input. Immunoprecipitated complexes were washed with six times with ice-cold wash buffer (50 mM Hepes-KOH, pH 7.6, 500 mM LiCl, 1 mM, EDTA, 1% NP-40, 0.7% Na-deoxycholate; Sigma) and once with cold Tris EDTA Buffer (Thermo Fisher Scientific) containing 50 mM NaCl (Sigma). Samples were

resuspended in 120 µL Tris EDTA Buffer (Thermo Fisher Scientific) containing 2% sodium dodecyl sulphate (SDS; Sigma) prior to the reversal of cross linking by incubation at 65 °C overnight. Samples were purified with PCR Purification Kit (Qiagen) and quantified by real-time PCR as described below.

2.1.5. Quantitative real-time PCR (qPCR)

Reverse transcription

cDNA was synthesised from RNA using the High Capacity cDNA Reverse Transcription Kit (Life Technologies) following the manufacturer's instructions. A minimum of one sample per experiment underwent the reverse transcription protocol without the addition of reverse transcriptase enzyme to serve a control for the presence of genomic DNA. Following reverse transcription samples were diluted 1:4 with RNase/DNase free H_2O (Invitrogen) and stored at -20 °C.

SYBR green based detection

Samples were quantified by qPCR using custom primers (listed below). qPCR was conducted in duplicate on 384 well plates (Life Technologies) using the following reaction:

Table 2.1. SYBR green qPCR reaction

Volume	***Reagent***
5 µL	Precision FAST MasterMix with low ROX premixed with SYBRgreen (Primer Design)
1 µL	RNase/DNase free H_2O (Invitrogen)
1 µL	5 µM stock of forward and reverse primers (final concentration 500 nM)
3 µL	Template cDNA or ChIP DNA

PCR reactions were run on the ViiA7 system (Life Technologies) using the following cycling program:

Table 2.2. SYBR green qPCR themocycling program

Step	***Time***	***Temperature (°C)***
Enzyme activation	3 min	95
Step 1	15 s	95
Step 2	35 s	60
Steps 1-2 are repeated 45 x		
Dissociation curve analysis		

The cycle threshold (Ct) is the number of cycles required for fluorescence (generated by intercalation of SYBR green dye into double stranded PCR products) to pass the background level.

Primers were designed using primer-BLAST (Ye et al., 2012) with amplicon sizes ranging from 120-200 b.p. and oligos were synthesised by Life Technologies. Prior to use primers were tested for efficiency by qPCR on serial dilutions of genomic DNA (gDNA) (six, ten fold dilutions), Ct values were then plotted against the log transformed gDNA concentration and a standard curve fitted by linear regression. Primer efficiency was calculated from the slope

of the standard curve as follows: efficiency = $(10^{(-1/slope)} - 1) \times 100$. All primers used had an efficiency of 100% (±10%). Additionally melt curves were assessed to ensure that each primer had a uniform melting temperature, indicating that a single PCR product was amplified.

Table 2.3. SYBR green qPCR primers

Target	***Forward primer***	***Reverse primer***
Tnf enhancer	CCTCGACTACAGGTTCTTGGGAAAA	TTCTTGGGCAACTAGAGATCCACAC
Tnf promoter (TSS -300)	GCTAAGTTCTTCCCCATGGATGTCCC	ACCCATTTCTTCTCTGTCCTCCAGAGC
Tnf 5' UTR	GGCCAGTGAGTGAAAGGGACAG	CAGCGAGGACAGCAAGGGACTA
Tnf exon1	GATCACCCCGAAGTTCAGTAGACAG	GAAGAGGCACTCCCCCAAAAGATG
Tnf exon1/intron1	ACTTCTTTCCCTCACACTGTCCTTC	GCCTATGTCTCAGCCTCTTCTCATT
Tnf intron3	CTGATGCCTTGCTTTTGAGTCACTG	GAGAATGAAGGGGCATGATTTTGGG
Tnf exon4	TCCTGGTATGAGATAGCAAATCGGC	GGCATGGATCTCAAAGACAACCAAC
Tnf TES	AATGGCCCAGGGGTATAAAGACTGA	CGCTACATCACTGAACCTCTGCTC
Tnf TES +544	TTTTCTCTTTCCAATCCACCCACCT	AAAGACACAGGGCTGAAAATGTGAC
Tnf TES +791	ACACTCTACAACAAGTCTCTGCACC	CAGGCTTGGATTTGATCCCAACACC
Tnf TES +1127	CTTATGTGCTTTGGACCTTCTGCAC	AGTCTAGGAGAGGGAGCTTGCTAAA
Tnf TES +1251	TCAACAATTTACCTGCCCCTACCTC	CAAAATTGGTCACCCTCTCACCCC
Hbb-b1	CAACTTCATCGGCGTTCACCTTTC	ACGTTTGCTTCTGATTCTGTTGTGT
Il12b enhancer	TACTAACCCGCACACTTTCTCTCAC	GAGGAGAGTTCAATGCACAGAGGAA
Il12b promoter	GCAAGGTAAGTTCTCTCCTCTTCCC	AATGACTATTTGAAGCCCCTGTCGT
Actb exon 4	GTGCTAGGAGCCAGAGCAGTAATC	AGTGTGACGTTGACATCCGTAAAGA
Actb exon4/intron5	AGCTCTCTGGGTGCTGGGATTC	ATGCAGAAGGAGATTACTGCTCTGG

Relative expression of primer targets were calculated using the Pffafl method (Pfaffl, 2001), utilising a standard curve on each plate run in parallel with samples to calculate the efficiency of each primer pair (as described above for testing primers). Data was therefore

corrected for primer efficiency. ChrRNA data were expressed relative to a reference gene, *Hbb-b1*. ChIP samples were expressed as % input for gene of interest over % input at control gene *Hbb-b1*.

TaqMan based detection

Total RNA was isolated from GM-BMDMs using RNeasy Mini kits (Qiagen) following the manufacturers instructions. An optional DNaseI digestion was performed to remove gDNA using the RNase-Free DNase kit (Qiagen). RNA concentration was determined using a NanoDrop UV-Vis Spectrophotometer (Thermo Fisher Scientific) and stored at -80 °C. mRNA was quantified by qPCR using TaqMan probes (listed below). qPCR was conducted in duplicate on 384 well plates (Life Technologies) using the following reaction:

Table 2.4. TaqMan qPCR reaction

Volume	***Reagent***
3 µL	Precision FAST MasterMix with ROX (Primer Design)
0.3 µL	RNase/DNase free H_2O (Invitrogen)
0.3 µL	TaqMan Probe
2.4 µL	Template cDNA

Reactions were run on ViiA7 system (Life Technologies) using the following cycling program:

Table 2.5. TaqMan qPCR thermocycling program

Step	***Time***	***Temperature (°C)***
Enzyme activation	3 min	95
Step 1	3 s	95
Step 2	30 s	60
Steps 1-2 are repeated 45 x		

TaqMan probes all have efficiencies of 100% therefore the ΔΔCt method was used for quantification of gene expression, in which samples are compared to a control and normalised to a reference gene. For TaqMan based qPCR the reference gene used was the

housekeeping gene *Hprt*. When comparing LPS stimulated and unstimulated samples the unstimulated sample was used as the control, in experiments comparing LPS stimulated WT and IRF5$^{-/-}$ samples the IRF5$^{-/-}$ unstimulated sample was used as the control. The following TaqMan probes were used for quantifying gene expression:

Table 2.6. TaqMan probes

Target	***Probe***
Ccl3	Mm00441259_g1
Il12b	Mm01288989_m1
Il6	Mm00446190_m1
Cxcl10	Mm00445235_m1
Alox5	Mm01182747_m1
Alox15	Mm00507789_m1
Gas6	Mm00490378_m1
Mmp14	Mm00485054_m1
Adam17	Mm00456428_m1
Hif1a	Mm00468869_m1
Runx1	Mm01213405_m1
Hprt	Mm03024075_m1

2.1.6. Assay for transposase accessible chromatin and sequencing (ATAC-seq)

Transposition

75x10^3 GM-BMDMs or BM neutrophils were pelleted by centrifugation at 500 g for 5 min at 4 °C. Pellets were washed with 50 µL ice cold PBS (Gibco) and pellet again as previously. Cell pellets were then lysed with a cytoplasmic lysis buffer (10 mM Tris-Cl pH 7.4, 10 mM NaCl, 3 mM $MgCl_2$, 0.1% w/v NP-40; Sigma) for 2 min on ice, and intact nuclei were pelleted by gentle centrifugation at 500 g for 10 min at 4 °C. Nuclei pellets were washed with 50 µL 1x TD buffer and centrifuged as previously. The nuclei were then resuspended in 50 µL transposition buffer (25 µL 2x TD buffer, 2.5 µL Tn5; from Illumina, and 22.5 µL RNase/DNase free H_2O; Invitrogen) and incubated for 30 min at 37 °C with gentle shaking at 300 rpm (Eppendorf Thermomixer). Following transposition samples were cooled on ice and

transposed DNA was purified using MinElute PCR Purification kits (Qiagen), following the manufacturers instructions.

PCR amplification

Samples were amplified by PCR in the following reaction:

Table 2.7. ATAC-seq PCR amplification

Volume	***Reagent***
10 µL	Transposed DNA
10 µL	RNase/DNase free H_2O (Invitrogen)
2.5 µL	Forward primer (from 25 µM stock)
2.5 µL	Reverse barcoded primer (from 25 µM stock)
25 µL	NEBNext High Fidelity 2x PCR Master Mix (NEB)

Using the following cycling program:

Table 2.8. ATAC-seq PCR amplification thermocycling program

Step	***Time***	***Temperature (°C)***
Initial extension	5 min	72
Step 1	30 s	98
Step 2	10 s	98
Step 3	30 s	63
Step 4	1 min	72
Steps 2-4 are repeated 5 x		

Primers for ATAC-seq library amplification were outlined in the ATAC-seq method publication (Buenrostro et al., 2013) and the following oligos were purchased from Life Technologies:

Table 2.9. ATAC-seq amplification primers

Primer	***Sequence***
Ad1 F	AATGATACGGCGACCACCGAGATCTACACTCGTCGGCAGCGTCAGATGTG
Ad2.1 R	TAAGGCGACAAGCAGAAGACGGCATACGAGATTCGCCTTAGTCTCGTGGGCTCGGAGATGT
Ad2.2 R	CGTACTAGCAAGCAGAAGACGGCATACGAGATCTAGTACGGTCTCGTGGGCTCGGAGATGT
Ad2.3 R	AGGCAGAACAAGCAGAAGACGGCATACGAGATTTCTGCCTGTCTCGTGGGCTCGGAGATGT
Ad2.4 R	TCCTGAGCCAAGCAGAAGACGGCATACGAGATGCTCAGGAGTCTCGTGGGCTCGGAGATGT
Ad2.5 R	GGACTCCTCAAGCAGAAGACGGCATACGAGATAGGAGTCCGTCTCGTGGGCTCGGAGATGT
Ad2.6 R	TAGGCATGCAAGCAGAAGACGGCATACGAGATCATGCCTAGTCTCGTGGGCTCGGAGATGT
Ad2.7 R	CTCTCTACCAAGCAGAAGACGGCATACGAGATGTAGAGAGGTCTCGTGGGCTCGGAGATGT
Ad2.8 R	CAGAGAGGCAAGCAGAAGACGGCATACGAGATCCTCTCTGGTCTCGTGGGCTCGGAGATGT
Ad2.9 R	GCTACGCTCAAGCAGAAGACGGCATACGAGATAGCGTAGCGTCTCGTGGGCTCGGAGATGT
Ad2.10 R	CGAGGCTGCAAGCAGAAGACGGCATACGAGATCAGCCTCGGTCTCGTGGGCTCGGAGATGT
Ad2.11 R	AAGAGGCACAAGCAGAAGACGGCATACGAGATTGCCTCTTGTCTCGTGGGCTCGGAGATGT
Ad2.12 R	GTAGAGGACAAGCAGAAGACGGCATACGAGATTCCTCTACGTCTCGTGGGCTCGGAGATGT

After an initial 5 cycles the PCR amplification was halted and kept on ice whilst qPCR was conducted on an aliquot of the PCR reaction to determine the saturation point of the reaction:

Table 2.10. ATAC-seq qPCR

Volume	***Reagent***
5 µL	PCR reaction aliqout
4.41 µL	RNase/DNase free H_2O (Invitrogen)
0.5 µL	Nextera primer mix (Illumina)
0.09 µL	100x SYBR Green I (Invitrogen)
5 µL	NEBNext High Fidelity 2x PCR Master Mix (NEB)

Table 2.11. ATAC-seq qPCR thermocycling program

Step	***Time***	***Temperature (°C)***
Step 1	30 s	98
Step 2	10 s	98
Step 3	30 s	63
Step 4	1 min	72
Steps 2-4 are repeated 40 x		

The point at which the fluorescence plateaus was taken as the saturation point, which was divided by three and the number of cycles taken to reach this threshold was determined graphically (as detailed in Chapter 3.2.1). The PCR amplification of ATAC-seq libraries was then extended by the appropriate number of additional cycles.

Library preparation and sequencing

Samples were prepared from two biological replicates. After PCR amplification samples were size selected using Agencourt AMPure XP beads (Beckman Coulter) to yield fragments ranging from 150-1,000 b.p. Size selection and 50 b.p. paired end sequencing of ATAC-seq

libraries was conducted by the Biomedical Sequencing Facility at CeMM Research Center for Molecular Medicine of the Austrian Academy of Sciences, Vienna, Austria.

M-BMDM ATAC-seq

Sample preparation of M-BMDMs ATAC-seq was conducted by Laurienne Edgar (Choudhury group, Radcliffe Department of Medicine, Oxford) as per the above protocol, and size selection and 50 b.p. single end sequencing was conducted by the Biomedical Sequencing Facility at CeMM Research Center for Molecular Medicine of the Austrian Academy of Sciences, Vienna, Austria.

2.1.7. mRNA sequencing (mRNA-seq)

mRNA-seq was performed by Dr. David Saliba (Udalova group) on $1X10^6$ GM-BMDMs from WT and $IRF5^{-/-}$ mice, either unstimulated or stimulated with LPS for 1, 2, 4, or 8 hours, as described previously. Two biological replicates were prepared for each condition. RNA was prepared using RNeasy Mini kits (Qiagen), including an optional DNaseI digestion with the RNase-Free DNase kit (Qiagen) as described above. Library preparation of poly(A)-selected mRNAs and 50 b.p. single end sequencing was conducted by the High-Throughput Genomics Group at the Wellcome Trust Centre for Human Genetics, Oxford.

2.2. Computational methods

2.2.1. ATAC-seq analysis

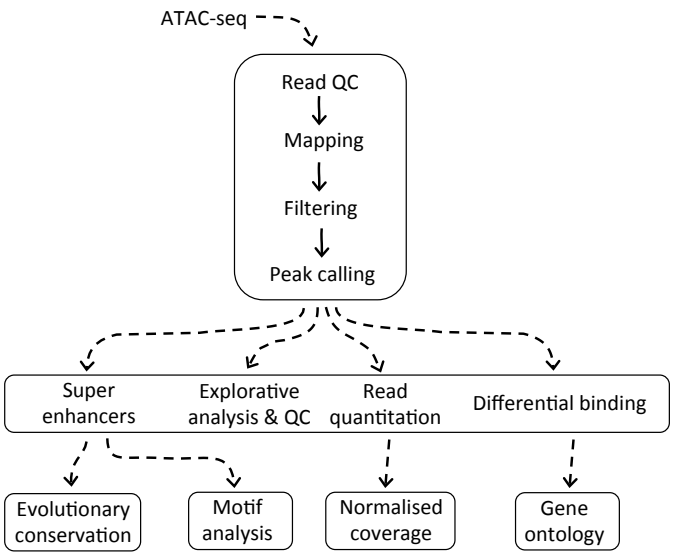

Figure 2.1. ATAC-seq analysis pipeline overview. ATAC-seq data were analysed using custom scripts, each of the stages outlined in the flow chart are described in detail below.

Data processing, mapping and peak calling

Read quality was assessed using FastQC (Andrews, 2010) and if necessary reads from Nextera Tn5 adaptors were removed using Cutadapt (Martin, 2011). Reads were mapped to the mouse mm10 reference genome using Bowtie2 (Langmead et al., 2009), with the "-X 2000" option for paired end reads to allow the mapping of reads with insert sizes up to 2 k.b. Reads mapping to chrM (mitochondrial DNA) were removed, as were PCR duplicates using Picard tools MarkDuplicates (Wysoker et al., 2017). Reads were also filtered on mapping scores, only retaining reads with MAPQ > 10 with SAMtools (H. Li et al., 2009). Peak calling was conducted using MACS2 (Y. Zhang et al., 2008) with options: "--nomodel --extsize 147 --gsize 1.87e9 --qvalue 0.01". Peaks in ENCODE ChIP blacklisted regions (ENCODE Project Consortium, 2012) and mitochondrial DNA homologues (Buenrostro et al., 2013) were removed prior to further analysis.

Read quantitation

Query peaks were merged and offset to the centre of the read pile ups ±250 b.p. to form a consensus peak set. Reads (or read pairs for paired end data) falling within the peak set were counted using BedTools (Quinlan and Hall, 2010) and counts were normalised for sequencing depth. For between sample comparisons read counts were upper quantile normalised.

Quality control and data exploration

Insert sizes were collected using Picard tools (Wysoker et al., 2017). Reads mapping to chrM were counted using SAMtools (H. Li et al., 2009). Fraction of reads in peaks (FRIP) was calculated using custom scripts, data expressed are the ratio of read counts inside peaks / read counts outside of peaks. Enrichment of ATAC-seq peaks at genomic regions was calculated using Genomic Annotation Test (GAT) (Heger et al., 2013), using the CGAT pipeline "pipeline_annotations.py" (https://github.com/CGATOxford/CGATPipelines). Principle component analysis (PCA) was conducted on normalised counts (as above) from all detected peaks.

Differential accessibility

Differential accessibility for paired end ATAC-seq data was conducted in R using DiffBind (Stark and Brown, 2011), briefly all peaks in comparisons were merged and offset to the peak center ±250 b.p. reads were then counted over the merged intervals and analysed using DESeq2. Peaks with a log2 fold change > 1.5 between conditions and false discovery rate (Benjamini-Hocheberg corrected p-value) < 0.05 were deemed differentially accessible. For comparisons between data sets (GM-BMDMs vs M-BMDMs) reads were quantified (as described above) over a merged set of peak intervals, consisting of all peaks detected in both data sets, counts were then log2 normalised (with the addition of a pseudo count) and

compared directly. Peaks that had >2 fold higher counts in either cell type were taken for gene ontology analysis.

Gene ontology

Gene ontology analysis for differentially accessible peaks was conducted using GREAT (McLean et al., 2010) using the basal plus extension association rule with default settings.

Super enhancer analysis

ATAC-seq peaks were annotated to the single nearest gene, up to a maximum distance of 1 m.b. Peaks within 2.5 k.b. of TSSs were designated as promoter peaks, peaks > 2.5 k.b. from genes were deemed enhancers. Enhancers within 12.5 k.b. intervals were merged to form potential super enhancer regions. Any promoter peaks or regions containing genes were subtracted from the merged peak set prior to subsequent analysis. Reads were quantitated over the merged peak set and normalised for sequencing depth as described above. To designate clusters of peaks as super enhancers the merged peaks were sorted by their normalised read counts and plotted by increasing signal intensity. An arbitrary cut-off was applied where the slope of the fitted line reaches one; all regions greater than the cut-off were designated super enhancers and regions below the cut-off traditional enhancers. Subsequent analysis of either super enhancers or traditional enhancers was performed on the individual ATAC-seq peaks from within the merged regions.

Coverage tracks, heat maps, and profiles

BigWigs of read coverage for visualisation were generated using DeepTools bamCoverage with the options: "--binSize 5 --normalizeUsingRPKM --smoothLength 20 --skipNAs --centerReads". For paired end data only correctly mapped read pairs were used, for single end data unmapped reads were excluded. Heat maps and coverage plots were produced using the DeepTools packages plotHeatmap and plotProfile (Ramírez et al., 2016). IGV

(Thorvaldsdóttir et al., 2013) was used to visualise ATAC-seq data. Pearson correlation matrix was generated as described in Chapter 2.2.2 – Pearson correlation, using normalised ATAC-seq and ChIP-seq reads counted over a merged peak set of ATAC-seq peaks from unstimulated GM-BMDMs and M-BMDMs.

Evolutionary conservation

Enrichment of mm10 60-way alignments from the UCSC genome browser (conserved regions identified with phastCons) (Tyner et al., 2017) were used for visualised over ATAC-seq peaks using DeepTools (Ramírez et al., 2016). Average phastCons scores in ATAC-seq peaks were also calculated and analysed in R.

Motif analysis

De novo motif discovery on DNA sequences from the central regions of query peaks was performed using MEME-ChIP (Machanick and Bailey, 2011). DNA sequences were either unmasked or softmasked to remove repetitive regions, and custom background sequences were created from the flanking regions of the DNA sequences with the "fasta-get-markov -m 2" command. MEME-ChIP was run with the options: "-meme-minw 5 -meme-maxw 30 -meme-nmotifs 3". The motif discovery mode ("-meme-mod") option was set to "any number of repetitions" (anr) for super enhancer ATAC-seq peaks.

2.2.2. ChIP-seq analysis

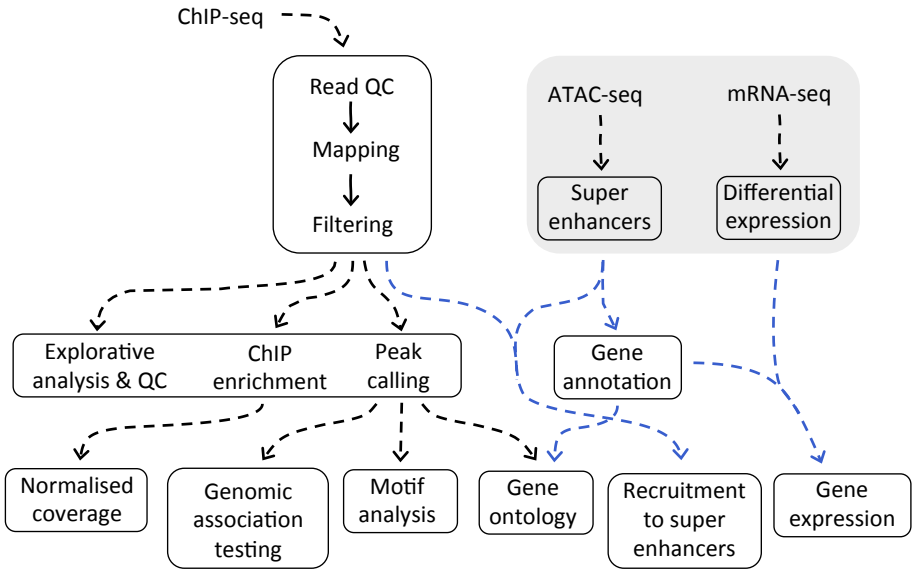

Figure 2.2. ChIP-seq analysis pipeline overview. ChIP-seq data were analysed using custom scripts, each of the stages outlined in the flow chart are described in detail below. Blue arrows indicate intersections of ChIP-seq with mRNA and ATAC -seq data sets (grey box). ATAC-seq and mRNA-seq analyses are described in Chapter 2.2.1 and 2.2.4, respectively.

ChIP-seq data sources

Table 2.12. ChIP-seq data samples and sources

ChIP	*Cell type*	*Lab*	*LPS stimulation (hr)*	*Accession ID*
H3K4me1	M-BMDM	Natoli	0, 4	GSE38377
H3K4me3	M-BMDM	Natoli	0, 4	GSE38377
H3K27ac	M-BMDM	Natoli	0, 4	GSE38377
H3K4me1	GM-BMDM	Amit	0, 2	GSE36104
H3K4me3	GM-BMDM	Amit	0, 2	GSE36104
H3K27ac	GM-BMDM	Amit	0, 2	GSE36104
C/EBPB	GM-BMDM	Amit	0, 2	GSE36104
Hif1a	GM-BMDM	Amit	0, 2	GSE36104
Maff	GM-BMDM	Amit	0, 2	GSE36104
Egr1	GM-BMDM	Amit	0, 2	GSE36104
Ets2	GM-BMDM	Amit	0, 2	GSE36104
E2f1	GM-BMDM	Amit	0, 2	GSE36104
E2f4	GM-BMDM	Amit	0, 2	GSE36104
Stat1	GM-BMDM	Amit	0, 2	GSE36104
Stat3	GM-BMDM	Amit	0, 2	GSE36104
RelB	GM-BMDM	Amit	0, 2	GSE36104
Rel	GM-BMDM	Amit	0, 2	GSE36104
IRF2	GM-BMDM	Amit	0, 2	GSE36104
IRF4	GM-BMDM	Amit	0, 2	GSE36104
IRF3	GM-BMDM	Smale	0, 2	GSE67357
RUNX1	GM-BMDM	Amit	0, 2	GSE36104
RUNX1	M-BMDM	Natoli	0, 4	Unpublished
PU.1	M-BMDM	Natoli	0, 4	GSE38377
IRF1	M-BMDM	Natoli	0, 2	GSE56123
IRF8	M-BMDM	Natoli	0, 2	GSE56123
JunB	M-BMDM	Natoli	0, 4	GSE38377
Srf	M-BMDM	Smale	0, 2	GSE67357
IRF5	GM-BMDM	Udalova	0, 2	E-MTAB-2661
RelA	GM-BMDM	Udalova	0, 2	E-MTAB-2031

Mapping

Paired and single end reads were mapped to the mouse genome (mm10) with Bowtie2 (Langmead et al., 2009), using default settings, and mapped reads were filtered by a minimum quality score (MAPQ) of 10.

Peak calling

Peak calling was conducted using the CGAT pipeline "pipeline_peakcalling.py" (https://github.com/CGATOxford/CGATPipelines), to run MACS2 (Y. Zhang et al., 2008) with the following settings: "--mfold 10 30 --gsize 1.87e9 --qvalue 0.10". Peaks falling within ENCODE blacklisted regions (ENCODE Project Consortium, 2012) were removed prior to further analysis. For IRF5 ChIP-seq only peaks detected in both replicates were used.

Read quantitation

Reads (or read pairs for paired end data) falling within the ATAC-seq peaks from LPS stimulated GM-BMDMs were counted using BedTools (Quinlan and Hall, 2010) and counts were normalised for sequencing depth and peak width. For between sample comparisons read counts were upper quantile normalised.

Pearson correlation

Reads were quantitated as above, counts from ChIP controls were subtracted before the addition of a pseudo count and log2 normalisation. Pearson correlation was performed in R using inbuilt functions. Heat maps were generated using ComplexHeatmap (Z. Gu et al., 2016) and hierarchical clustering was performed using the Ward method on Manhattan distances.

Differential binding

Differential binding analysis of transcription factors to super enhancers was conducted in R using DiffBind (Stark and Brown, 2011) briefly all ATAC-seq peaks in super enhancers were offset the peak center ±250 b.p. reads within the peak set were then counted and fold changes between unstimulated and LPS stimulated conditions calculated using DESeq2.

ChIP enrichment

The MACS2 --SPMR function (Y. Zhang et al., 2008) was used to obtain sequencing depth normalised read counts for ChIP and matching control samples (input or control ChIP). ChIP enrichment over control was then calculated from the normalised read counts using MACS2 bdgcmp (Y. Zhang et al., 2008). These data were converted to BigWigs for visualisation in IGV (Thorvaldsdóttir et al., 2013) and plotting with DeepTools (Ramírez et al., 2016).

Motif analysis

De novo motif discovery on DNA sequences from the central regions of query peaks was performed using MEME-ChIP (Machanick and Bailey, 2011). DNA sequences were either unmasked or softmasked to remove repetitive regions, and custom background sequences were created from the flanking regions of the DNA sequences with the "fasta-get-markov -m 2" command. MEME-ChIP was run with the options: "-meme-minw 5 -meme-maxw 30 -meme-nmotifs 3". The motif discovery mode ("-meme-mod") option was set to "zero or one occurrence per sequence" (zoops) for ChIP peaks.

Genomic association testing

Enrichment of ChIP-seq peaks at genomic regions was calculated with GAT (Heger et al., 2013), using the CGAT pipeline "pipeline_annotations.py" (https://github.com/CGATOxford/CGATPipelines). Association of ChIP peak overlaps was tested using GAT against a genomic background (consisting of ungapped contigs with ENCODE blacklisted regions subtracted) with 10,000 simulations. Associations of ChIP peak sets with ATAC-seq peaks in super or traditional enhancers were tested by the same procedure but with the use of all open chromatin (all ATAC-seq peaks) as a background.

Gene ontology

Gene ontology analysis for query peaks was conducted using GREAT (McLean et al., 2010) using the basal plus extension association rule with default settings.

2.2.3. chrRNA-seq analysis

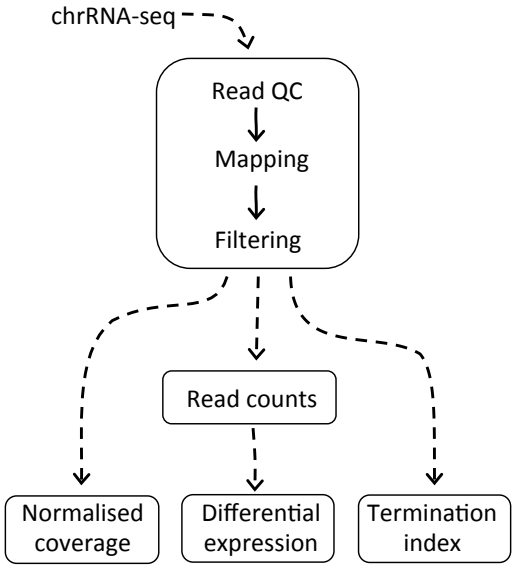

Figure 2.3. chrRNA-seq analysis pipeline overview. chrRNA-seq data were analysed using custom scripts, each of the stages outlined in the flow chart are described in detail below.

Mapping

Reads were trimmed with trimmomatic (Bolger et al., 2014) to remove TruSeq2 sequencing adapters with the "ILLUMINACLIP" option. Mapping was conducted using the CGAT pipeline "pipeline_mapping.py" (https://github.com/CGATOxford/CGATPipelines) using the Gsnap (T.D. Wu and Nacu, 2010) tool with options: "-m2 -N1 -B3 --maxsearch=1000 -w 500000 -n100 –Q" and mapped reads with MAPQ scores < 10 were discarded.

Differential expression

Differential expression of chrRNA read pairs counted within annotated genes (including introns and untranslated regions) were analysed with DESeq2 (Love et al., 2014). Analysis of chrRNA-seq differential expression and comparison of chrRNA-seq and mRNA-seq data sets was performed by Dr Stephen Sansom (Sansom Group, Kennedy Institute of Rheumatology).

Termination index

Genes were divided into gene body (middle 50% of TSS + 500 b.p. to TES) and gene end (TES to TES + 2,000 b.p.). Read pairs were counted over these intervals in a strand specific manner using BedTools multicov (Quinlan and Hall, 2010), and normalised for sequencing depth and interval length. The termination index was then calculated as:

Termination index = log2(gene body counts / gene end counts).

Coverage tracks, heat maps, and gene profiles

BigWigs were generated using DeepTools bamCoverage (Ramírez et al., 2016). The "--filterRNAstrand" option was used to generate separate tracks for forward and reverse strands. Additional options used were: "--binSize 5 –normalizeUsingRPKM --samFlagInclude 64 --centerReads --smoothLength 20". Heat maps and coverage profiles were produced using the DeepTools packages plotHeatmap and plotProfile. IGV (Thorvaldsdóttir et al., 2013) was used to visualise coverage tracks.

2.2.4. mRNA-seq analysis

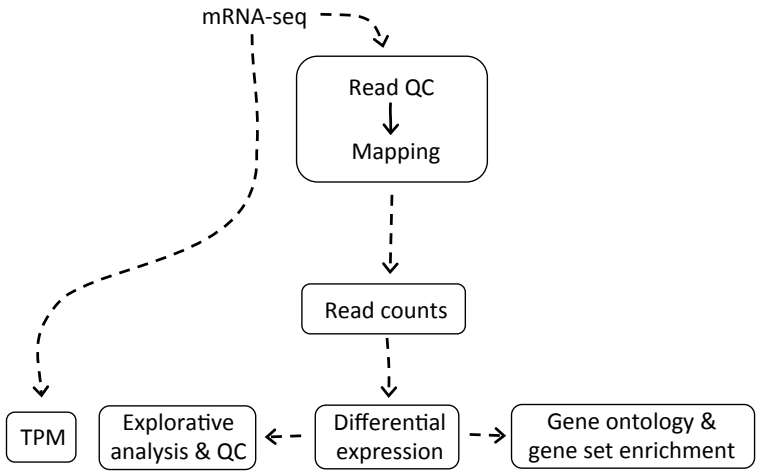

Figure 2.4. mRNA-seq analysis pipeline overview. mRNA-seq data were analysed using custom scripts, each of the stages outlined in the flow chart are described in detail below.

Mapping

Mapping was conducted using STAR (Dobin et al., 2013) with the options: "--runMode alignReads --outFilterMismatchNmax 2"

Differential expression

Uniquely mapped read pairs were counted over annotated genes using HTSeq-count (Anders et al., 2015) with the options: "-a 255 -s no -m union -t CDS". Differential expression was then analysed with DESeq2 (Love et al., 2014). Genes with an FDR < 0.05 and fold change > 1.5 were deemed to be differentially expressed.

Read quantitation

Transcripts per million (TPM) were calculated with Salmon (Patro et al., 2017) from unmapped reads using quasi-mapping for the mouse mm10 assembly.

Dimensionality reduction

Variance stabilised (VST) counts for all DESeq2 differentially expressed genes were used for dimensionality reduction and plotting. PCA was conducted on all samples using the prcomp function in R. T-Distributed Stochastic Neighbour Embedding (t-SNE) (Maaten and Hinton, 2008) was used with perplexity = 5. K-means clustering was used on the t-SNE results to highlight clusters of interest; the number of clusters best representing the data was determined using the "elbow" method.

Hierarchical clustering and heat map

VST counts from DESeq2 differentially expressed genes were used for hierarchical clustering, using the Ward method on Manhattan distances. Gene expression was normalised to the range of the data per row.

Gene set enrichment and gene ontology

Gene ontology terms for gene lists were retrieved using Enrichr (E.Y. Chen et al., 2013; Kuleshov et al., 2016). Gene set enrichment was conducted using Enrichr for ranked gene lists. Rankings are based on the DESeq2 fold changes between WT and IRF5$^{-/-}$ samples for each gene.

2.3. Statistical analysis

Statistical analyses were carried out with R (version 3.3.1), using Mann Whitney U test (for comparisons between groups) and Fisher's exact test (for comparisons between two categorical variables). GraphPad (version 6.0, GraphPad Software) was also used for conducting unpaired two-tailed T-test, Mann Whitney U test, and two-way ANOVA with Bonferroni's correction (for multiple comparisons) for grouped data. Additional statistical tests were carried out using computational methods and tools described above, where relevant, p-value cut-offs and false discovery rates (FDRs) are reported.

3. IRF5 and Efficiency of Transcription

3.1. Introduction

M-BMDMs are often described as alternatively activated macrophages, with reduced inflammatory capacity and distinct metabolic profiles (Joshi et al., 2014). IRF4 has been identified as a key mediator of M-BMDM development (Satoh et al., 2010). Conversely treatment of macrophages with GM-CSF promotes the transcription of IRF5 and polarization to an inflammatory phenotype (Krausgruber et al., 2011). IRF5 binds to regulatory elements of pro-inflammatory cytokines as a consequence of LPS stimulation, acting coordinately with RelA to promote transcription via increased Pol II recruitment (Krausgruber et al., 2011) (Saliba et al., 2014). Intriguingly, analysis of DNA sequences underlying IRF5-RelA binding sites revealed the presence of composite motifs consisting of ISRE half sites and PU.1 binding sites (Saliba et al., 2014). Transcription is a tightly regulated process, with many checks and balances via the activity of *cis*-regulatory elements to ensure coordinated transcription in response to exogenous signals. PU.1 plays a particularly important role in macrophages, specifying the repertoire of enhancers available for the subsequent recruitment of SDTFs (Ghisletti et al., 2010; Heinz et al., 2010), furthermore the presence of PU.1 at these pre-marked enhancers is required for the recruitment of such SDTFs (Escoubet-Lozach et al., 2011; Heinz et al., 2013). The formation of *de novo* enhancers, in regions of closed chromatin unmarked by PU.1 in response to stimuli provides an additional platform for SDTFs to operate on (Kaikkonen et al., 2013; Ostuni et al., 2013). NFκB is unable to bind enhancers obscured by closed chromatin (Lone et al., 2013), however such activity has been described for IRF8 (Mancino et al., 2015). We therefore hypothesised that IRF5 contributes to the remodeling of chromatin in response to stimulus leading to the formation of *de novo* enhancers. This uncovering of latent enhancers would thus allow increased binding of SDTFs and subsequent Pol II recruitment augmenting transcription.

Interestingly, IRF5 is also capable of binding the 3' regions of its target genes, binding to a distinct region immediately downstream of the *Tnf* gene (Krausgruber et al., 2010). This raises the question of other distinct forms of regulation by IRF5. In addition to activity at enhancers and promoters orchestrating the initiation of transcription, the termination of transcription and associated mRNA processing also represent key checkpoints at which gene expression can be regulated. Indeed, efficient termination of transcription has been shown to enhance mRNA translation promoting gene expression (West and Nicholas J Proudfoot, 2009; Nojima et al., 2013). Our second hypothesis is that the demonstrated 3' binding of IRF5 to the *Tnf* gene contributes to the efficient termination of transcription thus promoting gene expression. In this chapter we therefore investigate the effects of IRF5 on the efficiency of transcription, focusing on chromatin remodeling and the termination of transcription.

3.2. Results

3.2.1. IRF5 and Chromatin Accessibility

ATAC-seq makes use of a Tn5 transposase, pre-loaded with sequencing adaptors, to fragment accessible DNA whilst simultaneously tagging it with adaptors (Figure 3.1.A). This tagged DNA therefore consists of open chromatin at the time of transposition and can then be purified and amplified for sequencing. To ensure library complexity it is essential that samples are not over-amplified, which can result in the predominance of small fragments and PCR duplicates. This is accomplished by determining the saturation point of PCR amplification via a qPCR side reaction and amplifying samples to a third of this maximum (Figure 3.1.B). ATAC-seq library quality can be assessed by presence of characteristic nucleosomal phasing, indicated by peaks, or bands on a gel, corresponding to lengths of DNA associated with mononucleosomes (147 b.p.) and multiples thereof (Figure 3.1.C). To dissect IRF5 chromatin modulating activity we conducted ATAC-seq on WT and IRF5$^{-/-}$ GM-BMDMs, and BM neutrophils, which were either unstimulated or treated with LPS for two hours. Neutrophils were included as a control for comparative analysis with macrophages, as they fully differentiate in the bone marrow and were expected not to demonstrate the functional plasticity of macrophages. The sequencing and data analysis was conducted as described in (Chapter 2.1.6 and Chapter 2.2.1). Paired end sequencing allows us to determine the insert sizes of sequenced fragments, the majority of these are short fragments (first peak, <150 b.p.) indicative of accessible chromatin, whereas longer fragments (second peak, 150-220 b.p.) represent sites occupied by nucleosomes (Figure 3.1.D). One caveat of ATAC-seq is the presence of contaminating reads originating from mitochondrial DNA (Figure 3.1.E), which were removed, along with PCR duplicates prior to subsequent analysis.

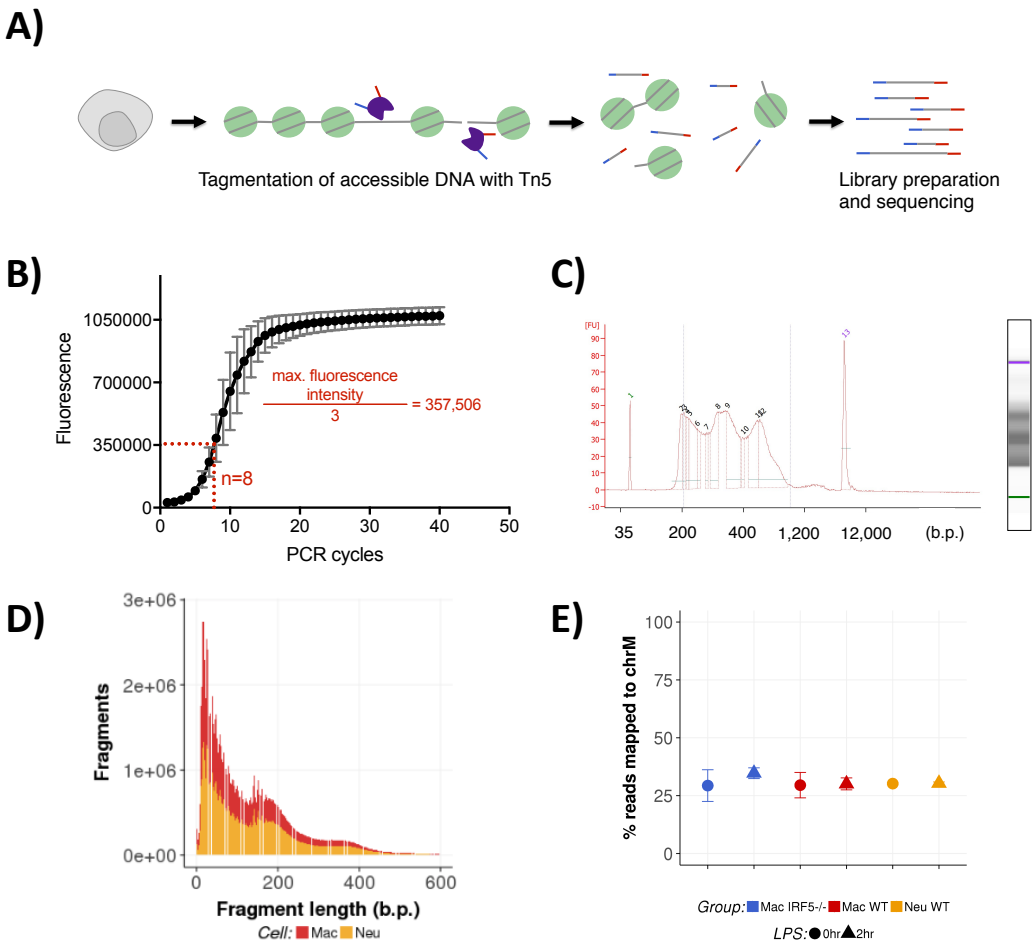

Figure 3.1. Analysis of chromatin accessibility by ATAC-seq. A) ATAC-seq method. Briefly, intact nuclei are incubated with Tn5 transposase, which fragments accessible DNA whilst simultaneously attaching sequencing adaptors a.k.a tagmentation. Tagmented DNA representative of open chromatin is then purified and used for library preparation. **B)** PCR amplification optimisation. After initial amplification PCR is halted, the saturation point of the PCR is then determined by qPCR and the remaining libraries are amplified for the optimal number of additional cycles. **C)** Representative Bioanalyser electropherogram of a size selected ATAC library. **D)** Fragment length distribution of sequenced ATAC-seq reads. **E)** Mitochondrial contamination of ATAC-seq data. Error bars indicate the standard deviation of two replicates.

Cis-regulatory elements (peaks of open chromatin) were identified with MACS2 as described in (Chapter 2.2.1). We uncovered 38,285, 29,568, and 29,610 peaks in unstimulated WT and IRF5$^{-/-}$ GM-BMDMs, and BM neutrophils, respectively. Which increased to 55,370, 49,246, and 35,784 peaks in LPS stimulated cells (Table 3.1). The numbers of LPS sensitive (gained or lost with stimulation) peaks between IRF5$^{-/-}$ and WT macrophages were very similar (~25,900), with neutrophils also demonstrating a surprising level of chromatin remodelling with LPS stimulation (9,730 LPS sensitive peaks).

	Mac.WT.Peaks	Mac.KO.Peaks	Neu.WT.Peaks
0hr	38,285	29,568	29,610
2hr	55,370	49,246	35,784
LPS gained	21,642	22,835	8,003
LPS lost	4,314	3,097	1,727
LPS sensitive	25,956	25,932	9,730

Table 3.1. MACS2 called peaks. ATAC-seq peaks in WT and IRF5$^{-/-}$ GM-BMDMs, and BM neutrophils, with and without LPS stimulation

Genomic association testing of ATAC-seq peak reveals that all of the samples are very promoter biased, with a high level of enrichment in 5' UTRs and 5' flanking regions (Figure 3.2.A). Examining the FRIP, a quality control metric indicative of signal/noise ratio, we noted that LPS stimulated macrophages had an increased FRIP compared to unstimulated cells, and interestingly, neutrophils had a still higher FRIP that wasn't affected by LPS (Figure 3.2.B). Figure 3.2.C shows normalised coverage of ATAC-seq at genes with more accessible chromatin in neutrophils (*Sod2, Il1b, Cxcr2*) and macrophages (*Cxcr1*, *Ccl5, Ccl9, Cd40*). The majority of ATAC-seq peaks at these regions are shared by both neutrophils and GM-BMDMs, though some cell-specific enhancers are also present. Notably IRF5 does not affect the accessibility of any of the loci shown in GM-BMDMs.

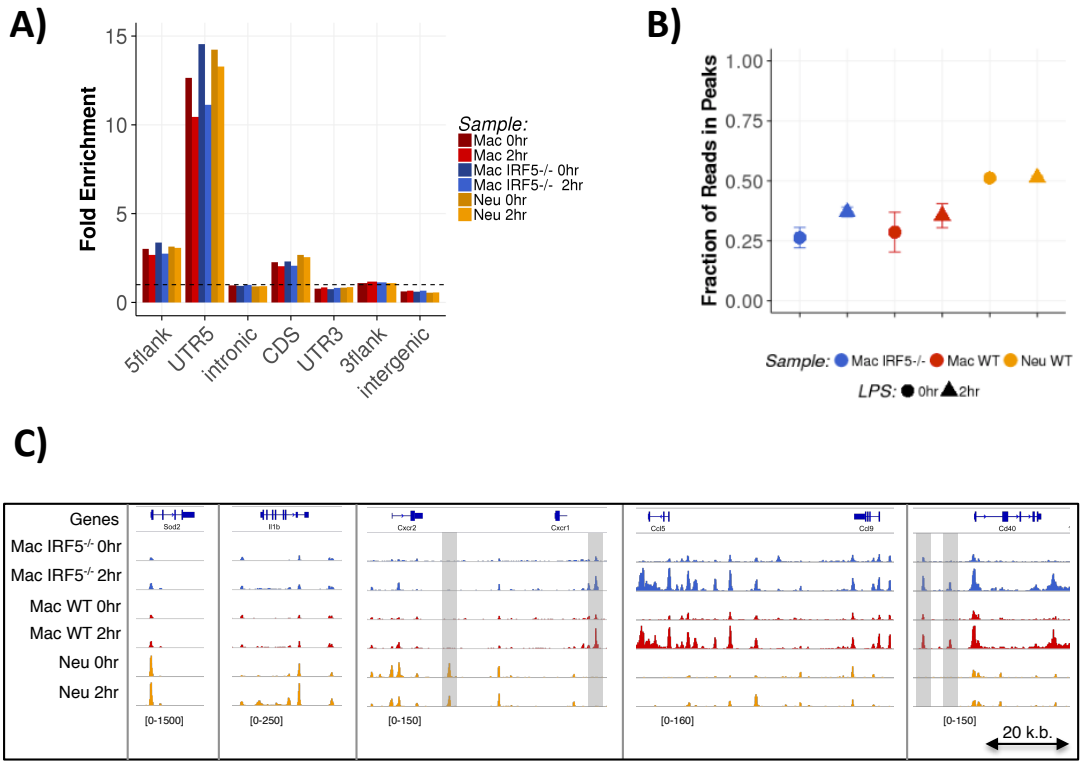

Figure 3.2. Distribution of ATAC-seq peaks genome-wide. A) Genomic association testing results depicting fold enrichment of ATAC peaks with features of interest against genomic background. All enrichments shown have an adjusted p-value (using the Benjamini-Hochberg procedure) of <0.05. **B)** Fraction of reads in peaks (FRIP). Error bars indicate the standard deviation of two replicates. **C)** Representative snapshots depicting ATAC-seq profiles in BM neutrophils and GM-BMDMs. Highlighted regions indicate cell specific enhancers. Tracks displayed correspond to Ensembl genes and normalised ATAC-seq signal (fragments per kilobase per million - FPKM). Scales are indicated on the plot.

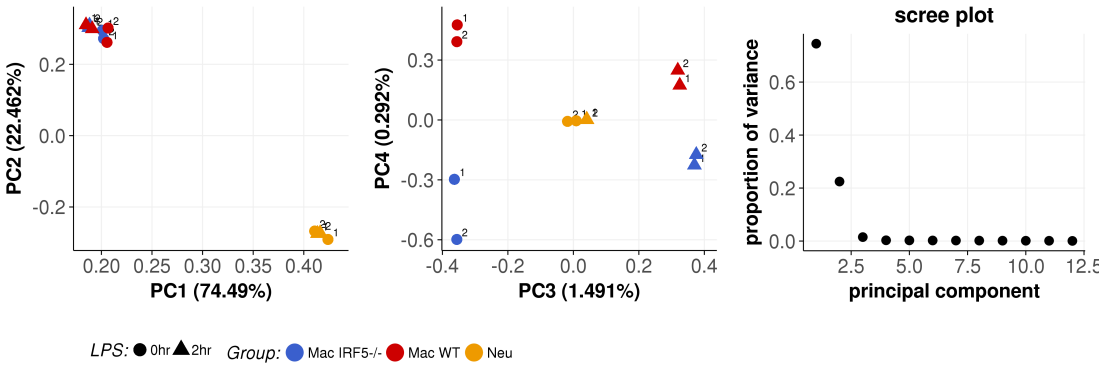

Figure 3.3. ATAC-seq principle component analysis. Comparative analysis is based on normalised read counts from a consensus peak set representing all open chromatin in BM neutrophils and GM-BMDMs. Principle components 1-4 are shown, the variance each component accounts for are indicated in brackets on the axis and the scree plot.

To obtain a broad overview of the data we used principal component analysis (PCA), based on normalised read counts (reads per million – RPM) of reads falling in a comprehensive peak set consisting of open chromatin in all of the samples (81,267 peaks) (as detailed in Chapter 2.2.1). This reveals that the main source of variance is cell type, with principal components one and two both separating neutrophils from macrophages (Figure 3.3). The next is LPS stimulation, which divides unstimulated and LPS treated macrophages. IRF5 separates macrophages on the fourth principle component, which accounts for 0.29% of the total variance. Interestingly neutrophils are relatively unaffected by LPS in comparison to macrophages.

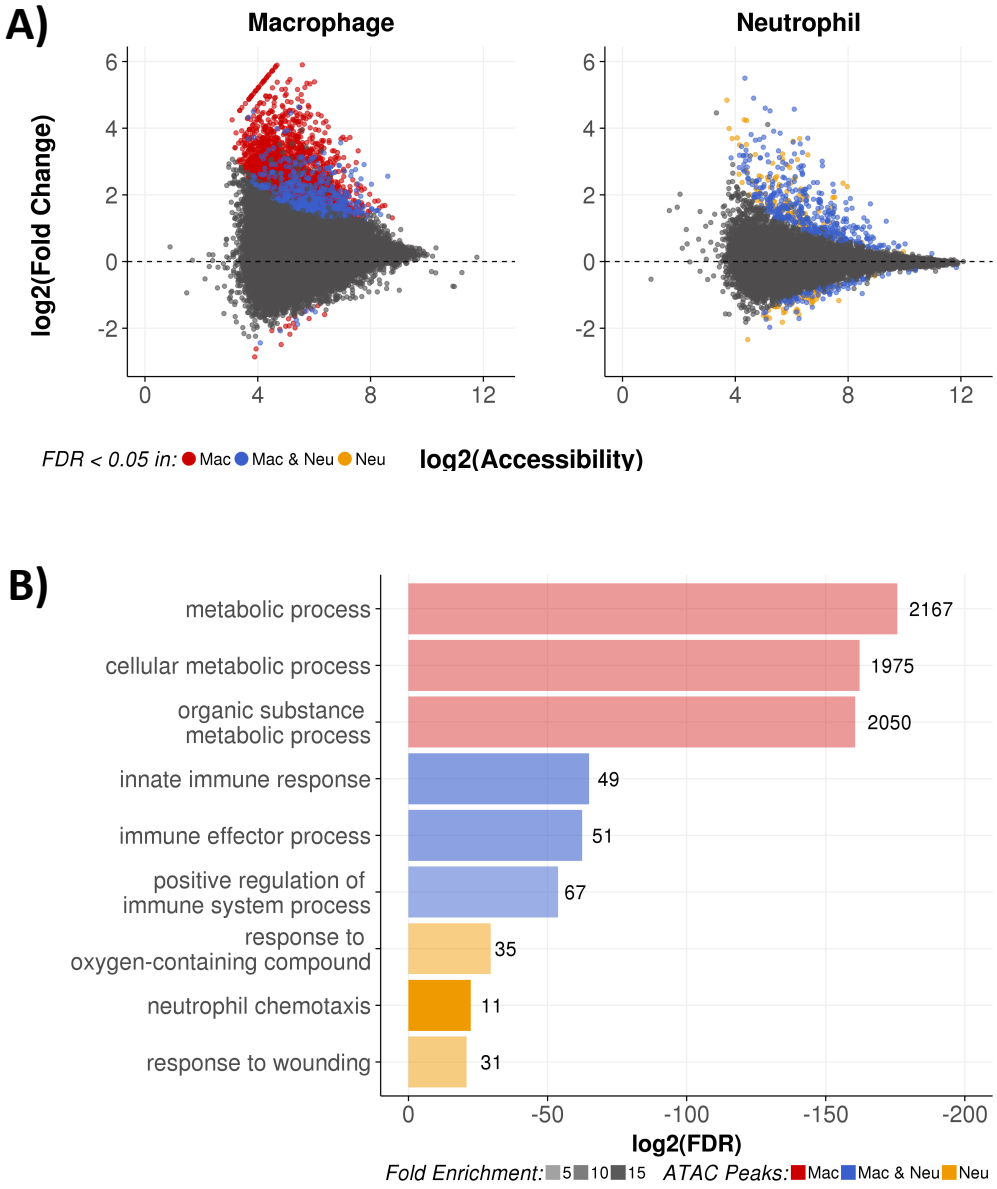

Figure 3.4. LPS modulated chromatin accessibility in macrophages and neutrophils. A) Differential accessibility of chromatin in GM-BMDMs and BM neutrophils in response to LPS stimulation. Highlighted differentially accessible peaks have an FDR < 0.05 in either GM-BMDMs (red), BM neutrophils (yellow) or both (blue). **B)** Representative gene ontology categories for BMDM specific (red), neutrophil specific (yellow), and shared (blue) differentially accessible ATAC-seq peaks. All ontologies shown have an adjusted binomial p-value < 0.05, density of shading indicates fold enrichment and annotations indicate the number of peaks corresponding to GO terms.

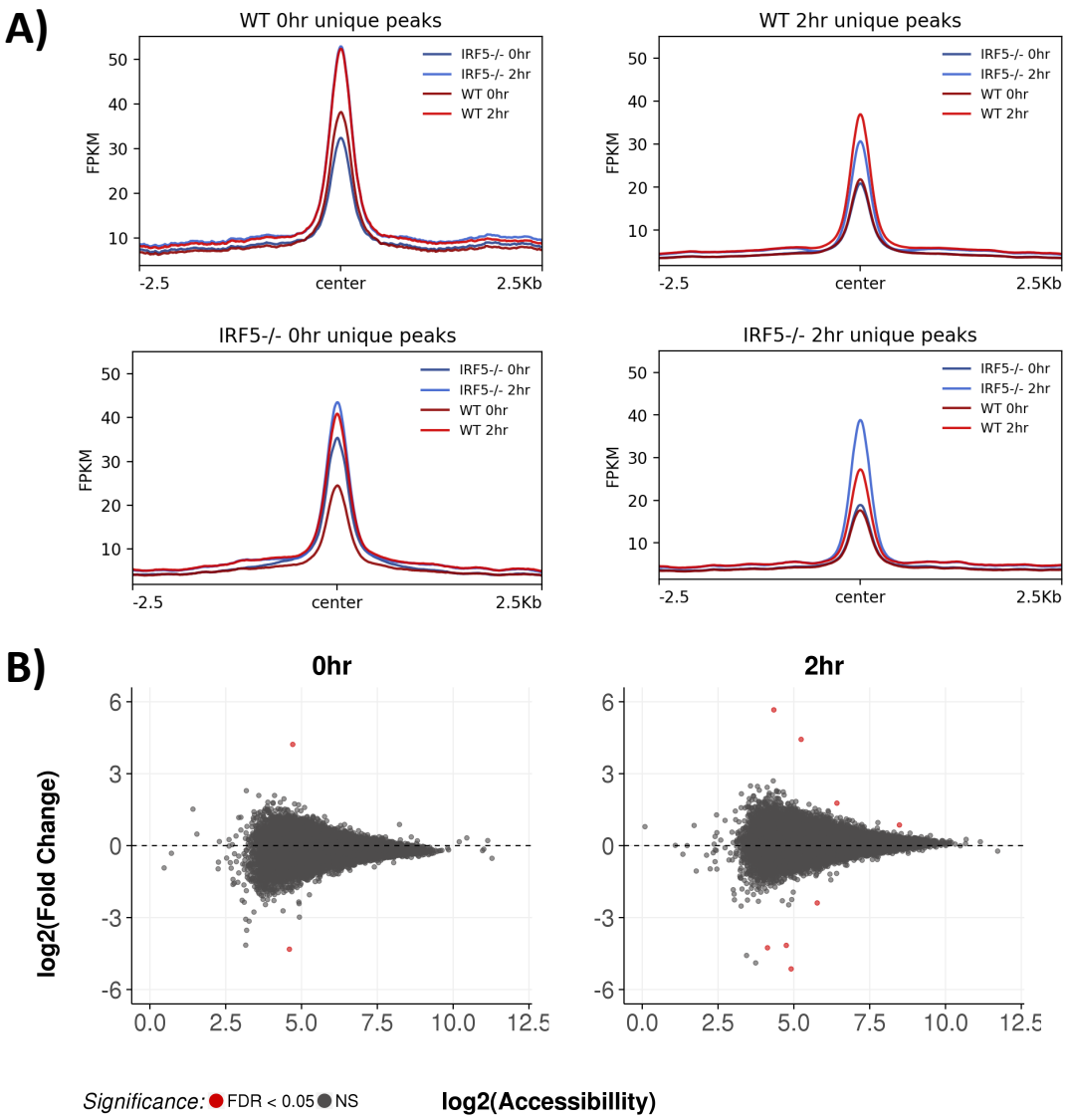

Figure 3.5. IRF5 mediated changes to chromatin accessibility. A) Average profiles of IRF5$^{-/-}$ and WT ATAC signal (fragments per kilobase per million – FPKM) plus and minus LPS at 0hr peaks and 2hr peaks detected in exclusively in WT or IRF5$^{-/-}$. **B)** Differential accessibility of all open chromatin in WT vs IRF5$^{-/-}$ GM-BMDMs at 0hr and 2hr time points. Highlighted differentially accessible peaks have an FDR < 0.05.

Quantitative assessment of peak accessibility was performed on macrophages and neutrophils separately (conducted as described in Chapter 2.2.1). This reveals LPS stimulated macrophages to have 3,838 differentially accessible peaks, and neutrophils to have 656 (FDR < 0.05), with the majority of these becoming more accessible in response to LPS in both cell types (Figure 3.4.A). Of, note we observed that a large proportion of differentially accessible peaks in neutrophils (534) overlapped with accessible peaks in macrophages, leaving 3,304 macrophage specific peaks and 193 neutrophil specific peaks. We utilised the GREAT gene ontology tool (McLean et al., 2010) to characterise the genes associated with these regions

(Figure 3.4.B). This analysis revealed that the peaks common to both cells largely represent the innate immune response, whereas macrophage specific peaks were enriched for metabolic process gene ontology terms, and neutrophil specific peaks pertained to the gene ontology terms: response to oxygen-containing compound, neutrophil chemotaxis, and response to wounding. An extended list of gene ontology terms is available in Chapter 8.1.1.

To examine the effect of IRF5 on chromatin accessibility, we first assessed the enrichment of ATAC-seq reads from WT and IRF5$^{-/-}$ macrophages over ATAC-seq peaks, which were present exclusively in WT or IRF5$^{-/-}$ (Figure 3.5.A). These data indicate that the peak calling is accurate with greater accessibility of WT samples at WT specific peaks and vice versa for IRF5$^{-/-}$ specific peaks. However, the differences are marginal with high read counts in both WT and IRF5$^{-/-}$. This likely reflects the influence of FDR cut-offs in the peak-calling algorithm, limiting the threshold of detection to avoid the presence of false positive results and biases in peak calling due to sequencing depth rather than biology, in the discrepancy in the total number of peaks detected in each condition. To quantify the effect of IRF5 on chromatin accessibility we therefore followed the procedure previously outlined, utilising a combined peak set of all peaks detected in IRF5$^{-/-}$ and WT macrophages to assess differential accessibility (Figure 3.5.B). This analysis reveals that IRF5 does not affect chromatin accessibility, with a total of ten peaks in both conditions being called as differentially accessible, out of a possible 58,261. Manual inspection reveals that these ten peaks do not reflect meaningful changes in chromatin accessibility between IRF5$^{-/-}$ and WT and are likely due to stochastic noise in the data (data not shown).

In order to assess if IRF5 played a role in maintaining chromatin accessibility after exposure to inflammatory stimuli we performed ChIP-qPCR (Figure 3.6.A) for the core nucleosome subunit H3 at *Tnf* and *Il12b cis*-regulatory regions (Figure 3.6.B), focussing on later time points after LPS stimulation (eight and twenty four hours). We observe a higher proportion of nucleosome occupancy at *Il12b* promoters and enhancers, which decreases with LPS

stimulation, than at those corresponding to the *Tnf* gene, which are very accessible in unstimulated conditions, and display reduced changes with LPS stimulation. This is in keeping with their status as SRGs and PRGs, respectively (discussed further in Chapter 4.3). Notably, we don't find any differences in nucleosome occupancy between WT and IRF5$^{-/-}$ GM-BMDMs, further confirming that IRF5 does not affect chromatin accessibility.

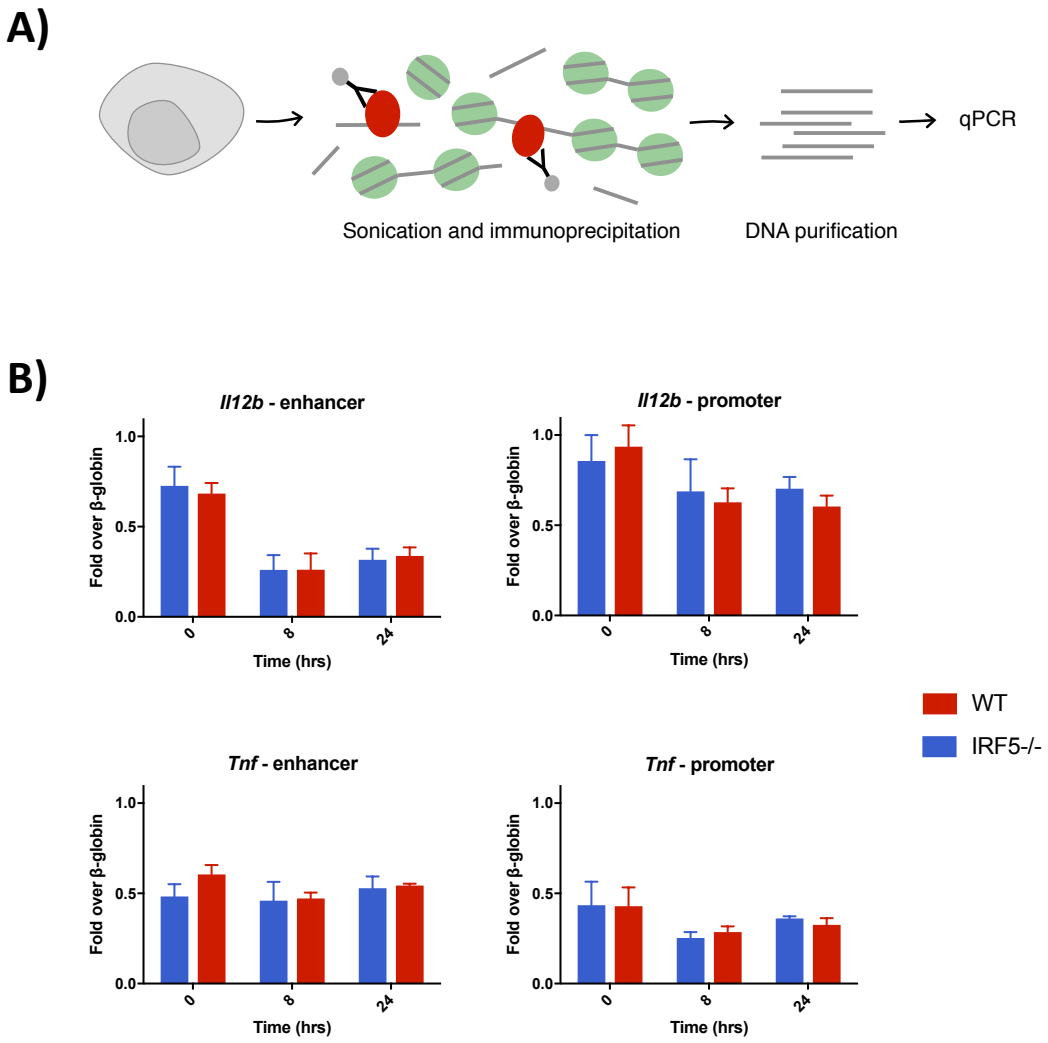

Figure 3.6. Nucleosome occupancy of *Tnf* and *Il12b cis*-regulatory regions. A) Overview of ChIP technique. Briefly, cells are cross linked and chromatin is fragmented by sonication, proteins of interest are then immunoprecipitated and the associated DNA is purified for downstream analysis. **B)** H3 ChIP-qPCR for *Tnf* and *Il12b cis*-regulatory regions, in unstimulated and LPS stimulated GM-BMDMs. Data are expressed as fold over β-globin (% input gene-specific / % input *Hbb-b1*). Data are mean values from n=3 ± SEM.

3.2.2. GM-CSF Priming of BMDMs

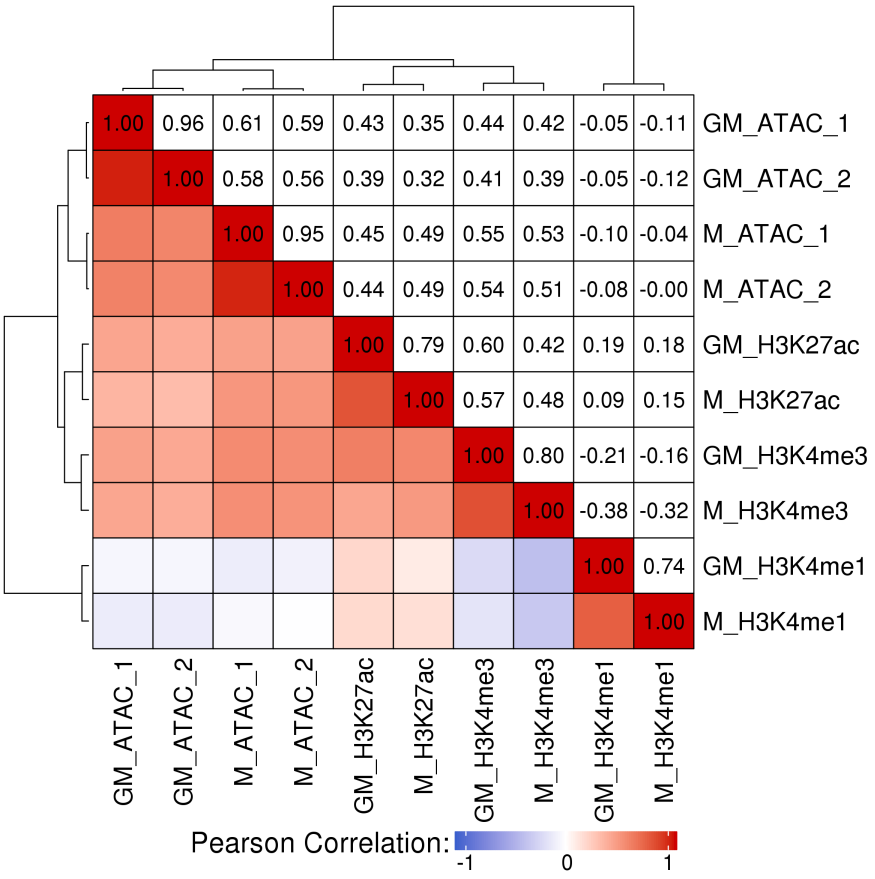

Figure 3.7. GM-BMDM vs M-BMDM chromatin correlation matrix. Pearson correlation matrix of ATAC-seq and H3K4me1, H3K4me3, and H3K27ac ChIP-seq data generated in unstimulated GM-BMDMs (GM) or M-BMDMs (M). Correlation coefficients for each comparison are indicated on the plot. Individual replicates for ATAC-seq data are shown.

In vitro differentiation of BMDMs in the presence of M-CSF and GM-CSF has been reported to affect macrophage functional responses (Murray et al., 2014; Murray, 2017). M-CSF differentiated BMDMs are typically attributed as having alternatively activated phenotypes, whereas GM-CSF differentiated BMDMs have a classic, pro-inflammatory phenotype. To assess the effect of GM-CSF priming we utilised publically available ChIP-seq data for H3K4me1, H3K4me3, and H3K27ac from GM-CSF (Accession: GSE36099) (Garber et al., 2012), and M-CSF (Accession: GSE38377 (Ostuni et al., 2013)) derived BMDMs, our own ATAC-seq generated in GM-BMDMs, and ATAC-seq generated by Laurienne Edgar in M-BMDMs. Data were analysed as described in (Chapter 2.2) and normalised reads over 66,283 peaks (representing all of the open chromatin in GM- and M- BMDMs) were used for Pearson correlation (Figure 3.7). Surprisingly this analysis reveals a strong correlation in

H3K4me1, H3K4me3, and H3K27ac ChIP-seq between M-BMDMs and GM-BMDMs (Pearson correlation coefficients of 0.74, 0.80, and 0.79, respectively). The ATAC-seq data revealed greater differences, with a mean correlation coefficient of 0.59 between GM-BMDM and M-BMDM datasets. Interestingly, we observe negative correlations of H3K4me1 with H3K4me3 and ATAC signal, likely due to a strong bias of the latter two towards promoters, from which H3K4me1 is depleted. H3K27ac, which is enriched at both enhancers and promoters, has a positive correlation with both H3K4me1 and H3K4me3.

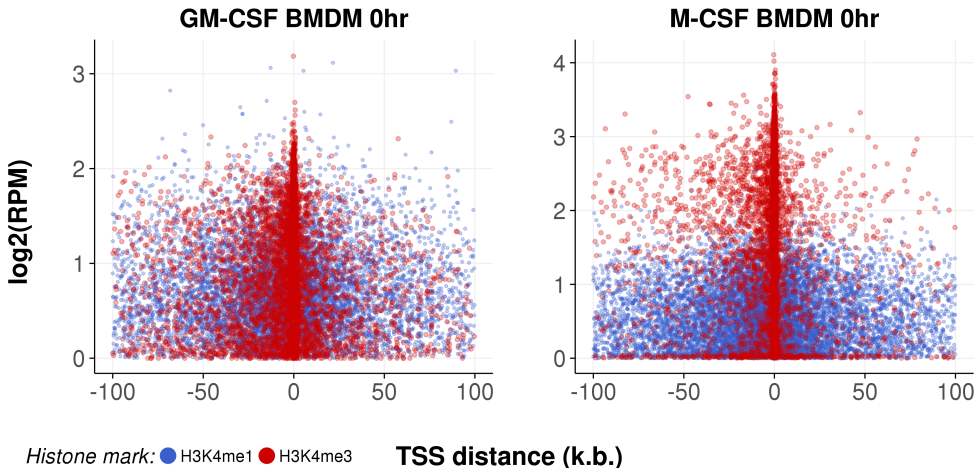

Figure 3.8. H3K4me1 and H3K4me3 ChIP signal at GM-BMDM ATAC-seq peaks. The plots indicate the position of ATAC-seq peaks in relation to the nearest transcription start sites (TSS), and the enrichment of H3K4me1 (blue) and H3K4me3 (red) at those peaks. Graphs compare ChIP data generated in GM-BMDMs (left) and M-BMDMs (right). Data are expressed as log2 reads per million (RPM) minus input.

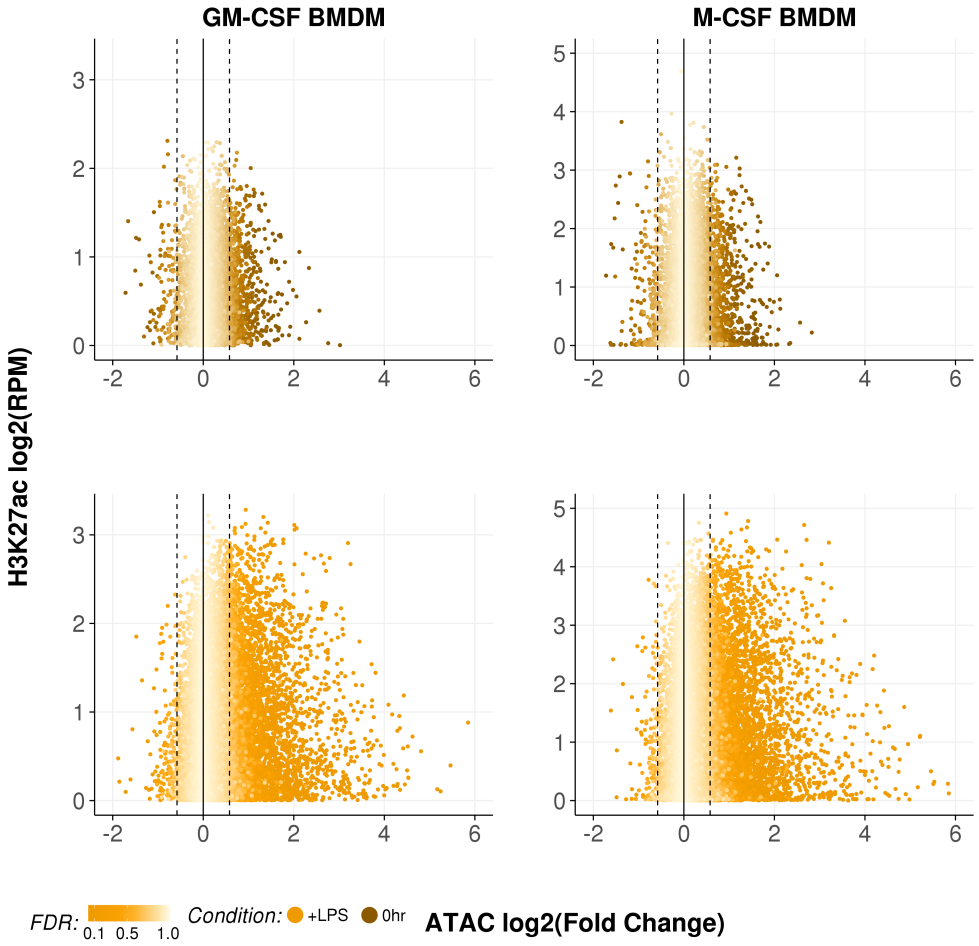

Figure 3.9. H3K27ac ChIP signal at differentially accessible GM-BMDM ATAC-seq peaks. The plots indicate the differential accessibility of ATAC-seq peaks with LPS stimulation, and the enrichment of H3K27ac at those peaks, for H3K27ac in unstimulated (brown) and LPS stimulated (yellow) BMDMs. Graphs compare ChIP data generated in GM-BMDMs (left) and M-BMDMs (right). Data are expressed as log2 reads per million (RPM) minus input. Shading indicates the FDR of changes in ATAC-seq peak accessibility with LPS stimulation.

Having observed that histone mark ChIP generated in GM- and M- BMDMs correlated remarkably well we sought to assess how well these data explained the chromatin landscape of GM-BMDMs captured by ATAC-Seq. H3K4me1 and H3K4me3 are well-described histone marks, indicative of the status of regulatory elements as either enhancers (high H3K4me1), or promoters (high H3K4me3). To check the applicability of this idiom with ChIP generated in both GM-BMDMs and M-BMDMs to our ATAC-seq data (from GM-BMDMs) we plotted the coverage of H3K4me1 and H3K4me3 at ATAC-seq peaks, organised by TSS distance (Figure 3.8). These plots show that H3K4me3 from both GM-BMDMs and M-BMDMs is enriched around TSSs in GM-BMDMs, whereas H3K4me1 (from both cell types) has a broader

distribution. Additionally we note that H3K4me3 from M-BMDMs has a narrower distribution and greater enrichment over TSS's than that generated in GM-BMDMs, this is likely due to differences in ChIP methodologies and overall quality of the data. We applied a similar procedure to test the correlation of H3K27ac ChIP from GM-BMDMs, and M-BMDMs with our ATAC-seq (Figure 3.9). The plots depict ChIP signal against ATAC-seq peak differential accessibility with LPS stimulation. This analysis shows that H3K27ac from both GM-BMDMs and M-BMDMs mark differentially accessible ATAC-seq peaks in GM-BMDMs. Again, we note that enrichment of H3K27ac from M-BMDM ChIP over ATAC peaks is greater than that of that in the GM-BMDM H3K27ac dataset, indicating greater quality of the M-BMDM ChIP dataset.

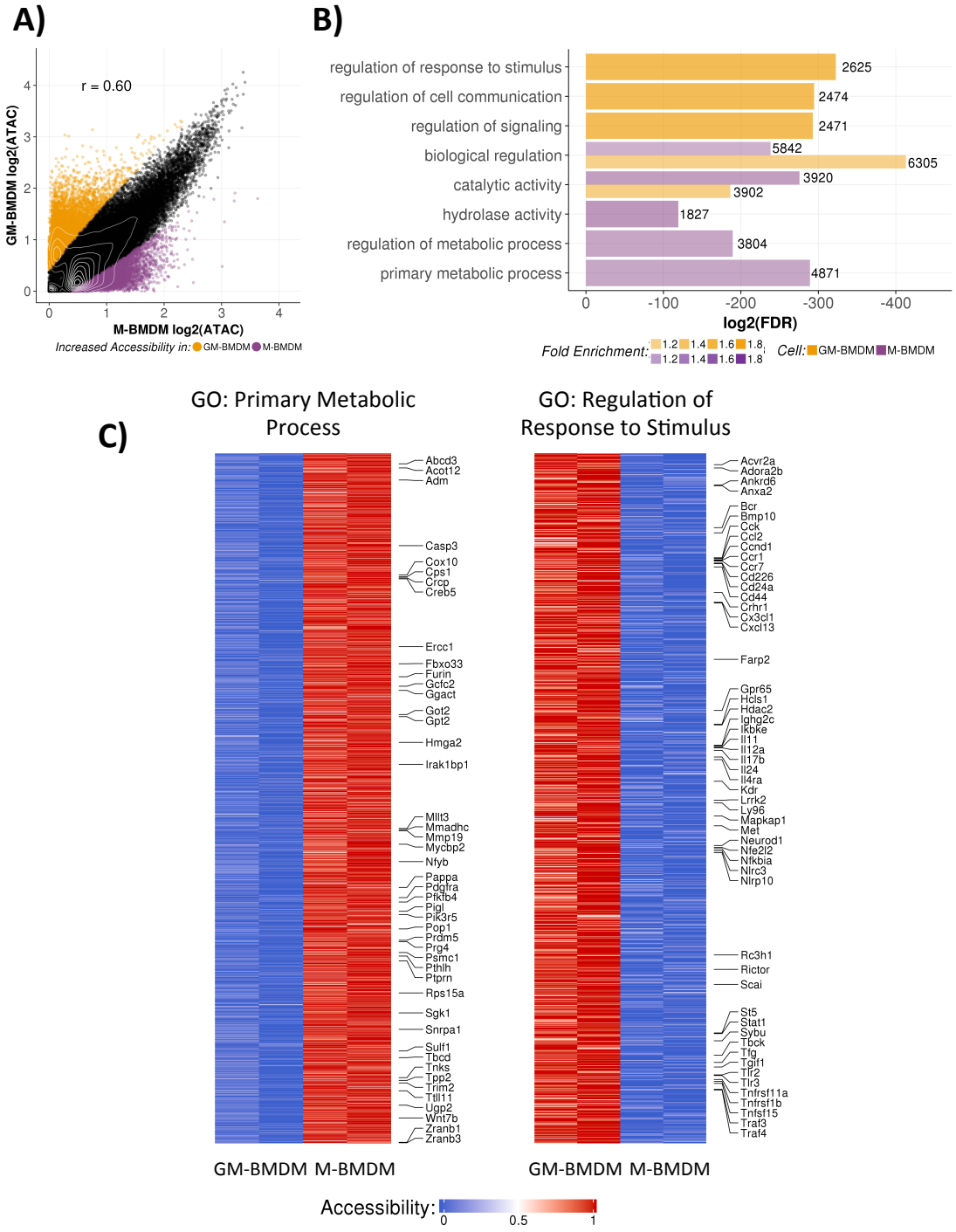

Figure 3.10. Chromatin accessibility in naïve M-BMDMs and GM-BMDMs. A) ATAC-seq signal (log2 reads per million – RPM) over all peaks in unstimulated GM- and M- BMDMs. Replicates from each condition are merged. Highlighted peaks have two fold greater ATAC signal in GM-BMDMs (yellow) or M-BMDMs (purple) than the other cell type. White density gradient shows overlapped points. **B)** Representative gene ontology categories for peaks identified in A. All categories shown have an FDR ≤ 0.05, fold enrichment is indicated by the density of shading, and the number of hits in each category are annotated in the graph. GO analysis was performed using rGREAT. **C)** Heat maps of accessibility at ATAC-seq peaks contributing to gene ontology categories. Scale indicates the relative accessibility of each peak. Representative genes from within each category are shown.

To investigate the observed variability in the ATAC-seq data between GM-BMDMs and M-BMDMs, we calculated normalised ATAC signal from both datasets over peaks representing all of the open chromatin GM- and M- BMDMs (Figure 3.10.A). We followed this procedure to account for differences in sequencing depth and methodologies between experiments. These analyses revealed two distinct groups of peaks, which had either a greater than two fold enrichment in GM-BMDMs (8,624 peaks) or M-BMDMs (8,295 peaks). The rest of the ATAC-seq peaks (49,353) were common between both cell types with a Pearson correlation coefficient of 0.88 (data not shown). To characterise the GM-BMDM and M-BMDM specific peaks we utilised gene ontology, which reveals GM-BMDM peaks to be associated with the regulation of response to stimulus and cell communication and M-BMDM peaks to be associated with metabolic processes (Figure 3.10.B). For an extended list of gene ontology terms see Chapter 8.1.2. Figure 3.10.C shows heat maps of the accessibility at the ATAC-seq peaks matching the gene ontology categories: primary metabolic process and regulation of response to stimulus in GM-BMDMs and M-BMDMs. Notably, many pro-inflammatory genes and cytokines are more accessible in GM-BMDMs than M-BMDMs, implying a role for GM-CSF for the chromatin remodelling of macrophages, priming them for inflammatory activity.

3.2.3. IRF5 and Transcriptional Termination

IRF5 is known to regulate the expression of the *Tnf* gene via its binding both 5' TSS proximal and 3' regions downstream of the TES (Krausgruber et al., 2010) suggesting a potential role for IRF5 in the regulation of the termination of transcription, promoting efficient transcription of *Tnf.* To further investigate this we biochemically isolated chromatin from GM-BMDMs (Figure 3.11.A). This is enriched for stable complexes of polymerase, template DNA, and nascent RNA, from which we extract the chromatin-associated (chrRNA). These transcripts are non-polyadenylated and indicative of active transcription, being enriched for splice junctions over the nucleoplasmic fraction, which contains a higher proportion of exons to immature transcripts containing splice sites (Figure 3.11.B). We therefore utilise nascent

chrRNA as a direct measure of transcription (Figure 3.11.C). We observed large increases in the quantity of *Tnf* transcripts detected by this method at the first exon of the *Tnf* gene in response to LPS stimulation, demonstrating increased transcription (Figure 3.12.B), which was significantly lower in IRF5$^{-/-}$ GM-BMDMs compared to WT (p=0.0016). To assess the effect of IRF5 on the level of read-through transcription past the TES, indicative of termination defects, we performed qPCR with primers mapped across the *Tnf* loci (Figures 3.12.A and 3.12.C), these data are normalised to *Tnf* exon1 (primer pair C) in order to assess changes in transcription profiles across the *Tnf* loci. The results indicate that the termination of *Tnf* transcription is unaffected by IRF5, occurring within 1 k.b. of the TES in both WT and IRF5$^{-/-}$.

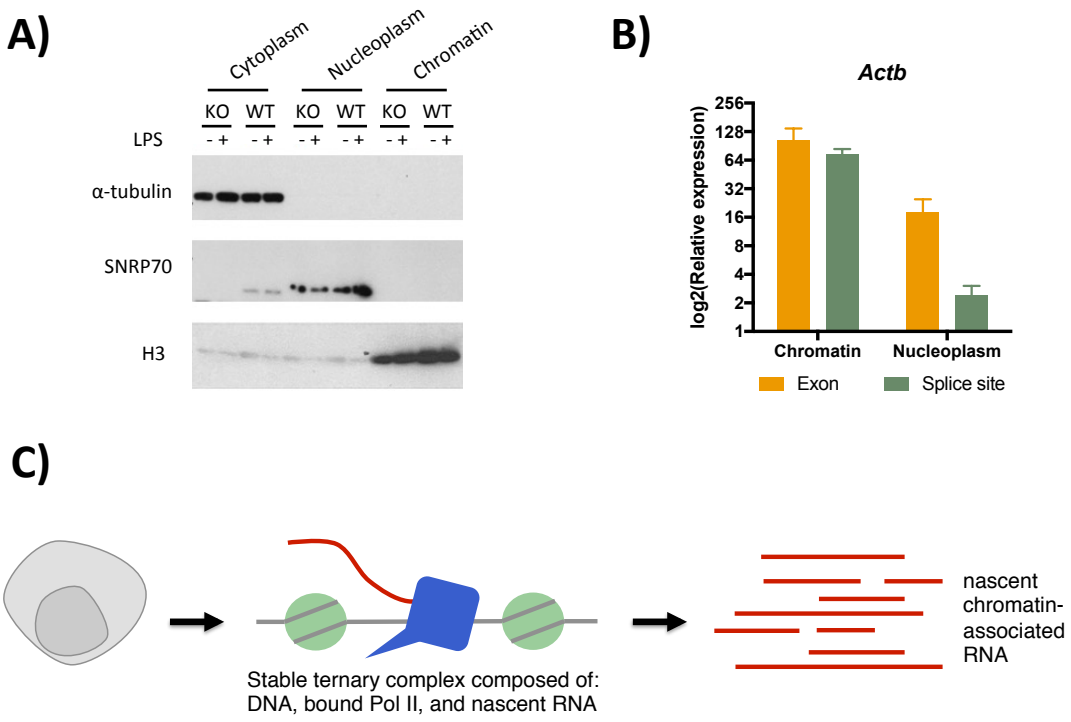

Figure 3.11. Chromatin-associated RNA (chrRNA) is representative of active transcription. A) Protein levels of α-tubulin, SNRP70, and H3 across subcellular fractions was determined by western blot. Experiment is representative of four independent experiments. **B)** qPCR of chrRNA and RNA from nucleoplasmic fraction from unstimulated WT GM-BMDMs, primers correspond to exons or exon intron junctions. Error bars represent standard error of the mean for n=4. **C)** chrRNA is isolated biochemically from chromatin, containing stable ternary complexes of RNA Pol II, the DNA template, and nascent RNA.

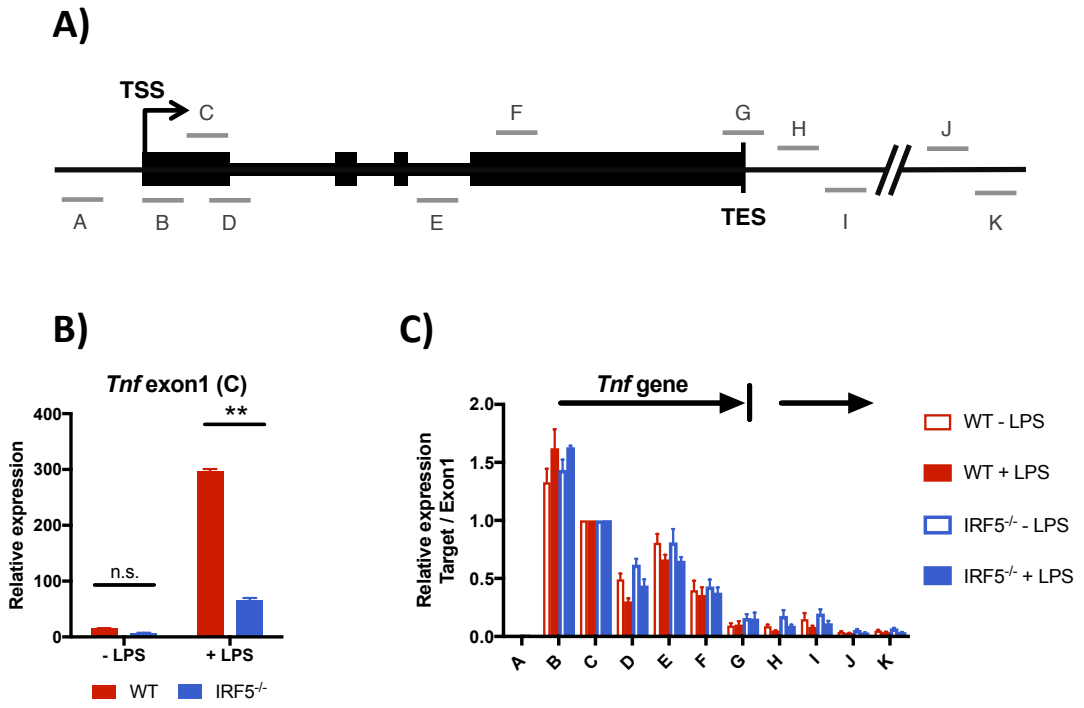

Figure 3.12. The effect of IRF5 on the termination of *Tnf* transcription. A) *Tnf* gene with approximate primer positions indicated. **B)** qPCR of *Tnf* exon1 (primer pair C) in chrRNA from WT and IRF5$^{-/-}$ GM-BMDMs, unstimulated or treated with LPS. **C)** qPCR of chrRNA from WT and IRF5$^{-/-}$ GM-BMDMs, unstimulated or treated with LPS. qPCR was performed with primers mapped over the *Tnf* loci, as in (A). Data from each sample are normalised to exon 1 to compare transcription profiles across the gene loci. Asterisks indicate significance thresholds (*p<0.05, **p≤0.001) of two-tailed unpaired t-test. Error bars represent standard deviation for n=3.

We conducted sequencing of chromatin-associated RNA (chrRNA-seq) to assess the effect of IRF5 on the termination of transcription genome wide. ChrRNA-seq was conducted and analysed as described in Chapter 2.1.2 and 2.2.3. These data are enriched for nascent transcripts and therefore contain introns, providing coverage over the entire transcription unit (Figure 3.13.A). We noted that some genes have higher coverage at exons than introns; this is likely due to co-transcriptional splicing. Visual assessment of quantitated reads shows that IRF5 binding to the 3' ends of genes does not appear to affect transcriptional termination, with the amount of read-through transcription past the annotated TES not differing between WT and IRF5$^{-/-}$ samples. We generated metagene profiles focussed on annotated TES's for all genes with IRF5 ChIP peaks (Saliba et al., 2014) (Figure 3.13.B). These average profiles also indicate that IRF5 has no effect on the termination of transcription, the only effect of IRF5 being increased levels of transcription prior to the TES. To assess this

quantitatively we calculated a termination index, based on the ratio of reads falling within the gene and downstream of the TES (as described in Chapter 2.2.3), which is representative of the efficiency of termination. Figure 3.13.C reveals that there is no significant difference in the efficiency of transcriptional termination due to the actions of IRF5.

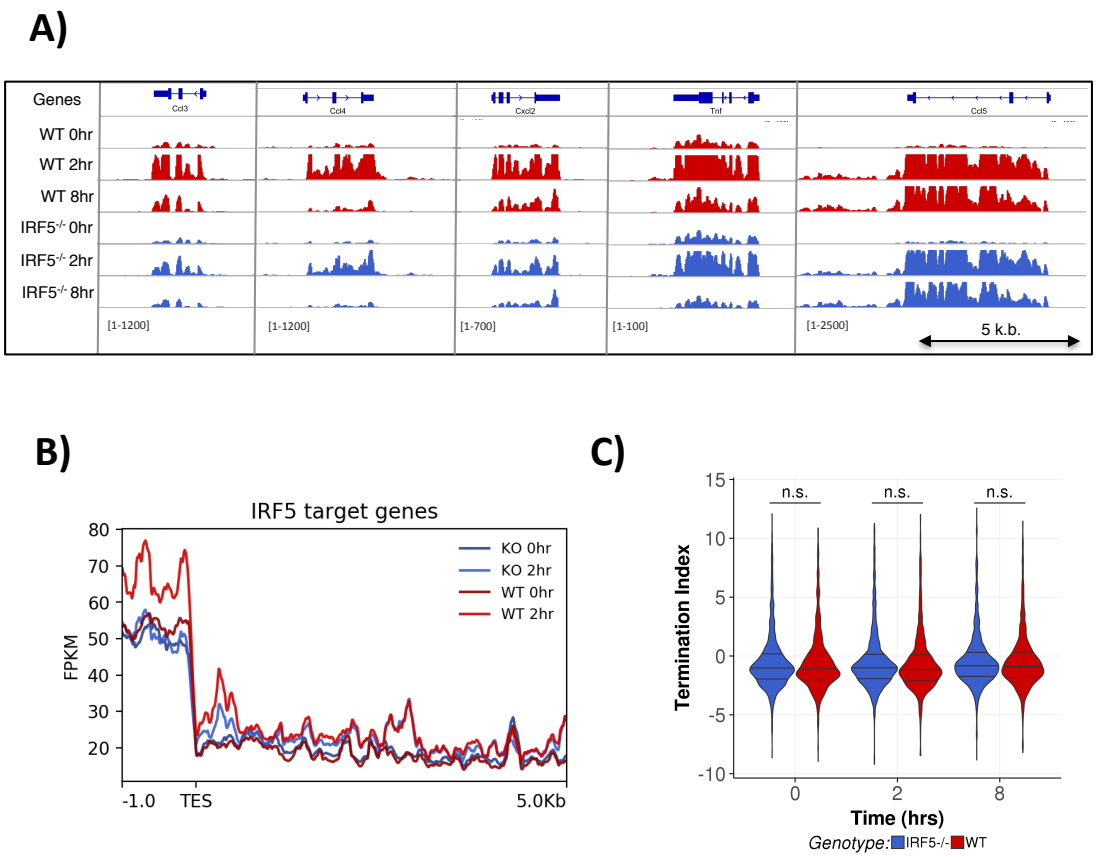

Figure 3.13. The effect of IRF5 on the termination of transcription genome wide. A) Representative snapshots depicting chrRNA profiles at the 3' ends of genes. Scales are indicated on the image, units are fragments per kilobase per million (FPKM). **B)** Meta-gene profile of chrRNA TES -1 k.b. to TES +5 k.b. of IRF5 target genes. **C)** Termination index for IRF5 target genes.

3.3. Discussion

Macrophages are attributed with a high degree of plasticity, able to adapt to their local environment and fulfil specific functions on the basis of stimuli and signals encountered. This plasticity is mediated by the processing of complex *milieu* of signals resulting in the modification of the underlying chromatin landscape. We therefore conducted ATAC-seq, a powerful technique for assaying chromatin accessibility (Figure 3.1) (Buenrostro et al., 2013). The aim of this investigation was to characterise the chromatin remodelling events mediating the phenotypic shift of macrophages with LPS stimulation, and to ascertain to what extent IRF5 contributed to this. We included neutrophils in our experimental design in order to contrast with macrophages, with the expectation that they would be relatively unaffected by LPS stimulation at the level of chromatin. Broadly the neutrophil data reflects that of the macrophages, with a strong bias towards promoters (Figure 3.2.A), and as we expected the main variation in the data is due to cell type, followed shortly by the effect of LPS stimulation on macrophages (Figure 3.3). However, to our surprise we note that neutrophils also possess a large proportion of LPS sensitive peaks (9,730 compared with 25,956 in WT macrophages) (Table 3.1). This observation stands up to closer scrutiny with 3,839 macrophage peaks being called as significantly differentially accessible in response to stimuli, along with 656 neutrophil peaks (Figure 3.4.A). Notably we did not detect any broad distribution of ATAC-seq signal indicative of widespread nuclear decondensation prior to NETosis described by others (X. Chen et al., 2016), however, LPS is often insufficient to induce NETs, rather a stimulus such as phorbol 12-myristate 13-acetate (PMA) as used by (X. Chen et al., 2016) is normally required. In fact our ATAC-seq in neutrophils had a higher FRIP than macrophages, indicating very specific enrichment at distinct foci (Figure 3.2.B).

Neutrophils are commonly cited as being short lived and transcriptionally quiescent, having fully differentiated in the bone marrow during which time they are pre-furnished with antimicrobial molecules, stored in granules, for release upon exposure to inflammatory stimuli. Nevertheless, a growing body of evidence supports the notion that neutrophils play

a more sophisticated role in inflammation, actively regulating inflammatory processes, and being able to release a variety of immunoregulatory cytokines contributing to both acute and chronic inflammation (Tecchio et al., 2014; Kolaczkowska and Kubes, 2013). The chromatin landscape and transcriptional responses of naïve neutrophils substantially differ from that of macrophages and monocytes (Lara-Astiaso et al., 2014). However, in the context of LPS stimulation we observe a large portion (534, out of 656) of differentially accessible peaks present in neutrophils overlapping with peaks of differentially accessible chromatin in macrophages (Figures 3.4.A and 3.2.C). These peaks correspond to inflammatory genes associated with the innate immune response, implying overlapping function of neutrophils and macrophages in the immediate response to infection (Figure 3.4.B). Examining the distance from TSS's of the shared macrophage and neutrophil peaks reveals that they are predominantly enriched proximal to promoters (data not shown). This coincides with interrogations of monocyte and neutrophil expression quantitative trait loci (eQTLs), which reveal that whilst there are some shared eQTLs, most are dependent on cellular context and subsequent enhancer status (Naranbhai et al., 2015). Neutrophil specific peaks encompass the migratory capacity of neutrophils to seek out sites of inflammation and to handle high levels of reactive oxygen species (ROS), whereas macrophage specific peaks pertain to metabolic processes, which are dynamically regulated under inflammatory conditions (O'Neill and Pearce, 2016).

IRF5 mRNA and protein levels have been shown to be induced by monocyte exposure to GM-CSF, the expression of which promotes a pro-inflammatory macrophage phenotype (Krausgruber et al., 2011). We therefore hypothesised that IRF5 may play a role in the establishment of de novo enhancers during activation of macrophages by inflammatory stimuli, leading to enhanced inflammatory cytokine production. However, we observed no differences due to the actions of IRF5 on macrophage chromatin accessibility in both unstimulated and LPS stimulated cells (Figure 3.5.B). Additionally, examining nucleosome occupancy at *cis*-regulatory elements of key IRF5 target genes *Tnf* and *Il12b* demonstrated

that IRF5 has no role in maintaining chromatin accessibility at these loci after LPS exposure (Figure 3.6.B). Recently, IFN-γ, another factor commonly used to polarise BMDMs towards an inflammatory phenotype (Murray, 2017), has been demonstrated to decommission enhancers associated with M2-like functions (Kang et al., 2017) in addition to its role in priming cis-regulatory elements associated with inflammatory genes, readying BMDMs for inflammatory responses, for which it's well known (J. Chen and Ivashkiv, 2010; Piccolo et al., 2017; Kang et al., 2017). We therefore investigated the effect of GM-CSF priming on BMDM cultures, contrasting histone marks indicative of chromatin status and ATAC-seq data from GM-BMDMs with that generated in M-BMDMs (Figure 3.7). This analysis reveals that histone mark ChIP is remarkably consistent between differentiation protocols, and that the key markers of enhancer and promoter status (H3K4me1, and H3K4me3, respectively) and activation (H3K27ac) generated in M-BMDMs are equally representative of chromatin status in GM-BMDMs (Figures 3.8 and 3.9). ATAC-seq provides a more sensitive measure of the chromatin landscape, directly assaying accessibility, thus uncovering distinct loci that exhibited a two fold increase in accessibility in either GM-BMDMs or M-BMDMs (Figure 3.10.A). Upon investigation we attributed M-BMDM enriched peaks with metabolic function, whereas GM-BMDM peaks were associated with inflammatory genes (Figure 3.10.B and C). Together these data suggest a role for GM-CSF in priming macrophages for activation, basally increasing the accessibility of *cis*-regulatory elements associated with inflammatory genes. This is in keeping with the biology of GM-CSF, which contrary to M-CSF, and in spite of its name, is not expressed at steady-state or required for myelopoiesis - with the exception of embryonically derived alveolar macrophages (Guilliams et al., 2013; Schneider et al., 2014). Rather its secretion by activated leukocytes at sites of tissue inflammation acts to promote myeloid inflammatory responses, broadly acting to promote tissue damage associated with chronic inflammation and autoimmune disorders (Becher et al., 2016). More specifically, GM-CSF has been demonstrated to promote inflammatory phenotypes of Ly6C^{hi} monocyte derived macrophages, inducing genes associated with their phagocytic ability, inflammasome activation, and chemotaxis (Croxford et al., 2015), although the precise

molecular mechanisms of the inflammatory activity of GM-CSF are not understood (Ushach and Zlotnik, 2016; Becher et al., 2016). Our data therefore reveals that GM-CSF primes macrophages at the chromatin level to respond to inflammatory stimuli, and that IRF5, despite being a target of GM-CSF signalling pathway (Krausgruber et al., 2011), is not involved in this process.

Based on our observations of IRF5 binding to both 5' and 3' regions of the *Tnf* gene (Krausgruber et al., 2010) we hypothesised that IRF5 may promote efficient transcription, by contributing to termination of transcription or gene looping. We investigated the effects of IRF5 on transcriptional termination by utilising chrRNA, which is enriched for nascent transcripts, indicative of active transcription (Figure 3.11). By assessing chrRNA profiles across the *Tnf* loci we demonstrate that IRF5 affects the total level of transcription (Figure 3.12.B), but does not have any effect on the termination of transcription (Figure 3.12.C). We extended these studies genome wide based on the observed enrichment of IRF5 at 3' ends of other inflammatory target genes (data not shown). However, analysis of these data confirms that termination of transcription at IRF5 target genes is not affected by IRF5 (Figure 3.13), rather, we observed increased transcription within the bodies of IRF5 regulated genes, indicative of increased Pol II recruitment via the 5' activity of IRF5. We therefore did not proceed to investigate the termination mechanisms discussed in Chapter 1.2.2. These data do not preclude the possibility of gene looping and increased efficiency of transcription mediated by Pol II recycling at the *Tnf* gene, however, to determine whether this is occurring data encompassing chromatin conformation generated by chromatin capture techniques (de Wit and de Laat, 2012) would be required.

4. IRF5 Regulated Gene Expression

4.1. Introduction

Macrophage inflammatory responses have typically been defined as fitting either the M1 (classically) or M2 (alternatively) activated phenotypes. However, appreciation of the *in vivo* complexity of the milieu of polarizing factors macrophages are exposed to and the resulting heterogeneity in macrophage responses is growing (Murray et al., 2014). The classic view of macrophage activation corresponds to *in vitro* polarization with pro-inflammatory stimuli such as IFNγ, and LPS, leading to robust inflammatory responses. Classically activated M1 macrophages are characterised by expression of key markers such as *Tnf*, *Il12a*, *Il12b*, *IL1a*, *Il1b*, *Il6*, *Il23a*, *Csf2* (GM-CSF), *Ccl1*, *Ccl11*, *Cxcl2*, *Cxcl13*, *Nos2*, and *Marco*. Alternative treatment with IL-4 or IL-13 stimulates M2 polarisation, which is distinguished by the markers: *Retnla* (FIZZ1), *Irf4*, *Mrc1* (mannose receptor), *Arg1* (arginase-1), *Clec7a* (dectin-1), *Socs2*, *Ppard* (PPARδ), and *Pparg* (PPARγ) (Murray, 2017). These alternatively activated macrophages are more capable at handling parasitic infection, wound healing, and repair related functions than their inflammatory counterparts, which mediate sterilising inflammation for the efficient killing of bacterial and intracellular pathogens. Within this context IRF5 has been shown to be a crucial mediator of inflammatory macrophages *in vivo* and classical macrophage activation *in vitro*. Its induction leads to TNF, IL-6, IL-12 and IL-23 secretion whilst simultaneously repressing IL-10 and TGF-β (Krausgruber et al., 2011; Ouyang et al., 2007; Dalmas et al., 2015). IRF5 expression is therefore integral for the inflammatory polarization of macrophages and has an immunomodulatory role, promoting Th1 and Th17 responses. We hypothesized that the contribution of IRF5 to changes in gene expression during macrophage activation is broader than the regulation of cytokines and chemokines previously described. To further dissect the role of IRF5 in the context of LPS stimulation, we utilize mRNA-seq and chrRNA-Seq approaches to uncover the effects of IRF5 on macrophage transcription.

4.2. Results

4.2.1. IRF5 in the macrophage inflammatory response

To elucidate the role of IRF5 in macrophage inflammatory responses we examined RNA sequencing of polyadenylated mRNAs in WT and IRF5$^{-/-}$ GM-BMDMs in unstimulated and LPS stimulated cells, through an eight-hour time course. mRNA-seq was performed by David Saliba and the data was processed as described in (Chapter 2.2.4). ChrRNA-seq, which is indicative of Pol II recruitment and active transcription, was conducted during the course of this study as described in Chapter 2.1.2. Analysis of the mRNA-seq dataset with DESeq2, reveals a total of 7,385 genes to be differentially expressed (FDR ≤ 0.05, fold change ≥ 1.5) throughout the time course and between IRF5$^{-/-}$ and WT GM-BMDMs. VST counts of differentially expressed genes were used for PCA of the data (Figure 4.1.A). This demonstrates that the largest principal component (56.32% of variance) describes changes in gene expression by time, from zero hours through to eight hours after LPS stimulation, sequentially. The next principal component separates unstimulated and late time points (four and eight hour) from the early time points (one and two hour) (16.22% of variance). Following this, the third principle component separates the samples by genotype, reflecting the effect of IRF5 on gene expression, and accounting for 12.95% of the total variance in the data. There is a drop in the proportion of variance explained by each principal component past the third component, illustrated in the scree plot, indicating that most of the variance is explained by these first three factors. A useful method of non-linear dimensionality reduction in large datasets is t-distributed stochastic neighbour embedding (t-SNE) (Maaten and Hinton, 2008), which differs from PCA in that it preserves local information. Figure 4.1.B shows this as a scatter plot, with additional annotations of clusters described by K-means clustering. Visualisation with t-SNE reflects the principal components, in that the data cluster primarily by time point. However, at the late time points (four and eight hours) the samples cluster instead by genotype (clusters B and D), implying a more pronounced role for IRF5 later in the LPS response. This is reflected in the chrRNA-seq data, analysis of which reveals

the greatest number of differentially expressed genes (1,029) (FDR ≤ 0.05, fold change ≥ 1.5) between WT and IRF5$^{-/-}$ after eight hours of LPS stimulation (data not shown).

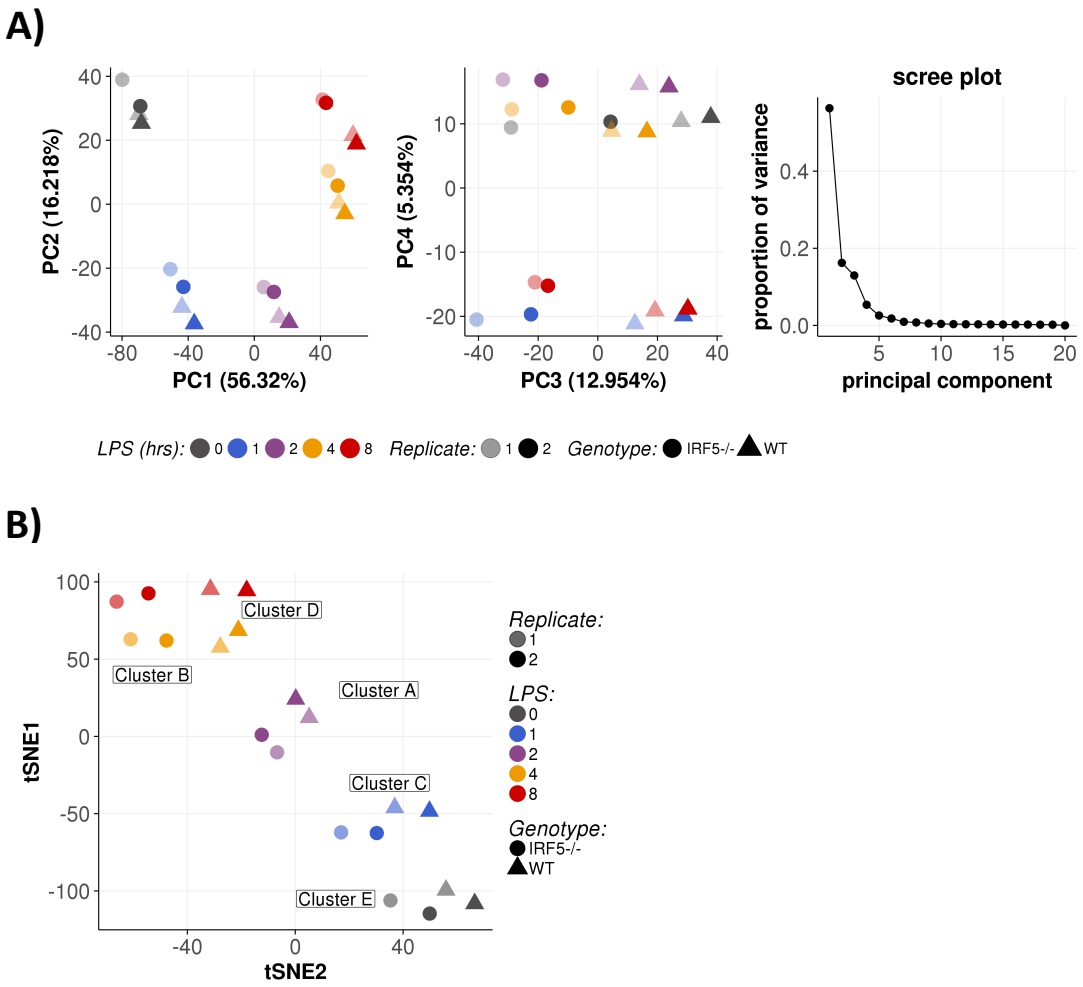

Figure 4.1. mRNA-seq dimensionality reduction. A) mRNA-seq data from wild type and IRF5$^{-/-}$ GM-BMDMs. Differential expression of protein coding genes was calculated with DESeq2 with an FDR of 0.05 and fold change > 1.5. Variance stabilised (VST) counts of 7,385 differentially expressed genes were then used for principal component analysis. The first 4 principle components are shown, in addition to a scree plot indicating the proportion of variance attributable to each component. **B)** t-Distributed Stochastic Neighbor Embedding (t-SNE) dimensionality reduction of VST counts of differentially expressed genes (perplexity=5), with annotated K-means clusters.

In order to assess the role of IRF5 within the LPS response we made direct comparisons between IRF5$^{-/-}$ and WT samples at each time point, which we compare with the total number of genes differentially expressed in response to LPS stimulation (FDR ≤ 0.05, fold change ≥ 1.5) (Table 4.1). Comparing LPS and IRF5 regulated genes throughout the time course we find that LPS leads to dynamic regulation of thousands of genes, with an even split between up- and down-regulated genes. IRF5 also mediates dynamic changes in gene

expression, with the number of up-regulated genes highest eight hours after LPS stimulation (948 genes) and the number of down-regulated genes highest at just one hour after LPS stimulation (1,200 genes), implying different kinetics for the different classes of genes under IRF5s control. Surprisingly, we also see IRF5 regulated genes in unstimulated cells, with 466 up-regulated, and 760 down-regulated genes. These data are represented graphically in Figure 4.2, for the zero, one, and eight -hour time points. Highlighted genes are hits for the top gene ontology terms corresponding to significantly up- and down- regulated genes in each condition (data not shown). These data indicate that LPS stimulation causes very pronounced changes in gene expression with genes pertaining to the inflammatory response, displaying large fold changes in their expression at both one and eight hours after LPS stimulation. LPS down-regulated genes display smaller fold changes with stimulation and decreased total expression levels than up-regulated genes. In contrast IRF5 mediates a much smaller degree of change, leading to up-regulation of TLRs, pro-inflammatory cytokines, and chemokines and down-regulation of genes associated with extracellular matrix remodelling.

	LPS.up	LPS.down	IRF5.up	IRF5.down
Unstimulated	0	0	466	760
1hr LPS	928	1,144	769	1,200
2hr LPS	1,807	2,142	603	572
4hr LPS	2,308	2,523	450	296
8hr LPS	2,357	2,584	948	576

Table 4.1. Number of LPS and IRF5 up- and down- regulated genes. DESeq2 differentially expressed genes in WT vs WT 0hr (LPS up/down) and WT vs IRF5$^{-/-}$ (IRF5 up/down). Number of genes displayed are differentially expressed with an FDR < 0.05 and fold change > 1.5.

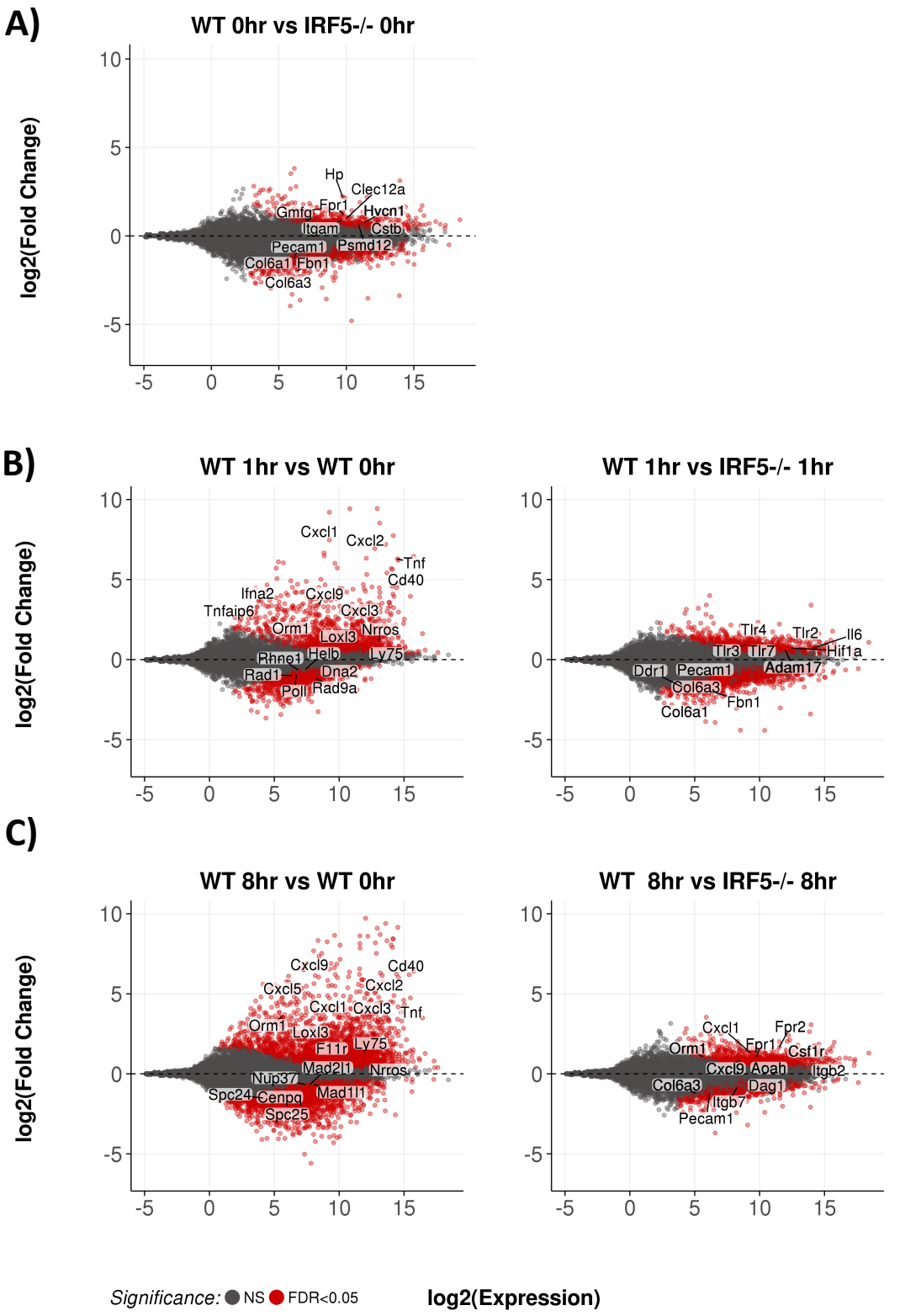

Figure 4.2. LPS & IRF5 differentially expressed genes. Differential expression of protein coding genes was calculated with DESeq2 with an FDR of 0.05. Labeled genes are from top gene ontology results for up- and down- regulated genes at each time point. **A)** MA plots indicating differentially expressed genes (red) between WT 0hr and IRF5$^{-/-}$ 0hr. **B)** Comparison between WT 1hr and WT 0hr, and WT 1hr and IRF5$^{-/-}$ 1hr. **C)** WT 8hr vs WT 0hr, and WT 8hr vs IRF5$^{-/-}$ 8hr.

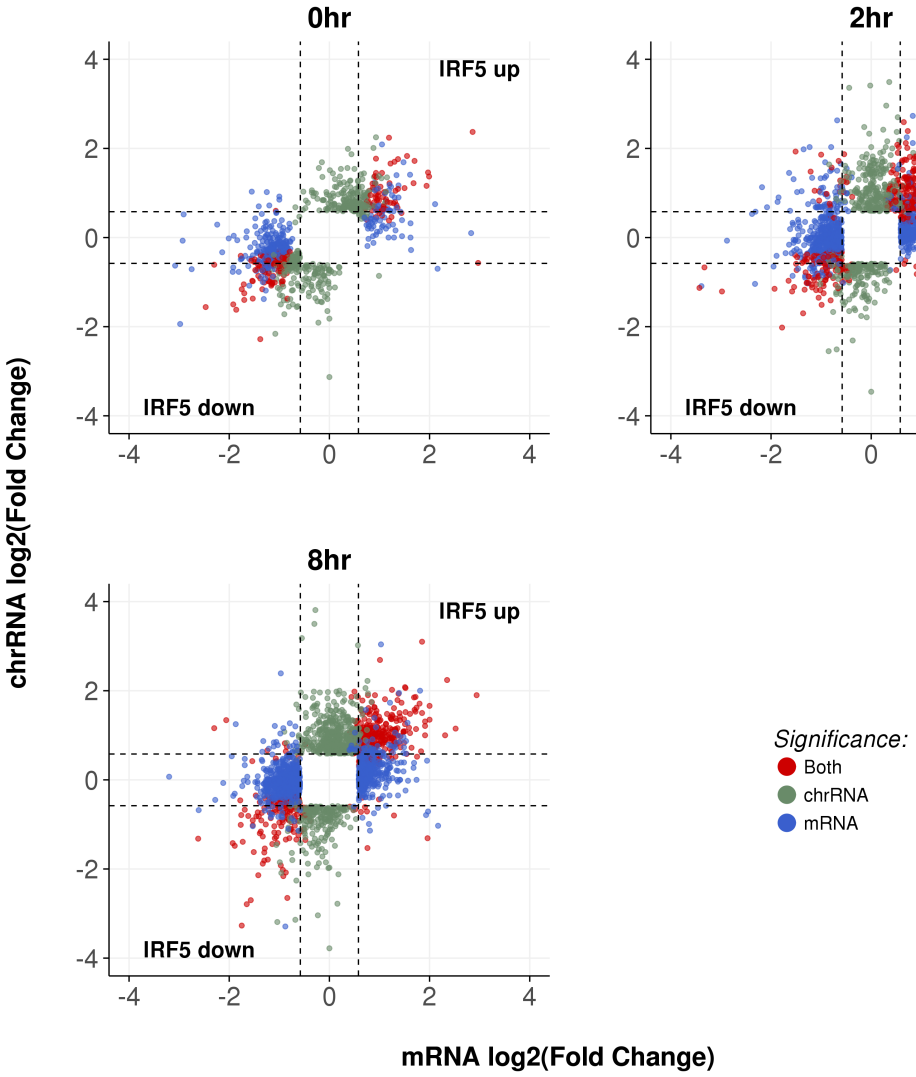

Figure 4.3. Comparison of IRF5 regulated genes detected by chrRNA-seq and mRNA-seq. chrRNA- vs mRNA- seq DESeq2 results, comparing WT and IRF5$^{-/-}$ at 0hr, 2hr, and 8hr time points. Significance threshold is a FDR of < 0.05 and fold change of > 1.5. Points are either significantly differentially expressed in the chrRNA-seq (green), mRNA-seq (blue), or both (red). chrRNA and mRNA -seq comparison was conducted by Dr. Stephen Sansom.

In order to validate our initial findings we made a comparison between genes differentially expressed by mRNA-seq with genes differentially expressed by chrRNA-seq, which is directly indicative of changes in transcription (Figure 4.3). These data reveal that transcriptional changes correlate very well with the detected mRNA levels, with the majority of IRF5 up-regulated genes detected by mRNA-seq displaying increased transcription by chrRNA-seq compared to the IRF5$^{-/-}$ and *vice versa* for IRF5 down-regulated genes. Interestingly with LPS stimulation, some genes displaying increased transcription in WT GM-BMDMs by chrRNA-

seq have decreased mRNA levels (this is particularly notable two hours after LPS stimulation), implying an active role for post-transcriptional processing in regulating mRNA levels in inflammatory responses and suggesting a role for IRF5 in the regulation of these processes (discussed further in Chapter 4.3).

4.2.2. LPS time course analysis

To characterise transcriptional responses more effectively we scaled the VST counts of all differentially expressed genes and focused on their relative expressions, performing hierarchical clustering and visualising the data as a heat map (Figure 4.4). Similar to the t-SNE (Figure 4.1.B) we see WT and IRF5$^{-/-}$ samples represented within each time point cluster, apart from at eight hours, where the IRF5$^{-/-}$ samples cluster with those at the four-hour time point. The differentially expressed genes split broadly into LPS up- and down- regulated categories, with a gain or loss of expression over time. Further sub-divisions are illustrated by coloured dendograms (clusters one to five). Cluster one represents rapidly up-regulated genes, which are induced with one hour of LPS stimulation and continue to be expressed at a greater level than in unstimulated cells. This cluster is enriched for gene ontology categories pertaining to chemokine and cytokine activity and the inflammatory response (see Chapter 8.2.1. for an extended list of gene ontology terms). IRF5 has the greatest effect on this category at the eight-hour time point. Cluster two genes are induced more slowly, with an increase in expression observable after two hours. These genes are associated with the IFN response and are less affected by IRF5. Cluster three represents genes that are associated with neutrophil degranulation, proteolysis, and NFκB signalling. These genes are only notably up regulated from their basal level of expression at the late (four and eight – hour) time points. Clusters four and five are both down-regulated with LPS stimulation. Cluster four has a marked difference between the WT and IRF5$^{-/-}$ in terms of basal expression levels and the level of down-regulation, with higher expression observed in the IRF5$^{-/-}$. Gene ontology categories for cluster four are: protein phosphorylation, actin

cytoskeletal organisation, and apoptotic cell clearance. Cluster five isn't obviously affected by IRF5 and corresponds to functions involving the cell cycle and protein phosphorylation.

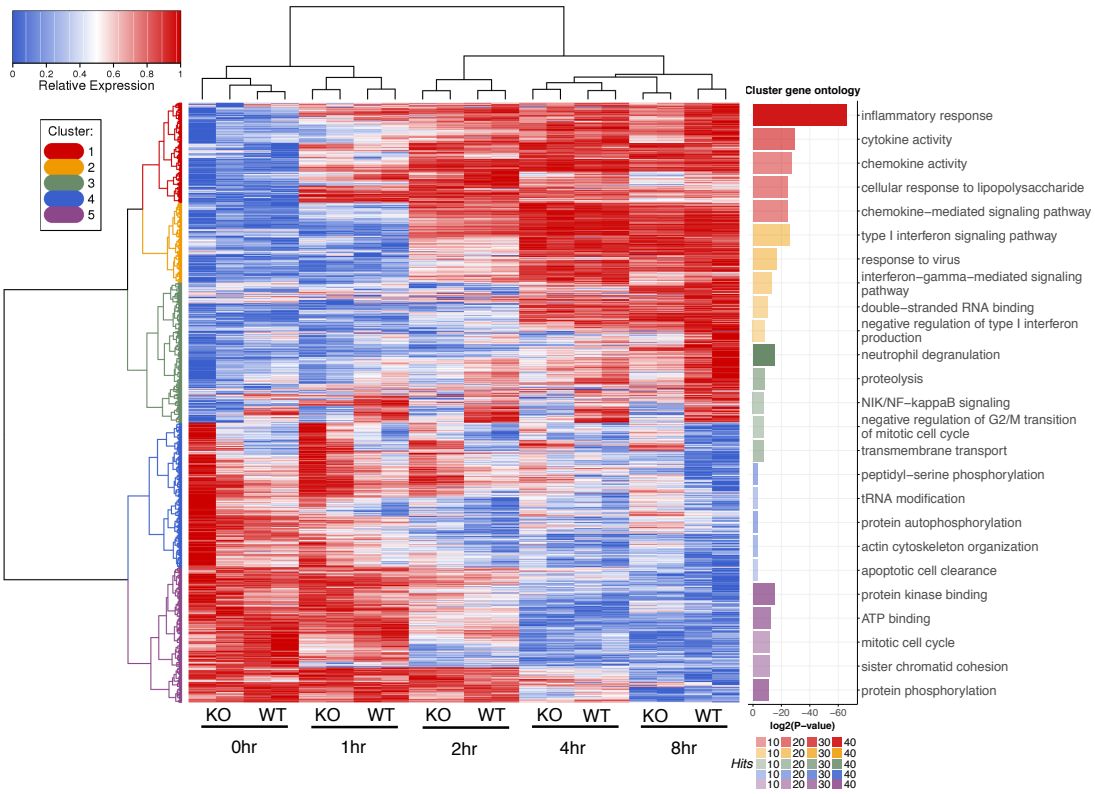

Figure 4.4. Effect of IRF5 on LPS responsive genes. Heat map shows 7,385 differentially expressed genes (FDR < 0.05). Data shown are relative variance stabilised counts, normalised to each gene. Hierarchical clustering was performed using the Ward method on Manhattan distances. Gene ontology categories for genes in each cluster were acquired using enrichr and representative results are shown.

To further characterise the identified clusters we intersected the expression data with our GM-BMDM ATAC-seq to functionally define promoters as peaks of open chromatin within 2.5 k.b. of gene TSSs (data not shown). We then examined the enrichment of: histone marks (H3K4me1, H3K4me3, and H3K27ac ChIP-seq generated from M-BMDMs, accession ID: GSE38377 (Ostuni et al., 2013)) as indicators of chromatin status, chrRNA (from GM-BMDMs) as a measure of transcriptional activity, and ATAC signal (from GM-BMDMs) as a measure of promoter accessibility, at these promoters (Figure 4.5). TSS proximal ATAC-seq peaks from all of the clusters are enriched for H3K4me3 and depleted of H3K4me1,

indicating their status as promoters, and both of these marks are refractory to LPS stimulation. Interestingly, promoters in every cluster have basal enrichment of ATAC-seq signal with only a slight increase in signal observable with LPS stimulation for clusters one, two, and three. H3K27ac is a marker of activation and increases with LPS stimulation at promoters of the up regulated clusters (one, two, and three), whereas clusters four and five, which are down regulated by LPS, lose H3K27 acetylation with stimulation. The chrRNA signal (representing active transcription) shows transcription to be initiating at the promoters identified. As a marker of promoter activity it is clear that transcription at clusters one and two increases markedly with stimulation, whereas cluster three has a higher level of transcription before stimulation and a smaller increase with LPS. On the other hand, clusters four and five are clearly down regulated with stimulation.

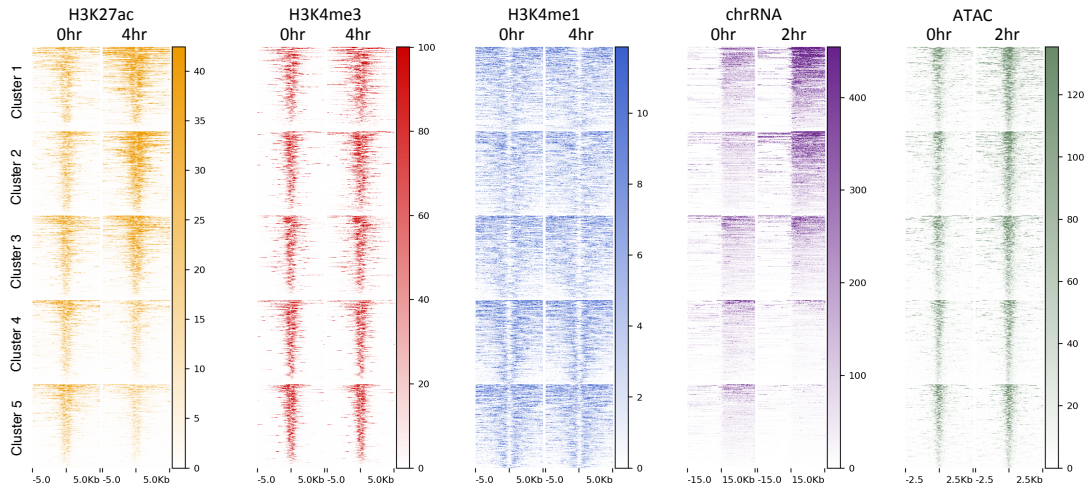

Figure 4.5. Promoter activity of genes in clusters. Heat maps depicting H3K27ac (yellow), H3K4me3 (red), H3K4me1 (blue), chrRNA (purple), and ATAC (green) coverage at promoters of the top 200 genes in each cluster (ranked by gene expression). ChIP data are expressed as fold enrichment over input, chrRNA and ATAC data are expressed as fragments per kilobase per million (FPKM). Distances from promoter ATAC peaks are indicated on the x-axis of each plot in kilobases (k.b.).

We next examined the average expression profiles of the constituent genes from each cluster (Figure 4.6.A). These data show that cluster 1 is rapidly induced upon LPS stimulation, the kinetics of which aren't affected by IRF5. Expression levels of genes in cluster one are very low prior to stimulation and plateau at ~60 TPM in the WT, and ~40 TPM in the $IRF5^{-/-}$. Genes in cluster two are induced more slowly, gradually rising to ~40 TPM by eight hours post LPS stimulation, with a small difference in the mean expression values between WT and $IRF5^{-/-}$ macrophages at the eight hour time point, otherwise IRF5 a negligible effect on their expression. Cluster three contains genes that are expressed basally, and are up regulated in response to LPS. Interestingly, basal gene expression is higher in the WT than the $IRF5^{-/-}$, as is gene expression at subsequent time points, however the kinetics are unaffected by IRF5. Genes in cluster four are expressed at a much lower level and are down regulated in response to LPS, expression levels in the $IRF5^{-/-}$ are higher at all of the time points than in the WT. Cluster five is also down-regulated in response to LPS, with no evident effect of IRF5. Expression levels for the top fifty expressed genes in each cluster are detailed in Chapter 8.2.2.

In order to more accurately ascertain whether IRF5 was having a significant effect of gene expression in each cluster we checked the fold change of genes between WT and $IRF5^{-/-}$ at each time point for all differentially expressed genes (Figure 4.6.B). Fold change values for the top fifty genes in each cluster, by gene expression, are listed in Chapter 8.2.3. From this analysis it is evident that IRF5 has the largest positive effect on gene expression for genes in cluster one and three, and negatively regulates genes in cluster four, whilst having little effect on cluster two and cluster five. Further details on the numbers of IRF5 up and down regulated genes in each cluster are tabulated in Chapter 8.2.4.

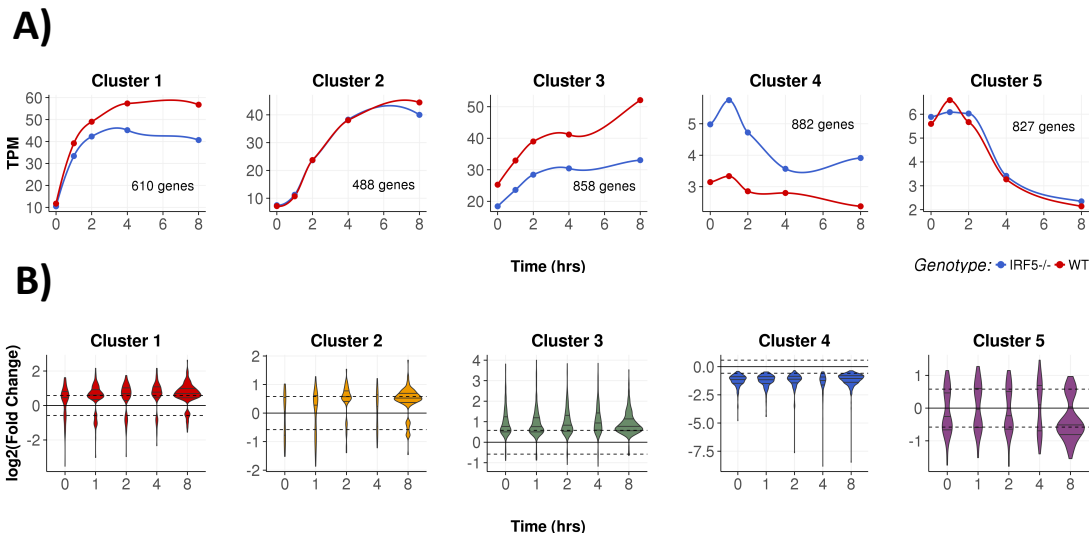

Figure 4.6. Kinetics and IRF5 dependency of clusters. A) Average expression (transcripts per million – TPM) profiles of genes in each cluster over time. Points are means of all expression values, curves are generated using locally weighted smoothing (LOESS) non-parametric regression. The number of genes within each cluster is indicated on the corresponding graphs. **B)** Fold change of differentially expressed genes (FDR < 0.05) within each cluster between WT and IRF5$^{-/-}$ macrophages (log2 scale). Violin widths are proportional to the number of differentially expressed genes at each time point. The median, upper, and lower quartiles are indicated by horizontal lines.

4.2.3. IRF5 regulated gene expression

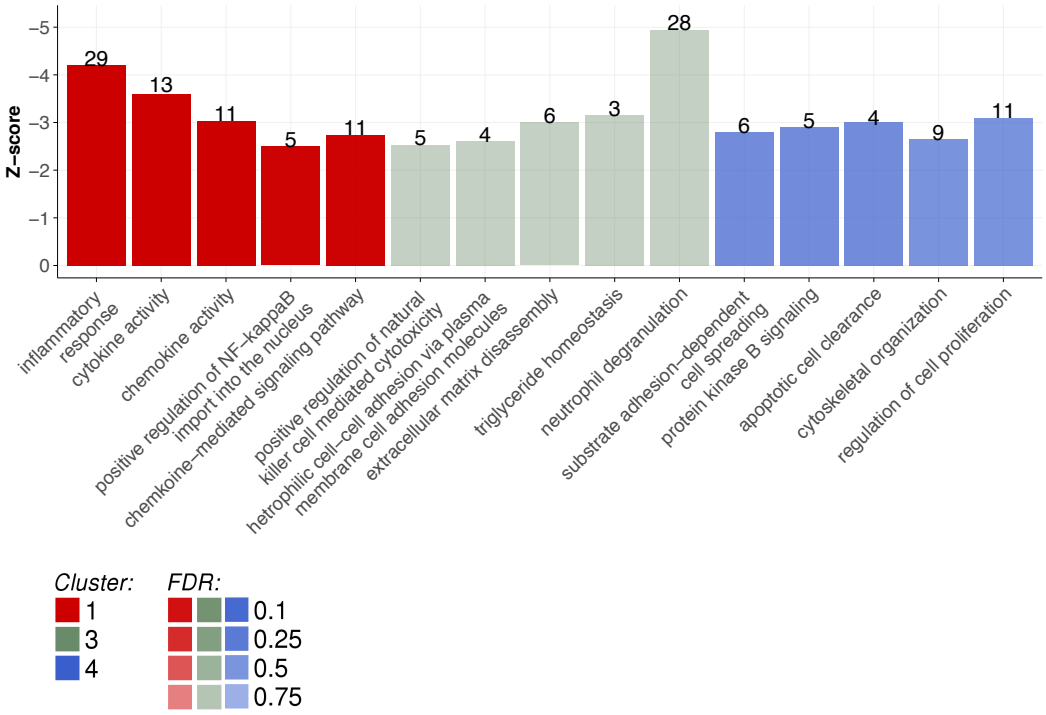

Figure 4.7. Gene set enrichment analysis for IRF5 dependent genes. Genes are weighted by their maximum fold change (WT vs IRF5$^{-/-}$) at any time point and ontologies obtained using Enrichr. Y axis shows the Z-score, which is based on a modified Fisher's exact test in which the expected enrichment of random gene lists for each ontology category is taken into account. Shading of bars indicates the FDR (Benjamini-Hochberg adjusted Fisher's exact test p-values), as does the order within each cluster. Text annotations show the number of hits within each gene ontology category.

To elucidate the functions of IRF5 regulated genes in the clusters exhibiting the highest levels of IRF5 dependency (clusters one, three, and four) we conducted gene set enrichment testing with Enrichr (E.Y. Chen et al., 2013; Kuleshov et al., 2016). Genes significantly differentially expressed between WT and IRF5$^{-/-}$ macrophages in each cluster (differentially expressed at least one time point with an FDR < 0.05) were scored on the basis of their maximum fold change between genotypes, this weighting represents their dependence on IRF5 and determines the level of membership of each gene to the set, allowing us to specifically retrieve gene ontology terms pertaining to genes which are functionally regulated by IRF5 (Figure 4.7). An extended list of Enrichr results is detailed in Chapter 8.2.5. This analysis reveals that cluster one is most associated with the inflammatory response, cytokine activity, and chemokine activity. Cluster three contains many genes associated with neutrophil degranulation, and is also enriched for the GO terms: extracellular matrix

disassembly, and positive regulation of natural killer cell mediated cytotoxicity. On the other hand, cluster four is associated with apoptotic cell clearance, substrate adhesion-dependent cell spreading, cytoskeletal organisation, and the regulation of cell proliferation.

IRF5 mediates the strongest level of regulation late in the LPS response; we therefore focussed our analysis on the eight-hour time point. Figure 4.8.A shows expression of genes in IRF5 regulated clusters in $IRF5^{-/-}$ vs WT macrophages, demonstrating that the majority of genes in clusters one and three are more highly expressed in the WT, and those in cluster four are more highly expressed in $IRF5^{-/-}$, as previously observed. Contrary to this when examining gene expression at cluster two and cluster five, we observe a much more limited effect of IRF5, with very little change in gene expression in these clusters (Figure 4.8.B). As indicated by the gene set enrichment (Figure 4.7), cluster one contains strikingly high numbers of inflammatory cytokines (*Il1b, Il12b, Il1a, Il6, Tnf*), and chemokines (*Ccl3, Cxcl2, Cxcl1, Cxcl3*), in addition to C-type lectin receptors (*Clec4e, Clec4d*), and anti-inflammatory regulators (*Anxa1, Ptx3, Acod1*). Cluster three genes are dominated by anti-microbial peptides, complement components, and genes associated with the oxidative burst (*Lyz2, C3, Cfb, Ctss, Sod2*). On the other hand cluster four contains genes involved in apoptotic clearance, cell adherence, metabolism, and other functions (*Tyro3, Mfge8, Gas6, Alox5/15*), which are down-regulated by IRF5. Cluster two is enriched for IFN response genes (ISGs) (*Mx1, Oas2, Oas3, Ifi206, Ifi213, Irf7, Irf9*) and is largely independent of IRF5, as is cluster five.

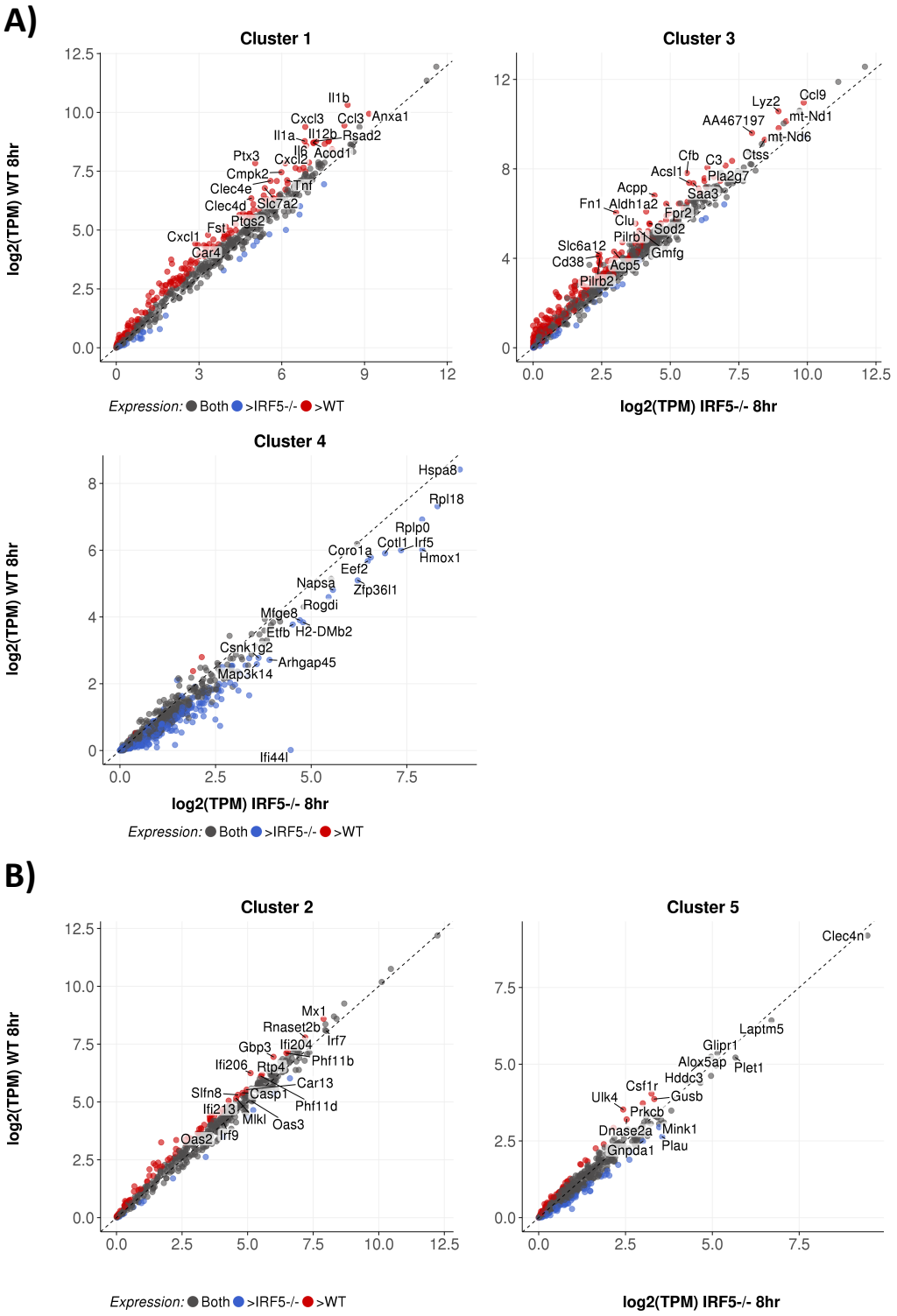

Figure 4.8. Gene expression in IRF5 dependent and independent clusters. Scatter plots show gene expression (log2 transcripts per million – TPM) in WT vs IRF5$^{-/-}$ macrophages for genes in clusters. Genes highlighted in red are expressed 50% higher in WT and blue indicates that expression is 50% higher in IRF5$^{-/-}$. Example genes in each cluster are annotated. **A)** IRF5 regulated clusters **B)** IRF5 independent clusters.

In order to validate these findings we focussed on representative genes from each category: pro-inflammatory chemokines (*Ccl3*, *Cxcl10*) and cytokines (*Il1b*, *Il6*, *Il12b*, *Tnf*) from cluster one, anti-bacterial peptides (*C3*, *Ctss*), enzymes (*Lyz2*, *Adam17*, *Mmp14*), and the transcription factor *Hif1a* from cluster three, and efferocytotic (*Tyro3*, *Mfge8*, *Gas6*) and pro-resolving genes (*Alox5*, *Alox15*, *Cat*) from cluster four; a representative selection of which were validated by qPCR (Figure 4.9).

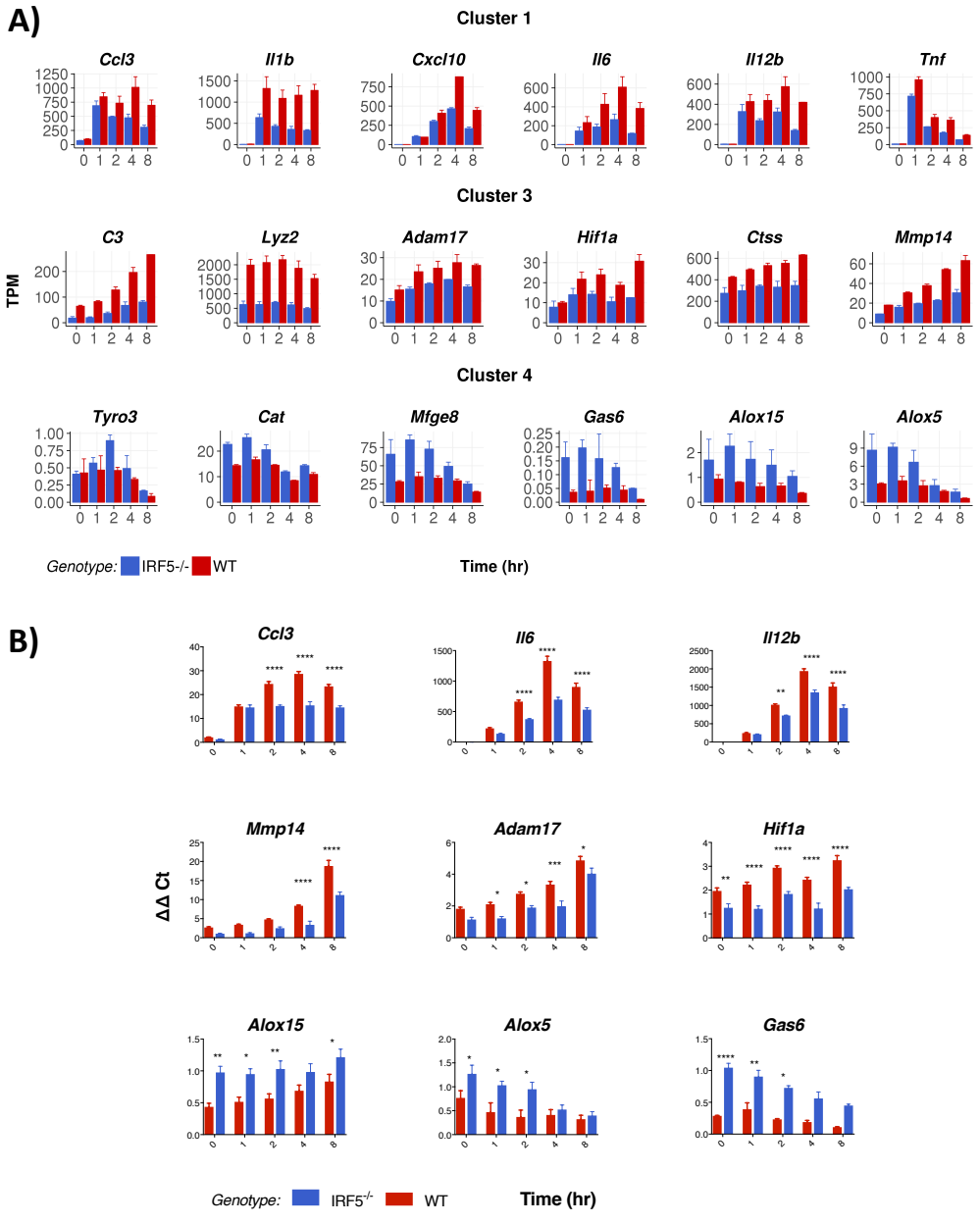

Figure 4.9. Validation of IRF5 regulated genes. A) Average transcripts per million (TPM) for selected genes from each cluster, ± SD. Genes shown are differentially expressed between IRF5$^{-/-}$ and WT macrophages with an FDR ≤ 0.05 at at least one time point. **B)** mRNA from IRF5 up- and down- regulated genes was quantified by qPCR, data shown are means with error bars representing the SEM for n=4. Statistical analysis was performed using two-way ANOVA with Bonferroni's multiple comparison. Asterisks represent significance thresholds: *p≤0.05, **p≤0.01, ***p≤0.001, ****p≤0.0001.

Having observed the somewhat unexpected presence of both PRGs (*e.g. Il1b, Tnf*) and SRGs (*e.g. Il12b, Il6*) in the rapidly induced cluster one, we examined the loci of archetypal genes from these categories more closely, in addition to example ISGs from the more slowly induced cluster two (Figure 4.10). ATAC-seq signal at the promoters of genes from all of the clusters in unstimulated cells indicates that they are basally accessible, although nascent RNA is detectable at PRGs and ISGs at the zero hour time point, but not at the SRGs. mRNA-seq profiles indicate that PRGs and SRGs share similar kinetics, being up-regulated rapidly in response to LPS. However, the SRGs are expressed at a high level for longer than the PRGs, which are more transient in their expression. Interestingly despite having accessible promoters and basal levels of transcription prior to LPS stimulation ISGs are not notably induced until two hours after LPS stimulation.

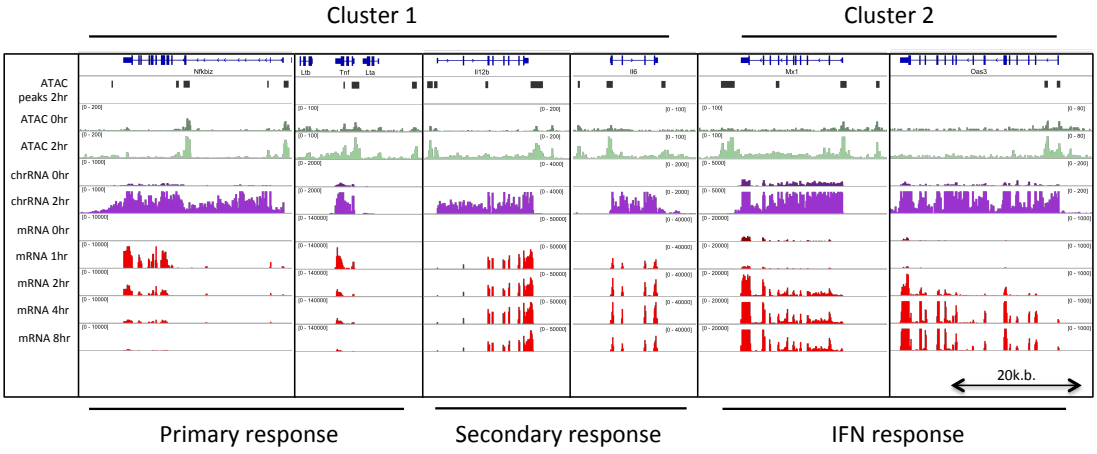

Figure 4.10. Chromatin accessibility and LPS induction of primary, secondary, and IFN response genes. Snapshots show ATAC-seq, chrRNA-seq, and mRNA-seq data in WT GM-BMDMs at primary and secondary response genes from cluster 1, and IFN response genes from cluster 2. Tracks shown are ATAC-seq peaks at the two hour time point and normalised coverage (FPKM) for all data sets. Scales for individual genes are shown.

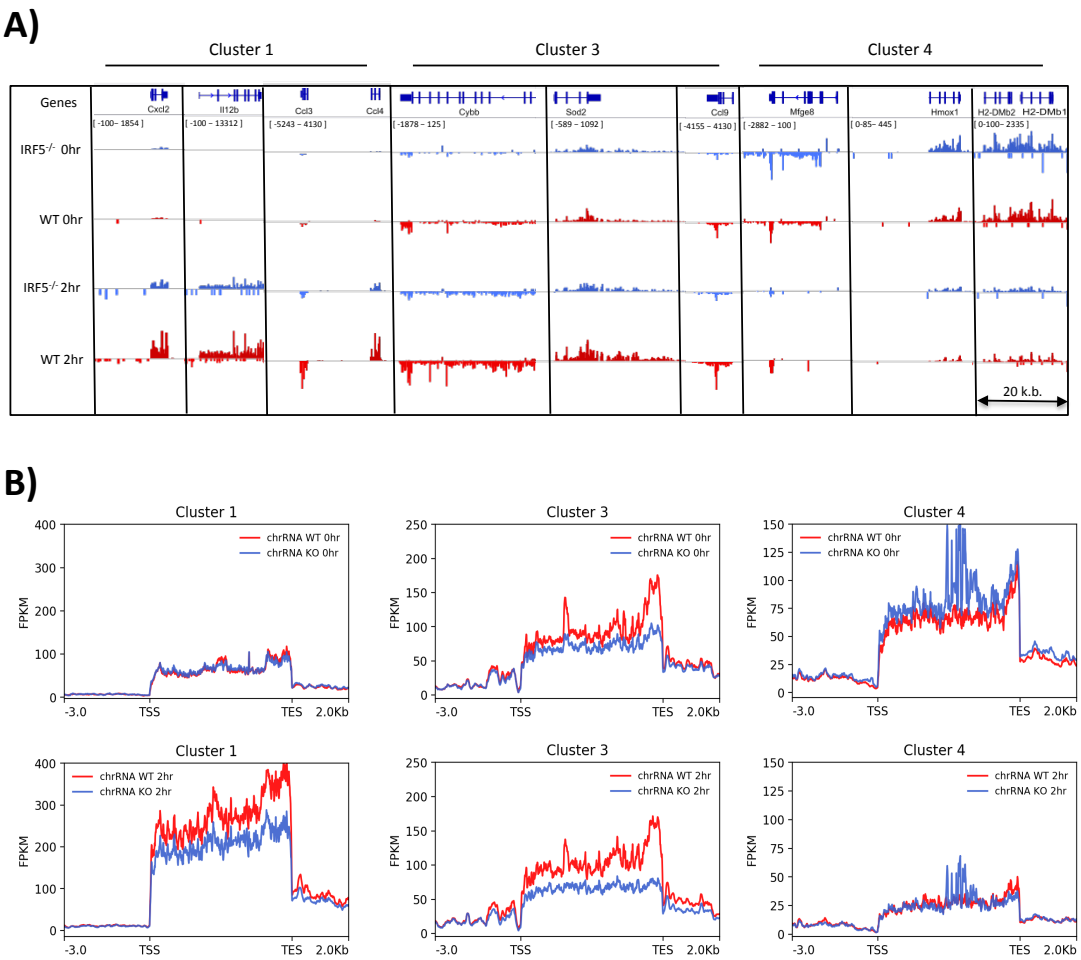

Figure 4.11. Transcriptional changes at genes from IRF5 regulated clusters. A) Snapshots of chrRNA in WT and IRF5$^{-/-}$ macrophages at genes differentially expressed by mRNA-seq (FDR < 0.05). Positive score represent reads on the sense strand and negative scores reads on the antisense strand. **B)** Meta-gene profiles of chrRNA signal (FPKM) over top 200 expressed genes in each cluster in naïve and LPS stimulated macrophages.

To confirm that IRF5 regulating these genes at the level of transcription we utilised our chrRNA data, which is indicative of Pol II recruitment and active transcription. First we examined the normalised coverage (FPKM) of WT and IRF5$^{-/-}$ chrRNA at genes of interest from each category (Figure 4.11.A). These data back up our previous observations: cluster 1 genes are induced with LPS stimulation, cluster 3 genes are expressed in naïve cells and up-regulated with LPS, and cluster 4 genes are down-regulated by LPS. Additionally, the direct effect of IRF5 on transcription can be observed, with reduced transcription in the IRF5$^{-/-}$ at genes in clusters one and three, and increased transcription at cluster four. Figure 4.11.B shows average chrRNA profiles over the top 200 genes in each cluster, indicating that IRF5

promotes inducible transcription of genes in cluster one, increases both the basal levels and inducible transcription of genes in cluster three, and represses transcription at cluster four.

4.2.4. Contribution of dendritic cells to GM-CSF bone marrow cultures

It has long been known that *in vitro* GM-CSF differentiated murine bone marrow cultures yield a heterogeneous population of cells (Inaba et al., 1992), commonly attributed with both inflammatory macrophage and DC phenotypes. However, more recently Heft *et al.* performed an in depth characterisation of GM-BMDMs, revealing the predominance of two main cell types, which they termed GM-DCs, and GM-Macs (Helft et al., 2015). In order to assess the contribution of dendritic cells to our GM-CSF bone marrow cultures, upon which our sequencing data are based, we examined gene expression by mRNA-seq of macrophage and dendritic cell signature genes, as defined by the ImmGen Consortium (J.C. Miller et al., 2012; Gautier et al., 2012) (Figure 4.12). Our data indicates that both of these gene signatures are present in our GM-CSF cultured cells, with little difference in the range of expression of either DC, or macrophage associated genes (bar chart). Hierarchical clustering reveals macrophage signature genes to be predominantly down-regulated by LPS, and DC signature genes to be up-regulated in response to stimulation. Furthermore, IRF5 appears to play a role in LPS mediated changes in gene expression for both subsets of genes. In unstimulated cells $IRF5^{-/-}$ and WT cells cluster together, however, subsequent to activation they cluster by genotype, suggesting the activity of IRF5 in mediating the expression of signature genes pertaining to cellular identity. Illustrating this, macrophage associated genes up-regulated by LPS are more strongly expressed in WT cells than $IRF5^{-/-}$ (bold clusters with solid dendograms leaves). On the other hand a subset of LPS up-regulated DC genes are more highly expressed in the absence of IRF5 (bold clusters with dashed dendograms leaves). Suggesting that IRF5 specifically promotes macrophage programs of transcription in response to activation and represses key DC genes.

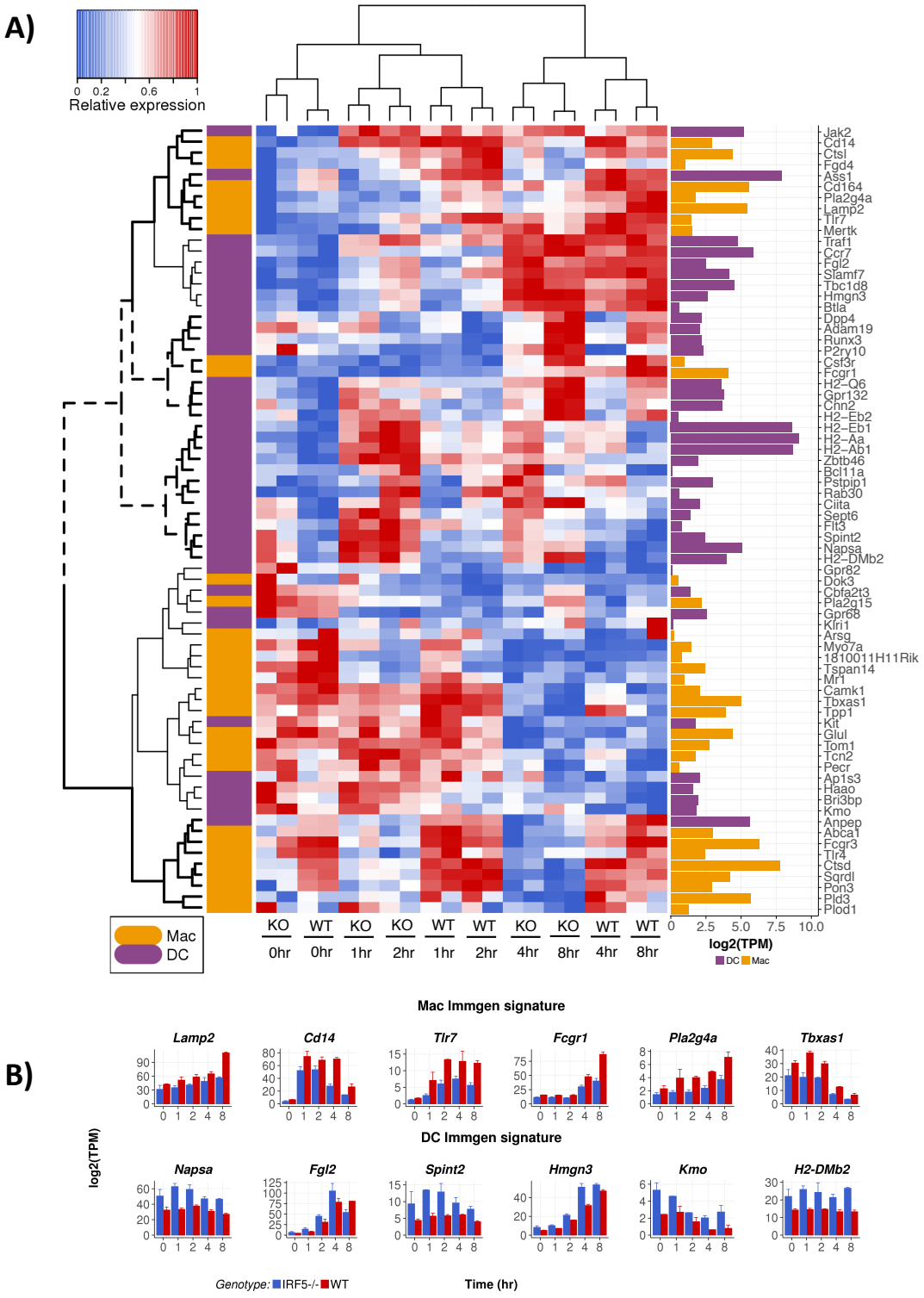

Figure 4.12. Macrophage and DC signature gene expression in GM-BMDMS. A) Heat map shows mRNA-seq expression of Immgen signature genes for dendritic cells (DC, purple) and macrophages (Mac, yellow) in GM-BMDMs. Expression data are log2(transcripts per million, TPM) scaled per gene, individual replicates are shown. Bold solid dendogram leaves indicate clusters with increased gene expression in WT, bold dashed dendogram leaves indicate clusters with increased expression in IRF5$^{-/-}$. Bar chart of average expression (log2 TPM) in WT unstimulated cells is shown on the right. **B)** Examples of differentially expressed (FDR < 0.05, fold change > 1.5, at at least one time point) Mac and DC signature genes between WT and IRF5$^{-/-}$.

4.3. Discussion

IRF5 has a crucial role in promoting pro-inflammatory responses as a consequence of TLR activation. Ablation of IRF5 function in $IRF5^{-/-}$ mice confers resistance to lethal endotoxic shock (Takaoka et al., 2005), highlighting the pro-inflammatory nature of this transcription factor. Previously studies of IRF5 transcriptional activity have focused primarily on the up-regulation of genes encoding pro-inflammatory cytokines (*e.g. Tnf, Il12b, Il6, Il1b*) and chemokines (*e.g. Ccl5, Ccl4, Cxcl2*) and down-regulation of anti-inflammatory cytokines such as IL-10 (Krausgruber et al., 2011; Saliba et al., 2014). To further characterise the transcriptional activity of IRF5 in response to LPS we examined gene expression by mRNA-seq and chrRNA-seq through a time course of LPS stimulated WT and $IRF5^{-/-}$ GM-BMDMs. Analysis of all differentially expressed genes by mRNA-seq with PCA and t-SNE reveals the driving force behind changes in gene expression to be LPS stimulation, with IRF5 accounting for smaller variations (Figure 4.1.A & B). PCA of chrRNA-seq differentially expressed genes supports this (data not shown). t-SNE provides an extra level of information over PCA by preserving local structure in the data, revealing that IRF5 has the most pronounced effects at four and eight hours after LPS stimulation (Figure 4.1.B). Examining differentially expressed genes reveals thousands of genes to be dynamically regulated by LPS, with activation causing large fold changes in the expression of up-regulated genes. IRF5 mediates the expression of a more restricted set of genes, also having both positive and negative effects on gene expression (Table 4.1) (Figure 4.2). This concurs with the known transcriptional activities of IRF5, acting to both promote the transcription of inflammatory cytokines and chemokines, and to down-regulate the production of anti-inflammatory mediators (Saliba et al., 2014; Krausgruber et al., 2010; Dalmas et al., 2015). However, surprisingly, we also observed IRF5 differentially expressed genes in unstimulated cells (Table 4.1) (Figure 4.2.A). This implies a basal level of IRF5 activity prior to LPS stimulation. This may be due to a contribution of IRF5 on the differentiation of macrophage progenitors or monocytes, aiding to promote an inflammatory macrophage phenotype. On the other hand, the death of cells in culture (such as neutrophils, which are prevalent in the bone

marrow) may coincide with the release of DAMPs, acting to promote IRF5 activity resulting in a basal level of activation.

The capacity of macrophages to respond dynamically to change is dependent not only on the inducing stimuli and the reactive transcription factors, but also on the chromatin state of the responding cell. It was first noted that NFκB could bind to some genes very rapidly, but was delayed in reaching others, indicating that chromatin remodeling was required to reveal the cognate binding site (Saccani et al., 2001). Reflecting this, macrophage gene transcription can be broadly divided into two categories; PRGs, the promoters of which are associated with permissive chromatin and are rapidly induced in response to stimuli, and SRGs, requiring chromatin remodeling at promoters for their induction. Many PRGs have accessible promoters and are basally associated with Pol II and markers of active gene transcription such as H3K27 acetylation (Ramirez-Carrozzi et al., 2009; Adelman et al., 2009; Hargreaves et al., 2009; Bhatt et al., 2012). Genes falling in this category are poised for transcription and are rapidly induced after sufficient stimulus. Whereas promoters at SRGs are dependent on nucleosome remodeling and protein synthesis for increased chromatin accessibility and transcription (Ramirez-Carrozzi et al., 2006; Ramirez-Carrozzi et al., 2009). Following the kinetics of LPS up-regulated genes, we observed three distinct clusters with differing kinetics (Figure 4.4, Figure 4.6.A). Clusters one and three are induced rapidly, whereas cluster two has slower kinetics, notably cluster three genes are expressed in naïve cells and are up-regulated further in response to LPS. On first inspection cluster one and two resemble the kinetics of PRGs and SRGs, however, these clusters do not correspond to the canonical PRG and SRG dichotomy. Rather, cluster one encompasses both PRG and SRG genes and cluster two contains LPS inducible ISGs. This is illustrated by the gene ontology for these categories (Figure 4.4), and by the presence of well-characterised PRGs (*e.g. Tnf, Ptgs2, Nfkbiz, Il1b*) and SRGs (*e.g. Il12b, Il6*) in cluster one (Figure 4.8.A), and IFN-response genes (*e.g. Mx1, Oas2, Oas3, Irf7, Irf9*) in cluster two (Figure 4.8.B). Upon assessing the chromatin architecture of promoters in clusters one, two, and three it became evident that

in GM-CSF derived BMDMs LPS up-regulated genes have basally accessible promoters, which increase in accessibility in response to LPS stimulation. This increased accessibility correlates with an increase in transcription and H3K27ac, indicating activation (Figure 4.5). The shared kinetics of PRGs and SRGs in GM-BMDMs can therefore be explained by the accessible state of promoter proximal chromatin in naïve cells (Figure 4.5 and 4.10), removing the barrier of chromatin remodeling for SRGs and allowing them to be rapidly transcribed in response to LPS due to binding of SDTFs. This reflects the conclusions drawn in Chapter 3 that GM-CSF acts to prime macrophages for inflammatory responses, increasing the accessibility of promoters of inflammatory response genes.

Interestingly, we also observe accessible promoters prior to LPS stimulation in cluster two, which contains many genes pertaining to the IFN response (Figures 4.4, 4.8.B). However, cluster two has distinctly slower kinetics, with genes being up regulated at two hours, rather than one-hour post-LPS (Figures 4.4, 4.6.A). This implies a dependency on a different set of transcription factors from those mediating the induction of clusters one and two, as there is no barrier of promoter accessibility restricting access of the activated factors. This observation can be explained by the powerful autocrine and paracrine signaling mediated by IFN-β, which is induced early in the LPS response and unaffected by IRF5 (data not shown) and acts to mediate the induction of ISGs as part of the LPS response in murine macrophages (K.E. Thomas et al., 2006). Notably, we find this process to be largely IRF5 independent (Figure 4.6.B), implying a distinct function of IRF5 in the up-regulation of pro-inflammatory cytokines and chemokines (cluster one) and anti-microbial proteins (cluster three), which differ from the IFN response (cluster two) both in terms of kinetics, and functionally. It is therefore likely that induction of cluster two genes is dependent upon the initial induction of *Ifnb1* by IRF3 and IRF7 (Honda et al., 2006; Takeuchi and Akira, 2010), which are induced via TLR4 signaling via TRIF in the MyD88 independent pathway (González-Navajas et al., 2012). Protein synthesis and subsequent release of IFN-β, is known to promote the induction of ISGs (cluster two) via IFNAR binding and the induction of the

STAT1-STAT2-IRF9 complex ISGF3 (González-Navajas et al., 2012) and STAT1-IRF8 (Mancino et al., 2015).

Sequencing of nascent RNA transcripts (chrRNA-seq) is indicative of Pol II recruitment and activity. Comparing chrRNA and mRNA –seq reveals that the majority of IRF5 differentially expressed genes coincide between data sets, however, with LPS stimulation a small minority are discordant, being up regulated at the chrRNA level and down regulated by mRNA-seq (Figure 4.3). This implies post-transcriptional regulation of mRNAs in LPS activated macrophages. Micro-RNAs (miRNAs) are major modulators of mRNA stability and act to dynamically regulate immune responses, contributing to macrophage gene expression and polarisation (Self-Fordham et al., 2017). ChrRNA-seq, being enriched for nascent RNA transcripts contains primary miRNA transcripts (pri-miRNAs), which are subsequently processed to yield mature miRNAs with regulatory activity. Utilising the chrRNA-seq data we were able to demonstrate that IRF5 promoted the transcription of several pri-miRNAs, however this did not translate to detectable change in the levels of mature miRNAs (data not shown). This is likely due to additional regulatory steps in the complex processes involved in miRNA processing subsequent to transcription (Ha and V.N. Kim, 2014). Although the presence of immuno-modulating miRNAs explains the observed discrepancies between chrRNA and mRNA -seq detected IRF5 regulated genes.

However, the chrRNA-seq does verify that IRF5 regulatory activity acts at the level of Pol II recruitment with decreased levels of transcription observed in $IRF5^{-/-}$ macrophages at genes from cluster one and cluster three, and increased levels of transcription in the $IRF5^{-/-}$ in unstimulated cells at cluster four genes (Figure 4.11). Interestingly, we observe full-length nascent transcripts at PRGs but not SRGs in cluster one, and at ISGs in cluster two (Figure 4.10). PRGs are commonly pre-associated with Pol II (Adelman et al., 2009), which is actively engaged in transcription but normally fails to progress into productive elongation, due to the actions of two negative regulators of transcription NELF and DSIF, which keep Pol II in a

paused state proximal to the TSS (C.-H. Wu et al., 2003; J. Li et al., 2013; Yamaguchi et al., 2013). SDTFs such as NF-κB act to regulate paused promoters at the transition from initiation and promoter-proximal pausing to productive elongation via the recruitment of P-TEFb (Barboric et al., 2001) and Brd4 (B. Huang et al., 2009). These kinases act to promote the transition of Pol II into productive elongation by phosphorylation of Pol II CTD Ser^2, providing a platform for the accumulation of factors associated with active transcription and RNA processing. P-TEFb also phosphorylates NELF and DSIF, releasing Pol II from active repression (Sims et al., 2004). The presence of full-length transcripts therefore implies a low level of active transcription, rather than promoter-proximal paused polymerase. The lack of nascent RNA at SRGs in unstimulated cells does not correlate with promoter accessibility, which is comparable between groups, and perhaps suggests the requirement of additional interactions between promoters of SRGs and distal regulatory elements upon LPS stimulation for the transition from initiation of transcription to productive elongation. Another possibility is that low level activation of SDTFs occurs in naïve cells through the release of DAMPs from dying cells during GM-BMDM culture, resulting in a basal level of transcription at strong IRF5 targets *e.g. Tnf* and at ISGs (via IFNAR). This would also account for the differential gene expression previously discussed between WT and $IRF5^{-/-}$ macrophages in unstimulated cells (Table 4.1).

LPS stimulation of macrophages results in the down-regulation of many basally transcribed genes, with a greater amount of genes down regulated by LPS than those induced (Table 4.1) (Bhatt et al., 2012). Both cluster four and cluster five are down regulated by LPS stimulation, which is associated with a loss of H3K27 acetylation at promoters and decreased transcriptional activity, although chromatin accessibility is maintained (Figure 4.5, Figure 4.6.A). Recently IFN-γ has been demonstrated to decommission enhancers associated with M2-like genes in monocyte-derived macrophages, this is associated with a loss of H3K27ac, PU.1 binding, and ATAC-seq signal. However, full enhancer disassembly only occurred at a small fraction of IFN-γ down regulated enhancers, with loss of H3K27ac only

occurring much more broadly at *cis*-regulatory elements associated with genes with decreased expression (Kang et al., 2017). Suggesting that down regulation of genes by inflammatory stimuli is mediated primarily by modulation of enhancer activity. IRF5 also acts to negatively regulate the expression of many target genes (Table 4.1, Figure 4.2, Figure 4.6). Intriguingly, IRF5 strongly down regulates genes in cluster four though not those in cluster five (Figure 4.6, Figure 4.8) implicating a stringent selection criteria for its selective recruitment to target genes. Gene set enrichment analysis reveals cluster four to be associated with resting macrophage functions such as apoptotic cell clearance and actin cytoskeletal organisation (Figure 4.7), which plays a major role in phagocytosis and efferocytosis (Erwig and Henson, 2008). These data indicate that cluster four contains genes are important for homeostatic macrophage function, such as the professional disposal of apoptotic cells in an immunologically silent manner (Gordon, 2016). This is reinforced by the differential expression of efferocytosis receptors *Tyro3*, and *Itgb3* and the efferocytosis regulating bridging molecules *Mfge8*, and *Gas6*, which are present in cluster four and down-regulated by IRF5 (Figure 4.9). Recently, IRF5 has been implicated in the pathogenesis of atherosclerosis by decreasing macrophage efferocytosis via the repression of *Mfge8* and *Itgb3*, resulting in failure to clear apoptotic cells in the necrotic core of atherosclerotic plaques (Seneviratne et al., 2017). Itgb3 forms a constituent part of the $\alpha_v\beta_3$ integrin, a potent mediator of efferocytosis via the cooperative binding of phosphatidylserine marked apoptotic cells with the bridging molecule Mfge8, a macrophage secreted glycoprotein (Hanayama et al., 2002). IRF5 therefore acts dynamically to down-regulate the uptake of apoptotic cells by efferocytosis whilst promoting phagocytic capacity by up-regulating anti-microbial genes for effective pathogen clearance in response to TLR4 sensing of PAMPs. Thus, prioritising macrophage function to that of pathogen clearance at the expense of homeostatic efferocytosis.

Overall, our data suggests that IRF5 is activated in response to TLR4 signaling, mediating a pro-inflammatory program of gene expression consisting of up-regulation of cytokines and

chemokines (cluster one) and enhancing anti-microbial activity (cluster three), at the expense of homeostatic and pro-resolution functions such as efferocytosis (cluster four) (Figure 4.7). This dynamic role of IRF5 effectively switches macrophage phenotypes from homeostasis to a program of inflammation and sterilising anti-microbial activity (Figure 4.13).

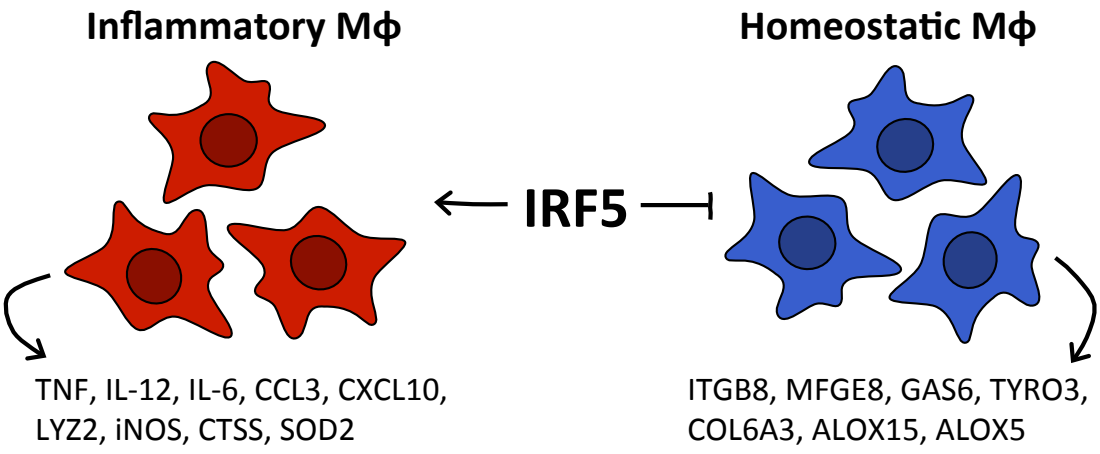

Figure 4.13. IRF5 promotes sterilising inflammation over homeostatic macrophage functions. IRF5 activation promotes a pro-inflammatory program of transcription, characterised by the up-regulation inflammatory cytokines, chemokines and anti-microbial genes, whilst repressing homeostatic and resolving macrophage functions such as efferocytosis and tissue remodeling.

To address the concern of the heterogeneous nature of GM-CSF BMDM cultures (Helft et al., 2015) we compared our mRNA-seq data to ImmGen identified lists of macrophage and DC signature genes (Gautier et al., 2012; J.C. Miller et al., 2012) (Figure 4.12). These data indicate that both macrophage and DC signature genes are expressed in GM-BMDMs, confirming that they are a mixed population of cells, consisting largely of monocyte derived macrophages and c-MoP derived DCs (Helft et al., 2015), both of which express IRF5 (data not shown). Interestingly, Heft et al. demonstrate that previously commonly utilised selection criteria, such as separating GM-CSF derived bone marrow cells on the basis of adherence, are inefficient, yielding mixed populations of cells (Helft et al., 2015). Due to differences in differentiation protocols, such as the length of culture time, tissue culture medium and fetal bovine serum used, and the use of tissue culture treated plastic, between

our differentiation protocol and the one used by Heft et al. the precise phenotypes of the resulting cells are likely to vary slightly. Our own studies have found roughly equal numbers of macrophage-like and DC-like components in our GM-BMDMs (data not shown). And, although neither GM-CSF derived macrophages nor GM-CSF derived DCs accurately represent *in vivo* populations, they do function as an effective *in vitro* model for IRF5 action in inflammatory conditions.

In terms of LPS induced gene expression, GM-CSF derived bone marrow DCs have been attributed with pro-inflammatory cytokine production (Dearman et al., 2009), however, the purity of these cells cannot be guaranteed, with the possibility of a macrophage contribution to cytokine production. Macrophages express very high levels of TLR4, with it being identified as a part of the core macrophage gene signature (Gautier et al., 2012) (Figure 4.12) and play a more dominant role in the modulation of immune responses via the release of secreted factors. By separating the constituent macrophages and dendritic cells from of GM-CSF bone marrow cultures it has been revealed that the bulk of inflammatory cytokine and chemokine expression does arise from the macrophage component (Helft et al., 2015). These data indicate that the IRF5 dependent up-regulation of pro-inflammatory mediators in cluster one (Figure 4.6, Figure 4.7, Figure 4.8) is likely reflective of changes in gene expression contributed by macrophages rather than DCs. Indeed, our data suggest that IRF5 plays a role in mediating the expression of signature genes pertaining to cellular identity, specifically promoting macrophage programs of transcription in response to activation. These data are indicative of a role for IRF5 in the differentiation of monocytes, promoting an inflammatory macrophage cell fate and supressing differentiation of monocyte to DCs. This concept is further explored in Chapter 6.

Macrophages and DCs, as professional phagocytes, share many functions in homeostasis, performing key regulatory activities such as the immunologically silent efferocytosis of apoptotic cells, preventing the release of potentially inflammatory molecules (Flannagan et

al., 2012). However, mechanisms of dealing with these ingested materials differ between the two populations; macrophages effectively catabolise phagocytosed debris down to the amino acid level, whereas DCs have limited lysosomal proteolysis thus preserving peptides for antigen presentation (Delamarre et al., 2005). This reflects the IRF5 mediated up-regulation of anti-microbial genes (*e.g. Cybb, Lyz2, C3*) (cluster three) (Figure 4.6, Figure 4.7, Figure 4.8.A) in contrast to DC signature genes encoding MHC class II molecules, which are also up-regulated by LPS, but unaffected or down-regulated (*e.g. H2-DMb2, Napsa*) by IRF5 (Figure 4.12, Figure 4.8.A). Indicating that the IRF5 dependent anti-microbial activity described is likely due to the effects of IRF5 on GM-CSF macrophages (GM-BMDMs), and not the contaminating DCs. In contrast to this the IRF5 mediated down-regulation of efferocytosis could be attributed to both macrophage and DCs, however, as previously discussed, IRF5 contributes to the negative regulation of efferocytosis by macrophages *in vivo* (Seneviratne et al., 2017), validating the conclusions drawn from these data.

5. IRF5 and Mechanisms of Function

5.1. Introduction

Macrophages are highly heterogeneous cells, able to take inputs from their tissue micro-environment and translate that signal into phenotypic adaptions via the induction of tissue-specific transcription factors (Rosas et al., 2014; Okabe and Medzhitov, 2014). This is mediated by the cooperation of induced transcription factors and PU.1, the master regulator of the macrophage transcription (Ghisletti et al., 2010; Heinz et al., 2010), to form new tissue-specific enhancers (Gosselin et al., 2014; Lavin et al., 2014). These nascent enhancers are distinct to the core macrophage enhancer landscape and are specific to macrophages from the tissue in question, with little over lap between macrophages from other compartments (Lavin et al., 2014). They act as key drivers in the expression of genes tailored to the needs of the tissue of residence such as: promoting lipid metabolism and storage capacity of alveolar macrophages in the lung (Schneider et al., 2014), and promoting iron homeostasis in splenic red pulp macrophages (Kohyama et al., 2008) (in response to PPAR-γ and Spi-C induction, respectively).

IRF5 has been shown to be a crucial mediator of inflammatory macrophages in vivo and classical macrophage activation in vitro. Its activation leads to TNF, IL-6, IL-12 and IL-23 secretion whilst simultaneously repressing IL-10 and TGF-β (Krausgruber et al., 2011) (Ouyang et al., 2007; Dalmas et al., 2015). Our earlier genome-wide analysis of IRF5 target genes in macrophages using ChIP-sequencing revealed that binding of IRF5 is highly LPS inducible associated with the transcription of chemokines and cytokines (Saliba et al., 2014; Weiss et al., 2015)

Upon re-examining the LPS inducible binding of IRF5 during the course of this study we noted that it rarely bound to isolated sites, instead favouring regions enriched for open chromatin (Figure 5.2.A). This, coupled with IRF5s strong enrichment at promoters formed

the basis of the hypothesis that IRF5 is preferentially recruited to key regulatory sites rich in open chromatin. To investigate this hypothesis we separated ATAC-seq peaks representing enhancers into traditional enhancers (representing both the constitutive and de novo enhancers examined in Chapter 3) and super enhancers, which are dense clusters of enhancers that preferentially mark key genes closely associated with cell identity and function (Whyte et al., 2013; Lovén et al., 2013). Additionally, super enhancers clearly delineate genes associated with core and macrophage tissue specific functions (Gosselin et al., 2014). We therefore utilise a commonly implemented bioinformatic procedure (Lovén et al., 2013; Semenkovich et al., 2016) to define super enhancers within the macrophage chromatin landscape, with the aim of identifying novel regulatory mechanisms governing macrophage transcription, within the context of the LPS response.

5.2. Results

5.2.1. The genomic context of IRF5 binding

In order to investigate the molecular targets of IRF5 binding, ChIP-seq was performed by David Saliba on GM-BMDMs, from both wild type and IRF5$^{-/-}$ mice (as a biological control). The cells were either unstimulated, or stimulated with LPS to induce activation of IRF5. The data were processed as described in (Chapter 2.2.2) and peaks were called against the IRF5$^{-/-}$ to obtain focal peaks of IRF5 binding indicative of recruitment. The data were deposited as accession number:E-MTAB-2661 in the ArrayExpress Archive of Functional Genomics Data and reported in (Saliba et al., 2014) along the original Chip-seq data obtained without the use of a biological control. The use of biological replicates and a biological control (rather than input DNA) results in fewer peaks being called: 3,591, 4,213 IRF5 peaks (0hr and 2hrs, first experiment) vs. 12, 1,842 IRF5 peaks (0hr, and 2hr second experiment), and provides us with greater certainty of identifying *bona fide* IRF5 binding sites. We are therefore able to probe IRF5 functionality more thoroughly than previously.

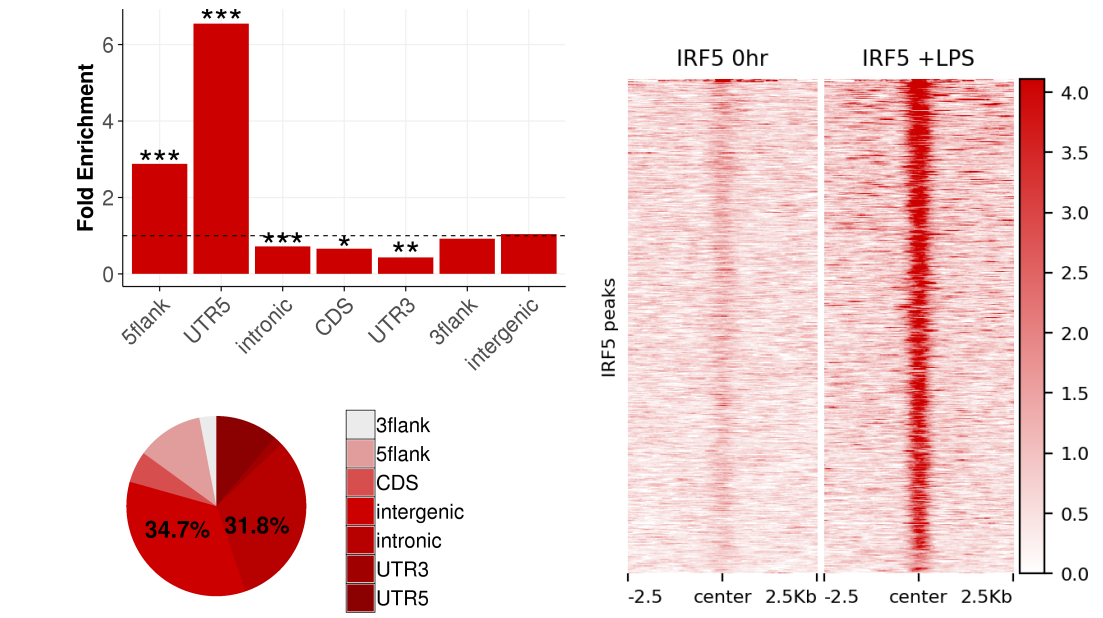

C)

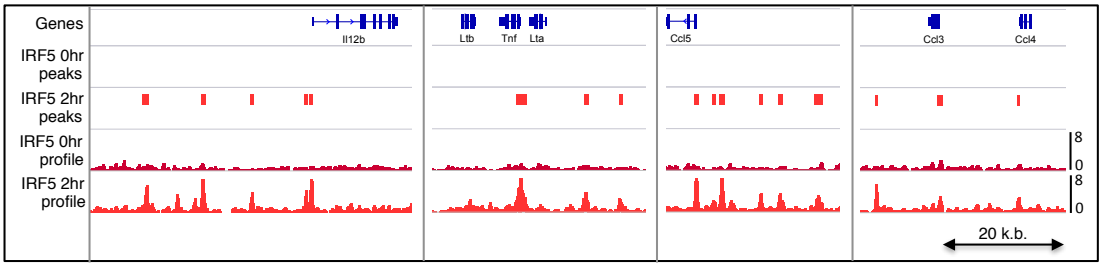

Figure 5.1. IRF5 ChIP-seq peak distribution and LPS inducible binding. A) Genomic association testing results depicting fold enrichment of IRF5 peaks with features of interest against genomic background and the relative proportions of IRF5 peaks falling within these categories. Asterisks indicate statistical significance according to adjusted p-values using the Benjamini-Hochberg procedure. **B)** Heatmap depicting linear scale IRF5 enrichment over 2.5 k.b. regions centered over the top 500 IRF5 ChIP peaks detected in LPS stimulated cells. IRF5 enrichment in unstimulated and LPS stimulated conditions are shown. **C)** Representative snapshots depicting IRF5 enrichment at detected peaks. Tracks displayed correspond to Ensembl genes, IRF5 called peaks, and linear scale enrichment over control ChIP. Scales are indicated on the image. Asterisks on plots indicate significance thresholds (*p<0.05, **P<0.001, ***p<0.001, ****p<0.0001)

Firstly, the enrichment of IRF5 peaks at regions of interest against genomic background was assessed quantitatively (Figure 5.1.A). These data indicate that IRF5 binding is very strongly enriched at 5' UTRs and 5' flanking regions, proximal to the TSS, with fold enrichments of 6.55 (p-value < 0.0001) and 2.9 (p-value < 0.0001), respectively. Enrichment at the 3' UTR, exons and intronic regions are somewhat less pronounced, though still significant, and IRF5 is not significantly enriched at 3' flanking and intergenic regions, in contrast to the 3' binding observed in the original ChIP-seq data (Saliba et al., 2014). The pie chart illustrating the distribution of IRF5 peaks indicates that although they are not relatively enriched in intronic and intergenic regions (due to the size of these features), the majority of IRF5 binding occurs there.

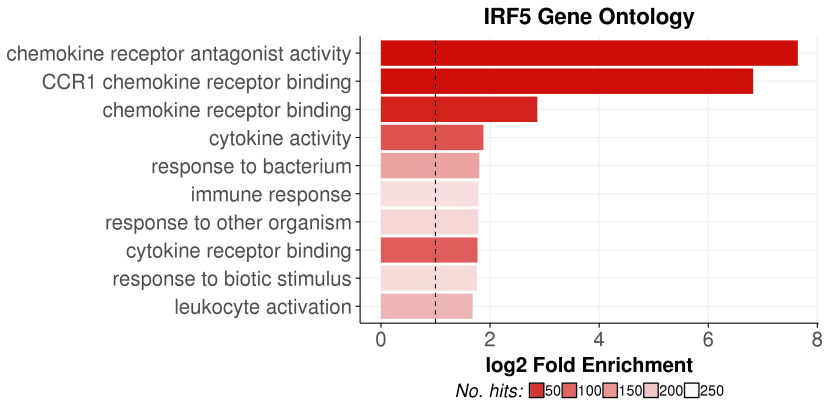

Figure 5.2. IRF5 ChIP-seq peak gene ontology. Representative gene ontology results for IRF5 ChIP-seq peaks. All ontologies shown have an adjusted binomial p-value < 0.05, results are displayed by descending fold enrichment (calculated over genomic background), and the number of observed region hits is indicated by the colour scale. GO analysis was performed using rGREAT.

Focussing on peaks which are consistent between the two IRF5 ChIP biological replicates reveals that IRF5 binds a total of 1,857 distinct genomic sites after activation with LPS, and just 15 binding sites were detected in unstimulated cells. The observed inducible binding of IRF5 concurs with the hypothesised mode of IRF5 activation; that it requires phosphorylation and dimerisation to translocate to the nucleus and bind DNA (W. Chen et al., 2008). Due to the very low number of IRF5 peaks in unstimulated cells the LPS responsive peaks were used for all subsequent analysis. Examining the enrichment of IRF5 at these peaks clearly demonstrates that IRF5 binding to its target regions is entirely LPS inducible (Figure 5.1.B). Focussing on specific IRF5 target genes (Figure 5.1.C) we observe that the trends outlined above hold true for loci such as *Il12b*, *Tnf*, *Ccl5*, with IRF5 peaks predominantly occurring at promoters, and at more distal enhancers, but not at the 3' ends of genes. To characterise the nature of IRF5s target genes, gene ontology analysis was conducted (Figure 5.2), revealing that the majority of IRF5s targets are involved in the inflammatory response and that it is particularly strongly enriched at genes pertaining to chemokine receptors and cytokines.

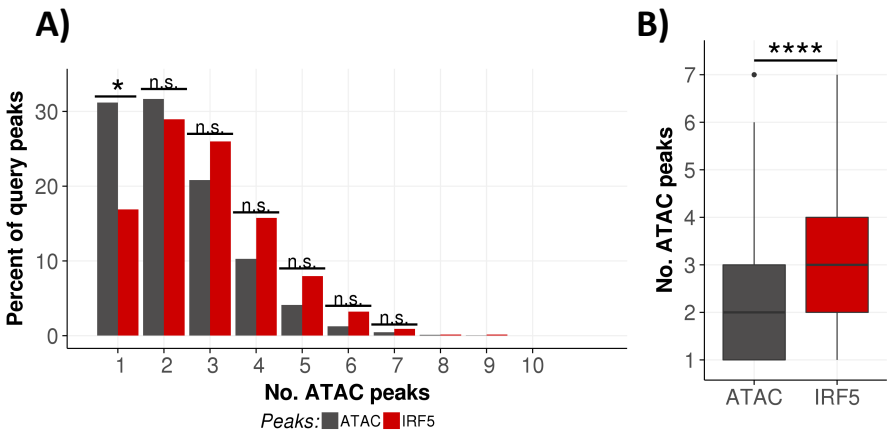

Figure 5.3. Genomic context of IRF5 binding. A) Association of IRF5 ChIP-seq and ATAC-seq peaks with nearby areas of open chromatin. Peaks were extended by 12.5 k.b. in either direction and adjacent ATAC-seq peaks falling within the extended intervals were counted. The number of areas of open chromatin associated with peaks are expressed as a histogram. Significance of enrichment / depletion of peaks in each bin was calculated using Fisher's exact test. **B)** Summary statistics for these data. Significance indicated was calculated using the Mann-Whitney U test. Asterisks indicate significance thresholds (*p<0.05, **p<0.001, ***p<0.001, ****p<0.0001)

To assess the chromatin context of IRF5 binding, we intersected IRF5 ChIP peaks with our ATAC-seq data (Chapter 3.1), which defines areas of open chromatin. In order to achieve this we extended IRF5 peaks by 12.5 k.b. in either direction and counted ATAC-seq peaks falling within these intervals. Extension lengths of 12.5 k.b. were chosen as this distance is commonly used in the literature to define regions enriched for enhancers (Pott and Lieb, 2015). The same procedure was applied to the ATAC-seq data as a control, and we reported how many ATAC-seq peaks overlapped with each extended query peak (Figure 5.3.A). We see significant depletion of IRF5 peaks in genomic regions with no neighbouring peak of open chromatin, compared with ATAC-seq peaks (p-value = 0.015), with just 16.9% of IRF5 peaks being isolated from other regions of open chromatin, compared with 31.1% of ATAC-seq peaks. Consequentially, IRF5 peaks tend to be in regions enriched for open chromatin. This trend is represented by a shift in the distribution of IRF5 peaks to the right of the histogram. Additionally, IRF5 has a median of three neighbouring ATAC-peaks, which is significantly higher than that of any given peak from the ATAC-seq dataset, implying that IRF5 selectively binds areas located in clusters of open chromatin (p-value = 2.1×10^{-16}) (Figure 5.3.B).

5.2.2. High order chromatin organisation

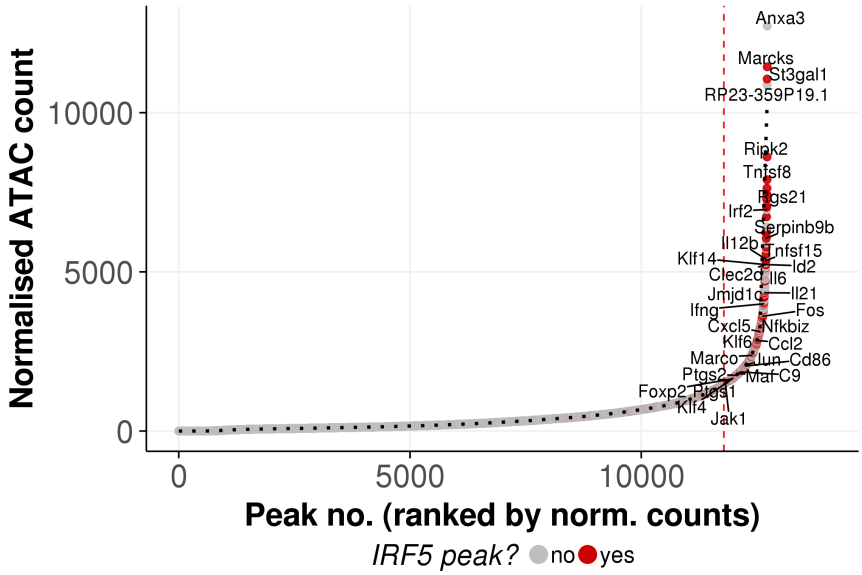

Figure 5.4. Super enhancer definition. ATAC-seq peaks within 12.5 k.b. intervals were merged into candidate super enhancer regions. ATAC-seq signal (reads per million - RPM) was then quantified over these intervals. Data plotted are candidate regions ranked by ascending ATAC-seq signal. Where the slope of the line equals 1 (red dotted line) an arbitrary cut off is applied and all regions past this point are classified as super enhancers. With everything falling short of this mark being termed a traditional enhancer. Enhancers with IRF5 ChIP peaks are indicated by red shading. Representative genes associated with super enhancers are labeled.

We therefore proceeded to utilise our ATAC-seq data to define regulatory units consisting of multiple enhancers within a short distance from each other, which some have termed super enhancers (Whyte et al., 2013). To do this we implemented a commonly used procedure to define super enhancers, which is dependent on the use of 12.5 k.b. as an arbitrary cut-off for the grouping of adjacent enhancers (Pott and Lieb, 2015). The candidate super enhancer intervals were generated by firstly, subtracting ATAC-seq peaks falling within genes or promoters (defined here as 2 k.b. windows around TSSs) from the total peak set, leaving enhancer peaks. Enhancer peaks within 12.5 k.b. of each other were then stitched together and sorted by their total chromatin accessibility, irrespective of enhancer length. A cut-off was applied where the slope of the fitted curve reaches one, with everything past the cut-off being defined as a super enhancer (full computational methods are detailed in Chapter 2.2.1). These regions represent areas with high chromatin accessibility; they're also enriched for IRF5 binding, and are associated with many pro-inflammatory genes (Figure 5.4).

Super enhancers make up a minority (7.4%) of the total enhancers within the cell, yet account for 37.4% of the ATAC-seq enhancer signal. They also account for a large proportion of IRF5 binding (of peaks in enhancers) and ATAC peaks (Figure 5.5.A). However, as a product of the analysis procedure both super enhancers, and traditional enhancers, are varied in length and may comprise of more than one ATAC-seq peak (Figure 5.5.C). They also vary in strength with extended clusters of weak enhancers and single, very active, enhancers being present in both groups (Figures 5.5.C and 5.6). Importantly, there is no observable difference in the distance of either class of enhancer with the nearest associated TSS (Figure 5.5.B). Furthermore, whilst at first glance traditional enhancers seem more responsive to LPS stimulation (with total numbers increasing from 8,633 peaks to 11,785 peaks) (Figure 5.5.D), compared to super enhancers (with 852 basal regions increasing to 939 after LPS stimulation); however, there is no significant difference between the proportions of constituent ATAC-seq peaks (making up the enhancers) that are lost, gained, or remain consistent with LPS stimulation between the enhancer groups (Figure 5.5.D).

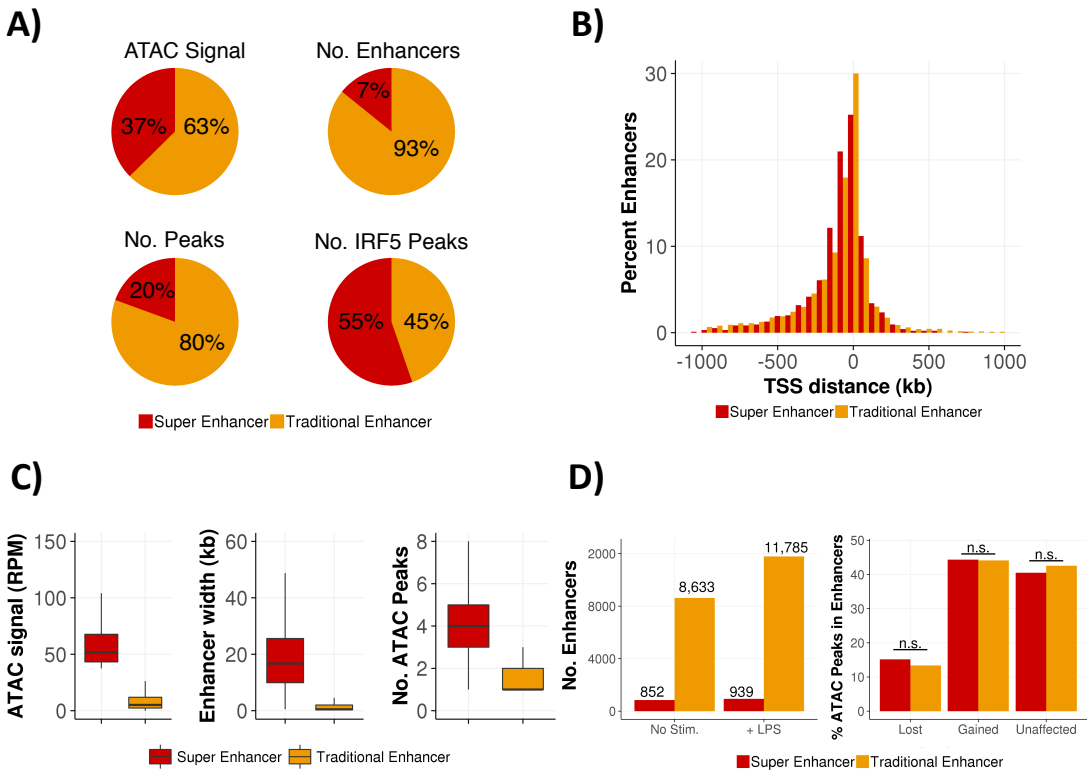

Figure 5.5. Super enhancer and traditional enhancer comparison. A) Pie charts depicting summary statistics for super enhancers (red) and traditional enhancers (yellow) **B)** Distance from enhancers in both groups from the nearest TSS, up to a maximum distance of 1,000 k.b. **C)** Boxplots of ATAC signal, interval width and number of ATAC-seq peaks of super enhancers and traditional enhancers. **D)** LPS inducibility of enhancers. Gross changes in the numbers of enhancers in each category pre- and post- LPS stimulation and the effect of LPS on the loss or gain of the constituent ATAC-seq peaks of enhancers. Significance was tested using Fisher's exact test (n.s. indicates p-value > 0.05).

To validate our categorisation of macrophage enhancers we utilised publically available histone tail modification and PU.1 ChIP-seq datasets generated in M-BMDMs and stimulated with LPS for 4 hours or left untreated (GEO Accession: GSE38377, (Ostuni et al., 2013)) (the raw data were analysed as described in Chapter 2.2.2). BMDM differentiation methods differ between our ATAC-seq and the publically available ChIP-seq data used, however, as addressed in Chapter 3.2.2 histone mark ChIP from GM-BMDMs and M-BMDMs correlate very well. Figure 5.6 shows the normalised enrichment for H3K4me1, H3K4me3, H3K27ac, and normalised ATAC signal at selected examples of super enhancers and traditional enhancers. All of the enhancers depicted have high H3K4me1, typical of distal regulatory regions, and show enrichment of H3K27 acetylation. These representative images also demonstrate the heterogeneity of both groups of enhancers, with each consisting of a

mixture of single focal peaks, and extended regions composed of clusters of peaks. However, it can be observed that the super enhancers typically comprise ATAC-seq peaks of higher signal intensity than traditional enhancers.

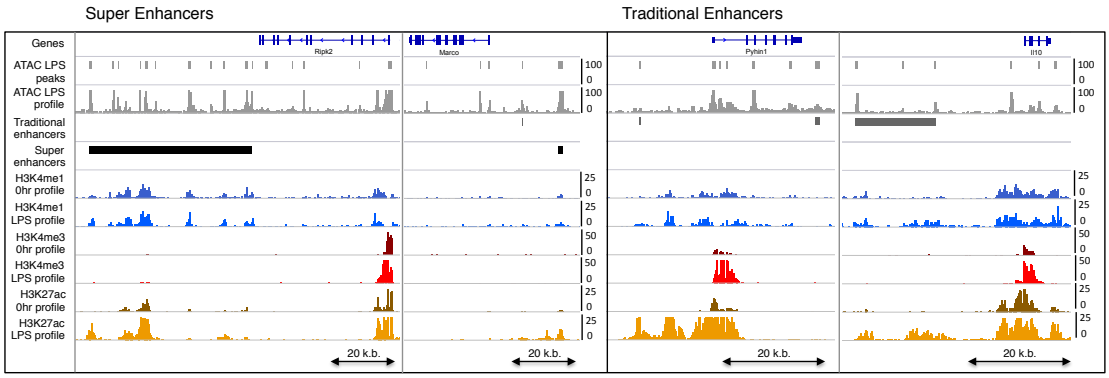

Figure 5.6. Super enhancer and traditional enhancer loci. Representative snapshots showing histone mark ChIP-seq and ATAC-seq signal, in addition to ATAC-seq peaks, and super and traditional enhancer tracks. Profiles correspond to linear scale fold enrichment over control for ChIP data, and RPKM for ATAC-seq signal. Scales are indicated on the plot.

Meta analysis on all ATAC-seq peaks falling in enhancers and promoters (Figure 5.7) shows enhancers from both groups have high H3K4me1/H3K4me3 ratios, whereas H3K4me3 is highly enriched at promoters, which bear little to no H3K4me1. There is minimal change in the H3K4me1 and H3K4me3 profiles between enhancer sub-classes. However, H3K27ac is greatly enriched over super-enhancers in naïve cells and increases still further with LPS stimulation, whilst traditional enhancers have a low level of H3K27ac that is not LPS responsive. Notably both classes of enhancer are enriched for PU.1, the binding of which is unaffected by LPS treatment, though super enhancers have greater PU.1 enrichment than both traditional enhancers and promoters. As expected ATAC signal is approximately two fold higher in super enhancers vs. traditional enhancers, and increases still further with LPS stimulation. ChrRNA is enriched for nascent, unprocessed RNA, and is therefore representative of active transcription (Chapter 3.3), we therefore examined chrRNA-seq signal at enhancer subsets and promoters. Promoter profiles indicate that they are active sources of productive transcription. Traditional enhancers are devoid of chrRNA transcripts, and super enhancers exhibit a low level of transcription, originating at ATAC-seq peak

centres and quickly decreasing to baseline. These data indicate that super enhancers are more transcriptionally active than traditional enhancers, but that these transcripts are unstable and rapidly degraded.

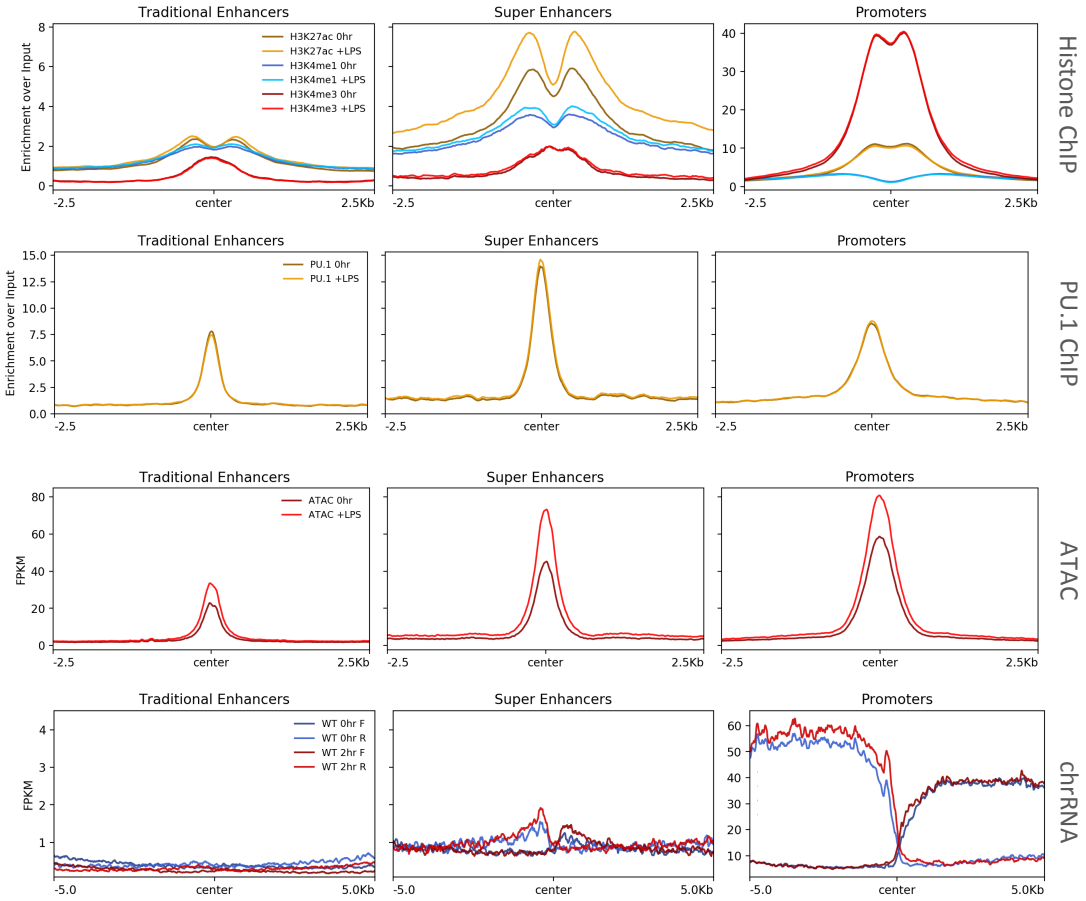

Figure 5.7. Super enhancer and traditional enhancer meta-profiles. ChIP-seq, ATAC-seq, and chrRNA-seq profiles at traditional enhancers, super enhancers, and promoters. Data are expressed as linear fold enrichment over input (ChIP) or FPKM (ATAC and chrRNA) over 2.5 - 5 k.b. windows centered over the ATAC-seq peaks within each region.

To establish whether there are biological differences between super enhancers and traditional enhancers we performed gene ontology to give an indication of the function of the associated genes (Figure 5.8). From this we can see that traditional enhancers are primarily associated with genes pertaining to metabolic processes. On the other hand super enhancers are highly enriched for GO terms pertaining to inflammatory processes, functions they do not seem to share with traditional enhancers. There is some overlap between the enhancer groups, with redundancy noticeable for DNA binding, biological regulation, and some metabolic processes.

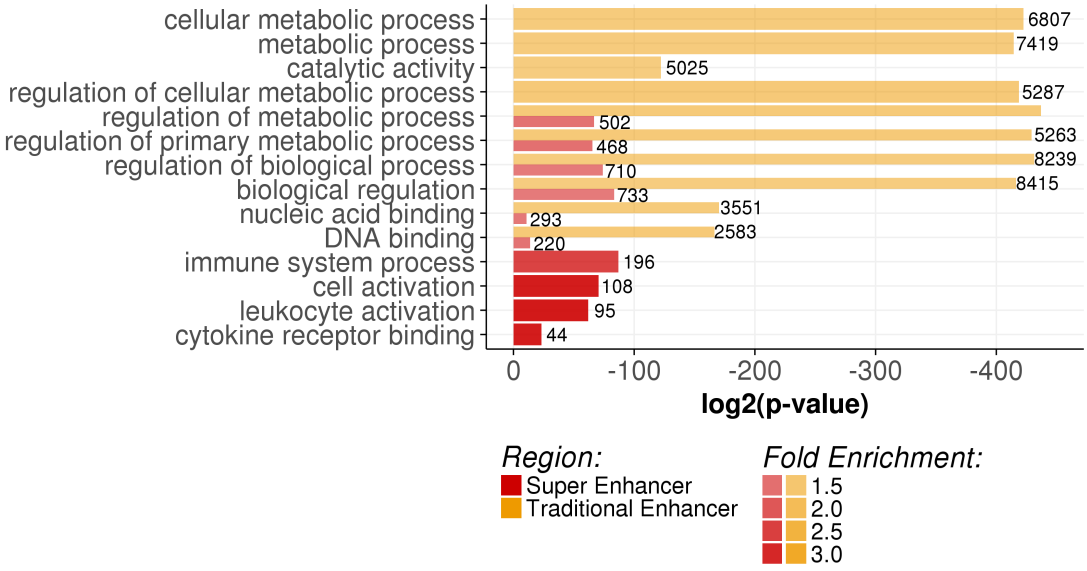

Figure 5.8. Super enhancer and traditional enhancer gene ontology. Representative gene ontology results for super enhancers (red) and traditional enhancers (yellow). All ontologies shown have an adjusted binomial p-value < 0.001, density of shading indicates fold enrichment (calculated over genomic background), and the number of observed region hits is indicated on the graphs. GO analysis was performed using rGREAT.

In order to examine whether these enhancer subclasses may have distinct effects on gene expression we utilised our mRNA-seq data from wild type GM-BMDMs, comparing the LPS inducibility of genes associated with traditional enhancer and those associated with super enhancers. We observe that the range of gene expression and fold change with LPS stimulation is concordant between both groups (Figure 5.9.A). The data also clearly highlights that super enhancers drive the expression of highly inflammatory genes, such as *Ptgs2*, *Il12B*, *Il6*, *Nkbiz, Tnfsf15*. Contrary to this traditional enhancers promote the expression of a much wider range of genes, including those related to metabolism (*Faah*, *Parap14*, *Nts*, *Macc1*, *Hamp*), and to the interferon response (*Pyhin1*, *Ifnb1*, *Mnda*, *Pydc3*). Although the range of expression and fold change of target genes was consistent between traditional- and super- enhancers, tracking the enhancer-associated genes through an eight hour time course reveals that super enhancer associated genes are significantly more up-regulated in response to LPS than those associated with traditional enhancers, at all of the time points examined (p-value < 0.0001 for all comparisons). Additionally, super enhancer induced gene expression is maintained at a high level throughout the time course, whilst fold induction of gene expression driven by traditional enhancers decreases with time (Figure 5.9.B).

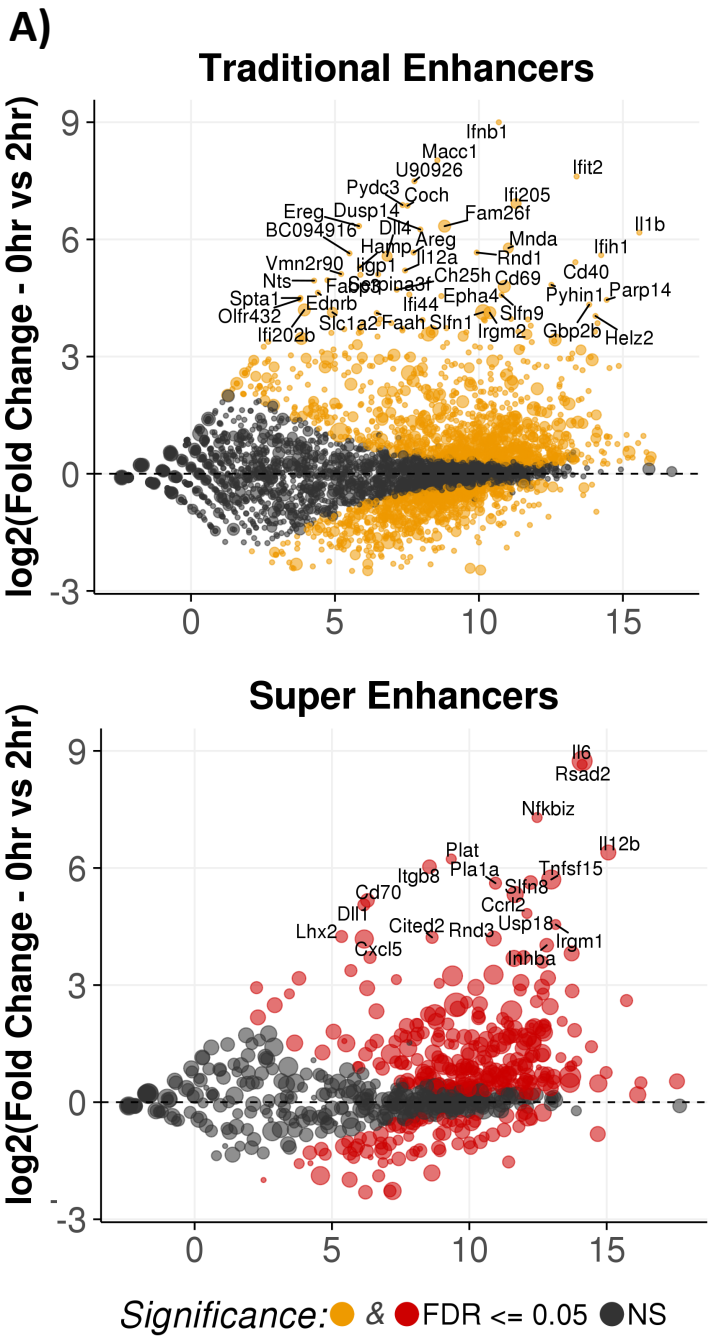
A)
Traditional Enhancers
log2(Fold Change - 0hr vs 2hr)
Ifnb1
Macc1
U90926
Ifit2
Pydc3
Coch
Ifi205
Ereg
Dusp14
Fam26f
Il1b
BC094916
Dll4
Areg
Mnda
Hamp
Ifih1
Vmn2r90
Igp1
Il12a
Rnd1
Nts
Ch25h
Cd69
Cd40
Spta1
Epha4
Pyhin1
Parp14
Ednrb
Ifi44
Olfr432
Slc1a2
Faah
Slfn1
Slfn9
Irgm2
Gbp2b
Helz2
Ifi202b
Super Enhancers
log2(Fold Change - 0hr vs 2hr)
Il6
Rsad2
Nfkbiz
Il12b
Plat
Pla1a
Tnfsf15
Itgb8
Slfn8
Cd70
Ccrl2
Dll1
Lhx2
Cited2
Rnd3
Usp18
Irgm1
Cxcl5
Inhba
Significance: & FDR <= 0.05 NS
B)
log2(Expression)
log2(Fold Change - 0hr vs LPS)
****
****
****
****
1hr
2hr
4hr
8hr
Time (hr)
Super Enhancer
Traditional Enhancer

Figure 5.9. Expression of super enhancer and traditional enhancer associated genes. A) mRNA-seq data from WT GM-BMDMs at 0hrs and WT 2hrs post LPS-stimulation. Differential expression of protein coding genes calculated with DESeq2 with an FDR of 0.05. Genes associated with traditional enhancers (yellow) or super enhancers (red) are shown on separate plots. Only the gene expression data for the nearest gene to each enhancer is shown. Point size is proportional to the number of ATAC-seq peaks associated with each gene. **B)** Gene expression data across all time points for genes associated with enhancer classes. Statistical significance of differential expression data as in A. Significance between groups was calculated using the Mann-Whitney U Test, asterisks indicate significance thresholds (*p<0.05, **P<0.001, ***p<0.001, ****p<0.0001).

Our data indicate that ATAC-seq peaks within super enhancers are a subset of strong enhancers, characterised by a high level of chromatin accessibility, H3K27ac, PU.1 occupancy, and transcription; acting to regulate key inflammatory genes in macrophages. We therefore examined the sequence conservation of ATAC-seq peaks comprising super and traditional enhancers, with the hypothesis that super enhancers are more representative of core cellular functions and exhibit greater conservation. Comparison with UCSC phastcons indicates that super enhancers are more enriched for evolutionarily conserved ATAC-seq peaks than traditional enhancers (Figure 5.10.A and B) with fewer peaks with low conservation scores and a shift in the upper quartile of the data, however this is a very mild effect (Figure 5.10.B).

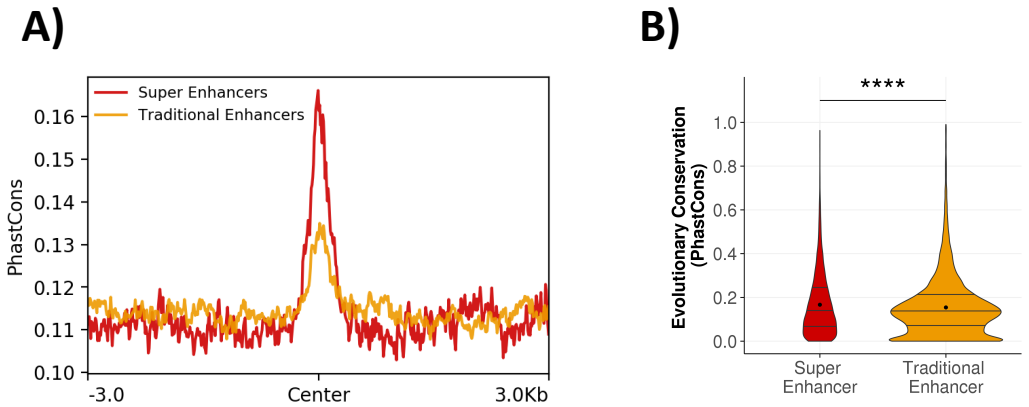

Figure 5.10. Conservation of ATAC-seq peaks comprising super and traditional enhancers. A) Average vertebrate PhastCon scores for regions +/- 3 k.b. from super and traditional enhancer ATAC-seq peaks in LPS stimulated macrophages. **B)** PhastCons scores for all peaks falling within super enhancers and traditional enhancers. Violin width is proportional to the number of peaks, horizontal lines indicate median, upper, and lower quartiles, points indicate the mean. Significance between groups was calculated using the Mann-Whitney U Test, asterisks indicate significance thresholds (*p<0.05, **P<0.001, ***p<0.001, ****p<0.0001).

5.2.3. Macrophage SDTF activity

Super enhancers are well described as having high transcription factor occupancy. We therefore set out to investigate which transcription factors were recruited to super enhancers, contributing to the observed changes in the expression of associated genes. In order to fully explore this we assessed 23 publically accessible datasets, comprising transcription factor ChIP-seq in pre- and post- LPS stimulated GM- and M- BMDMs. These data were analysed as described in Chapter 2.2.2.

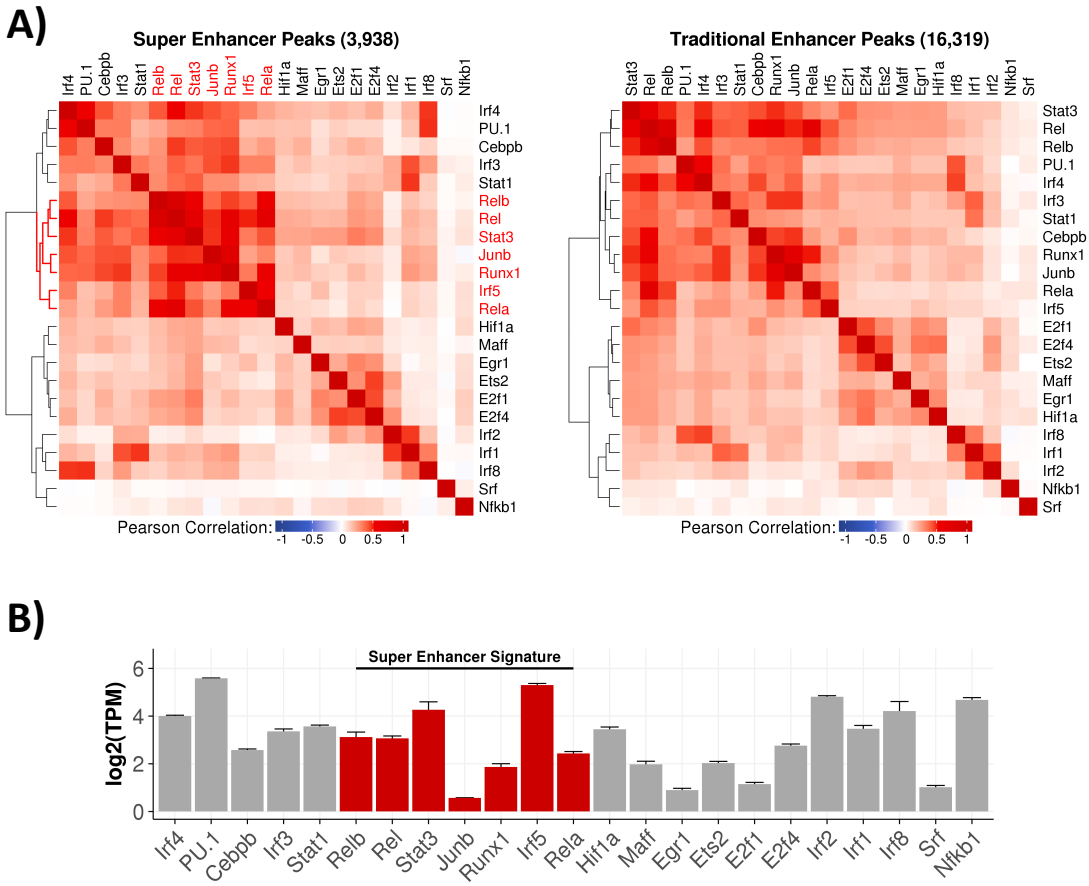

Figure 5.11. Super enhancer transcription factor signature. A) Reads were quantitated over 500 b.p. windows centered over ATAC-seq peaks from within super (left) or traditional enhancers (right) and the normalised counts were used for the calculation of Pearson correlation coefficients (indicated by colour scale). Hierarchical clustering was conducted using the Ward method on Manhattan distances. Transcription factors with similar binding profiles at super enhancers are highlighted in red. **B)** mRNA-seq data from unstimulated WT GM-BMDMs. Data shown are log2 transformed average transcripts per million (TPM) for transcription factors. Error bars indicate the standard deviation between two biological replicates. Transcription factors comprising the super enhancer signature are highlighted red.

To characterise the nature of transcription factor binding at super enhancers, we first compared the binding profiles of all 23 transcription factors at both classes of enhancer under LPS stimulated conditions. To accomplish this, reads were quantitated over all ATAC-seq peaks from within super and traditional enhancers (as described in Chapter 2.2.2) and the binding profiles compared using Pearson correlation. The correlation matrix (Figure 5.11.A) indicates a high degree of similarity in the binding profiles of: RelB, Rel, Stat3, JunB, RUNX1, IRF5, and RelA at super enhancers. Interestingly this tight correlation is absent at traditional enhancers, indicating that these factors represent a specific super enhancer signature. Notably we observe the independent clustering of closely associated lineage defining and homeostatic transcription factors PU.1, CEBPβ, and IRF4. It is therefore interesting to observe the presence of RUNX1 in the super enhancer signature, which largely consists of SDTFs, rather than in the cluster of regulatory transcription factors. We checked the expression of each tested transcription factor using mRNA-seq in unstimulated WT GM-BMDMs (Figure 5.11.B). This demonstrates that all of the transcription factors tested are expressed and that their binding profiles do not correlate with expression, varying from very high levels of expression (PU.1, IRF5) to lowly expressed (JunB, Srf).

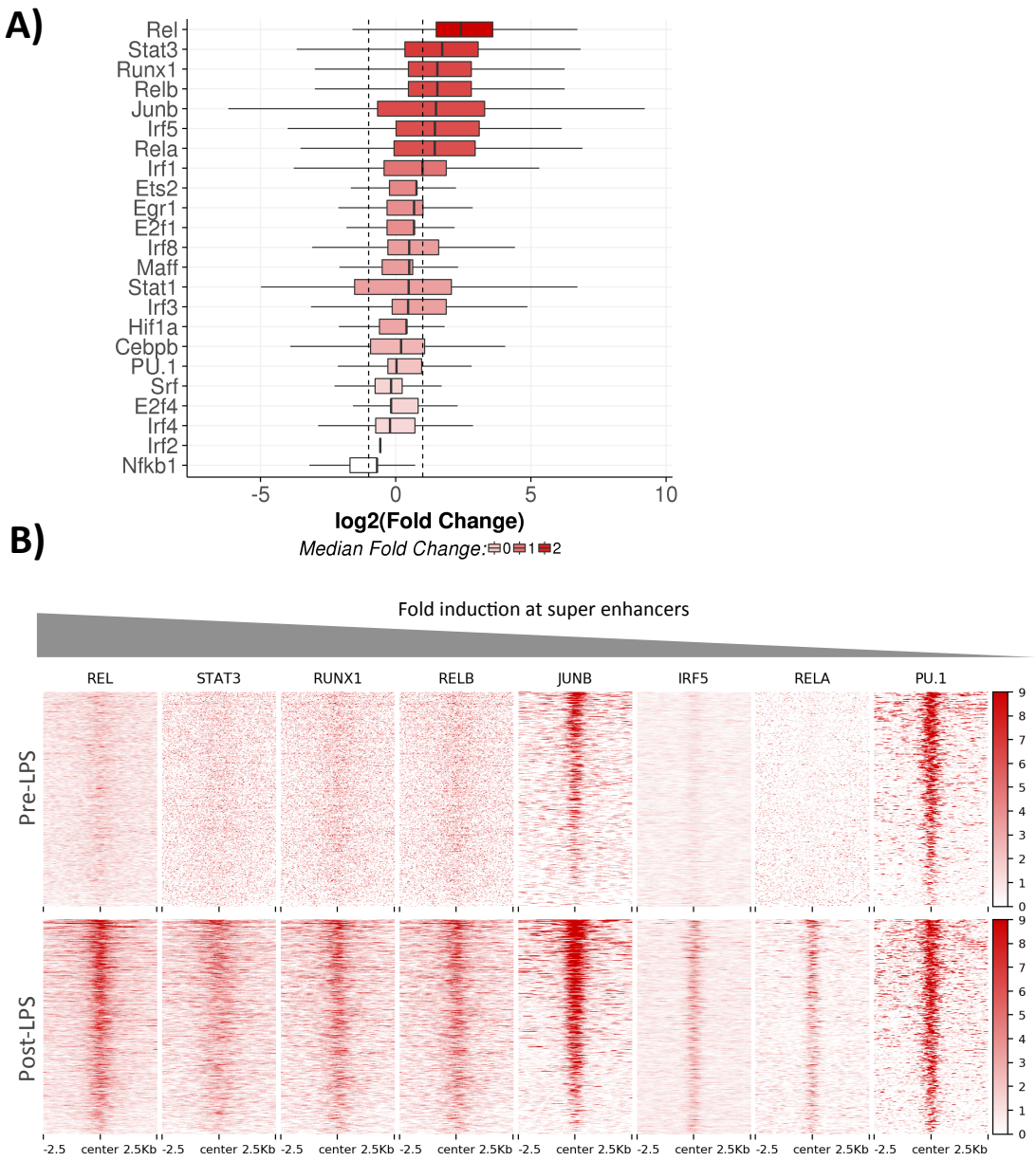

Figure 5.12. Inducible binding of transcription factors to super enhancers. A) Fold change of LPS stimulated vs unstimulated transcription factor ChIP-seq enrichment at super enhancers. **B)** Heatmap depicting enrichment of super enhancer signature transcription factors and PU.1, at 0 hrs and post-LPS. Regions are the top 500 ATAC-seq peaks from within super enhancers ±2.5 k.b. Enrichment values shown are linear scale fold enrichment over control.

To further explore the binding profiles of the identified super enhancer signature transcription factors we examined LPS inducible recruitment of all twenty-three transcription factors to super enhancers. To do this we calculated the fold enrichment of each transcription factor's occupancy of super enhancers in LPS stimulated conditions compared with that at the zero hour time point (Figure 5.12.A). From the data it is clear that

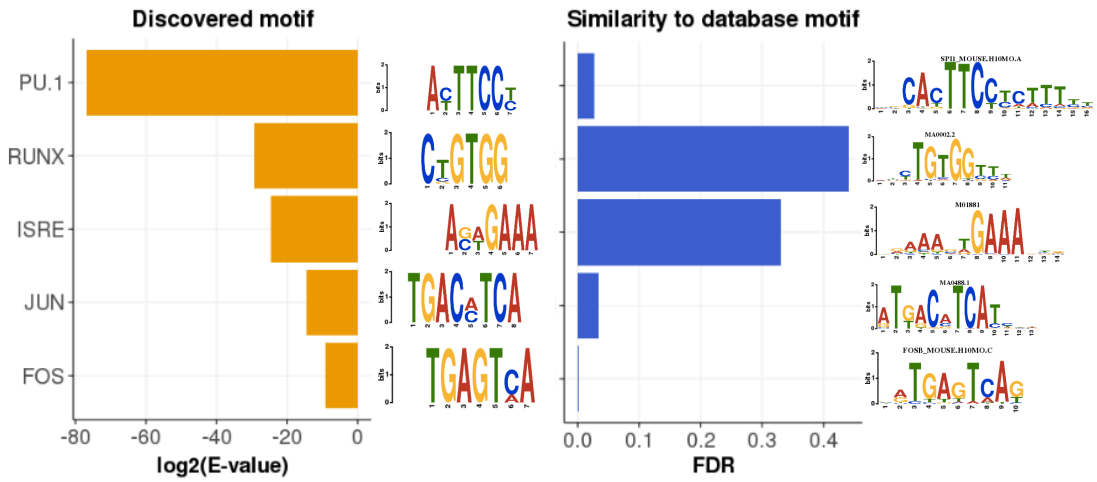

Figure 5.13. Super enhancer motifs. Motif analysis was performed on the top 1,000 ATAC-seq peaks from super enhancer regions. Sequences obtained from a 200 b.p. window over the peak center, background sequences are the flanking regions of the central window. Significance of the discovered motifs is indicated by the x axis (log2, yellow), and significance of the similarity between the discovered motifs and database matches is indicated by Benjamini-Hochberg corrected p-value (false discovery rate - FDR, blue).

the majority of macrophage transcription factors do not bind super enhancers inducibly, with fold change values of less than two (log2 fold change < 1). The largest recruitment following LPS stimulation is that of the super enhancer signature transcription factors, all of which demonstrated fold changes of more than two. Surprisingly, amongst these we see a high level of inducible RUNX1 recruitment. Macrophage transcription factors known as pioneering lineage-specific and environmental signal-independent factors, such as PU.1 and CEBPβ, have a median fold change close to zero. To ensure the inducible binding observed was genuine, and that the transcription factors assessed are present at meaningful levels, we checked their enrichment at the constituent ATAC-seq peaks from within the super enhancer regions in naïve and LPS stimulated cells (Figure 5.12.B). This demonstrates that the super enhancer signature factors we identified are recruited inducibly to super enhancers; with specific enrichment at ATAC-seq defined open chromatin peaks within super enhancers. In contrast to super enhancer occupancy by PU.1 is observable at a high level in both naïve and LPS stimulated cells. Interestingly, we note that JunB has a particularly high enrichment at zero hours, which is further increased with stimulation. To investigate whether the super enhancer transcription factor signature was reflected in the

sequence composition we conducted *de novo* motif discovery on the open chromatin peaks within super enhancers (Figure 5.13). This uncovered motifs corresponding to PU.1, but also ISRE half sites, RUNX, and AP-1 motifs.

5.2.4. IRF5-RUNX1 interactions

We observe a high level of RUNX1 recruitment in an LPS inducible manner to regions indicative of core macrophage inflammatory function. Runx1 is best known for its role in haematopoiesis (de Bruijn and Dzierzak, 2017), however the functions of RUNX1 in the context of inflammation are poorly understood. Thus we now focus our attention on RUNX1. First we validated *Runx1* expression by qPCR (Figure 5.14.A), finding it to be basally expressed with LPS down regulating its expression. We then compared a newly generated RUNX1 ChIP-seq data set kindly provided to us by G. Natoli (IEO, Milan) (hereafter referred to as "Natoli RUNX1 dataset") to the publically available RUNX1 ChIP-seq data (GEO Accession: GSE36104) (Garber et al., 2012) (referred to as "Amit RUNX1 dataset") and confirm that both experiments exhibit LPS inducible RUNX1 binding to super enhancers with a median fold change of more than 2 (Figure 5.14.B), and have centralised RUNX1 coverage over open chromatin in super enhancers in LPS stimulated conditions (Figure 5.14.C).

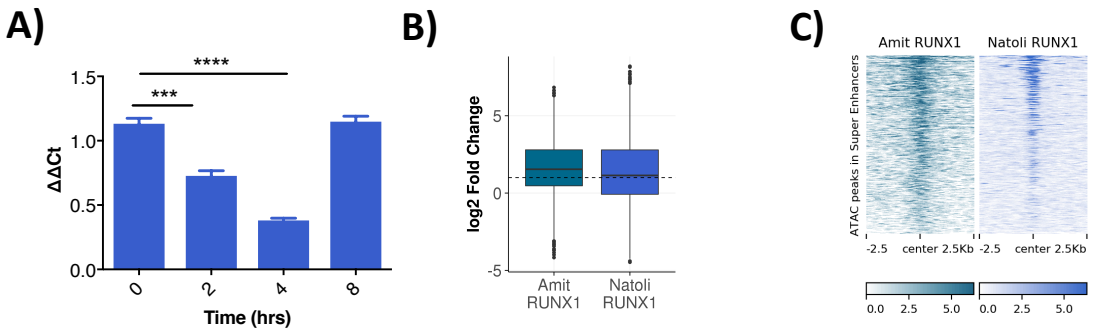

Figure 5.14. RUNX1 ChIP-seq comparison. A) RUNX1 expression by qPCR in WT GM-BMDMs stimulated with LPS. Asterisks indicate significance thresholds (*p<0.05, **p≤0.001, ***p<0.001, ****p<0.0001) of two-tailed unpaired t-test. Error bars represent SEM for n=4. **B)** log2 fold change values for LPS inducible binding of both RUNX1 ChIPs at super enhancers. **D)** Comparison of RUNX1 datasets. RUNX1 enrichment values shown are linear scale fold enrichment over control, generated with MACS2. Intervals are the top 500 ATAC-seq peaks from super enhancer regions.

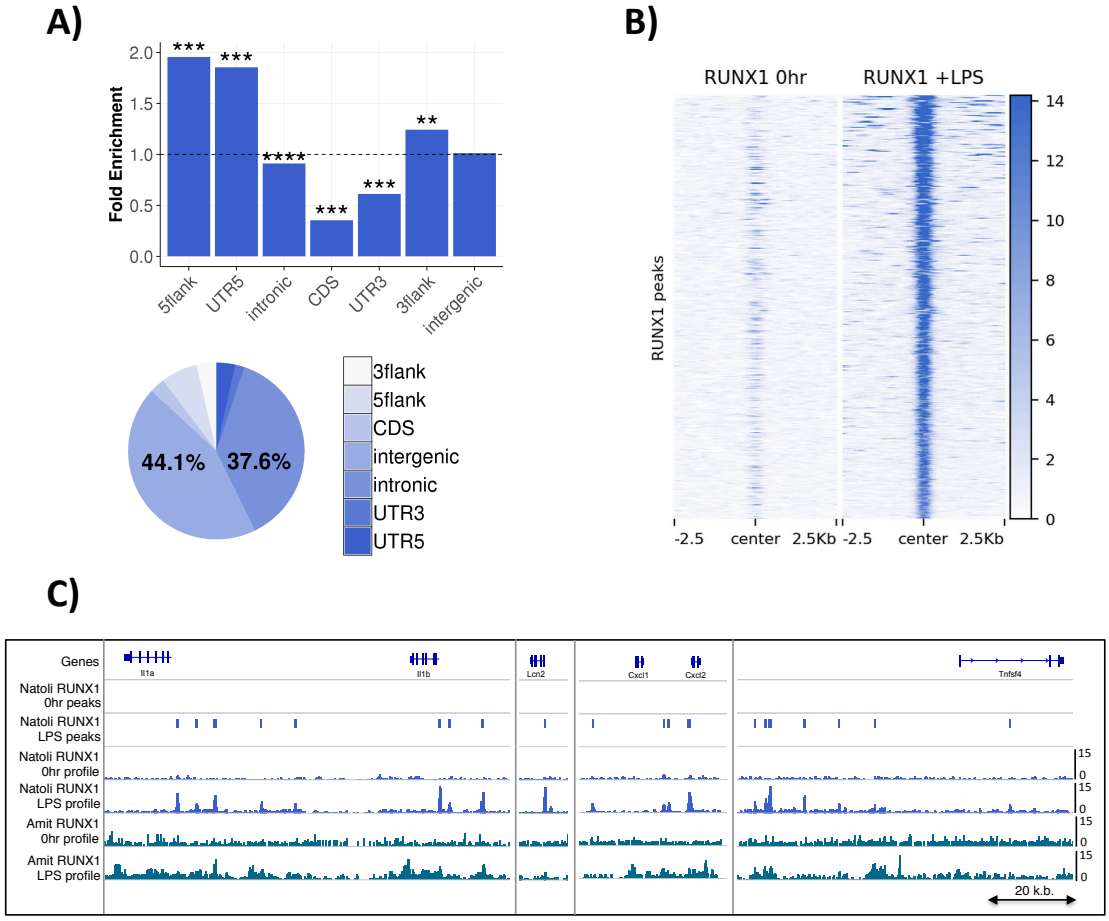

Figure 5.15. RUNX1 ChIP-seq peak distribution and LPS inducible binding. A) Genomic association testing results depicting fold enrichment of RUNX1 peaks at features of interest against genomic background and the relative proportions of RUNX1 peaks falling within these categories. Asterisks indicate statistical significance according to multiple testing corrected p-value using the Benjamini-Hochberg procedure. Asterisks indicate significance thresholds (*p<0.05, **P<0.001, ***p<0.001, ****p<0.0001). **B)** Heatmap of RUNX1 enrichment at the top 500 RUNX1 peaks, at 0hrs and after LPS stimulation. Enrichment values shown are linear scale fold enrichment over input **C)** RUNX1 called peaks at representative genes and fold enrichment over input for Natoli and Amit RUNX1 ChIP-seq data sets, scales are indicated in the figure.

Global assessment of RUNX1 binding reveals it to be a highly inducible transcription factor in mature macrophages, with 505 detected peaks prior to LPS stimulation and 4,277 peaks after LPS treatment (data not shown). Figure 5.15.B shows the enrichment of RUNX1 at detected peaks in basal and LPS stimulated conditions, demonstrating the inducible nature of this transcription factor. RUNX1 has a similar distribution to IRF5, with the majority of peaks falling in intergenic and intronic regions but being significantly enriched over the 5' ends of genes, with lesser fold enrichment at the 3' ends and within genes themselves

(Figure 5.15.A). Upon manual inspection we also note the binding of RUNX1 to inflammatory genes such as *Il1a, Il1b, Cxcl1, Cxcl2* (Figure 5.15.C). It is also worth noting that although both datasets are generally similar, with RUNX1 enrichment over the same broad areas, the Natoli RUNX1 dataset has much lower background than the Amit RUNX1 dataset with clearer LPS inducibility at peaks.

We next examined the gene ontology enrichment for RUNX1 peaks. The data show a very strong bias toward genes associated with the immune response and response to LPS, with no other categories appearing in the top ten biological process and molecular function results (Figure 5.16). Given the strong LPS induction of RUNX1 binding, the inflammatory nature of its target genes, its enrichment at super enhancers, and strong correlation in occupancy profiles with key macrophage SDTFs, we next investigated the potential causes of inducible RUNX1 recruitment. To do this we applied *de novo* motif discovery analysis to the sequences beneath RUNX1 peaks, in order to uncover the motifs of potential co-factors. We found PU.1 and RUNX motifs to be the most significant discoveries (the motifs of which are very strong matches to the database motifs) (Figure 5.17). Additionally, we uncovered Jun motifs, ISRE half sites, and a composite RUNX-ISRE motif. However, the *de novo* discovered ISRE half motif is only a weak match for the full-length database motif, most likely due to its truncation.

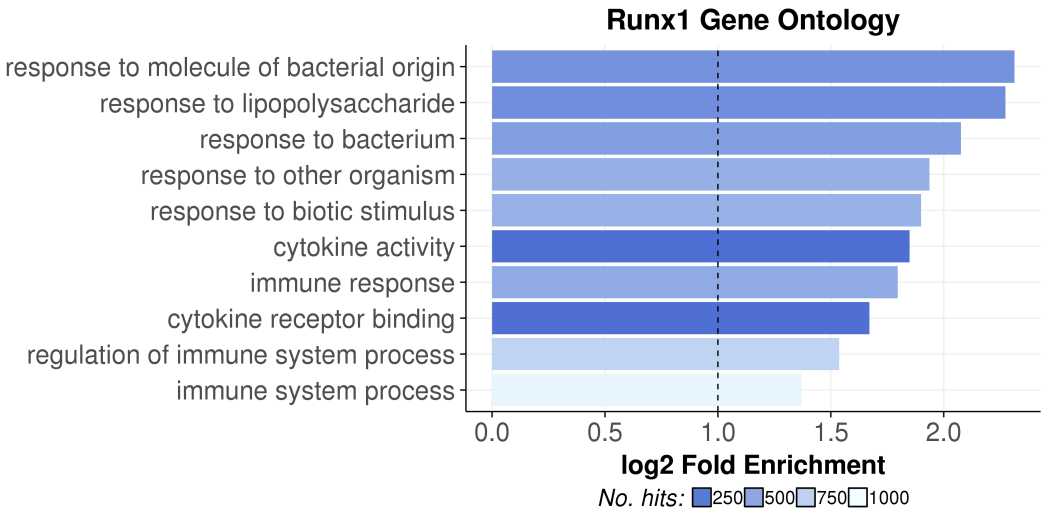

Figure 5.16. RUNX1 ChIP-seq peak gene ontology. Representative gene ontology results for RUNX1 ChIP-seq peaks. All ontologies shown have an adjusted binomial p-value ≤ 0.05, results are displayed by descending fold enrichment (calculated over genomic background), and the number of observed region hits is indicated by the colour scale. GO analysis was performed using rGREAT.

As a result of the discovery of the composite RUNX-ISRE motif, and ISRE half-sites, underneath RUNX1 binding sites; we hypothesised that RUNX1 may be binding cooperatively with an IRF transcription factor. We selected IRF1 and IRF5 as likely candidates, as they were both identified as also inducibly binding to super enhancers (with fold changes > 2) (Figure 5.12.A). Figure 5.18.A shows enrichment of RUNX1 at IRF1, IRF5, and RUNX1 peaks; clearly illustrating that there is considerable RUNX1 enrichment at IRF5 peaks, but not at those of IRF1. To be thorough we tested the association of both IRFs with RUNX1 peaks against a genomic background and found IRF1 to be six fold enriched at RUNX1 peaks, whereas IRF5 is 232 fold enriched at RUNX1 peaks, both with an adjusted p-value of ≤ 0.001 (Figure 5.18.B). We therefore proceeded to analyse the intersection between IRF5 and RUNX1, which totalled 472 peaks. Figure 5.18.D shows the enrichment of both IRF5 and RUNX1 at these intersections, indicating that both of these factors are more than two fold enriched at the shared peaks we identified. Figure 5.18.E illustrates the inducible binding of both IRF5 and RUNX1 to the overlapping peak set. The distribution of IRF5 and RUNX1 co-binding peaks also indicate that they have a propensity to occur in clusters (*e.g. Socs3*, *Skil*, and *Etv3*), in close proximity to each other. Furthermore, Hayley

Eames conducted IRF5 pull-downs in TLR4-CD14/Md2 expressing HEK293 cells, transfected with onestrep-IRF5 or empty vector, demonstrating that IRF5 is able to directly interact with RUNX1 (Figure 5.18.C).

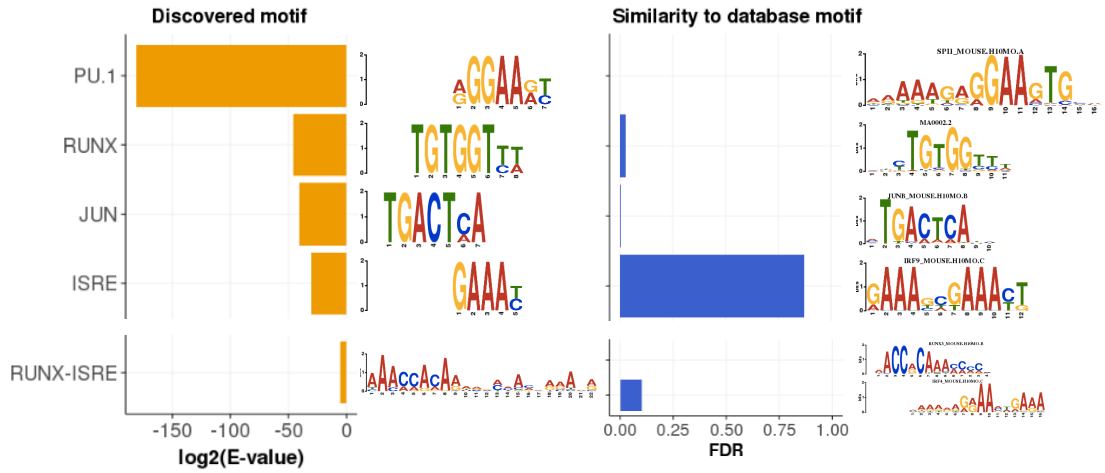

Figure 5.17. RUNX1 ChIP-seq peak motifs. Motif analysis performed on top 1,000 RUNX1 ChIP peaks. Sequences obtained from a 100 b.p. window over the peak center, background sequences are the flanking regions of the central window. Significance of the discovered motifs is indicated by the x axis (log2, yellow), and significance of the similarity between the discovered motifs and database matches is indicated by Benjamini-Hochberg corrected p-value (false discovery rate - FDR, blue).

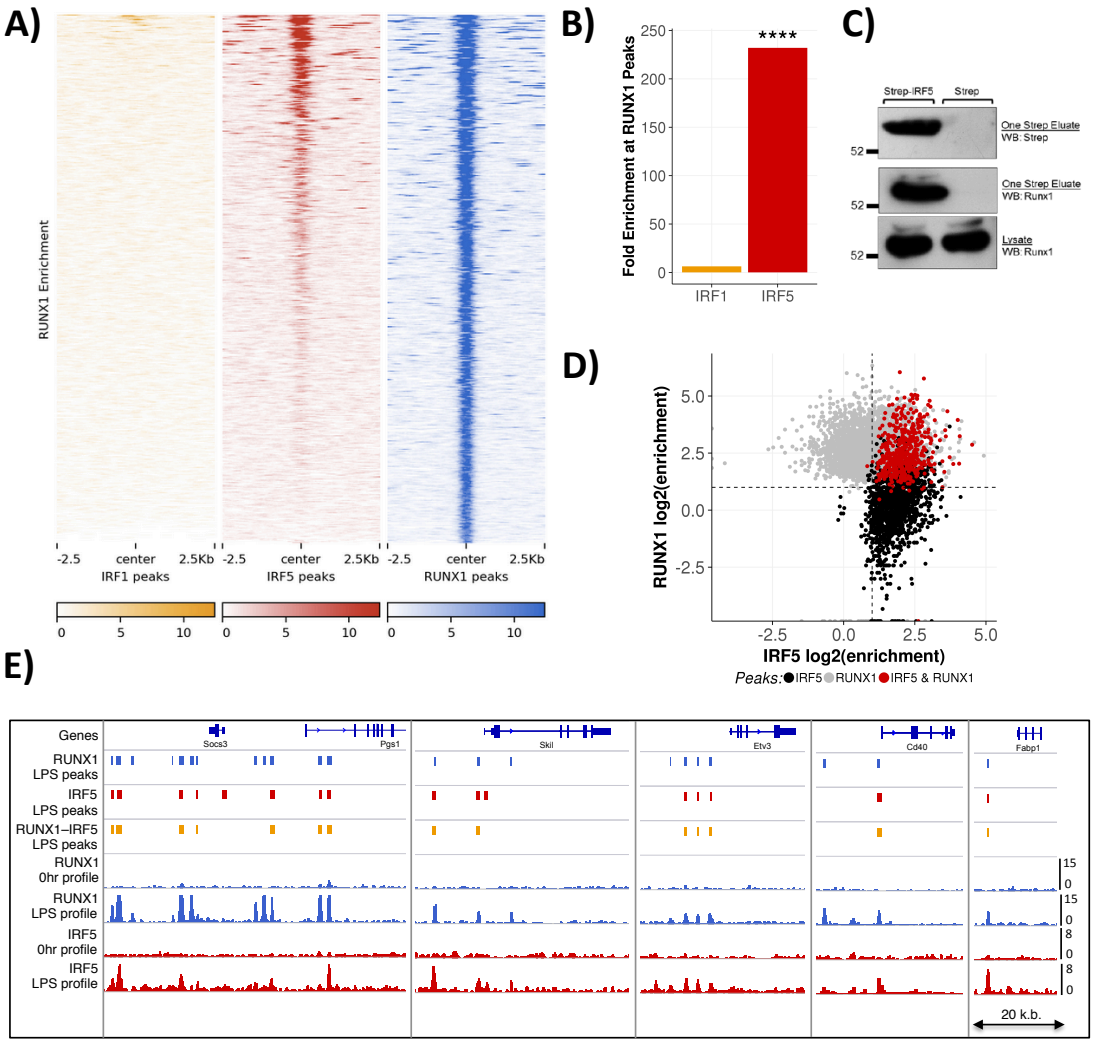

Figure 5.18. IRF5-RUNX1 interactions. A) Heatmap of RUNX1 enrichment at top 500 IRF1, IRF5, and RUNX1 peaks. **B)** Genomic association testing between IRF1 or IRF5 peaks and RUNX1 peaks, against genomic background. Asterisks indicate statistical significance according to multiple testing corrected p-value using the Benjamini-Hochberg procedure (significance thresholds *p<0.05, **P<0.001, ***p<0.001, ****p<0.0001). **C)** HEK293-TLR4-CD14/Md2 cells adenovirally infected with onestrep-IRF5 or empty vector. Nuclear lysates purified on streptactin columns & eluates were immuno-blotted with Runx1 antibody (ab23980, Abcam). Courtesy of Hayley Eames. **D)** Scatterplot depicting RUNX1 and IRF5 enrichment over control (log2) at RUNX1, IRF5, and RUNX1-IRF5 overlapping peaks. **E)** Snapshot of representative IRF5-RUNX1 overlapping peaks and target genes. Tracks correspond to: RUNX1 peaks, IRF5 peaks, and overlapping peaks in LPS stimulated conditions, and fold enrichment over control for both transcription factors in stimulated and unstimulated conditions. Scales are indicated in the figure.

Gene ontology for IRF5 and RUNX1 ChIP-peaks indicates that both factors have highly similar roles (Figure 5.19), acting to regulate the immune response subsequent to activation by pathogenic stimuli. Shared gene ontology categories include: cytokine activity, response to bacterium, immune response, response to biotic stimulus. Nonetheless each factor has its own specific roles with IRF5 only being enriched for chemokine receptor binding and organic cyclic compound binding, and RUNX1 being specifically associated with kinase binding, catalytic activity, and response to molecule of bacterial origin.

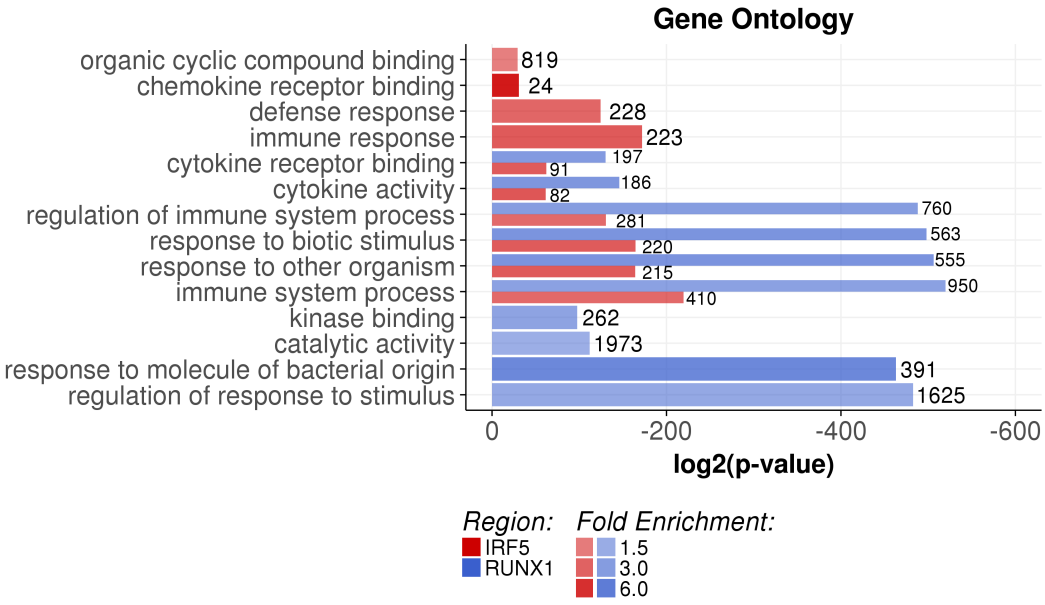

Figure 5.19. IRF5 vs RUNX1 gene ontology. Representative gene ontology results for enhancer subsets. All ontologies shown have an adjusted binomial p-value < 0.05, density of shading indicates fold enrichment (calculated over genomic background), and the number of observed region hits is annotated on the plot. GO analysis was performed using rGREAT.

5.2.5. Enrichment of IRF5 interactions at enhancer clusters

Examining the enrichment of IRF5 and RUNX1 over enhancer subsets demonstrates that there is a greater degree of overlap between IRF5 and RUNX1 at ATAC-seq peaks within super enhancers than traditional enhancers (though there are IRF5 and RUNX1 co-bound peaks in traditional enhancers too), and that the strength of enrichment at overlapping sites is also greater at super enhancers than traditional enhancers (Figure 5.20.A). We therefore examined the association of peaks that only have IRF5 binding, IRF5 and RUNX1 overlapping

peaks, and RUNX1 only peaks with genomic regulatory features (Figure 5.20.B). This revealed that IRF5 and RUNX1 overlapping peaks were the most enriched at super enhancers, with a fold enrichment of 4.3 (vs a stringent background of all open chromatin), whereas IRF5 and RUNX1 both have a lower enrichment at super enhancers of 2.6 and 2.9 fold respectively (at a p-value of ≤ 0.0001). After super enhancers, IRF5 peaks are next most enriched at promoters, whereas RUNX1 peaks are more enriched at traditional enhancers (Figure 5.20.B). The distribution of ChIP peaks reflects this, with IRF5 being most prevalent in promoters (32.3%), RUNX1 in traditional enhancers (25.2%), and IRF5-RUNX1 peaks in super enhancers (28.7%) (Figure 5.20.C).

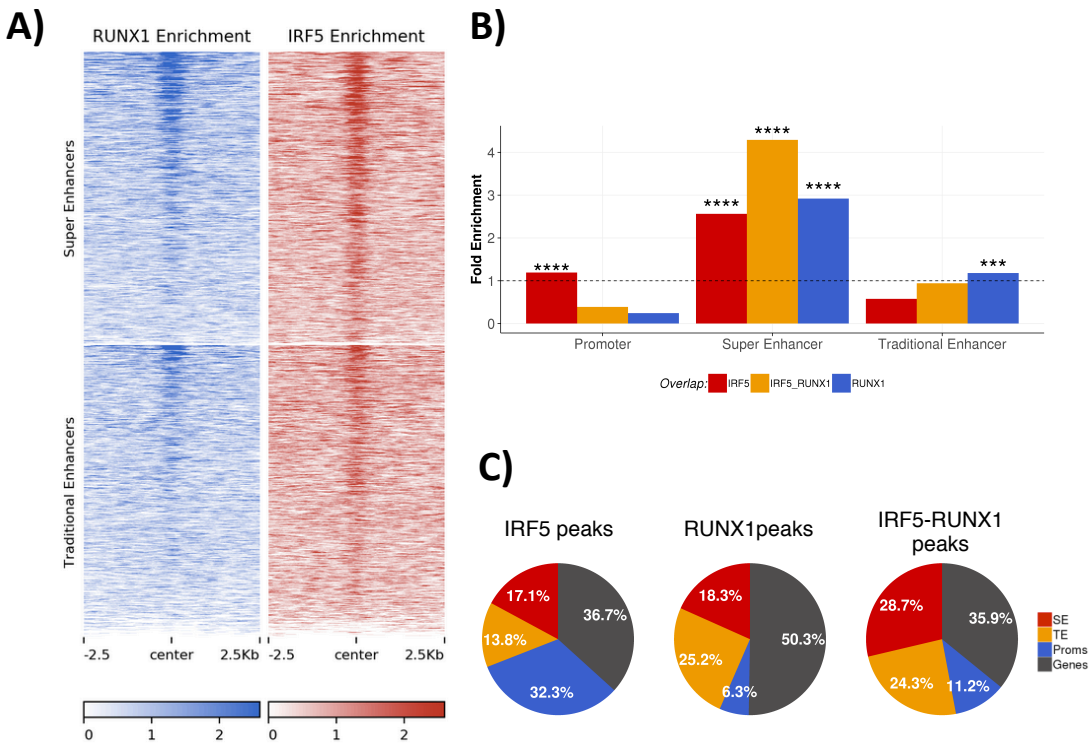

Figure 5.20. IRF5-RUNX1 peaks are enriched at super enhancers. A) Heatmap of IRF5 and RUNX1 enrichment over the top 500 ATAC peaks from within super enhancers (top panel) and traditional enhancers (bottom panel) **B)** Genomic association testing between ChIP-peak overlaps and regulatory regions (against a background of all open chromatin). Asterisks indicate statistical significance according to adjusted p-values using the Benjamini-Hochberg procedure. **C)** Proportion of ChIP peaks falling within each annotation category. Asterisks on plots indicate significance thresholds (*p<0.05, **P<0.001, ***p<0.001, ****p<0.0001).

We have previously described an interaction between IRF5 and RelA (Saliba et al., 2014) using our original IRF5 ChIP-Seq dataset with input DNA control. We therefore checked whether we could detect the same association with the second IRF5 ChIP-Seq dataset with a biological ($IRF5^{-/-}$) control. Figure 5.21.A shows high levels of RelA enrichment over IRF5 peaks, which is confirmed by genomic association testing for both RelA and RUNX1 peaks against IRF5 peaks; demonstrating that both factors are significantly enriched at IRF5 peaks vs genomic background by 397 and 223 fold, respectively (at a p-value of ≤ 0.0001) (Figure 5.21.B). In terms of functional significance the size of the IRF5–RUNX1 and IRF5–RelA overlaps are comparable (472 IRF5–RUNX1 peaks vs 423 IRF5–RelA peaks) (Figure 5.21.C). Figure 5.21.D shows that IRF5–RelA overlapping peaks are enriched for both transcription factors by greater than two fold over the control, further validating our observations. We next tested whether IRF5–RelA peaks also have a greater affinity for super enhancers than peaks bound by a single transcription factor, and found that, similarly to the RUNX1-IRF5 interacting peaks, they have greater fold enrichment at super enhancers than either IRF5, or RelA peaks on their own (Figure 5.21.E).

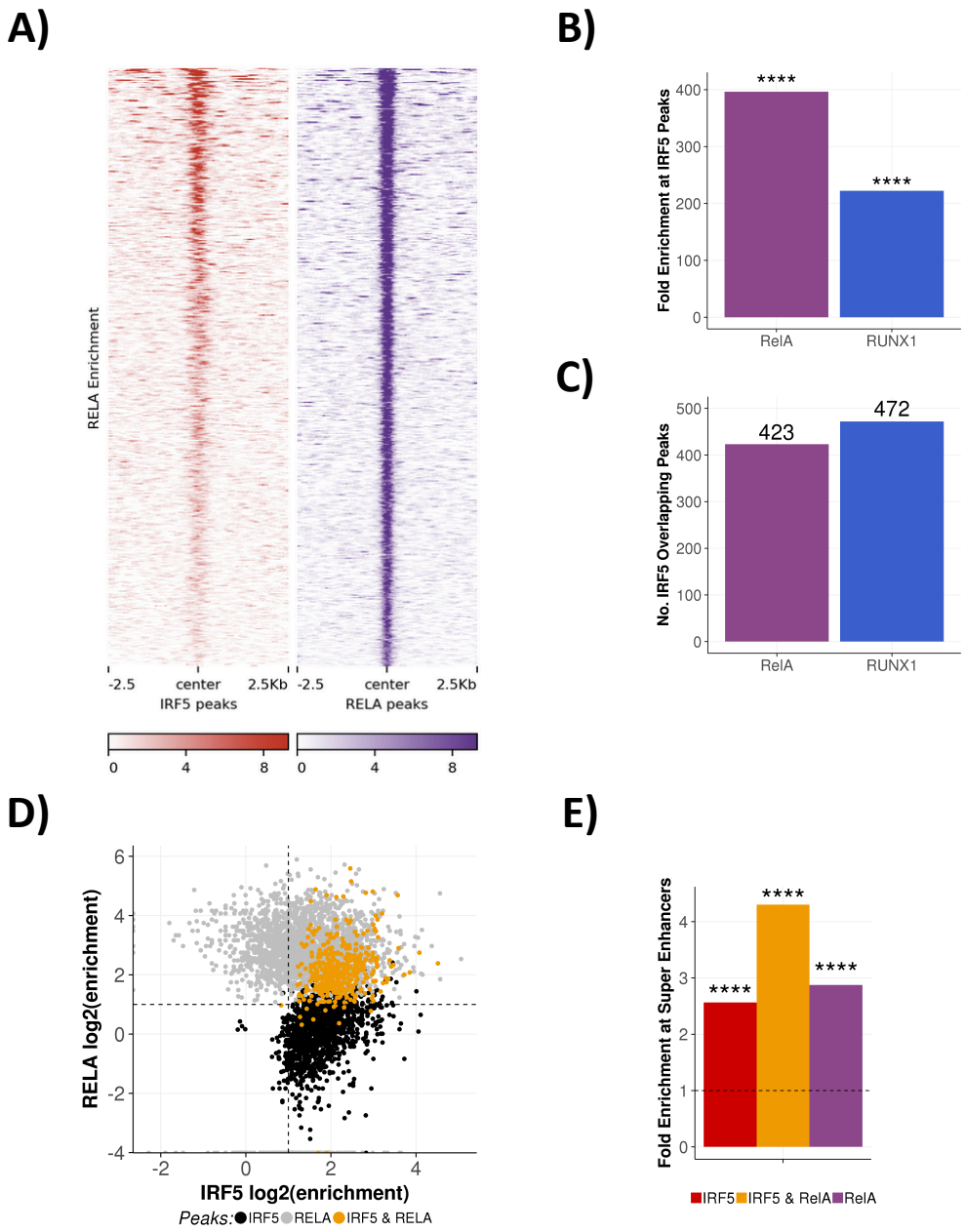

Figure 5.21. IRF5-RelA interactions. A) Heatmap of RelA enrichment at top 500 IRF5 and RelA peaks. **B)** Genomic association testing between RelA and RUNX1 ChIP peaks and IRF5 peaks (against genomic background). Asterisks indicate statistical significance according to adjusted p-values using the Benjamini-Hochberg procedure **C)** Size of RelA and RUNX1 peak overlaps with IRF5. **D)** Scatterplot depicting RelA and IRF5 enrichment over control (log2) at RelA, IRF5, and RelA-IRF5 overlapping peaks. **E)** Genomic association testing between ChIP-peak overlaps and regulatory regions (against a background of all open chromatin). Asterisks indicate statistical significance according to adjusted p-values using the Benjamini-Hochberg procedure. Significance thresholds (*p<0.05, **P<0.001, ***p<0.001, ****p<0.0001)

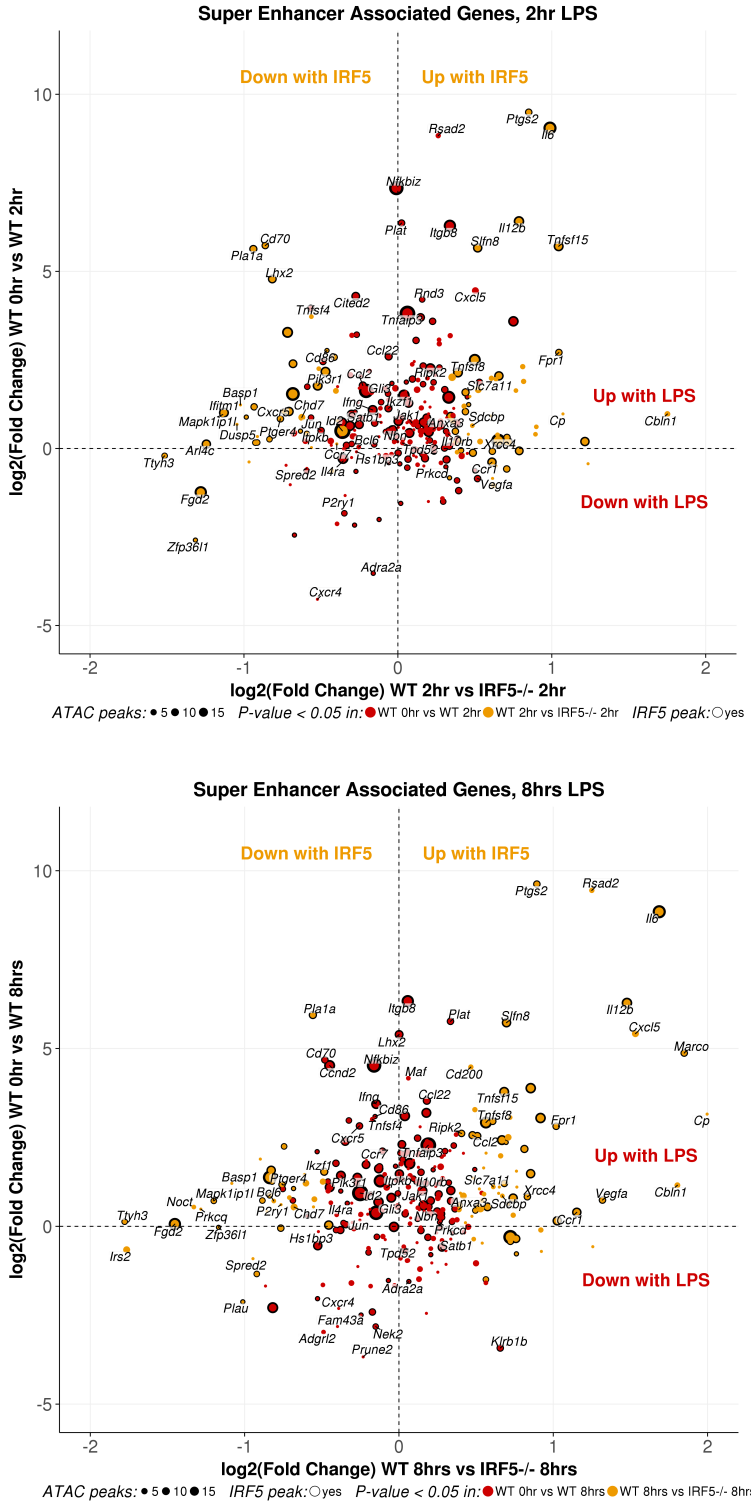

Figure 5.22. Differential expression of super enhancer associated genes. mRNA-seq data from wild type and IRF5$^{-/-}$ GM-BMDMs at 0hrs, 2hrs, and 8hrs post LPS-stimulation. Differential expression of protein coding genes was calculated with DESeq2 with an FDR of 0.05. Shown are significant (log2) fold change values for genes associated with super enhancers, which are either: differentially expressed with LPS stimulation (red), or differentially expressed between WT and IRF5$^{-/-}$ in LPS stimulated conditions (yellow). Genes with IRF5 ChIP-seq peaks are circled in black, point size is proportional to the number of ATAC-seq peaks associated with the gene.

Following these analysis we queried the effect of IRF5 on super enhancer mediated gene expression. To investigate this we integrated gene expression data from WT and IRF5$^{-/-}$ GM-BMDMs, IRF5 ChIP-seq, and ATAC-seq data (Figure 5.22). As previously (Figure 5.9), we observe a robust increase in the expression of the majority of genes under the control of super enhancers, concomitant to LPS stimulation, with a smaller proportion of genes being down regulated. Interestingly, we see a differential effect of IRF5, with both positive and negative contributions to gene expression, predominantly at direct IRF5 targets at the 2hr time point and additionally to non-IRF5 target genes at the 8hr time point. We also observe that the majority of highly LPS up-regulated genes are sensitive to IRF5 binding (*Ptgs2*, *Rsad2*, *Il6*, *Il12b*, *Cxcl5*, *Tnfsf15*) and that their fold induction remains high at the 8hr time point. Next we asked whether the cooperative binding of transcription factors to super enhancers had an impact on subsequent gene expression (Figure 5.23). These data indicate that RelA and IRF5 co-binding of super enhancers causes increased up-regulation of the associated genes in response to LPS, compared to IRF5 alone (p-value = 0.029), and a similar trend was observed for RUNX1. Furthermore, super enhancers targeted by all three transcription factors demonstrate a clear trend, with increased LPS inducibility over those bound by two transcription factors. This pattern of increasing transcription factor occupancy yielding increased induction of associated genes implicates cooperation in the recruitment of IRF5-RUNX1, and IRF5-RelA.

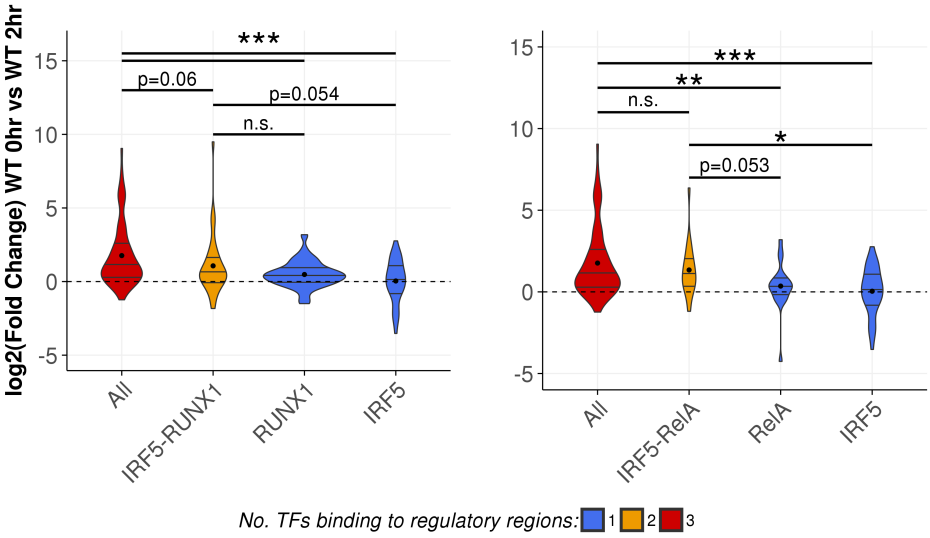

Figure 5.23. Effect of SDTF cooperation on gene expression. mRNA-seq data from wild type and IRF5$^{-/-}$ GM-BMDMs at 0hrs and 2hrs post LPS-stimulation. Differential expression of protein coding genes was calculated with DESeq2 with an FDR of 0.05. Shown are significant (log2) fold change values for genes associated with super enhancers. Super enhancers are binned into groups based on the binding of IRF5, RUNX1, and RelA. Lines within violins indicate upper, median, and lower quartiles, and points indicate the mean. Significance indicated was calculated using the Mann-Whitney U test. Asterisks indicate significance thresholds *p<0.05, **p<0.01, ***p<0.001.

5.3. Discussion

Previously my laboratory has demonstrated that IRF5 is a crucial mediator of inflammatory macrophages *in vivo* and classical macrophage activation *in vitro* and controls the transcription of various inflammatory cytokines and chemokines (Krausgruber et al., 2010; Krausgruber et al., 2011; Eames et al., 2012; Saliba et al., 2014; Weiss et al., 2013; Weiss et al., 2015; Dalmas et al., 2015; Byrne et al., 2016). My analysis reveals that (1) binding of IRF5 is highly LPS inducible and that it has a strong preference for promoters over other genomic regions (2) outside of promoter regions, IRF5 is preferentially recruited to key regulatory sites rich in open chromatin, so called super enhancers, and (3) interacts with RUNX1 (and RelA) to increase up-regulation of the associated genes in response to LPS.

The classification of super enhancers as a distinct entity to normal or traditional enhancers is a contentious issue, with little agreement as to what functionally defines a super enhancer other than the analysis procedure commonly used to find them. This procedure, consisting of merging nearby enhancers (within 12.5 k.b.) and ranking them by enrichment of enhancer-associated markers (detailed in section 2.2.1) was initially outlined by (Whyte et al., 2013; Lovén et al., 2013), using enrichment of Mediator (Med1) to characterise super enhancers. It was noted that very high levels of H3K27ac, Brd4, and DNase1 accessibility were also characteristic of super enhancers (Whyte et al., 2013). Subsequently, additional co-activators and histone marks themselves (such as p300 and H3K27ac) have been used to identify super enhancers (Witte et al., 2015; Chapuy et al., 2014; Ding et al., 2015). Thus, analysis of ChIP-seq datasets for super-enhancers has become routine, with NGS analysis suites such as HOMER and ROSE providing tools for defining super enhancers (Heinz et al., 2010; Lovén et al., 2013). In addition, specific pipelines for the utilisation of ATAC-seq data in a similar capacity have also been developed (Semenkovich et al., 2016). However, there still lacks a clear consensus on what makes an enhancer super, and if there is any functional significance of this delineation.

Our own analysis indicates that although super enhancers represent a minority of the total macrophage enhancer landscape, they account for a large proportion of the total ATAC-seq enhancer signal (Figure 5.5.A). This concurs with other observations of ATAC-seq defined super enhancers (Semenkovich et al., 2016). It is unclear to what extent traditional and super enhancers are separate entities: they both have the same distribution in relation to their target genes (Figure 5.5.B), and they both contain a variable number of enhancers, and therefore have a variable width (Figure 5.5.C). In terms of LPS inducibility, traditional enhancers exhibit more dynamic changes in gross numbers between unstimulated and LPS stimulated conditions, but examining changes at the level of the constituent ATAC-seq peaks making up the enhancer subgroups reveals that there is no significant difference between the two (Figure 5.5.D). This contrasts with other reports of super enhancer formation in inflammation, which possit super enhancers as being highly dynamic in response to stimuli; with large scale decommissioning of basal super enhancers in favour of their inflammatory replacements (Brown et al., 2014). However, this could be due to differences in the cell types examined, with endothelial cells having to modulate their chromatin structure to a much greater extent in order to implement an inflammatory program of gene expression compared to GM-BMDMs, which exist in a basally primed state (Chapter 3.2), with high IRF5 expression (Krausgruber et al., 2011) and increased responsiveness to inflammatory stimuli (Sorgi et al., 2012). That being said, chromatin remodelling is not a phenomenon restricted to super enhancers.

Histone marks are key indicators of the status of regulatory features, and the relative enrichment of H3K4me1, H3K4me3, and H3K27ac at the discrete ATAC-seq peaks falling within promoters, and traditional, or super, enhancers helps to differentiate these features (Figure 5.7). Firstly, both classes of enhancer have a greater H3K4me1:H3K4me3 ratio than promoter peaks, which are very strongly enriched for H3K4me3. More interestingly, we see specific differences between enhancer subgroups in terms of their H3K27 acetylation profile, with peaks within super enhancers exhibiting greater H3K4me1 and H3K27ac, and further

increases in H3K27ac with LPS stimulation. The implication being that super enhancers are more active than traditional enhancers, since this mark is commonly associated with enhancer activation (Kaikkonen et al., 2013; Zhu et al., 2013; Glass and Natoli, 2015). Our chrRNA data reinforces this hypothesis, with enhancer RNA (eRNA) observable at super enhancer but not traditional enhancers. This implies that super enhancers are active points of transcription, this is in line with other reports of super enhancer associated eRNA (Hnisz et al., 2013; Hah et al., 2015). The decreased quantity and focal enrichment of chrRNA at super enhancers compared to promoters is indicative of non-productive transcription. Indeed it has been observed that actively-enforce early termination is required to keep non-productive transcription arising from *cis*-regulatory elements in check (Austenaa et al., 2015). PU.1 is a key orchestrator of macrophage chromatin architecture (Barozzi et al., 2014) and has been associated with super enhancers in B cells (Whyte et al., 2013). Concordant with this we find PU.1 enrichment at super enhancers to be approximately two fold higher than in either traditional enhancers or promoters (Figure 5.7). This indicates a key regulatory role for super enhancers in macrophage function. Additionally, we find that ATAC-seq peaks in super enhancers are more accessible than those in traditional enhancers; indeed they are more comparable to promoters (Figure 5.7). Suggesting that super enhancers are enriched for strong enhancers a.k.a. hotspots (Siersbæk et al., 2014), such as that present upstream of *Marco* (Figure 5.6), in addition to clusters of individual enhancers *e.g.* at *Ripk2* (Figure 5.6). Out of the three classes of regulatory elements super enhancers also have the greatest change in accessibility in response to LPS, implicating them closely with inflammatory processes and as potential targets for SDTFs.

In line with this we find super enhancers to be preferentially associated with inflammatory processes, whereas traditional enhancers are more associated with metabolic function (Figure 5.8). Other reports reinforce this observation, documenting super enhancers as being highly associated with core cellular functions (Hnisz et al., 2013; Whyte et al., 2013; Parker et al., 2013). Super enhancers have been attributed to mediating stronger, more

robust changes in gene expression than other enhancers (Whyte et al., 2013; Hnisz et al., 2015). However, we see no differences in the range of gene expression, or fold change, between super enhancers and traditional enhancers (Figure 5.9.A). However, super enhancers are much more strongly associated with LPS up-regulated genes than traditional enhancers; further implicating them as core regulators of the macrophage inflammatory response (Figure 5.9.B). Upon examination of the sequence conservation of enhancer ATAC peaks we found that super enhancers are more enriched for evolutionary conserved enhancers than traditional enhancers (Figure 5.10). The clusters of ATAC peaks comprising super enhancers could therefore reflect an evolutionary selection pressure for tight regulation of the associated genes, which are crucial for cellular identity and function.

Combined, our data can be taken to infer that, rather than being a distinct regulatory entity, super enhancers more probably represent dense clusters of enhancers and strong individual enhancers. The degree to which super enhancer constituents contribute to changes in gene expression is a hotly debated topic, with some positing that they form cooperative networks collaboratively regulating gene expression (Hnisz et al., 2017). Supporting this increased chromatin interactions between super enhancer constituents have been observed, suggesting complex interactions in the mediation of gene expression (Dowen et al., 2014). Indeed it has been reported that super enhancers are gained or lost as units (Hnisz et al., 2013), with some being particularly labile, the deletion of single cofactors or constituents leading to their decommissioning and collapse (Lovén et al., 2013; Mansour et al., 2014). Recently, CRISPR-Cas9 has been utilised in the design of elegant studies to elucidate the functions of the constituent peaks comprising individual super enhancers. Hnisz et al. demonstrate variable levels of constituent enhancer contributions to gene expression, with all of the *Sik1* super enhancer constituents contributing to stable gene expression, whereas at *Prdm14* one dominant constituent enhancer drives gene expression (Hnisz et al., 2015). Removal of constituent enhancers from within the *Nr4a1* super enhancer also have varied effects on gene expression, the majority of them minor, however ablation of a single

dominant constituent results in prevention of subsequent gene expression. These data implicate redundancy in the *Nr4a1* super enhancer, with one constituent enhancer being necessary and sufficient for gene expression (G.D. Thomas et al., 2016). Furthermore, dissection of the canonical α-globin locus control region (or super enhancer), in which activity of its constituent enhancers are individually abrogated, reveals that they have no cooperative or synergistic activities (Hay et al., 2016). More work is needed to fully elucidate the function of super enhancers, but it is likely that these trends are more generally applicable, with variable contributions of constituent enhancers to gene expression. That being said super enhancers still represent a useful feature to uniformly locate and identify powerful regulatory elements, which are closely associated with cellular identity and function, and can be used to distinguish macrophage specific functions (Gosselin et al., 2014).

Lineage determining, and cell specific, transcription factors are known to be highly enriched at super enhancers, which are attributed as having roughly ten fold the density of transcriptional regulators than traditional enhancers. (Hnisz et al., 2013; Lovén et al., 2013; Whyte et al., 2013). In order to investigate the key macrophage SDTFs we therefore utilise the identified super enhancers as characteristic markers of the core macrophage enhancer landscape and assess the LPS inducible binding of twenty-three transcription factors to these regions. Using this unbiased approach, we define a core super enhancer signature (RelB, Rel, Stat3, JunB, RUNX1, IRF5, RelA) (Figure 5.11.A). We further characterised these transcription factors, demonstrating that LPS promotes their recruitment to super enhancers (Figure 5.12.A and B). The majority of these factors are known for mediating macrophage inflammatory responses, however, strikingly we also observe a high level of inducible RUNX1 recruitment and concurrent strong enrichment for RUNX motifs (Figure 5.13). Together these data implicate super enhancers as nodes for focussing extracellular derived signals at the level of chromatin; selectively regulating LPS induced inflammatory genes, and implicate RUNX1 as a core orchestrator of the macrophage inflammatory responses.

RUNX1 is primarily known for its role in definitive adult haematopoiesis (Okuda et al., 1996; Wang et al., 1996; Cai et al., 2000; M.J. Chen et al., 2009). It is part of the RUNX family of transcription factors, which share the Runt-related domain for DNA binding, an evolutionary conserved domain with high homology to the *Drosphilia Melanogaster* transcription factor Runt, from whence the family derives its name (Runt-related proteins) (van Wijnen et al., 2004). RUNX1 is essential for macrophage development; in its absence primitive yolk-sac macrophages are severely depleted (Frame et al., 2016). RUNX1 is expressed as early as E7.5 in development (North et al., 1999) and initiates the subsequent expression of PU.1 (G. Huang et al., 2007; Hoogenkamp et al., 2009). Aside from its role in development the function of RUNX1 in macrophages is little understood.

In macrophages RUNX1 is known to regulate the transcription of the M-CSF receptor, contributing to the regulation of macrophage proliferation and survival (D.E. Zhang et al., 1996; Himes et al., 2005), in addition to regulating the integrin LFA-1 (Puig-Kröger et al., 2003), and recently has been linked with IL-6 and IL-1β expression (Luo et al., 2016). Additional data implicate Runx1 in Th1/Th2 and regulatory T cell (Treg) specification and function, in addition to the maintenance of immature B cells (Voon et al., 2015). Our data indicate that RUNX1 binding is highly LPS-inducible, genome wide (Figures 5.15.B, 5.15.C), and that RUNX1 targets are inflammatory in nature (Figure 16).

DNA binding of RUNX1 is autoinhibited by sequences flanking its Runt DNA-binding domain (W.Y. Kim et al., 1999; T.L. Gu et al., 2000). RUNX1 activity therefore requires its obligate cofactor core binding factor β (CBFβ) for relief of inhibition and activity (Ogawa et al., 1993; Tahirov et al., 2001). However, cooperation between RUNX1 and additional factors is also described. For example, in T cells RUNX1 has been shown to interact with ETS1 via co-recruitment to composite motifs enriched at genes relating to inflammatory function (Hollenhorst et al., 2007; Hollenhorst et al., 2009). Additionally, RUNX1 has been

demonstrated to directly interact with Foxp3 to regulate Treg function (Ono et al., 2007). Direct protein interactions and binding of a shared composite motif have also been described for RUNX1 and the AP-1 family members c-Fos and c-Jun, via the RUNX1 cofactor CBFα (D'Alonzo et al., 2002). It therefore stands that RUNX1 could exert its inflammatory activities in macrophages inducibly, by cooperatively binding RUNX-ISRE composite motifs we identified under RUNX1 ChIP peaks (Figure 5.17). Furthermore, we see significant overlaps between RUNX1 and IRF5, which are not shared by other inducible IRF family members (Figure 5.18.A and B). This implicates IRF5 as a RUNX1 cofactor in macrophages, able to interact with IRF5 directly (Figure 5.18.C). IRF5 is well known to function in a signal dependent manner, requiring inflammatory stimuli for activation (Ryzhakov et al., 2015), and could therefore represent the inducible signal required for relief of RUNX1 auto-inhibition. Gene expression data for RUNX1 supports this model with mRNA levels transiently decreasing post LPS stimulation (Figure 5.14.A), which may be a regulatory mechanism to control excessive inflammatory action by RUNX1.

IRF5 is also known to interact with the NFκB subunit RelA, mediating a similar inflammatory cistrome (Saliba et al., 2014). We are able to reproduce this finding with our more recent IRF5 ChIP-seq (Figure 5.21), furthermore we show that the IRF5-RUNX1 cistrome is of a comparable size of that mediated by IRF5-RelA (Figure 5.21.C), implying equal biological relevance. Intriguingly, both IRF5-RUNX1 and IRF5-RelA peaks show enhanced enrichment at super enhancers, compared to non-overlapping transcription factor peaks (Figures 5.20.B, 5.21.E). Enhancers have long since been known to function via the collaborative binding of transcription factors (Wathelet et al., 1998; Carey et al., 1990; Giese et al., 1995; T.K. Kim and Maniatis, 1997; Thanos and Maniatis, 1995) thought to be mediated by changes to DNA conformation induced by binding of the initial factor and promoting subsequent transcription factor recruitment (Falvo et al., 1995), by co-recruitment of transcriptional co-activators (Merika et al., 1998), and via direct protein – protein interactions (Johnson et al., 1979). We investigated the combinatorial binding of IRF5, RelA, and RUNX1 to super

enhancers (Figure 5.23), demonstrating that they had cooperative effects, acting to incrementally promote the transcription of associated genes.

The increased cooperative binding of SDTFs observed at enhancer clusters could provide a mechanism for greater transcriptional control of associated genes, as has been shown at other enhancer loci (Carey, 1998) and been described of super enhancers (Hnisz et al., 2015). In macrophages this could explain the high degree of association between super enhancers and inflammatory target genes (Figure 5.8 and 5.9.A), the expression of which requires tight regulation to balance beneficial sterilising inflammation and chronic inflammation leading to pathology (Karin et al., 2006). In order to investigate the effect of IRF5 on this system we examined the expression of super enhancer associated genes in both WT GM-BMDMs and IRF5$^{-/-}$ cells (Figure 5.22). Contrary to our expectations IRF5 has both positive and negative effects on the expression of LPS regulated genes under the control of super enhancers. IRF5 positively regulates the expression of many highly LPS inducible genes, such as *Ptgs2*, *Il6*, *Il12b*, and *Tnfsf15*, leading to a pro-inflammatory macrophage phenotype. Whilst simultaneously downregulating the expression of key genes associated with: antigen presentation (*Cd86*, *Tnfsf4*), leukocyte trafficking to efferent lymphatics (*Ccr7*, *Cxcr5*), down-regulation of inflammatory signalling (*Dusp5* (Moon et al., 2014), *Pi3kr1* (Luyendyk et al., 2008)), transcriptional regulators (*Id2, Lhx2, Fgd2*, *Zfp36l1*, *Chd7*), and fatty acid metabolism and signalling (*Pla1a*, *Ptger4*). Notably, the majority of IRF5 down-regulated genes are induced by LPS. IRF5 therefore seems to be acting in a modulatory capacity, fine tuning transcriptional responses to promote a classic macrophage inflammatory phenotype.

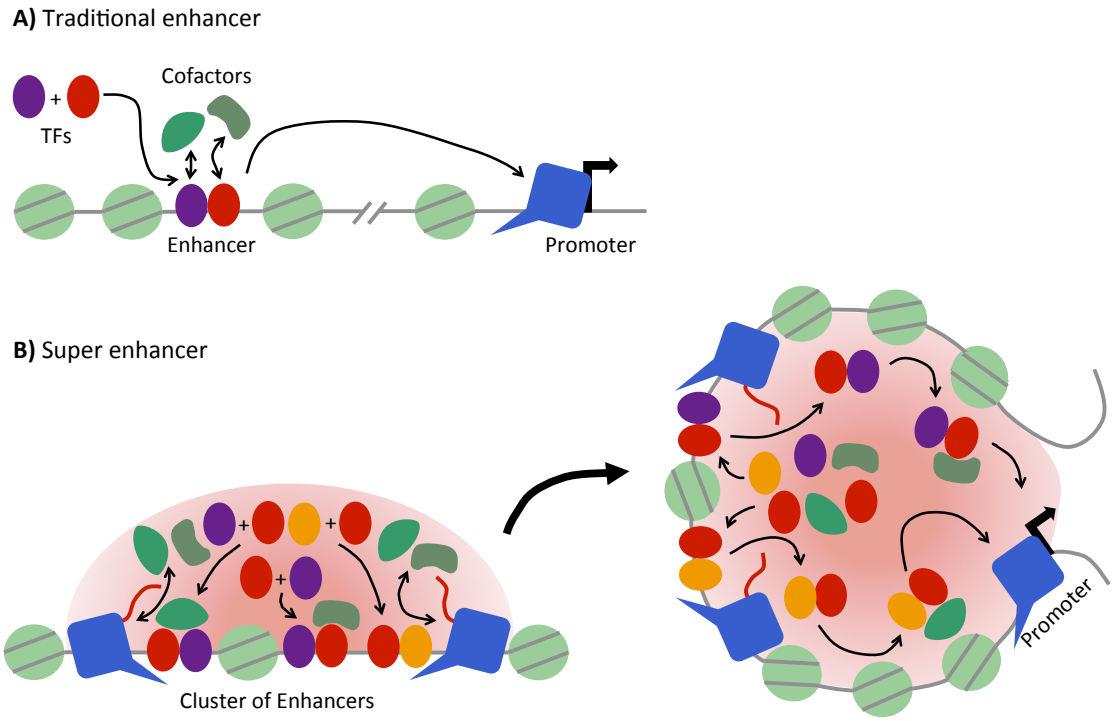

Figure 5.24. Phase separation model favours transcription factor cooperativity at enhancer clusters. A) Signal dependent transcription factors (SDTFs) are recruited to open chromatin. Low level binding to traditional enhancers mediates Pol II recruitment and transcription of the associated gene. **B)** Clusters of open chromatin at super enhancers increase local concentrations of SDTFs, cofactors, Pol II, and nascent RNA. Increasing the rate of reversible post-translational modifications of highly phosphorylated proteins, such as the Pol II CTD, H3 tails, TFs, and cofactors, promoting transient "cross-links" between transcriptional machinery. These contribute to the phase separation of enhancers and target genes in liquid-like droplets, enhancing TF interactions, cofactor recruitment, and enhancer – promoter interactions; mediating the fine-tuning of transcriptional control.

In summation we uncovered a novel role for the RUNX1 transcription factor in macrophage inflammatory responses, via the use of super enhancers as representative markers of core macrophage function. Subsequently, we observe cooperative binding of IRF5 with both RUNX1 and RelA, which is enriched at super enhancers compared to other regulatory regions, functioning to promote the transcription of pro-inflammatory genes. However, upon abrogating IRF5 function we see contrasting effects on the expression of super enhancer associated genes, with a reduction in the expression of highly pro-inflammatory genes (in the absence of IRF5), and an increase in the expression of other LPS dependent inflammatory genes corresponding to a shift in macrophage function; promoting antigen presentation and the dampening of inflammation.

We therefore conclude that IRF5 acts in a highly cooperative manner, interacting with RUNX1 and RelA to mediate a program of inflammatory gene expression, furthermore it is likely that IRF5 has additional binding partners not yet identified, which could play a role in the down-regulation of target genes. Our data indicate that the clustering of enhancers (identified as super enhancers) could act as focal points for the recruitment of transcriptional machinery, leading to increased local concentrations of SDTFs, promoting their interactions and cooperative binding. This ties in closely with the newly described phase separation model for enhancer function, in which clusters of enhancers (or super enhancers) promote the local concentrations of transcriptional machinery. Dynamic post-translational modifications of H3 tails, Pol II CTD, transcription factors, and cofactors, all act to increase the rate of the formation of transient "cross-links" between interacting transcriptional machinery with nascent RNA species further contributing to this molecular glue. The result is the phase separation of highly active chromatin hubs into water-like droplets (Hnisz et al., 2017). This model allows the incorporation of classic features of enhancers with more novel observations such as the phenomenon of transcriptional bursting and the simultaneous activation of multiple genes by a single enhancer (Zhao et al., 2016). Phase separation would also contribute to the increased transcription factor interactions observed at super enhancers by concentrating these factors in a defined area (Figure 5.24). Super enhancers therefore provide a unique mechanism for the integration of extracellular derived signals at the level of chromatin to tailor transcriptional responses to a myriad of potential scenarios.

6. General Discussion

Macrophages are crucial regulators of inflammation; armed with an impressive arsenal of PRRs they are able to effectively gauge the environment and respond accordingly, shaping the progress of ensuing immune reactions. Recent studies have highlighted the heterogeneity of macrophage populations (Lavin et al., 2014) and revealed distinct ontogenies of tissue-resident macrophages (Ginhoux and Guilliams, 2016), which act to perform a range of tissue-specific functions in addition to acting as the primary sentinels of inflammation, initiating inflammation in response to exogenous stimuli (Ginhoux et al., 2015). In such a reaction the predominant incoming mononuclear phagocyte is the monocyte, which has the capacity to differentiate into both macrophages and DCs. Monocyte-derived macrophages are major inflammatory mediators of immune responses, however, they are not uniform populations, exhibiting considerable heterogeneity (Kratofil et al., 2017). The DCs arising from tissue-infiltrating monocytes are also pro-inflammatory in nature, characterised by the production of TNF and iNOS (Serbina et al., 2003), in contrast to cDCs, which are highly motile and efficient at antigen presentation, rapidly migrating to lymph nodes shortly after activation. Furthermore, the distinction between monocyte-derived macrophages and DCs is unclear, and is typically based on characteristic markers; all monocyte derived cells are capable of expressing CD11c and MHC class II, whereas the expression of MERTK, F4/80, and CD64 is deemed macrophage specific (Guilliams et al., 2014). Notably, the functional capacities of the monocyte derived cells differs, with cells exhibiting either predominantly macrophage attributes (*e.g.* high phagocytic capacity, anti-microbial, poor migration) or DC attributes (*e.g.* migration to lymph nodes, enhanced antigen presentation) (Jakubzick et al., 2017). These functional changes are accompanied by gross phenotypic differences between monocyte precursors and their progeny, this is best exemplified by changes in the size of cells, with influxing monocytes averaging diameters of 7-8 µm and differentiated monocyte-derived macrophages reaching 15-20 µm (Jakubzick et al., 2017). However, the extent to which monocyte-derived DCs and macrophages represent

terminally differentiated cells or poles of continuum is unknown, but it can be appreciated that profound transcriptional changes must mediate the observed phenotypic diversity.

IRF5 has been identified as a key transcription factor regulating pro-inflammatory macrophage polarisation (Krausgruber et al., 2011), and mediating the transcription of inflammatory chemokines and cytokines (Krausgruber et al., 2010; Krausgruber et al., 2011; Saliba et al., 2014). In this thesis we explored the transcriptional activity of IRF5, revealing that in addition to inducing inflammatory chemokines and cytokines, IRF5 has a key role in the up regulation of anti-microbial genes whilst supressing homeostatic macrophage function (Chapter 4). These data suggest that IRF5 is an important mediator of pro-inflammatory responses to bacterial stimuli, at the expense of steady-state tissue-resident macrophage function such as efferocytosis. The extent to which IRF5 contributes to transcriptional responses in tissue-resident macrophages vs monocyte-derived macrophage is not known, however, it is likely that basal levels of IRF5 expression in tissue-resident populations is low, as it has been demonstrated that inflammatory stimuli such as GM-CSF and IFN-γ induce IRF5 expression (Krausgruber et al., 2011), and that tissue-resident macrophages are not pro-inflammatory at homeostasis (Davies et al., 2013). Consequently, it follows that low levels of IRF5 in tissue-resident macrophages likely induces key target genes, such as the chemokines and cytokines under the control of super enhancers. In conditions of inflammation incoming Ly6C^{hi} monocytes are exposed to such factors as GM-CSF, and express high levels IRF5 (G.D. Thomas et al., 2016), the activity of which would contribute to their strong anti-microbial phenotype.

Recently it has been suggested that Ly6C^{hi} monocytes can be subdivided into two precursor populations, which subsequently differentiate into either DCs or macrophages (Menezes et al., 2016). However, subsequent single-cell RNA-seq analyses of murine monocytes have reported homogeneity of Ly6C^{hi} monocytes (Mildner et al., 2017). Indeed the micro-environment into which monocytes arrive seems to be a key factor in cell fate, favouring

either DC or macrophage phenotypes (Zigmond et al., 2012; Bain et al., 2013; Goudot et al., 2017). Utilising an *in vitro* cell system in which monocytes are cultured with M-CSF, IL-4, and TNF to yield mixed populations of monocyte-derived macrophages and DCs, (Goudot et al., 2017) report that the default fate of monocytes is to progress into monocyte-derived macrophages in inflammatory conditions, which is mediated by the transcription factor MafB. However, micro-environmental signals acting to induce IRF4 and the nuclear receptor Ahr act as a molecular switch, promoting DC-like maturation.

It is interesting to speculate on the role of IRF5 in shaping monocyte fate, as in a guided analysis of key macrophage and DC markers identified by the ImmGen Consortium (J.C. Miller et al., 2012; Gautier et al., 2012) we observed that core macrophages markers (*e.g. Lamp2, Cd14, Tlr7, Tbxas1, Fcgr1, Pla2g4a*) were more highly expressed in WT GM-BMDMs and that DC markers (*e.g. Napsa, Fgl2, Spint2, Hmgn3, Kmo, H2-Dmb2*) were expressed at a greater level in IRF5$^{-/-}$ GM-BMDMs (Chapter 4). Furthermore when focussing on super enhancer associated genes, we found similar results, with IRF5 acting to promote the transcription of inflammatory cytokines and down regulate genes associated with antigen presentation and leukocyte trafficking to efferent lymphatics (Chapter 5). In monocytes, basally expressed IRF5 (G.D. Thomas et al., 2016) and MafB (Goudot et al., 2017) may therefore act to jointly promote differentiation to macrophages, encompassing the default maturation pathway. IRF4 has been demonstrated to compete directly with IRF5 for activation by MyD88 binding (Negishi et al., 2005), furthermore IRF4 negatively regulates IRF5 expression through repression of the IRF5 promoter (Xu et al., 2011), and down regulates IRF5 target genes (Negishi et al., 2005). The induction of IRF4 in monocytes may therefore counteract the activities of IRF5 thus promoting a shift from a macrophage to DC phenotype. However, what mediates the bifurcation of homogenous monocyte precursors, exposed to the same stimuli, into distinct DC and macrophage like populations remains an unanswered question. Heterogeneity in the underlying chromatin landscape could in part explain the distinct responses to the same stimuli. Furthermore, a phase-separated model of

transcription (Hnisz et al., 2017) in which the clustering of enhancers concentrates extracellular derived signals at the level of chromatin, in a manner highly susceptible to perturbation by the decrease or absence of constituent factors, could give rise to the apparent stochastic nature of monocyte transcriptional outcomes. To investigate the role of IRF5 in monocyte differentiation a single cell RNA-seq approach would be best suited, to capture the full heterogeneity of responses. Additional data such as chromatin accessibility provided by single cell ATAC-seq (Buenrostro et al., 2015) could be leveraged alongside the gene expression data to infer the transcription factors driving this differentiation process through the analysis of motifs at differentially accessible ATAC-seq peaks and corresponding changes to gene expression.

To dissect the transcriptional regulation of macrophage inflammatory responses we used an *in vitro* system of GM- and M- differentiated BMDMs, the enhancer landscape of which is very similar in unstimulated conditions, aside from the priming of inflammatory genes by GM-CSF and altered metabolic profile of M-BMDMs (Chapter 3). To mitigate these differences we focussed on highly active clusters of enhancers, known as super enhancers, which are representative of cellular identity and function (Hnisz et al., 2013; Whyte et al., 2013). We utilised publically available data sets, in combination with our own data and that from collaborators, to investigate the roles of twenty-three transcription factors in BMDMs. Analysis of the binding profiles of these factors at super enhancers revealed a core set of SDTFs, which are inducibly recruited to PU.1 marked super enhancers. Further interrogation of these transcription factors revealed novel interactions between IRF5 and RUNX1 and recapitulated previous observations of IRF5-RelA interactions (Krausgruber et al., 2010; Saliba et al., 2014). This is the first study that highlights a possible involvement of RUNX1 in the inflammatory response, and thus extending its functions in macrophages from regulation of cell development to regulation of cell function. Furthermore, we observed that IRF5, RUNX1, and RelA interactions proceeded in a combinatorial fashion, acting to incrementally increase the expression of super enhancer associated genes. We have

previously demonstrated the requirement of RelA for IRF5 binding to co-occupied peaks (Saliba et al., 2014). However, to further interrogate the dynamics of RUNX1-IRF5 binding we plan to knockdown RUNX1 in GM-BMDMs, utilising RUNX1-flox mice and adenoviral delivery of Cre recombinase (as implemented for RelA knockdown in (Saliba et al., 2014)). Utilising this system we will examine the effects of RUNX1 on gene expression by mRNA-seq and interrogate the requirement of IRF5 for RUNX1 recruitment and *vice versa* at specific loci by ChIP-qPCR.

Our data supports the recently described phase separation model of transcription (Hnisz et al., 2017), with increased transcription factor occupancy at super enhancers acting to promote SDTF interactions and the LPS dependent transcription of associated genes, both of which are greater than at traditional enhancers (Chapter 5). Notably this model is dependent on the presence of extensive enhancer promoter interactions, application of 3C based technologies, such as Capture-C (Hughes et al., 2014) to simultaneously assay the interaction of hundreds of constituent ATAC-seq peaks making up extended super enhancer regions would therefore be very informative in the context of macrophage activation. Of particular interest would be the individual abrogation of super enhancer binding SDTFs and Capture-C and mRNA-seq to examine the effects on chromatin architecture and associated transcriptional responses.

In addition to its transcription stimulating activity, we also described a large subset of IRF5 regulated genes that were repressed by IRF5 (Chapter 4). Additional work is required to elucidate the molecular mechanisms by which IRF5 down regulates pro-resolving and homeostatic target genes, however, it is likely that IRF5 interacts with transcriptional co-repressors, either directly or via additional SDTF interactions. Transient changes in gene expression observed at down regulated genes were concomitant with a loss of H3K27 acetylation and reduced transcription; it is therefore likely that IRF5 interacts with a histone deacetylases (HDACs) to mediate these changes shortly after LPS stimulation. Previously an

IRF5-TRIM28 interaction has been described (Eames et al., 2012). TRIM28 is a transcriptional co-repressor interacting with chromatin remodelling factors including HDACs and histone methyltransferases (HMTs). Indeed, IRF5 forms a complex with TRIM28 and the HMT SETDB1, acting to promote deposition of the H3K9me3 mark (Eames et al., 2012). H3K9me3 is a repressive chromatin mark inducing the recruitment of HP1 and heterochromatin formation. We did not observe any changes to chromatin accessibility mediated by IRF5 (Chapter 1), however, our studies were limited to two hours post-LPS activation. It is possible that over a longer time period the promoters of IRF5 down-regulated become less accessible, mediated by IRF5 induced loss of H3K27ac, and gain of the repressive H3K9me3 mediating subsequent recruitment of HP1 and DNA methylation. Recently IFN-γ stimulation of macrophages has been demonstrated to decommission promoters of down regulated genes, which is associated with a similar chain of events (Kang et al., 2017).

In summary, IRF5 is a potent regulator of macrophage transcription, acting dynamically to promote pro-inflammatory module of transcription via the modulation of Pol II recruitment to *cis*-regulatory regions; promoting the transcription of inflammatory and anti-microbial genes, whilst repressing the transcription of genes associated with resolution and homeostasis. Furthermore, IRF5 activity is highly cooperative, demonstrating direct interactions and co-recruitment with both RUNX1 and RelA to inflammatory target genes. IRF5 is therefore a key mediator of macrophage pro-inflammatory responses, and may also act as a regulator of monocyte to macrophage differentiation, due to its activity in supressing the transcription of DC marker genes and promotion of pro-inflammatory macrophage phenotypes in GM-BMDMs.

7. Bibliography

Adelman, K. and Lis, J.T. 2012. Promoter-proximal pausing of RNA polymerase II: emerging roles in metazoans. *Nature Reviews Genetics*. **13**(10),pp.720–731.

Adelman, K., Kennedy, M.A., Nechaev, S., Gilchrist, D.A., Muse, G.W., Chinenov, Y. and Rogatsky, I. 2009. Immediate mediators of the inflammatory response are poised for gene activation through RNA polymerase II stalling. *Proceedings of the National Academy of Sciences*. **106**(43),pp.18207–18212.

Aikawa, Y., Katsumoto, T., Zhang, P., Shima, H., Shino, M., Terui, K., Ito, E., Ohno, H., Stanley, E.R., Singh, H., Tenen, D.G. and Kitabayashi, I. 2010. PU.1-mediated upregulation of CSF1R is crucial for leukemia stem cell potential induced by MOZ-TIF2. *Nature medicine*. **16**(5),pp.580–5– 1p following 585.

Ajuebor, M.N., Das, A.M., Virág, L., Flower, R.J., Szabó, C. and Perretti, M. 1999. Role of resident peritoneal macrophages and mast cells in chemokine production and neutrophil migration in acute inflammation: evidence for an inhibitory loop involving endogenous IL-10. *The Journal of Immunology*. **162**(3),pp.1685–1691.

Anders, S., Pyl, P.T. and Huber, W. 2015. HTSeq—a Python framework to work with high-throughput sequencing data. *Bioinformatics*. **31**(2),pp.166–169.

Andrews, S. 2010. FastQC: a quality control tool for high throughput sequence data. Available online at: http://www.bioinformatics.babraham.ac.uk/projects/fastqc

Arnosti, D.N. and Kulkarni, M.M. 2005. Transcriptional enhancers: Intelligent enhanceosomes or flexible billboards? *Journal of cellular biochemistry*. **94**(5),pp.890–898.

Arthur, J.S.C. and Ley, S.C. 2013. Mitogen-activated protein kinases in innate immunity. *Nature reviews. Immunology*. **13**(9),pp.679–692.

Aschoff, I.L. 1924. Das reticulo-endotheliale System. *Ergebn. Inn. Med. Kinderheilk*. **26**.

Austenaa, L.M.I., Barozzi, I., Simonatto, M., Masella, S., Chiara, Della, G., Ghisletti, S., Curina, A., de Wit, E., Bouwman, B.A.M., de Pretis, S., Piccolo, V., Termanini, A., Prosperini, E., Pelizzola, M., de Laat, W. and Natoli, G. 2015. Transcription of Mammalian cis-Regulatory Elements Is Restrained by Actively Enforced Early Termination. *Molecular Cell*. **60**(3),pp.460–474.

Back, J., Allman, D., Chan, S. and Kastner, P. 2005. Visualizing PU.1 activity during hematopoiesis. *Experimental hematology*. **33**(4),pp.395–402.

Bain, C.C., Bravo-Blas, A., Scott, C.L., Gomez Perdiguero, E., Geissmann, F., Henri, S., Malissen, B., Osborne, L.C., Artis, D. and Mowat, A.M. 2014. Constant replenishment from circulating monocytes maintains the macrophage pool in the intestine of adult mice. *Nature immunology*. **15**(10),pp.929–937.

Bain, C.C., Scott, C.L., Uronen-Hansson, H., Gudjonsson, S., Jansson, O., Grip, O., Guilliams, M., Malissen, B., Agace, W.W. and Mowat, A.M. 2013. Resident and pro-inflammatory macrophages in the colon represent alternative context-dependent fates of the same Ly6Chi monocyte precursors. *Mucosal Immunology*. **6**(3),pp.498–510.

Ban, T., Sato, G.R., Nishiyama, A., Akiyama, A., Takasuna, M., Umehara, M., Suzuki, S., Ichino,

M., Matsunaga, S., Kimura, A., Kimura, Y., Yanai, H., Miyashita, S., Kuromitsu, J., Tsukahara, K., Yoshimatsu, K., Endo, I., Yamamoto, T., Hirano, H., Ryo, A., Taniguchi, T. and Tamura, T. 2016. Lyn Kinase Suppresses the Transcriptional Activity of IRF5 in the TLR-MyD88 Pathway to Restrain the Development of Autoimmunity. *Immunity*. **45**(2),pp.319–332.

Banerji, J., Rusconi, S. and Schaffner, W. 1981. Expression of a beta-globin gene is enhanced by remote SV40 DNA sequences. *Cell*. **27**(2 Pt 1),pp.299–308.

Barboric, M., Nissen, R.M., Kanazawa, S., Jabrane-Ferrat, N. and Peterlin, B.M. 2001. NF-kappaB binds P-TEFb to stimulate transcriptional elongation by RNA polymerase II. *Molecular Cell*. **8**(2),pp.327–337.

Barish, G.D., Yu, R.T., Karunasiri, M., Ocampo, C.B., Dixon, J., Benner, C., Dent, A.L., Tangirala, R.K. and Evans, R.M. 2010. Bcl-6 and NF-kappaB cistromes mediate opposing regulation of the innate immune response. *Genes & development*. **24**(24),pp.2760–2765.

Barnes, B.J., Kellum, M.J., Field, A.E. and Pitha, P.M. 2002. Multiple regulatory domains of IRF-5 control activation, cellular localization, and induction of chemokines that mediate recruitment of T lymphocytes. *Molecular and cellular biology*. **22**(16),pp.5721–5740.

Barozzi, I., Simonatto, M., Bonifacio, S., Yang, L., Rohs, R., Ghisletti, S. and Natoli, G. 2014. Coregulation of Transcription Factor Binding and Nucleosome Occupancy through DNA Features of Mammalian Enhancers. *Molecular Cell*. **54**(5),pp.844–857.

Becher, B., Tugues, S. and Greter, M. 2016. GM-CSF: From Growth Factor to Central Mediator of Tissue Inflammation. *Immunity*. **45**(5),pp.963–973.

Bhatt, D.M., Pandya-Jones, A., Tong, A.-J., Barozzi, I., Lissner, M.M., Natoli, G., Black, D.L. and Smale, S.T. 2012. Transcript dynamics of proinflammatory genes revealed by sequence analysis of subcellular RNA fractions. *Cell*. **150**(2),pp.279–290.

Bleriot, C., Dupuis, T., Jouvion, G., Eberl, G., Disson, O. and Lecuit, M. 2015. Liver-resident macrophage necroptosis orchestrates type 1 microbicidal inflammation and type-2-mediated tissue repair during bacterial infection. *Immunity*. **42**(1),pp.145–158.

Bolger, A.M., Lohse, M. and Usadel, B. 2014. Trimmomatic: a flexible trimmer for Illumina sequence data. *Bioinformatics*. **30**(15),pp.2114–2120.

Borregaard, N. 2010. Neutrophils, from marrow to microbes. *Immunity*. **33**(5),pp.657–670.

Brown, J.D., Lin, C.Y., Duan, Q., Griffin, G., Federation, A.J., Paranal, R.M., Bair, S., Newton, G., Lichtman, A.H., Kung, A.L., Yang, T., Wang, H., Luscinskas, F.W., Croce, K.J., Bradner, J.E. and Plutzky, J. 2014. NF-κB Directs Dynamic Super Enhancer Formation in Inflammation and Atherogenesis. *Molecular Cell*. **56**(2),pp.219–231.

Buenrostro, J.D., Giresi, P.G., Zaba, L.C., Chang, H.Y. and Greenleaf, W.J. 2013. Transposition of native chromatin for fast and sensitive epigenomic profiling of open chromatin, DNA-binding proteins and nucleosome position. *Nature Methods*. **10**(12),pp.1213–1218.

Buenrostro, J.D., Wu, B., Litzenburger, U.M., Ruff, D., Gonzales, M.L., Snyder, M.P., Chang, H.Y. and Greenleaf, W.J. 2015. Single-cell chromatin accessibility reveals principles of regulatory variation. *Nature*. **523**(7561),pp.486–490.

Bulger, M. and Groudine, M. 2011. Functional and mechanistic diversity of distal

transcription enhancers. *Cell*. **144**(3),pp.327–339.

Byrne, A.J., Weiss, M., Mathie, S.A., Walker, S.A., Eames, H.L., Saliba, D., Lloyd, C.M. and Udalova, I.A. 2016. A critical role for IRF5 in regulating allergic airway inflammation. *Mucosal Immunology*.

Cai, Z., de Bruijn, M., Ma, X., Dortland, B., Luteijn, T., Downing, J.R. and Dzierzak, E. 2000. Haploinsufficiency of AML1 Affects the Temporal and Spatial Generation of Hematopoietic Stem Cells in the Mouse Embryo. *Immunity*. **13**(4),pp.423–431.

Cailhier, J.F., Partolina, M., Vuthoori, S., Wu, S., Ko, K., Watson, S., Savill, J., Hughes, J. and Lang, R.A. 2005. Conditional macrophage ablation demonstrates that resident macrophages initiate acute peritoneal inflammation. *The Journal of Immunology*. **174**(4),pp.2336–2342.

Calderon, B., Carrero, J.A., Ferris, S.T., Sojka, D.K., Moore, L., Epelman, S., Murphy, K.M., Yokoyama, W.M., Randolph, G.J. and Unanue, E.R. 2015. The pancreas anatomy conditions the origin and properties of resident macrophages. *Journal of Experimental Medicine*. **212**(10),pp.1497–1512.

Carey, M. 1998. The enhanceosome and transcriptional synergy. *Cell*. **92**(1),pp.5–8.

Carey, M., Leatherwood, J. and Ptashne, M. 1990. A potent GAL4 derivative activates transcription at a distance in vitro. *Science (New York, N.Y.)*. **247**(4943),pp.710–712.

Chapuy, B., McKeown, M.R., Lin, C.Y., Monti, S., Roemer, M.G.M., Qi, J., Rahl, P.B., Sun, H.H., Yeda, K.T., Doench, J.G., Reichert, E., Kung, A.L., Rodig, S.J., Young, R.A., Shipp, M.A. and Bradner, J.E. 2014. Discovery and Characterization of Super-Enhancer-Associated Dependencies in Diffuse Large B Cell Lymphoma. *Cancer Cell*. **25**(4),pp.545–546.

Chen, E.Y., Tan, C.M., Kou, Y., Duan, Q., Wang, Z., Meirelles, G.V., Clark, N.R. and Ma'ayan, A. 2013. Enrichr: interactive and collaborative HTML5 gene list enrichment analysis tool. *BMC bioinformatics*. **14**(1),p.128.

Chen, J. and Ivashkiv, L.B. 2010. IFN-γ abrogates endotoxin tolerance by facilitating Toll-like receptor-induced chromatin remodeling. *Proceedings of the National Academy of Sciences of the United States of America*. **107**(45),pp.19438–19443.

Chen, M.J., Yokomizo, T., Zeigler, B.M., Dzierzak, E. and Speck, N.A. 2009. Runx1 is required for the endothelial to haematopoietic cell transition but not thereafter. *Nature*. **457**(7231),pp.887–891.

Chen, W., Lam, S.S., Srinath, H., Jiang, Z., Correia, J.J., Schiffer, C.A., Fitzgerald, K.A., Lin, K. and Royer, W.E. 2008. Insights into interferon regulatory factor activation from the crystal structure of dimeric IRF5. *Nature structural & molecular biology*. **15**(11),pp.1213–1220.

Chen, X., Shen, Y., Draper, W., Buenrostro, J.D., Litzenburger, U., Cho, S.W., Satpathy, A.T., Carter, A.C., Ghosh, R.P., East-Seletsky, A., Doudna, J.A., Greenleaf, W.J., Liphardt, J.T. and Chang, H.Y. 2016. ATAC-see reveals the accessible genome by transposase-mediated imaging and sequencing. *Nature Methods*. **13**(12),pp.1013–1020.

Croxford, A.L., Lanzinger, M., Hartmann, F.J., Schreiner, B., Mair, F., Pelczar, P., Clausen, B.E., Jung, S., Greter, M. and Becher, B. 2015. The Cytokine GM-CSF Drives the Inflammatory Signature of CCR2+ Monocytes and Licenses Autoimmunity. *Immunity*. **43**(3),pp.502–514.

D'Alonzo, R.C., Selvamurugan, N., Karsenty, G. and Partridge, N.C. 2002. Physical interaction of the activator protein-1 factors c-Fos and c-Jun with Cbfa1 for collagenase-3 promoter activation. *Journal of Biological Chemistry*. **277**(1),pp.816–822.

Dalmas, E., Toubal, A., Alzaid, F., Blazek, K., Eames, H.L., Lebozec, K., Pini, M., Hainault, I., Montastier, E., Denis, R.G.P., Ancel, P., Lacombe, A., Ling, Y., Allatif, O., Cruciani-Guglielmacci, C., André, S., Viguerie, N., Poitou, C., Stich, V., Torcivia, A., Foufelle, F., Luquet, S., Aron-Wisnewsky, J., Langin, D., Clément, K., Udalova, I.A. and Venteclef, N. 2015. Irf5 deficiency in macrophages promotes beneficial adipose tissue expansion and insulin sensitivity during obesity. *Nature medicine*. **21**(6),pp.610–618.

Davies, L.C., Jenkins, S.J., Allen, J.E. and Taylor, P.R. 2013. Tissue-resident macrophages. *Nature immunology*. **14**(10),pp.986–995.

Dawson, M.A., Prinjha, R.K., Dittmann, A., Giotopoulos, G., Bantscheff, M., Chan, W.-I., Robson, S.C., Chung, C.-W., Hopf, C., Savitski, M.M., Huthmacher, C., Gudgin, E., Lugo, D., Beinke, S., Chapman, T.D., Roberts, E.J., Soden, P.E., Auger, K.R., Mirguet, O., Doehner, K., Delwel, R., Burnett, A.K., Jeffrey, P., Drewes, G., Lee, K., Huntly, B.J.P. and Kouzarides, T. 2011. Inhibition of BET recruitment to chromatin as an effective treatment for MLL-fusion leukaemia. *Nature*. **478**(7370),pp.529–533.

de Bruijn, M. and Dzierzak, E. 2017. Runx transcription factors in the development and function of the definitive hematopoietic system. *Blood*.

de Wit, E. and de Laat, W. 2012. A decade of 3C technologies: insights into nuclear organization. *Genes & development*. **26**(1),pp.11–24.

Dearman, R.J., Cumberbatch, M., Maxwell, G., Basketter, D.A. and Kimber, I. 2009. Toll-like receptor ligand activation of murine bone marrow-derived dendritic cells. *Immunology*. **126**(4),pp.475–484.

Dekker, J., Rippe, K., Dekker, M. and Kleckner, N. 2002. Capturing chromosome conformation. *Science (New York, N.Y.)*. **295**(5558),pp.1306–1311.

DeKoter, R.P. and Singh, H. 2000. Regulation of B lymphocyte and macrophage development by graded expression of PU.1. *Science (New York, N.Y.)*. **288**(5470),pp.1439–1441.

Delamarre, L., Pack, M., Chang, H., Mellman, I. and Trombetta, E.S. 2005. Differential lysosomal proteolysis in antigen-presenting cells determines antigen fate. *Science (New York, N.Y.)*. **307**(5715),pp.1630–1634.

Di Paolo, N.C., Doronin, K., Baldwin, L.K., Papayannopoulou, T. and Shayakhmetov, D.M. 2013. The transcription factor IRF3 triggers 'defensive suicide' necrosis in response to viral and bacterial pathogens. *CellReports*. **3**(6),pp.1840–1846.

Ding, J., Huang, X., Shao, N., Zhou, H., Lee, D.-F., Faiola, F., Fidalgo, M., Guallar, D., Saunders, A., Shliaha, P.V., Wang, H., Waghray, A., Papatsenko, D., Sánchez-Priego, C., Li, D., Yuan, Y., Lemischka, I.R., Shen, L., Kelley, K., Deng, H., Shen, X. and Wang, J. 2015. Tex10 Coordinates Epigenetic Control of Super-Enhancer Activity in Pluripotency and Reprogramming. *Cell Stem Cell*. **16**(6),pp.653–668.

Dobin, A., Davis, C.A., Schlesinger, F., Drenkow, J., Zaleski, C., Jha, S., Batut, P., Chaisson, M. and Gingeras, T.R. 2013. STAR: ultrafast universal RNA-seq aligner. *Bioinformatics*. **29**(1),pp.15–21.

Dostie, J., Richmond, T.A., Arnaout, R.A., Selzer, R.R., Lee, W.L., Honan, T.A., Rubio, E.D.,

Krumm, A., Lamb, J., Nusbaum, C., Green, R.D. and Dekker, J. 2006. Chromosome Conformation Capture Carbon Copy (5C): a massively parallel solution for mapping interactions between genomic elements. *Genome Research*. **16**(10),pp.1299–1309.

Dowen, J.M., Fan, Z.P., Hnisz, D., Ren, G., Abraham, B.J., Zhang, L.N., Weintraub, A.S., Schujiers, J., Lee, T.I., Zhao, K. and Young, R.A. 2014. Control of cell identity genes occurs in insulated neighborhoods in mammalian chromosomes. *Cell*. **159**(2),pp.374–387.

Doyle, S., Vaidya, S., O'Connell, R., Dadgostar, H., Dempsey, P., Wu, T., Rao, G., Sun, R., Haberland, M., Modlin, R. and Cheng, G. 2002. IRF3 mediates a TLR3/TLR4-specific antiviral gene program. *Immunity*. **17**(3),pp.251–263.

Dye, M.J. and Proudfoot, N J 2001. Multiple transcript cleavage precedes polymerase release in termination by RNA polymerase II. *Cell*. **105**(5),pp.669–681.

Eames, H.L., Saliba, D.G., Krausgruber, T., Lanfrancotti, A., Ryzhakov, G. and Udalova, I.A. 2012. KAP1/TRIM28: an inhibitor of IRF5 function in inflammatory macrophages. *Immunobiology*. **217**(12),pp.1315–1324.

Ehrlich, P. 1880. Methodologische beiträge zur physiologie und pathologie der verschiedenen formen der leukocyten. *Z Klin Med*. **1**(1),pp.553–560.

Elliott, M.R., Koster, K.M. and Murphy, P.S. 2017. Efferocytosis Signaling in the Regulation of Macrophage Inflammatory Responses. *Journal of immunology (Baltimore, Md. : 1950)*. **198**(4),pp.1387–1394.

ENCODE Project Consortium 2012. An integrated encyclopedia of DNA elements in the human genome. *Nature*. **489**(7414),pp.57–74.

Epelman, S., Lavine, K.J., Beaudin, A.E., Sojka, D.K., Carrero, J.A., Calderon, B., Brija, T., Gautier, E.L., Ivanov, S., Satpathy, A.T., Schilling, J.D., Schwendener, R., Sergin, I., Razani, B., Forsberg, E.C., Yokoyama, W.M., Unanue, E.R., Colonna, M., Randolph, G.J. and Mann, D.L. 2014. Embryonic and adult-derived resident cardiac macrophages are maintained through distinct mechanisms at steady state and during inflammation. *Immunity*. **40**(1),pp.91–104.

Erwig, L.-P. and Henson, P.M. 2008. Clearance of apoptotic cells by phagocytes. *Cell death and differentiation*. **15**(2),pp.243–250.

Escoubet-Lozach, L., Benner, C., Kaikkonen, M.U., Lozach, J., Heinz, S., Spann, N.J., Crotti, A., Stender, J., Ghisletti, S., Reichart, D., Cheng, C.S., Luna, R., Ludka, C., Sasik, R., Garcia-Bassets, I., Hoffmann, A., Subramaniam, S., Hardiman, G., Rosenfeld, M.G. and Glass, C.K. 2011. Mechanisms establishing TLR4-responsive activation states of inflammatory response genes. A. Akhtar, ed. *PLoS genetics*. **7**(12),p.e1002401.

Falvo, J.V., Thanos, D. and Maniatis, T. 1995. Reversal of intrinsic DNA bends in the IFN beta gene enhancer by transcription factors and the architectural protein HMG I(Y). *Cell*. **83**(7),pp.1101–1111.

Feng, D., Sangster-Guity, N., Stone, R., Korczeniewska, J., Mancl, M.E., Fitzgerald-Bocarsly, P. and Barnes, B.J. 2010. Differential requirement of histone acetylase and deacetylase activities for IRF5-mediated proinflammatory cytokine expression. *The Journal of Immunology*. **185**(10),pp.6003–6012.

Fenouil, R., Cauchy, P., Koch, F., Descostes, N., Cabeza, J.Z., Innocenti, C., Ferrier, P., Spicuglia, S., Gut, M., Gut, I. and Andrau, J.-C. 2012. CpG islands and GC content dictate

nucleosome depletion in a transcription-independent manner at mammalian promoters. *Genome Research*. **22**(12),pp.2399–2408.

Flannagan, R.S., Jaumouillé, V. and Grinstein, S. 2012. The cell biology of phagocytosis. *Annual review of pathology*. **7**(1),pp.61–98.

Frame, J.M., Fegan, K.H., Conway, S.J., McGrath, K.E. and Palis, J. 2016. Definitive Hematopoiesis in the Yolk Sac Emerges from Wnt-Responsive Hemogenic Endothelium Independently of Circulation and Arterial Identity. *Stem cells (Dayton, Ohio)*. **34**(2),pp.431–444.

Fukaya, T., Lim, B. and Levine, M. 2016. Enhancer Control of Transcriptional Bursting. *Cell*. **166**(2),pp.358–368.

Garber, M., Yosef, N., Goren, A., Raychowdhury, R., Thielke, A., Guttman, M., Robinson, J., Minie, B., Chevrier, N., Itzhaki, Z., Blecher-Gonen, R., Bornstein, C., Amann-Zalcenstein, D., Weiner, A., Friedrich, D., Meldrim, J., Ram, O., Cheng, C., Gnirke, A., Fisher, S., Friedman, N., Wong, B., Bernstein, B.E., Nusbaum, C., Hacohen, N., Regev, A. and Amit, I. 2012. A high-throughput chromatin immunoprecipitation approach reveals principles of dynamic gene regulation in mammals. *Molecular Cell*. **47**(5),pp.810–822.

Gautier, E.L., Shay, T., Miller, J., Greter, M., Jakubzick, C., Ivanov, S., Helft, J., Chow, A., Elpek, K.G., Gordonov, S., Mazloom, A.R., Ma'ayan, A., Chua, W.-J., Hansen, T.H., Turley, S.J., Merad, M., Randolph, G.J.Immunological Genome Consortium 2012. Gene-expression profiles and transcriptional regulatory pathways that underlie the identity and diversity of mouse tissue macrophages. *Nature immunology*. **13**(11),pp.1118–1128.

Geissmann, F., Jung, S. and Littman, D.R. 2003. Blood monocytes consist of two principal subsets with distinct migratory properties. *Immunity*. **19**(1),pp.71–82.

Ghisletti, S., Barozzi, I., Mietton, F., Polletti, S., De Santa, F., Venturini, E., Gregory, L., Lonie, L., Chew, A., Wei, C.-L., Ragoussis, J. and Natoli, G. 2010. Identification and Characterization of Enhancers Controlling the Inflammatory Gene Expression Program in Macrophages. *Immunity*. **32**(3),pp.1–12.

Giese, K., Kingsley, C., Kirshner, J.R. and Grosschedl, R. 1995. Assembly and function of a TCR alpha enhancer complex is dependent on LEF-1-induced DNA bending and multiple protein-protein interactions. *Genes & development*. **9**(8),pp.995–1008.

Ginhoux, F. and Guilliams, M. 2016. Tissue-Resident Macrophage Ontogeny and Homeostasis. *Immunity*. **44**(3),pp.439–449.

Ginhoux, F. and Jung, S. 2014. Monocytes and macrophages: developmental pathways and tissue homeostasis. *Nature reviews. Immunology*. **14**(6),pp.392–404.

Ginhoux, F., Bleriot, C. and Lecuit, M. 2017. Dying for a Cause: Regulated Necrosis of Tissue-Resident Macrophages upon Infection. *Trends in immunology*.

Ginhoux, F., Schultze, J.L., Murray, P.J., Ochando, J. and Biswas, S.K. 2015. New insights into the multidimensional concept of macrophage ontogeny, activation and function. *Nature immunology*. **17**(1),pp.34–40.

Glass, C.K. and Natoli, G. 2015. Molecular control of activation and priming in macrophages. *Nature immunology*. **17**(1),pp.26–33.

Glass, C.K. and Saijo, K. 2010. Nuclear receptor transrepression pathways that regulate

inflammation in macrophages and T cells. *Nature reviews. Immunology*. **10**(5),pp.365–376.

González-Navajas, J.M., Lee, J., David, M. and Raz, E. 2012. Immunomodulatory functions of type I interferons. *Nature reviews. Immunology*. **12**(2),pp.125–135.

Gordon, S. 2016. Elie Metchnikoff, the Man and the Myth. *Journal of innate immunity*. **8**(3),pp.223–227.

Gordon, S. 2016. Phagocytosis: An Immunobiologic Process. *Immunity*. **44**(3),pp.463–475.

Gosselin, D., Link, V.M., Romanoski, C.E., Fonseca, G.J., Eichenfield, D.Z., Spann, N.J., Stender, J.D., Chun, H.B., Garner, H., Geissmann, F. and Glass, C.K. 2014. Environment Drives Selection and Function of Enhancers Controlling Tissue-Specific Macrophage Identities. *Cell*. **159**(6),pp.1327–1340.

Goudot, C., Coillard, A., Villani, A.-C., Gueguen, P., Cros, A., Sarkizova, S., Tang-Huau, T.-L., Bohec, M., Baulande, S., Hacohen, N., Amigorena, S. and Segura, E. 2017. Aryl Hydrocarbon Receptor Controls Monocyte Differentiation into Dendritic Cells versus Macrophages. *Immunity*. **47**(3),pp.582–596.e6.

Gómez-Marín, C., Tena, J.J., Acemel, R.D., López-Mayorga, M., Naranjo, S., la Calle-Mustienes, de, E., Maeso, I., Beccari, L., Aneas, I., Vielmas, E., Bovolenta, P., Nobrega, M.A., Carvajal, J. and Gómez-Skarmeta, J.L. 2015. Evolutionary comparison reveals that diverging CTCF sites are signatures of ancestral topological associating domains borders. *Proceedings of the National Academy of Sciences of the United States of America*. **112**(24),pp.7542–7547.

Gromak, N., West, S. and Proudfoot, N.J. 2006. Pause sites promote transcriptional termination of mammalian RNA polymerase II. *Molecular and cellular biology*. **26**(10),pp.3986–3996.

Gu, T.L., Goetz, T.L., Graves, B.J. and Speck, N.A. 2000. Auto-inhibition and partner proteins, core-binding factor beta (CBFbeta) and Ets-1, modulate DNA binding by CBFalpha2 (AML1). *Molecular and cellular biology*. **20**(1),pp.91–103.

Gu, Z., Eils, R. and Schlesner, M. 2016. Complex heatmaps reveal patterns and correlations in multidimensional genomic data. *Bioinformatics*. **32**(18),pp.2847–2849.

Guilliams, M., De Kleer, I., Henri, S., Post, S., Vanhoutte, L., De Prijck, S., Deswarte, K., Malissen, B., Hammad, H. and Lambrecht, B.N. 2013. Alveolar macrophages develop from fetal monocytes that differentiate into long-lived cells in the first week of life via GM-CSF. *Journal of Experimental Medicine*. **210**(10),pp.1977–1992.

Guilliams, M., Ginhoux, F., Jakubzick, C., Naik, S.H., Onai, N., Schraml, B.U., Segura, E., Tussiwand, R. and Yona, S. 2014. Dendritic cells, monocytes and macrophages: a unified nomenclature based on ontogeny. *Nature reviews. Immunology*.

Guo, Y., Xu, Q., Canzio, D., Shou, J., Li, J., Gorkin, D.U., Jung, I., Wu, H., Zhai, Y., Tang, Y., Lu, Y., Wu, Y., Jia, Z., Li, W., Zhang, M.Q., Ren, B., Krainer, A.R., Maniatis, T. and Wu, Q. 2015. CRISPR Inversion of CTCF Sites Alters Genome Topology and Enhancer/Promoter Function. *Cell*. **162**(4),pp.900–910.

Ha, M. and Kim, V.N. 2014. Regulation of microRNA biogenesis. *Nature reviews. Molecular cell biology*. **15**(8),pp.509–524.

Hah, N., Benner, C., Chong, L.-W., Yu, R.T., Downes, M. and Evans, R.M. 2015. Inflammation-sensitive super enhancers form domains of coordinately regulated enhancer RNAs. *Proceedings of the National Academy of Sciences of the United States of America*. **112**(3),pp.E297–302.

Haldar, M., Kohyama, M., So, A.Y.-L., Kc, W., Wu, X., Briseño, C.G., Satpathy, A.T., Kretzer, N.M., Arase, H., Rajasekaran, N.S., Wang, L., Egawa, T., Igarashi, K., Baltimore, D., Murphy, T.L. and Murphy, K.M. 2014. Heme-mediated SPI-C induction promotes monocyte differentiation into iron-recycling macrophages. *Cell*. **156**(6),pp.1223–1234.

Hanayama, R., Tanaka, M., Miwa, K., Shinohara, A., Iwamatsu, A. and Nagata, S. 2002. Identification of a factor that links apoptotic cells to phagocytes. *Nature*. **417**(6885),pp.182–187.

Hargreaves, D.C., Horng, T. and Medzhitov, R. 2009. Control of Inducible Gene Expression by Signal-Dependent Transcriptional Elongation. *Cell*. **138**(1),pp.129–145.

Harlen, K.M. and Churchman, L.S. 2017. The code and beyond: transcription regulation by the RNA polymerase II carboxy-terminal domain. *Nature reviews. Molecular cell biology*. **18**(4),pp.263–273.

Hay, D., Hughes, J.R., Babbs, C., Davies, J.O.J., Graham, B.J., Hanssen, L.L.P., Kassouf, M.T., Oudelaar, A.M., Sharpe, J.A., Suciu, M.C., Telenius, J., Williams, R., Rode, C., Li, P.-S., Pennacchio, L.A., Sloane-Stanley, J.A., Ayyub, H., Butler, S., Sauka-Spengler, T., Gibbons, R.J., Smith, A.J.H., Wood, W.G. and Higgs, D.R. 2016. Genetic dissection of the α-globin super-enhancer in vivo. *Nature Genetics*. **48**(8),pp.895–903.

Heger, A., Webber, C., Goodson, M., Ponting, C.P. and Lunter, G. 2013. GAT: a simulation framework for testing the association of genomic intervals. *Bioinformatics*. **29**(16),pp.2046–2048.

Heidemann, M., Hintermair, C., Voß, K. and Eick, D. 2013. Dynamic phosphorylation patterns of RNA polymerase II CTD during transcription. *Biochimica et biophysica acta*. **1829**(1),pp.55–62.

Heintzman, N.D., Stuart, R.K., Hon, G., Fu, Y., Ching, C.W., Hawkins, R.D., Barrera, L.O., Van Calcar, S., Qu, C., Ching, K.A., Wang, W., Weng, Z., Green, R.D., Crawford, G.E. and Ren, B. 2007. Distinct and predictive chromatin signatures of transcriptional promoters and enhancers in the human genome. *Nature Genetics*. **39**(3),pp.311–318.

Heinz, S., Benner, C., Spann, N., Bertolino, E., Lin, Y.C., Laslo, P., Cheng, J.X., Murre, C., Singh, H. and Glass, C.K. 2010. Simple Combinations of Lineage-Determining Transcription Factors Prime cis-Regulatory Elements Required for Macrophage and B Cell Identities. *Molecular Cell*. **38**(4),pp.576–589.

Heinz, S., Romanoski, C.E., Benner, C., Allison, K.A., Kaikkonen, M.U., Orozco, L.D. and Glass, C.K. 2013. Effect of natural genetic variation on enhancer selection and function. *Nature*. **503**(7477),pp.487–492.

Helft, J., Böttcher, J., Chakravarty, P., Zelenay, S., Huotari, J., Schraml, B.U., Goubau, D. and Sousa, C.R.E. 2015. GM-CSF Mouse Bone Marrow Cultures Comprise a Heterogeneous Population of CD11c+MHCII+ Macrophages and Dendritic Cells. *Immunity*. **42**(6),pp.1197–1211.

Heng, T.S.P., Painter, M.W.Immunological Genome Project Consortium 2008. The Immunological Genome Project: networks of gene expression in immune cells. *Nature*

immunology. **9**(10),pp.1091–1094.

Hettinger, J., Richards, D.M., Hansson, J., Barra, M.M., Joschko, A.-C., Krijgsveld, J. and Feuerer, M. 2013. Origin of monocytes and macrophages in a committed progenitor. *Nature immunology*. **14**(8),pp.821–830.

Himes, S.R., Cronau, S., Mulford, C. and Hume, D.A. 2005. The Runx1 transcription factor controls CSF-1-dependent and -independent growth and survival of macrophages. *Oncogene*. **24**(34),pp.5278–5286.

Hnisz, D., Abraham, B.J., Lee, T.I., Lau, A., Saint-André, V., Sigova, A.A., Hoke, H.A. and Young, R.A. 2013. Super-Enhancers in the Control of Cell Identity and Disease. *Cell*. **155**(4),pp.934–947.

Hnisz, D., Schuijers, J., Lin, C.Y., Weintraub, A.S., Abraham, B.J., Lee, T.I., Bradner, J.E. and Young, R.A. 2015. Convergence of developmental and oncogenic signaling pathways at transcriptional super-enhancers. *Molecular Cell*. **58**(2),pp.362–370.

Hnisz, D., Shrinivas, K., Young, R.A., Chakraborty, A.K. and Sharp, P.A. 2017. A Phase Separation Model for Transcriptional Control. *Cell*. **169**(1),pp.13–23.

Hoeffel, G., Chen, J., Lavin, Y., Low, D., Almeida, F.F., See, P., Beaudin, A.E., Lum, J., Low, I., Forsberg, E.C., Poidinger, M., Zolezzi, F., Larbi, A., Ng, L.G., Chan, J.K.Y., Greter, M., Becher, B., Samokhvalov, I.M., Merad, M. and Ginhoux, F. 2015. C-Myb(+) erythro-myeloid progenitor-derived fetal monocytes give rise to adult tissue-resident macrophages. *Immunity*. **42**(4),pp.665–678.

Hohaus, S., Petrovick, M.S., Voso, M.T., Sun, Z., Zhang, D.E. and Tenen, D.G. 1995. PU.1 (Spi-1) and C/EBP alpha regulate expression of the granulocyte-macrophage colony-stimulating factor receptor alpha gene. *Molecular and cellular biology*. **15**(10),pp.5830–5845.

Hollenhorst, P.C., Chandler, K.J., Poulsen, R.L., Johnson, W.E., Speck, N.A. and Graves, B.J. 2009. DNA specificity determinants associate with distinct transcription factor functions. M. Snyder, ed. *PLoS genetics*. **5**(12),p.e1000778.

Hollenhorst, P.C., Shah, A.A., Hopkins, C. and Graves, B.J. 2007. Genome-wide analyses reveal properties of redundant and specific promoter occupancy within the ETS gene family. *Genes & development*. **21**(15),pp.1882–1894.

Honda, K. and Taniguchi, T. 2006. IRFs: master regulators of signalling by Toll-like receptors and cytosolic pattern-recognition receptors. *Nature reviews. Immunology*. **6**(9),pp.644–658.

Honda, K., Takaoka, A. and Taniguchi, T. 2006. Type I inteferon gene induction by the interferon regulatory factor family of transcription factors. *Immunity*.

Hoogenkamp, M., Lichtinger, M., Krysinska, H., Lancrin, C., Clarke, D., Williamson, A., Mazzarella, L., Ingram, R., Jorgensen, H., Fisher, A., Tenen, D.G., Kouskoff, V., Lacaud, G. and Bonifer, C. 2009. Early chromatin unfolding by RUNX1: a molecular explanation for differential requirements during specification versus maintenance of the hematopoietic gene expression program. *Blood*. **114**(2),pp.299–309.

Hsin, J.-P. and Manley, J.L. 2012. The RNA polymerase II CTD coordinates transcription and RNA processing. *Genes & development*. **26**(19),pp.2119–2137.

Huang, B., Yang, X.-D., Zhou, M.-M., Ozato, K. and Chen, L.-F. 2009. Brd4 coactivates transcriptional activation of NF-kappaB via specific binding to acetylated RelA. *Molecular and cellular biology*. **29**(5),pp.1375–1387.

Huang, G., Zhang, P., Hirai, H., Elf, S., Yan, X., Chen, Z., Koschmieder, S., Okuno, Y., Dayaram, T., Growney, J.D., Shivdasani, R.A., Gilliland, D.G., Speck, N.A., Nimer, S.D. and Tenen, D.G. 2007. PU.1 is a major downstream target of AML1 (RUNX1) in adult mouse hematopoiesis. *Nature Genetics*. **40**(1),pp.51–60.

Hughes, J.R., Roberts, N., McGowan, S., Hay, D., Giannoulatou, E., Lynch, M., De Gobbi, M., Taylor, S., Gibbons, R. and Higgs, D.R. 2014. Analysis of hundreds of cis-regulatory landscapes at high resolution in a single, high-throughput experiment. *Nature Genetics*. **46**(2),pp.205–212.

Imperato, M.R., Cauchy, P., Obier, N. and Bonifer, C. 2015. The RUNX1–PU.1 axis in the control of hematopoiesis. *International Journal of Hematology*. **101**(4),pp.319–329.

Inaba, K., Inaba, M., Romani, N., Aya, H., Deguchi, M., Ikehara, S., Muramatsu, S. and Steinman, R.M. 1992. Generation of large numbers of dendritic cells from mouse bone marrow cultures supplemented with granulocyte/macrophage colony-stimulating factor. *The Journal of experimental medicine*. **176**(6),pp.1693–1702.

Ivashkiv, L.B. and Donlin, L.T. 2014. Regulation of type I interferon responses. *Nature reviews. Immunology*. **14**(1),pp.36–49.

Iwafuchi-Doi, M. and Zaret, K.S. 2014. Pioneer transcription factors in cell reprogramming. *Genes & development*. **28**(24),pp.2679–2692.

Jakubzick, C.V., Randolph, G.J. and Henson, P.M. 2017. Monocyte differentiation and antigen-presenting functions. *Nature reviews. Immunology*. **17**(6),pp.349–362.

Jeronimo, C. and Robert, F. 2014. Kin28 regulates the transient association of Mediator with core promoters. *Nature structural & molecular biology*. **21**(5),pp.449–455.

Jeronimo, C. and Robert, F. 2017. The Mediator Complex: At the Nexus of RNA Polymerase II Transcription. *Trends in cell biology*.

Jin, Q., Yu, L.-R., Wang, L., Zhang, Z., Kasper, L.H., Lee, J.-E., Wang, C., Brindle, P.K., Dent, S.Y.R. and Ge, K. 2011. Distinct roles of GCN5/PCAF-mediated H3K9ac and CBP/p300-mediated H3K18/27ac in nuclear receptor transactivation. *The EMBO journal*. **30**(2),pp.249–262.

Johnson, A.D., Meyer, B.J. and Ptashne, M. 1979. Interactions between DNA-bound repressors govern regulation by the lambda phage repressor. *Proceedings of the National Academy of Sciences*. **76**(10),pp.5061–5065.

Jonkers, I. and Lis, J.T. 2015. Getting up to speed with transcription elongation by RNA polymerase II. *Nature reviews. Molecular cell biology*. **16**(3),pp.167–177.

Jorgensen, I., Zhang, Y., Krantz, B.A. and Miao, E.A. 2016. Pyroptosis triggers pore-induced intracellular traps (PITs) that capture bacteria and lead to their clearance by efferocytosis. *Journal of Experimental Medicine*. **213**(10),pp.2113–2128.

Joshi, S., Singh, A.R., Zulcic, M., Bao, L., Messer, K., Ideker, T., Dutkowski, J. and Durden, D.L. 2014. Rac2 controls tumor growth, metastasis and M1-M2 macrophage differentiation in vivo. M. Chrzanowska-Wodnicka, ed. *PloS one*. **9**(4),p.e95893.

Junion, G., Spivakov, M., Girardot, C., Braun, M., Gustafson, E.H., Birney, E. and Furlong, E.E.M. 2012. A transcription factor collective defines cardiac cell fate and reflects lineage history. *Cell*. **148**(3),pp.473–486.

Kaikkonen, M.U., Spann, N.J., Heinz, S., Romanoski, C.E., Allison, K.A., Stender, J.D., Chun, H.B., Tough, D.F., Prinjha, R.K., Benner, C. and Glass, C.K. 2013. Remodeling of the Enhancer Landscape during Macrophage ActivationIs Coupled to Enhancer Transcription. *Molecular Cell*. **51**(3),pp.310–325.

Kang, K., Park, S.-H., Chen, J., Qiao, Y., Giannopoulou, E., Berg, K., Hanidu, A., Li, J., Nabozny, G., Kang, K., Park-Min, K.-H. and Ivashkiv, L.B. 2017. Interferon-γ Represses M2 Gene Expression in Human Macrophages by Disassembling Enhancers Bound by the Transcription Factor MAF. *Immunity*. **47**(2),pp.235–250.e4.

Karin, M., Lawrence, T. and Nizet, V. 2006. Innate Immunity Gone Awry: Linking Microbial Infections to Chronic Inflammation and Cancer. *Cell*. **124**(4),pp.823–835.

Kay, A.B. 2016. Paul Ehrlich and the Early History of Granulocytes. *Microbiology Spectrum*. **4**(4).

Kieusseian, A., Brunet de la Grange, P., Burlen-Defranoux, O., Godin, I. and Cumano, A. 2012. Immature hematopoietic stem cells undergo maturation in the fetal liver. *Development (Cambridge, England)*. **139**(19),pp.3521–3530.

Kim, T.K. and Maniatis, T. 1997. The mechanism of transcriptional synergy of an in vitro assembled interferon-beta enhanceosome. *Molecular Cell*. **1**(1),pp.119–129.

Kim, W.Y., Sieweke, M., Ogawa, E., Wee, H.J., Englmeier, U., Graf, T. and Ito, Y. 1999. Mutual activation of Ets-1 and AML1 DNA binding by direct interaction of their autoinhibitory domains. *The EMBO journal*. **18**(6),pp.1609–1620.

Kohyama, M., Ise, W., Edelson, B.T., Wilker, P.R., Hildner, K., Mejia, C., Frazier, W.A., Murphy, T.L. and Murphy, K.M. 2008. Role for Spi-C in the development of red pulp macrophages and splenic iron homeostasis. *Nature*. **457**(7227),pp.318–321.

Kolaczkowska, E. and Kubes, P. 2013. Neutrophil recruitment and function in health and inflammation. *Nature reviews. Immunology*. **13**(3),pp.159–175.

Kolb, J.P., Oguin, T.H., III, Oberst, A. and Martinez, J. 2017. Programmed Cell Death and Inflammation: Winter Is Coming. *Trends in immunology*.pp.1–14.

Kolev, N.G., Yario, T.A., Benson, E. and Steitz, J.A. 2008. Conserved motifs in both CPSF73 and CPSF100 are required to assemble the active endonuclease for histone mRNA 3'-end maturation. *EMBO reports*. **9**(10),pp.1013–1018.

Kratofil, R.M., Kubes, P. and Deniset, J.F. 2017. Monocyte Conversion During Inflammation and Injury. *Arteriosclerosis, thrombosis, and vascular biology*. **37**(1),pp.35–42.

Krausgruber, T., Blazek, K., Smallie, T., Alzabin, S., Lockstone, H., Sahgal, N., Hussell, T., Feldmann, M. and Udalova, I.A. 2011. IRF5 promotes inflammatory macrophage polarization and T. *Nature immunology*. **12**(3),pp.231–238.

Krausgruber, T., Saliba, D., Ryzhakov, G., Lanfrancotti, A., Blazek, K. and Udalova, I.A. 2010. IRF5 is required for late-phase TNF secretion by human dendritic cells. *Blood*. **115**(22),pp.4421–4430.

Kuleshov, M.V., Jones, M.R., Rouillard, A.D., Fernandez, N.F., Duan, Q., Wang, Z., Koplev, S., Jenkins, S.L., Jagodnik, K.M., Lachmann, A., McDermott, M.G., Monteiro, C.D., Gundersen, G.W. and Ma'ayan, A. 2016. Enrichr: a comprehensive gene set enrichment analysis web server 2016 update. *Nucleic acids research*. **44**(W1),pp.W90–7.

Kumaravelu, P., Hook, L., Morrison, A.M., Ure, J., Zhao, S., Zuyev, S., Ansell, J. and Medvinsky, A. 2002. Quantitative developmental anatomy of definitive haematopoietic stem cells/long-term repopulating units (HSC/RUs): role of the aorta-gonad-mesonephros (AGM) region and the yolk sac in colonisation of the mouse embryonic liver. *Development (Cambridge, England)*. **129**(21),pp.4891–4899.

Kwak, H. and Lis, J.T. 2013. Control of Transcriptional Elongation. *Annual review of genetics*. **47**(1),pp.483–508.

Langmead, B., Trapnell, C., Pop, M. and Salzberg, S.L. 2009. Ultrafast and memory-efficient alignment of short DNA sequences to the human genome. *Genome Biology*. **10**(3),p.R25.

Lara-Astiaso, D., Weiner, A., Lorenzo-Vivas, E., Zaretsky, I., Jaitin, D.A., David, E., Keren-Shaul, H., Mildner, A., Winter, D., Jung, S., Friedman, N. and Amit, I. 2014. Chromatin state dynamics during blood formation. *Science (New York, N.Y.)*. **345**(6199),pp.1256271–949.

Laslo, P., Spooner, C.J., Warmflash, A., Lancki, D.W., Lee, H.-J., Sciammas, R., Gantner, B.N., Dinner, A.R. and Singh, H. 2006. Multilineage transcriptional priming and determination of alternate hematopoietic cell fates. *Cell*. **126**(4),pp.755–766.

Lavin, Y., Winter, D., Blecher-Gonen, R., David, E., Keren-Shaul, H., Merad, M., Jung, S. and Amit, I. 2014. Tissue-Resident Macrophage Enhancer Landscapes Are Shaped by the Local Microenvironment. *Cell*. **159**(6),pp.1312–1326.

Li, H., Handsaker, B., Wysoker, A., Fennell, T., Ruan, J., Homer, N., Marth, G., Abecasis, G., Durbin, R.1000 Genome Project Data Processing Subgroup 2009. The Sequence Alignment/Map format and SAMtools. *Bioinformatics*. **25**(16),pp.2078–2079.

Li, J., Liu, Y., Rhee, H.S., Ghosh, S.K.B., Bai, L., Pugh, B.F. and Gilmour, D.S. 2013. Kinetic competition between elongation rate and binding of NELF controls promoter-proximal pausing. *Molecular Cell*. **50**(5),pp.711–722.

Lieberman-Aiden, E., van Berkum, N.L., Williams, L., Imakaev, M., Ragoczy, T., Telling, A., Amit, I., Lajoie, B.R., Sabo, P.J., Dorschner, M.O., Sandstrom, R., Bernstein, B., Bender, M.A., Groudine, M., Gnirke, A., Stamatoyannopoulos, J., Mirny, L.A., Lander, E.S. and Dekker, J. 2009. Comprehensive mapping of long-range interactions reveals folding principles of the human genome. *Science (New York, N.Y.)*. **326**(5950),pp.289–293.

Lim, C.-A., Yao, F., Wong, J.J.-Y., George, J., Xu, H., Chiu, K.P., Sung, W.-K., Lipovich, L., Vega, V.B., Chen, J., Shahab, A., Zhao, X.D., Hibberd, M., Wei, C.-L., Lim, B., Ng, H.-H., Ruan, Y. and Chin, K.-C. 2007. Genome-wide mapping of RELA(p65) binding identifies E2F1 as a transcriptional activator recruited by NF-kappaB upon TLR4 activation. *Molecular Cell*. **27**(4),pp.622–635.

Lone, I.N., Shukla, M.S., Charles Richard, J.L., Peshev, Z.Y., Dimitrov, S. and Angelov, D. 2013. Binding of NF-κB to Nucleosomes: Effect of Translational Positioning, Nucleosome Remodeling and Linker Histone H1 D. Schübeler, ed. *PLoS genetics*. **9**(9),p.e1003830.

Long, H.K., Prescott, S.L. and Wysocka, J. 2016. Ever-Changing Landscapes: Transcriptional Enhancers in Development and Evolution. *Cell*. **167**(5),pp.1170–1187.

Love, M.I., Huber, W. and Anders, S. 2014. Moderated estimation of fold change and dispersion for RNA-seq data with DESeq2. *Genome Biology*. **15**(12),p.550.

Lovén, J., Hoke, H.A., Lin, C.Y., Lau, A., Orlando, D.A., Vakoc, C.R., Bradner, J.E., Lee, T.I. and Young, R.A. 2013. Selective Inhibition of Tumor Oncogenes by Disruption of Super-Enhancers. *Cell*. **153**(2),pp.320–334.

Lu, H., Flores, O., Weinmann, R. and Reinberg, D. 1991. The nonphosphorylated form of RNA polymerase II preferentially associates with the preinitiation complex. *Proceedings of the National Academy of Sciences*. **88**(22),pp.10004–10008.

Luo, M.-C., Zhou, S.-Y., Feng, D.-Y., Xiao, J., Li, W.-Y., Xu, C.-D., Wang, H.-Y. and Zhou, T. 2016. Runt-related Transcription Factor 1 (RUNX1) Binds to p50 in Macrophages and Enhances TLR4-triggered Inflammation and Septic Shock. *Journal of Biological Chemistry*. **291**(42),pp.22011–22020.

Luyendyk, J.P., Schabbauer, G.A., Tencati, M., Holscher, T., Pawlinski, R. and Mackman, N. 2008. Genetic analysis of the role of the PI3K-Akt pathway in lipopolysaccharide-induced cytokine and tissue factor gene expression in monocytes/macrophages. *The Journal of Immunology*. **180**(6),pp.4218–4226.

Maaten, L.V.D. and Hinton, G. 2008. Visualizing Data using t-SNE. *Journal of Machine Learning Research*. **9**(Nov),pp.2579–2605.

Machanick, P. and Bailey, T.L. 2011. MEME-ChIP: motif analysis of large DNA datasets. *Bioinformatics*. **27**(12),pp.1696–1697.

Mancino, A., Termanini, A., Barozzi, I., Ghisletti, S., Ostuni, R., Prosperini, E., Ozato, K. and Natoli, G. 2015. A dual cis-regulatory code links IRF8 to constitutive and inducible gene expression in macrophages. *Genes & development*. **29**(4),pp.394–408.

Mansour, M.R., Abraham, B.J., Anders, L., Berezovskaya, A., Gutierrez, A., Durbin, A.D., Etchin, J., Lawton, L., Sallan, S.E., Silverman, L.B., Loh, M.L., Hunger, S.P., Sanda, T., Young, R.A. and Look, A.T. 2014. Oncogene regulation. An oncogenic super-enhancer formed through somatic mutation of a noncoding intergenic element. *Science (New York, N.Y.)*. **346**(6215),pp.1373–1377.

Martin, M. 2011. Cutadapt removes adapter sequences from high-throughput sequencing reads. *EMBnet journal*. **17**(1),pp.pp. 10–12.

Martinez, F.O., Helming, L. and Gordon, S. 2009. Alternative Activation of Macrophages: An Immunologic Functional Perspective. *Annual review of immunology*. **27**(1),pp.451–483.

Matharu, N. and Ahituv, N. 2015. Minor Loops in Major Folds: Enhancer-Promoter Looping, Chromatin Restructuring, and Their Association with Transcriptional Regulation and Disease. E. M. C. Fisher, ed. *PLoS genetics*. **11**(12),p.e1005640.

Matsuyama, T., Kimura, T., Kitagawa, M., Pfeffer, K., Kawakami, T., Watanabe, N., Kündig, T.M., Amakawa, R., Kishihara, K. and Wakeham, A. 1993. Targeted disruption of IRF-1 or IRF-2 results in abnormal type I IFN gene induction and aberrant lymphocyte development. *Cell*. **75**(1),pp.83–97.

Maus, U.A., Koay, M.A., Delbeck, T., Mack, M., Ermert, M., Ermert, L., Blackwell, T.S., Christman, J.W., Schlöndorff, D., Seeger, W. and Lohmeyer, J. 2002. Role of resident alveolar macrophages in leukocyte traffic into the alveolar air space of intact mice. *American journal of physiology. Lung cellular and molecular physiology*.

282(6),pp.L1245–52.

McAndrew, M.J., Gjidoda, A., Tagore, M., Miksanek, T. and Floer, M. 2016. Chromatin Remodeler Recruitment during Macrophage Differentiation Facilitates Transcription Factor Binding to Enhancers in Mature Cells. *Journal of Biological Chemistry*. **291**(35),pp.18058–18071.

McCracken, S., Fong, N., Yankulov, K., Ballantyne, S., Pan, G., Greenblatt, J., Patterson, S.D., Wickens, M. and Bentley, D.L. 1997. The C-terminal domain of RNA polymerase II couples mRNA processing to transcription. *Nature*. **385**(6614),pp.357–361.

McLean, C.Y., Bristor, D., Hiller, M., Clarke, S.L., Schaar, B.T., Lowe, C.B., Wenger, A.M. and Bejerano, G. 2010. GREAT improves functional interpretation of cis-regulatory regions. *Nature Biotechnology*. **28**(5),pp.495–501.

Medzhitov, R., Preston-Hurlburt, P. and Janeway, C.A. 1997. A human homologue of the Drosophila Toll protein signals activation of adaptive immunity. *Nature*. **388**(6640),pp.394–397.

Menezes, S., Melandri, D., Anselmi, G., Perchet, T., Loschko, J., Dubrot, J., Patel, R., Gautier, E.L., Hugues, S., Longhi, M.P., Henry, J.Y., Quezada, S.A., Lauvau, G., Lennon-Duménil, A.-M., Gutiérrez-Martínez, E., Bessis, A., Gomez Perdiguero, E., Jacome-Galarza, C.E., Garner, H., Geissmann, F., Golub, R., Nussenzweig, M.C. and Guermonprez, P. 2016. The Heterogeneity of Ly6Chi Monocytes Controls Their Differentiation into iNOS+ Macrophages or Monocyte-Derived Dendritic Cells. *Immunity*. **45**(6),pp.1205–1218.

Merika, M., Williams, A.J., Chen, G., Collins, T. and Thanos, D. 1998. Recruitment of CBP/p300 by the IFN beta enhanceosome is required for synergistic activation of transcription. *Molecular Cell*. **1**(2),pp.277–287.

Mildner, A., Schönheit, J., Giladi, A., David, E., Lara-Astiaso, D., Lorenzo-Vivas, E., Paul, F., Chappell-Maor, L., Priller, J., Leutz, A., Amit, I. and Jung, S. 2017. Genomic Characterization of Murine Monocytes Reveals C/EBPβ Transcription Factor Dependence of Ly6C- Cells. *Immunity*. **46**(5),pp.849–862.e7.

Miller, J.A. and Widom, J. 2003. Collaborative competition mechanism for gene activation in vivo. *Molecular and cellular biology*. **23**(5),pp.1623–1632.

Miller, J.C., Brown, B.D., Shay, T., Gautier, E.L., Jojic, V., Cohain, A., Pandey, G., Leboeuf, M., Elpek, K.G., Helft, J., Hashimoto, D., Chow, A., Price, J., Greter, M., Bogunovic, M., Bellemare-Pelletier, A., Frenette, P.S., Randolph, G.J., Turley, S.J., Merad, M.Immunological Genome Consortium 2012. Deciphering the transcriptional network of the dendritic cell lineage. *Nature immunology*. **13**(9),pp.888–899.

Min, I.M., Waterfall, J.J., Core, L.J., Munroe, R.J., Schimenti, J. and Lis, J.T. 2011. Regulating RNA polymerase pausing and transcription elongation in embryonic stem cells. *Genes & development*. **25**(7),pp.742–754.

Miyamoto, M., Fujita, T., Kimura, Y., Maruyama, M., Harada, H., Sudo, Y., Miyata, T. and Taniguchi, T. 1988. Regulated expression of a gene encoding a nuclear factor, IRF-1, that specifically binds to IFN-beta gene regulatory elements. *Cell*. **54**(6),pp.903–913.

Molawi, K., Wolf, Y., Kandalla, P.K., Favret, J., Hagemeyer, N., Frenzel, K., Pinto, A.R., Klapproth, K., Henri, S., Malissen, B., Rodewald, H.-R., Rosenthal, N.A., Bajenoff, M., Prinz, M., Jung, S. and Sieweke, M.H. 2014. Progressive replacement of embryo-derived cardiac macrophages with age. *Journal of Experimental Medicine*. **211**(11),pp.2151–

2158.

Moon, S.-J., Lim, M.-A., Park, J.-S., Byun, J.-K., Kim, S.-M., Park, M.-K., Kim, E.-K., Moon, Y.-M., Min, J.-K., Ahn, S.-M., Park, S.-H. and Cho, M.-L. 2014. Dual-specificity phosphatase 5 attenuates autoimmune arthritis in mice via reciprocal regulation of the Th17/Treg cell balance and inhibition of osteoclastogenesis. *Arthritis & rheumatology (Hoboken, N.J.)*. **66**(11),pp.3083–3095.

Mukundan, L., Odegaard, J.I., Morel, C.R., Heredia, J.E., Mwangi, J.W., Ricardo-Gonzalez, R.R., Goh, Y.P.S., Eagle, A.R., Dunn, S.E., Awakuni, J.U.H., Nguyen, K.D., Steinman, L., Michie, S.A. and Chawla, A. 2009. PPAR-delta senses and orchestrates clearance of apoptotic cells to promote tolerance. *Nature medicine*. **15**(11),pp.1266–1272.

Munder, M., Eichmann, K. and Modolell, M. 1998. Alternative metabolic states in murine macrophages reflected by the nitric oxide synthase/arginase balance: competitive regulation by CD4+ T cells correlates with Th1/Th2 phenotype. *The Journal of Immunology*. **160**(11),pp.5347–5354.

Munder, M., Eichmann, K., Morán, J.M., Centeno, F., Soler, G. and Modolell, M. 1999. Th1/Th2-regulated expression of arginase isoforms in murine macrophages and dendritic cells. *The Journal of Immunology*. **163**(7),pp.3771–3777.

Murray, P.J. 2017. Macrophage Polarization. *Annual Review of Physiology*. **79**(1),pp.541–566.

Murray, P.J., Allen, J.E., Biswas, S.K., Fisher, E.A., Gilroy, D.W., Goerdt, S., Gordon, S., Hamilton, J.A., Ivashkiv, L.B., Lawrence, T., Locati, M., Mantovani, A., Martinez, F.O., Mege, J.-L., Mosser, D.M., Natoli, G., Saeij, J.P., Schultze, J.L., Shirey, K.A., Sica, A., Suttles, J., Udalova, I., van Ginderachter, J.A., Vogel, S.N. and Wynn, T.A. 2014. Macrophage Activation and Polarization: Nomenclature and Experimental Guidelines. *Immunity*. **41**(1),pp.14–20.

Naik, S.H., Sathe, P., Park, H.-Y., Metcalf, D., Proietto, A.I., Dakic, A., Carotta, S., O'Keeffe, M., Bahlo, M., Papenfuss, A., Kwak, J.-Y., Wu, L. and Shortman, K. 2007. Development of plasmacytoid and conventional dendritic cell subtypes from single precursor cells derived in vitro and in vivo. *Nature immunology*. **8**(11),pp.1217–1226.

Naranbhai, V., Fairfax, B.P., Makino, S., Humburg, P., Wong, D., Ng, E., Hill, A.V.S. and Knight, J.C. 2015. Genomic modulators of gene expression in human neutrophils. *Nature Communications*. **6**,p.7545.

Negishi, H., Ohba, Y., Yanai, H., Takaoka, A., Honma, K., Yui, K., Matsuyama, T., Taniguchi, T. and Honda, K. 2005. Negative regulation of Toll-like-receptor signaling by IRF-4. *Proceedings of the National Academy of Sciences of the United States of America*. **102**(44),pp.15989–15994.

Netea, M.G., Joosten, L.A.B., Latz, E., Mills, K.H.G., Natoli, G., Stunnenberg, H.G., O'Neill, L.A.J. and Xavier, R.J. 2016. Trained immunity: A program of innate immune memory in health and disease. *Science (New York, N.Y.)*. **352**(6284),pp.aaf1098–aaf1098.

Nojima, T., Dienstbier, M., Murphy, S., Proudfoot, N.J. and Dye, M.J. 2013. Definition of RNA polymerase II CoTC terminator elements in the human genome. *CellReports*. **3**(4),pp.1080–1092.

Nojima, T., Gomes, T., Grosso, A.R.F., Kimura, H., Dye, M.J., Dhir, S., Carmo-Fonseca, M. and Proudfoot, N.J. 2015. Mammalian NET-Seq Reveals Genome-wide Nascent Transcription

Coupled to RNA Processing. *Cell*. **161**(3),pp.526–540.

Nora, E.P., Lajoie, B.R., Schulz, E.G., Giorgetti, L., Okamoto, I., Servant, N., Piolot, T., van Berkum, N.L., Meisig, J., Sedat, J., Gribnau, J., Barillot, E., Blüthgen, N., Dekker, J. and Heard, E. 2012. Spatial partitioning of the regulatory landscape of the X-inactivation centre. *Nature*. **485**(7398),pp.381–385.

North, T., Gu, T.L., Stacy, T., Wang, Q., Howard, L., Binder, M., Marin-Padilla, M. and Speck, N.A. 1999. Cbfa2 is required for the formation of intra-aortic hematopoietic clusters. *Development (Cambridge, England)*. **126**(11),pp.2563–2575.

Nussenzweig, M.C. and Steinman, R.M. 1980. Contribution of dendritic cells to stimulation of the murine syngeneic mixed leukocyte reaction. *The Journal of experimental medicine*. **151**(5),pp.1196–1212.

Nutt, S.L., Metcalf, D., D'Amico, A., Polli, M. and Wu, L. 2005. Dynamic regulation of PU.1 expression in multipotent hematopoietic progenitors. *The Journal of experimental medicine*. **201**(2),pp.221–231.

Ogawa, E., Inuzuka, M., Maruyama, M., Satake, M., Naito-Fujimoto, M., Ito, Y. and Shigesada, K. 1993. Molecular cloning and characterization of PEBP2 beta, the heterodimeric partner of a novel Drosophila runt-related DNA binding protein PEBP2 alpha. *Virology*. **194**(1),pp.314–331.

Okabe, Y. and Medzhitov, R. 2016. Tissue biology perspective on macrophages. *Nature Publishing Group*. **17**(1),pp.9–17.

Okabe, Y. and Medzhitov, R. 2014. Tissue-Specific Signals Control Reversible Program of Localization and Functional Polarization of Macrophages. *Cell*. **157**(4),pp.832–844.

Okuda, T., van Deursen, J., Hiebert, S.W., Grosveld, G. and Downing, J.R. 1996. AML1, the Target of Multiple Chromosomal Translocations in Human Leukemia, Is Essential for Normal Fetal Liver Hematopoiesis. *Cell*. **84**(2),pp.321–330.

Olson, M.C., Scott, E.W., Hack, A.A., Su, G.H., Tenen, D.G., Singh, H. and Simon, M.C. 1995. PU. 1 is not essential for early myeloid gene expression but is required for terminal myeloid differentiation. *Immunity*. **3**(6),pp.703–714.

Onai, N., Obata-Onai, A., Schmid, M.A., Ohteki, T., Jarrossay, D. and Manz, M.G. 2007. Identification of clonogenic common Flt3+M-CSFR+ plasmacytoid and conventional dendritic cell progenitors in mouse bone marrow. *Nature immunology*. **8**(11),pp.1207–1216.

Ong, C.-T. and Corces, V.G. 2011. Enhancer function: new insights into the regulation of tissue-specific gene expression. *Nature Reviews Genetics*. **12**(4),pp.283–293.

Ono, M., Yaguchi, H., Ohkura, N., Kitabayashi, I., Nagamura, Y., Nomura, T., Miyachi, Y., Tsukada, T. and Sakaguchi, S. 2007. Foxp3 controls regulatory T-cell function by interacting with AML1/Runx1. *Nature*. **446**(7136),pp.685–689.

Ostuni, R., Piccolo, V., Barozzi, I., Polletti, S., Termanini, A., Bonifacio, S., Curina, A., Prosperini, E., Ghisletti, S. and Natoli, G. 2013. Latent Enhancers Activatedby Stimulation in Differentiated Cells. *Cell*. **152**(1-2),pp.157–171.

Ouyang, X., Negishi, H., Takeda, R., Fujita, Y., Taniguchi, T. and Honda, K. 2007. Cooperation between MyD88 and TRIF pathways in TLR synergy via IRF5 activation. *Biochemical and*

biophysical research communications. **354**(4),pp.1045–1051.

O'Neill, L.A.J. and Pearce, E.J. 2016. Immunometabolism governs dendritic cell and macrophage function. *Journal of Experimental Medicine*. **213**(1),pp.15–23.

Parker, S.C.J., Stitzel, M.L., Taylor, D.L., Orozco, J.M., Erdos, M.R., Akiyama, J.A., van Bueren, K.L., Chines, P.S., Narisu, N., NISC Comparative Sequencing Program, Black, B.L., Visel, A., Pennacchio, L.A., Collins, F.S., National Institutes of Health Intramural Sequencing Center Comparative Sequencing Program AuthorsNISC Comparative Sequencing Program Authors 2013. Chromatin stretch enhancer states drive cell-specific gene regulation and harbor human disease risk variants. *Proceedings of the National Academy of Sciences of the United States of America*. **110**(44),pp.17921–17926.

Parkhomchuk, D., Borodina, T., Amstislavskiy, V., Banaru, M., Hallen, L., Krobitsch, S., Lehrach, H. and Soldatov, A. 2009. Transcriptome analysis by strand-specific sequencing of complementary DNA. *Nucleic acids research*. **37**(18),pp.e123–e123.

Patro, R., Duggal, G., Love, M.I., Irizarry, R.A. and Kingsford, C. 2017. Salmon provides fast and bias-aware quantification of transcript expression. *Nature Methods*. **14**(4),pp.417–419.

Pfaffl, M.W. 2001. A new mathematical model for relative quantification in real-time RT-PCR. *Nucleic acids research*. **29**(9),p.e45.

Piccolo, V., Curina, A., Genua, M., Ghisletti, S., Simonatto, M., Sabò, A., Amati, B., Ostuni, R. and Natoli, G. 2017. Opposing macrophage polarization programs show extensive epigenomic and transcriptional cross-talk. *Nature immunology*. **18**(5),pp.530–540.

Poltorak, A., He, X., Smirnova, I., Liu, M.Y., Van Huffel, C., Du, X., Birdwell, D., Alejos, E., Silva, M., Galanos, C., Freudenberg, M., Ricciardi-Castagnoli, P., Layton, B. and Beutler, B. 1998. Defective LPS signaling in C3H/HeJ and C57BL/10ScCr mice: mutations in Tlr4 gene. *Science (New York, N.Y.)*. **282**(5396),pp.2085–2088.

Poon, I.K.H., Lucas, C.D., Rossi, A.G. and Ravichandran, K.S. 2014. Apoptotic cell clearance: basic biology and therapeutic potential. *Nature reviews. Immunology*. **14**(3),pp.166–180.

Pott, S. and Lieb, J.D. 2015. What are super-enhancers? *Nature Publishing Group*. **47**(1),pp.8–12.

Proudfoot, N J and Brownlee, G.G. 1976. 3' non-coding region sequences in eukaryotic messenger RNA. *Nature*. **263**(5574),pp.211–214.

Proudfoot, Nick J 2011. Ending the message: poly(A) signals then and now. *Genes & development*. **25**(17),pp.1770–1782.

Proudfoot, Nick J 2016. Transcriptional termination in mammals: Stopping the RNA polymerase II juggernaut. *Science (New York, N.Y.)*. **352**(6291),pp.aad9926–aad9926.

Puig-Kröger, A., Sanchez-Elsner, T., Ruiz, N., Andreu, E.J., Prosper, F., Jensen, U.B., Gil, J., Erickson, P., Drabkin, H., Groner, Y. and Corbí, A.L. 2003. RUNX/AML and C/EBP factors regulate CD11a integrin expression in myeloid cells through overlapping regulatory elements. *Blood*. **102**(9),pp.3252–3261.

Purtha, W.E., Swiecki, M., Colonna, M., Diamond, M.S. and Bhattacharya, D. 2012. Spontaneous mutation of the Dock2 gene in Irf5-/- mice complicates interpretation of

type I interferon production and antibody responses. *Proceedings of the National Academy of Sciences of the United States of America*. **109**(15),pp.E898–904.

Quinlan, A.R. and Hall, I.M. 2010. BEDTools: a flexible suite of utilities for comparing genomic features. *Bioinformatics*. **26**(6),pp.841–842.

Ramirez-Carrozzi, V.R., Braas, D., Bhatt, D.M., Cheng, C.S., Hong, C., Doty, K.R., Black, J.C., Hoffmann, A., Carey, M. and Smale, S.T. 2009. A unifying model for the selective regulation of inducible transcription by CpG islands and nucleosome remodeling. *Cell*. **138**(1),pp.114–128.

Ramirez-Carrozzi, V.R., Nazarian, A.A., Li, C.C., Gore, S.L., Sridharan, R., Imbalzano, A.N. and Smale, S.T. 2006. Selective and antagonistic functions of SWI/SNF and Mi-2beta nucleosome remodeling complexes during an inflammatory response. *Genes & development*. **20**(3),pp.282–296.

Ramírez, F., Ryan, D.P., Grüning, B., Bhardwaj, V., Kilpert, F., Richter, A.S., Heyne, S., Dündar, F. and Manke, T. 2016. deepTools2: a next generation web server for deep-sequencing data analysis. *Nucleic acids research*. **44**(W1),pp.W160–5.

Rieger, M.A., Hoppe, P.S., Smejkal, B.M., Eitelhuber, A.C. and Schroeder, T. 2009. Hematopoietic cytokines can instruct lineage choice. *Science (New York, N.Y.)*. **325**(5937),pp.217–218.

Robinson, P.J., Trnka, M.J., Bushnell, D.A., Davis, R.E., Mattei, P.-J., Burlingame, A.L. and Kornberg, R.D. 2016. Structure of a Complete Mediator-RNA Polymerase II Pre-Initiation Complex. *Cell*. **166**(6),pp.1411–1422.e16.

Roeder, R.G. 1996. The role of general initiation factors in transcription by RNA polymerase II. *Trends in biochemical sciences*. **21**(9),pp.327–335.

Rosas, M., Davies, L.C., Giles, P.J., Liao, C.-T., Kharfan, B., Stone, T.C., O'Donnell, V.B., Fraser, D.J., Jones, S.A. and Taylor, P.R. 2014. The transcription factor Gata6 links tissue macrophage phenotype and proliferative renewal. *Science (New York, N.Y.)*. **344**(6184),pp.645–648.

Roszer, T., Menéndez-Gutiérrez, M.P., Lefterova, M.I., Alameda, D., Núñez, V., Lazar, M.A., Fischer, T. and Ricote, M. 2011. Autoimmune kidney disease and impaired engulfment of apoptotic cells in mice with macrophage peroxisome proliferator-activated receptor gamma or retinoid X receptor alpha deficiency. *Journal of immunology (Baltimore, Md. : 1950)*. **186**(1),pp.621–631.

Ryzhakov, G., Eames, H.L. and Udalova, I.A. 2015. Activation and Function of Interferon Regulatory Factor 5. *Journal of Interferon & Cytokine Research*. **35**(2),pp.71–78.

Saccani, S., Pantano, S. and Natoli, G. 2001. Two waves of nuclear factor kappaB recruitment to target promoters. *The Journal of experimental medicine*. **193**(12),pp.1351–1359.

Saliba, D.G., Heger, A., Eames, H.L., Oikonomopoulos, S., Teixeira, A., Blazek, K., Androulidaki, A., Wong, D., Goh, F.G., Weiss, M., Byrne, A., Pasparakis, M., Ragoussis, J. and Udalova, I.A. 2014. IRF5:RelA Interaction Targets Inflammatory Genes in Macrophages. *CellReports*. **8**(5),pp.1308–1317.

Sathe, P., Metcalf, D., Vremec, D., Naik, S.H., Langdon, W.Y., Huntington, N.D., Wu, L. and Shortman, K. 2014. Lymphoid tissue and plasmacytoid dendritic cells and macrophages do not share a common macrophage-dendritic cell-restricted progenitor. *Immunity*.

41(1),pp.104–115.

Satoh, T., Takeuchi, O., Vandenbon, A., Yasuda, K., Tanaka, Y., Kumagai, Y., Miyake, T., Matsushita, K., Okazaki, T., Saitoh, T., Honma, K., Matsuyama, T., Yui, K., Tsujimura, T., Standley, D.M., Nakanishi, K., Nakai, K. and Akira, S. 2010. The Jmjd3-Irf4 axis regulates M2 macrophage polarization and host responses against helminth infection. *Nature immunology*. **11**(10),pp.936–944.

Schiltz, R.L., Mizzen, C.A., Vassilev, A., Cook, R.G., Allis, C.D. and Nakatani, Y. 1999. Overlapping but distinct patterns of histone acetylation by the human coactivators p300 and PCAF within nucleosomal substrates. *Journal of Biological Chemistry*. **274**(3),pp.1189–1192.

Schmidt, S.V., Krebs, W., Ulas, T., Xue, J., Baßler, K., Günther, P., Hardt, A.-L., Schultze, H., Sander, J., Klee, K., Theis, H., Kraut, M., Beyer, M. and Schultze, J.L. 2016. The transcriptional regulator network of human inflammatory macrophages is defined by open chromatin. *Nature Publishing Group*. **26**(2),pp.151–170.

Schneider, C., Nobs, S.P., Kurrer, M., Rehrauer, H., Thiele, C. and Kopf, M. 2014. Induction of the nuclear receptor PPAR-γ by the cytokine GM-CSF is critical for the differentiation of fetal monocytes into alveolar macrophages. *Nature immunology*. **15**(11),pp.1026–1037.

Schultz, D.C., Ayyanathan, K., Negorev, D., Maul, G.G. and Rauscher, F.J. 2002. SETDB1: a novel KAP-1-associated histone H3, lysine 9-specific methyltransferase that contributes to HP1-mediated silencing of euchromatic genes by KRAB zinc-finger proteins. *Genes & development*. **16**(8),pp.919–932.

Scott, C.L., Zheng, F., De Baetselier, P., Martens, L., Saeys, Y., De Prijck, S., Lippens, S., Abels, C., Schoonooghe, S., Raes, G., Devoogdt, N., Lambrecht, B.N., Beschin, A. and Guilliams, M. 2016. Bone marrow-derived monocytes give rise to self-renewing and fully differentiated Kupffer cells. *Nature Communications*. **7**,p.10321.

Scott, E.W., Simon, M.C., Anastasi, J. and Singh, H. 1994. Requirement of transcription factor PU.1 in the development of multiple hematopoietic lineages. *Science (New York, N.Y.)*. **265**(5178),pp.1573–1577.

Self-Fordham, J.B., Naqvi, A.R., Uttamani, J.R., Kulkarni, V. and Nares, S. 2017. MicroRNA: Dynamic Regulators of Macrophage Polarization and Plasticity. *Frontiers in immunology*. **8**,p.1062.

Semenkovich, N.P., Planer, J.D., Ahern, P.P., Griffin, N.W., Lin, C.Y. and Gordon, J.I. 2016. Impact of the gut microbiota on enhancer accessibility in gut intraepithelial lymphocytes. *Proceedings of the National Academy of Sciences of the United States of America*. **113**(51),pp.14805–14810.

Seneviratne, A.N., Edsfeldt, A.O., Cole, J.E., Kassiteridi, C., Swart, M., Park, I., Green, P., Khoyratty, T.E., Saliba, D.G., Goddard, M.E., Sansom, S.N., Goncalves, I., Krams, R., Udalova, I.A. and Monaco, C. 2017. Interferon Regulatory Factor 5 Controls Necrotic Core Formation in Atherosclerotic Lesions by Impairing Efferocytosis. *Circulation*.p.CIRCULATIONAHA.117.027844.

Serbina, N.V., Salazar-Mather, T.P., Biron, C.A., Kuziel, W.A. and Pamer, E.G. 2003. TNF/iNOS-producing dendritic cells mediate innate immune defense against bacterial infection. *Immunity*. **19**(1),pp.59–70.

Sheng, J., Ruedl, C. and Karjalainen, K. 2015. Most Tissue-Resident Macrophages Except

Microglia Are Derived from Fetal Hematopoietic Stem Cells. *Immunity*. **43**(2),pp.382–393.

Siersbæk, R., Rabiee, A., Nielsen, R., Sidoli, S., Traynor, S., Loft, A., La Cour Poulsen, L., Rogowska-Wrzesinska, A., Jensen, O.N. and Mandrup, S. 2014. Transcription factor cooperativity in early adipogenic hotspots and super-enhancers. *CellReports*. **7**(5),pp.1443–1455.

Sims, R.J., Belotserkovskaya, R. and Reinberg, D. 2004. Elongation by RNA polymerase II: the short and long of it. *Genes & development*. **18**(20),pp.2437–2468.

Skourti-Stathaki, K. and Proudfoot, Nicholas J 2014. A double-edged sword: R loops as threats to genome integrity and powerful regulators of gene expression. *Genes & development*. **28**(13),pp.1384–1396.

Skourti-Stathaki, K., Kamieniarz-Gdula, K. and Proudfoot, N.J. 2014. R-loops induce repressive chromatin marks over mammalian gene terminators. *Nature*. **516**(7531),pp.436–439.

Skourti-Stathaki, K., Proudfoot, N.J. and Gromak, N. 2011. Human senataxin resolves RNA/DNA hybrids formed at transcriptional pause sites to promote Xrn2-dependent termination. *Molecular Cell*. **42**(6),pp.794–805.

Sorgi, C.A., Rose, S., Court, N., Carlos, D., Paula-Silva, F.W.G., Assis, P.A., Frantz, F.G., Ryffel, B., Quesniaux, V. and Faccioli, L.H. 2012. GM-CSF priming drives bone marrow-derived macrophages to a pro-inflammatory pattern and downmodulates PGE2 in response to TLR2 ligands. D. S. Zamboni, ed. *PloS one*. **7**(7),p.e40523.

Soufi, A., Garcia, M.F., Jaroszewicz, A., Osman, N., Pellegrini, M. and Zaret, K.S. 2015. Pioneer Transcription Factors Target Partial DNA Motifs on Nucleosomes to Initiate Reprogramming. *Cell*. **161**(3),pp.555–568.

Spitz, F. and Furlong, E.E.M. 2012. Transcription factors: from enhancer binding to developmental control. *Nature Reviews Genetics*. **13**(9),pp.613–626.

Sripathy, S.P., Stevens, J. and Schultz, D.C. 2006. The KAP1 corepressor functions to coordinate the assembly of de novo HP1-demarcated microenvironments of heterochromatin required for KRAB zinc finger protein-mediated transcriptional repression. *Molecular and cellular biology*. **26**(22),pp.8623–8638.

Stark, R., and Brown, G., 2011. DiffBind: differential binding analysis of ChIP-Seq peak data. *Bioconductor.* Available at: http://bioconductor.org/packages/release/bioc/vignettes/DiffBind/inst/doc/DiffBind.pdf

Steinman, R.M. and Cohn, Z.A. 1973. Identification of a novel cell type in peripheral lymphoid organs of mice. I. Morphology, quantitation, tissue distribution. *The Journal of experimental medicine*. **137**(5),pp.1142–1162.

Swirski, F.K., Nahrendorf, M., Etzrodt, M., Wildgruber, M., Cortez-Retamozo, V., Panizzi, P., Figueiredo, J.-L., Kohler, R.H., Chudnovskiy, A., Waterman, P., Aikawa, E., Mempel, T.R., Libby, P., Weissleder, R. and Pittet, M.J. 2009. Identification of splenic reservoir monocytes and their deployment to inflammatory sites. *Science (New York, N.Y.)*. **325**(5940),pp.612–616.

Tahirov, T.H., Inoue-Bungo, T., Morii, H., Fujikawa, A., Sasaki, M., Kimura, K., Shiina, M., Sato, K., Kumasaka, T., Yamamoto, M., Ishii, S. and Ogata, K. 2001. Structural analyses of DNA

recognition by the AML1/Runx-1 Runt domain and its allosteric control by CBFbeta. *Cell*. **104**(5),pp.755–767.

Takaoka, A., Yanai, H., Kondo, S., Duncan, G., Negishi, H., Mizutani, T., Kano, S.-I., Honda, K., Ohba, Y., Mak, T.W. and Taniguchi, T. 2005. Integral role of IRF-5 in the gene induction programme activated by Toll-like receptors. *Nature*. **434**(7030),pp.243–249.

Takeda, K., Tanaka, T., Shi, W., Matsumoto, M., Minami, M., Kashiwamura, S., Nakanishi, K., Yoshida, N., Kishimoto, T. and Akira, S. 1996. Essential role of Stat6 in IL-4 signalling. *Nature*. **380**(6575),pp.627–630.

Takeuchi, O. and Akira, S. 2010. Pattern recognition receptors and inflammation. *Cell*. **140**(6),pp.805–820.

Tamoutounour, S., Guilliams, M., Montanana Sanchis, F., Liu, H., Terhorst, D., Malosse, C., Pollet, E., Ardouin, L., Luche, H., Sanchez, C., Dalod, M., Malissen, B. and Henri, S. 2013. Origins and functional specialization of macrophages and of conventional and monocyte-derived dendritic cells in mouse skin. *Immunity*. **39**(5),pp.925–938.

Tamura, T., Nagamura-Inoue, T., Shmeltzer, Z., Kuwata, T. and Ozato, K. 2000. ICSBP directs bipotential myeloid progenitor cells to differentiate into mature macrophages. *Immunity*. **13**(2),pp.155–165.

Tanaka, N., Kawakami, T. and Taniguchi, T. 1993. Recognition DNA sequences of interferon regulatory factor 1 (IRF-1) and IRF-2, regulators of cell growth and the interferon system. *Molecular and cellular biology*. **13**(8),pp.4531–4538.

Tecchio, C., Micheletti, A. and Cassatella, M.A. 2014. Neutrophil-derived cytokines: facts beyond expression. *Frontiers in immunology*. **5**,p.508.

Thanos, D. and Maniatis, T. 1995. Virus induction of human IFN beta gene expression requires the assembly of an enhanceosome. *Cell*. **83**(7),pp.1091–1100.

Thomas, G.D., Hanna, R.N., Vasudevan, N.T., Hamers, A.A., Romanoski, C.E., McArdle, S., Ross, K.D., Blatchley, A., Yoakum, D., Hamilton, B.A., Mikulski, Z., Jain, M.K., Glass, C.K. and Hedrick, C.C. 2016. Deleting an Nr4a1 Super-Enhancer Subdomain Ablates Ly6C(low) Monocytes while Preserving Macrophage Gene Function. *Immunity*. **45**(5),pp.975–987.

Thomas, K.E., Galligan, C.L., Newman, R.D., Fish, E.N. and Vogel, S.N. 2006. Contribution of interferon-beta to the murine macrophage response to the toll-like receptor 4 agonist, lipopolysaccharide. *Journal of Biological Chemistry*. **281**(41),pp.31119–31130.

Thorvaldsdóttir, H., Robinson, J.T. and Mesirov, J.P. 2013. Integrative Genomics Viewer (IGV): high-performance genomics data visualization and exploration. *Briefings in bioinformatics*. **14**(2),pp.178–192.

Tillo, D., Kaplan, N., Moore, I.K., Fondufe-Mittendorf, Y., Gossett, A.J., Field, Y., Lieb, J.D., Widom, J., Segal, E. and Hughes, T.R. 2010. High nucleosome occupancy is encoded at human regulatory sequences. S. Hannenhalli, ed. *PloS one*. **5**(2),p.e9129.

Tyner, C., Barber, G.P., Casper, J., Clawson, H., Diekhans, M., Eisenhart, C., Fischer, C.M., Gibson, D., Gonzalez, J.N., Guruvadoo, L., Haeussler, M., Heitner, S., Hinrichs, A.S., Karolchik, D., Lee, B.T., Lee, C.M., Nejad, P., Raney, B.J., Rosenbloom, K.R., Speir, M.L., Villarreal, C., Vivian, J., Zweig, A.S., Haussler, D., Kuhn, R.M. and Kent, W.J. 2017. The UCSC Genome Browser database: 2017 update. *Nucleic acids research*. **45**(D1),pp.D626–

D634.

Ushach, I. and Zlotnik, A. 2016. Biological role of granulocyte macrophage colony-stimulating factor (GM-CSF) and macrophage colony-stimulating factor (M-CSF) on cells of the myeloid lineage. *Journal of leukocyte biology*. **100**(3),pp.481–489.

Van Furth, R. 1981. Identification of mononuclear phagocytes: overview and definitions. *Methods Jor studying mononuclear phagocytes, Adams, et al.(eds) p*. **243**.

Van Furth, R., Cohn, Z.A., Hirsch, J.G., Humphrey, J.H., Spector, W.G. and Langevoort, H.L. 1972. [Mononuclear phagocytic system: new classification of macrophages, monocytes and of their cell line]. *Bulletin of the World Health Organization*. **47**(5),pp.651–658.

van Wijnen, A.J., Stein, G.S., Peter Gergen, J., Groner, Y., Hiebert, S.W., Ito, Y., Liu, P., Neil, J.C., Ohki, M. and Speck, N. 2004. Nomenclature for Runt-related (RUNX) proteins. *Oncogene*. **23**(24),pp.4209–4210.

Varga, T., Mounier, R., Horvath, A., Cuvellier, S., Dumont, F., Poliska, S., Ardjoune, H., Juban, G., Nagy, L. and Chazaud, B. 2016. Highly Dynamic Transcriptional Signature of Distinct Macrophage Subsets during Sterile Inflammation, Resolution, and Tissue Repair. *Journal of immunology (Baltimore, Md. : 1950)*. **196**(11),pp.4771–4782.

Varinou, L., Ramsauer, K., Karaghiosoff, M., Kolbe, T., Pfeffer, K., Müller, M. and Decker, T. 2003. Phosphorylation of the Stat1 transactivation domain is required for full-fledged IFN-gamma-dependent innate immunity. *Immunity*. **19**(6),pp.793–802.

Voon, D.C.-C., Hor, Y.T. and Ito, Y. 2015. The RUNX complex: reaching beyond haematopoiesis into immunity. *Immunology*. **146**(4),pp.523–536.

Waddington, C.H., 1957. The strategy of the genes. *London: Allen*, *86*.

Wang, Q., Stacy, T., Binder, M., Marin-Padilla, M., Sharpe, A.H. and Speck, N.A. 1996. Disruption of the Cbfa2 gene causes necrosis and hemorrhaging in the central nervous system and blocks definitive hematopoiesis. *Proceedings of the National Academy of Sciences*. **93**(8),pp.3444–3449.

Wathelet, M.G., Lin, C.H., Parekh, B.S., Ronco, L.V., Howley, P.M. and Maniatis, T. 1998. Virus infection induces the assembly of coordinately activated transcription factors on the IFN-beta enhancer in vivo. *Molecular Cell*. **1**(4),pp.507–518.

Weiss, M., Blazek, K., Byrne, A.J., Perocheau, D.P. and Udalova, I.A. 2013. IRF5 is a specific marker of inflammatory macrophages in vivo. *Mediators of inflammation*. **2013**(8),pp.245804–9.

Weiss, M., Byrne, A.J., Blazek, K., Saliba, D.G., Pease, J.E., Perocheau, D., Feldmann, M. and Udalova, I.A. 2015. IRF5 controls both acute and chronic inflammation. *Proceedings of the National Academy of Sciences of the United States of America*. **112**(35),pp.11001–11006.

West, S. and Proudfoot, Nicholas J 2009. Transcriptional Termination Enhances Protein Expression in Human Cells. *Molecular Cell*. **33**(3),pp.354–364.

West, S., Proudfoot, N.J. and Dye, M.J. 2008. Molecular dissection of mammalian RNA polymerase II transcriptional termination. *Molecular Cell*. **29**(5),pp.600–610.

Whyte, W.A., Orlando, D.A., Hnisz, D., Abraham, B.J., Lin, C.Y., Kagey, M.H., Rahl, P.B., Lee,

T.I. and Young, R.A. 2013. Master Transcription Factors and Mediator Establish Super-Enhancers at Key Cell Identity Genes. *Cell*. **153**(2),pp.307–319.

Wilson, A., Murphy, M.J., Oskarsson, T., Kaloulis, K., Bettess, M.D., Oser, G.M., Pasche, A.-C., Knabenhans, C., Macdonald, H.R. and Trumpp, A. 2004. c-Myc controls the balance between hematopoietic stem cell self-renewal and differentiation. *Genes & development*. **18**(22),pp.2747–2763.

Witte, S., Bradley, A., Enright, A.J. and Muljo, S.A. 2015. High-density P300 enhancers control cell state transitions. *BMC Genomics*. **16**(1),p.307.

Wong, K.H., Jin, Y. and Struhl, K. 2014. TFIIH phosphorylation of the Pol II CTD stimulates mediator dissociation from the preinitiation complex and promoter escape. *Molecular Cell*. **54**(4),pp.601–612.

Wu, C.-H., Yamaguchi, Y., Benjamin, L.R., Horvat-Gordon, M., Washinsky, J., Enerly, E., Larsson, J., Lambertsson, A., Handa, H. and Gilmour, D. 2003. NELF and DSIF cause promoter proximal pausing on the hsp70 promoter in Drosophila. *Genes & development*. **17**(11),pp.1402–1414.

Wu, T.D. and Nacu, S. 2010. Fast and SNP-tolerant detection of complex variants and splicing in short reads. *Bioinformatics*. **26**(7),pp.873–881.

Wuarin, J. and Schibler, U. 1994. Physical isolation of nascent RNA chains transcribed by RNA polymerase II: evidence for cotranscriptional splicing. *Molecular and cellular biology*. **14**(11),pp.7219–7225.

Wysoker, A., Tibbetts, K., and Fennell, T. 2017. Picard tools version 2.0.1. Available online at: http://broadinstitute.github.io/picard/

Xu, D., Meyer, F., Ehlers, E., Blasnitz, L. and Zhang, L. 2011. Interferon regulatory factor 4 (IRF-4) targets IRF-5 to regulate Epstein-Barr virus transformation. *Journal of Biological Chemistry*. **286**(20),pp.18261–18267.

Yamaguchi, Y., Shibata, H. and Handa, H. 2013. Transcription elongation factors DSIF and NELF: promoter-proximal pausing and beyond. *Biochimica et biophysica acta*. **1829**(1),pp.98–104.

Yang, Z., Yik, J.H.N., Chen, R., He, N., Jang, M.K., Ozato, K. and Zhou, Q. 2005. Recruitment of P-TEFb for stimulation of transcriptional elongation by the bromodomain protein Brd4. *Molecular Cell*. **19**(4),pp.535–545.

Yatim, N., Jusforgues-Saklani, H., Orozco, S., Schulz, O., Barreira da Silva, R., Reis e Sousa, C., Green, D.R., Oberst, A. and Albert, M.L. 2015. RIPK1 and NF-κB signaling in dying cells determines cross-priming of $CD8^+$ T cells. *Science (New York, N.Y.)*. **350**(6258),pp.328–334.

Ye, J., Coulouris, G., Zaretskaya, I., Cutcutache, I., Rozen, S. and Madden, T.L. 2012. Primer-BLAST: A tool to design target-specific primers for polymerase chain reaction. *BMC bioinformatics*. **13**(1),p.134.

Yona, S. and Gordon, S. 2015. From the Reticuloendothelial to Mononuclear Phagocyte System - The Unaccounted Years. *Frontiers in immunology*. **6**,p.328.

Yona, S., Kim, K.-W., Wolf, Y., Mildner, A., Varol, D., Breker, M., Strauss-Ayali, D., Viukov, S., Guilliams, M., Misharin, A., Hume, D.A., Perlman, H., Malissen, B., Zelzer, E. and Jung, S.

2013. Fate mapping reveals origins and dynamics of monocytes and tissue macrophages under homeostasis. *Immunity*. **38**(1),pp.79–91.

Zabidi, M.A. and Stark, A. 2016. Regulatory Enhancer-Core-Promoter Communication via Transcription Factors and Cofactors. *Trends in genetics : TIG*. **32**(12),pp.801–814.

Zaret, K.S. and Carroll, J.S. 2011. Pioneer transcription factors: establishing competence for gene expression. *Genes & development*. **25**(21),pp.2227–2241.

Zhang, D.E., Hetherington, C.J., Meyers, S., Rhoades, K.L., Larson, C.J., Chen, H.M., Hiebert, S.W. and Tenen, D.G. 1996. CCAAT enhancer-binding protein (C/EBP) and AML1 (CBF alpha2) synergistically activate the macrophage colony-stimulating factor receptor promoter. *Molecular and cellular biology*. **16**(3),pp.1231–1240.

Zhang, Y., Liu, T., Meyer, C.A., Eeckhoute, J., Johnson, D.S., Bernstein, B.E., Nusbaum, C., Myers, R.M., Brown, M., Li, W. and Liu, X.S. 2008. Model-based analysis of ChIP-Seq (MACS). *Genome Biology*. **9**(9),p.R137.

Zhao, Z.W., White, M.D., Bissiere, S., Levi, V. and Plachta, N. 2016. Quantitative imaging of mammalian transcriptional dynamics: from single cells to whole embryos. *BMC biology*. **14**(1),p.115.

Zhu, Y., Sun, L., Chen, Z., Whitaker, J.W., Wang, T. and Wang, W. 2013. Predicting enhancer transcription and activity from chromatin modifications. *Nucleic acids research*. **41**(22),pp.10032–10043.

Zigmond, E., Varol, C., Farache, J., Elmaliah, E., Satpathy, A.T., Friedlander, G., Mack, M., Shpigel, N., Boneca, I.G., Murphy, K.M., Shakhar, G., Halpern, Z. and Jung, S. 2012. Monocytes in the Inflamed Colon Give Rise to Proinflammatory Effector Cellsand Migratory Antigen-Presenting Cells. *Immunity*. **37**(6),pp.1076–1090.

8. Appendix

8.1. Chapter 3 – supplementary tables

8.1.1 ATAC-seq GM-BMDM vs BM neutrophil - top gene ontology results

GO ID	Name	Binom_Observed_Region_Hits	Binom_Fold_Enrichment	AdjustedBinomPValue	FDR	Cell
GO:0008152	metabolic process	2167	1.26	3.72E-53	1.24E-53	Mac
GO:0044238	primary metabolic process	2015	1.28	9.04E-50	1.81E-50	Mac
GO:0044237	cellular metabolic process	1975	1.28	8.97E-49	1.49E-49	Mac
GO:0071704	organic substance metabolic process	2050	1.27	3.65E-48	4.57E-49	Mac
GO:0019222	regulation of metabolic process	1646	1.35	3.35E-47	3.72E-48	Mac
GO:0080090	regulation of primary metabolic process	1530	1.37	8.71E-47	8.71E-48	Mac
GO:0005515	protein binding	1999	1.27	1.07E-45	5.37E-46	Mac
GO:0031323	regulation of cellular metabolic process	1528	1.36	8.76E-44	7.30E-45	Mac
GO:0009987	cellular process	2808	1.14	1.40E-43	1.08E-44	Mac
GO:0060255	regulation of macromolecule metabolic process	1441	1.38	1.76E-43	1.26E-44	Mac
GO:0045087	innate immune response	49	6.15	2.01E-19	2.88E-20	Mac & Neu
GO:0002252	immune effector process	51	5.61	1.26E-18	1.58E-19	Mac & Neu
GO:0043900	regulation of multi-organism process	40	6.92	4.39E-17	4.39E-18	Mac & Neu
GO:0006950	response to stress	165	2.04	4.11E-16	3.42E-17	Mac & Neu
GO:0002684	positive regulation of immune system process	67	3.71	8.46E-16	6.51E-17	Mac & Neu
GO:0050776	regulation of immune response	58	4.14	2.26E-15	1.62E-16	Mac & Neu
GO:0009615	response to virus	35	6.92	1.33E-14	8.85E-16	Mac & Neu
GO:0031347	regulation of defense response	50	4.29	2.00E-13	1.18E-14	Mac & Neu
GO:0002697	regulation of immune effector process	40	5.29	4.15E-13	2.19E-14	Mac & Neu
GO:0006954	inflammatory response	29	6.86	5.37E-12	1.08E-12	Neu
GO:1901700	response to oxygen-containing compound	47	3.15	1.27E-08	1.27E-09	Neu
GO:1901701	cellular response to oxygen-containing compound	35	4.07	1.77E-08	1.61E-09	Neu
GO:0071219	cellular response to molecule of bacterial origin	17	9.35	7.45E-08	6.21E-09	Neu
GO:0071216	cellular response to biotic stimulus	17	8.66	2.42E-07	1.86E-08	Neu
GO:0070887	cellular response to chemical stimulus	56	2.55	2.63E-07	1.88E-08	Neu
GO:0071222	cellular response to lipopolysaccharide	16	9.16	4.20E-07	2.80E-08	Neu
GO:0030593	neutrophil chemotaxis	11	15.05	3.19E-06	1.77E-07	Neu
GO:0004982	N-formyl peptide receptor activity	5	97.64	9.32E-06	9.32E-06	Neu
GO:0009611	response to wounding	31	3.55	1.01E-05	5.03E-07	Neu
GO:0005143	interleukin-12 receptor binding	6	24.47	8.32E-04	2.08E-04	Mac & Neu

8.1.2. GM-BMDM vs M-BMDM ATAC-seq peaks - top gene ontology results

ID	Name	Binom_Observed_Region_Hits	Binom_Fold_Enrichment	AdjustedBinomPValue	FDR	Cell
GO:0009987	cellular process	7413	1.15	3.36E-142	3.36E-142	GM-BMDM
GO:0065007	biological regulation	6305	1.20	4.03E-125	2.01E-125	GM-BMDM
GO:0050789	regulation of biological process	6145	1.21	5.53E-121	1.84E-121	GM-BMDM
GO:0050794	regulation of cellular process	5977	1.21	8.19E-116	2.05E-116	GM-BMDM
GO:0048583	regulation of response to stimulus	2625	1.47	7.93E-98	1.59E-98	GM-BMDM
GO:0044237	cellular metabolic process	4982	1.24	2.91E-93	4.85E-94	GM-BMDM
GO:0008152	metabolic process	5433	1.21	4.07E-92	5.82E-93	GM-BMDM
GO:0071704	organic substance metabolic process	5170	1.23	3.26E-90	4.07E-91	GM-BMDM
GO:0010646	regulation of cell communication	2474	1.47	2.31E-89	2.56E-90	GM-BMDM
GO:0023051	regulation of signaling	2471	1.47	7.10E-89	7.10E-90	GM-BMDM
GO:0005488	binding	7055	1.16	1.31E-130	1.31E-130	GM-BMDM
GO:0005515	protein binding	5092	1.24	4.78E-95	2.39E-95	GM-BMDM
GO:0003824	catalytic activity	3902	1.23	7.93E-57	2.64E-57	GM-BMDM
GO:0043167	ion binding	4391	1.19	4.64E-49	1.16E-49	GM-BMDM
GO:0043168	anion binding	2339	1.31	4.65E-43	9.30E-44	GM-BMDM
GO:0019899	enzyme binding	1095	1.55	2.54E-42	4.24E-43	GM-BMDM
GO:0030234	enzyme regulator activity	955	1.53	2.05E-34	2.93E-35	GM-BMDM
GO:0008289	lipid binding	867	1.55	3.63E-32	4.12E-33	GM-BMDM
GO:0097159	organic cyclic compound binding	3695	1.18	3.70E-32	4.12E-33	GM-BMDM
GO:0005083	small GTPase regulator activity	424	1.90	1.09E-30	1.09E-31	GM-BMDM
GO:0009987	cellular process	7097	1.15	4.20E-127	4.20E-127	M-BMDM
GO:0008152	metabolic process	5286	1.23	2.86E-101	1.43E-101	M-BMDM
GO:0044237	cellular metabolic process	4800	1.24	1.54E-91	5.15E-92	M-BMDM
GO:0071704	organic substance metabolic process	4995	1.23	2.09E-91	5.22E-92	M-BMDM
GO:0044238	primary metabolic process	4871	1.23	9.07E-88	1.81E-88	M-BMDM
GO:0065007	biological regulation	5842	1.16	1.73E-72	2.88E-73	M-BMDM
GO:0050789	regulation of biological process	5686	1.16	1.36E-69	1.95E-70	M-BMDM
GO:0050794	regulation of cellular process	5498	1.16	1.11E-61	1.39E-62	M-BMDM
GO:0019222	regulation of metabolic process	3804	1.24	8.35E-58	9.27E-59	M-BMDM
GO:0044763	single-organism cellular process	5923	1.13	5.13E-54	5.13E-55	M-BMDM
GO:0005488	binding	6680	1.15	2.15E-98	2.15E-98	M-BMDM
GO:0003824	catalytic activity	3920	1.29	1.05E-83	5.24E-84	M-BMDM
GO:0005515	protein binding	4707	1.19	1.25E-57	4.18E-58	M-BMDM
GO:0043167	ion binding	4237	1.20	2.73E-49	6.83E-50	M-BMDM
GO:0016787	hydrolase activity	1827	1.34	1.23E-36	2.47E-37	M-BMDM
GO:0043168	anion binding	2198	1.28	9.14E-34	1.52E-34	M-BMDM
GO:0030234	enzyme regulator activity	894	1.49	3.12E-28	4.45E-29	M-BMDM
GO:0042578	phosphoric ester hydrolase activity	452	1.76	1.06E-25	1.32E-26	M-BMDM
GO:0016788	hydrolase activity, acting on ester bonds	679	1.54	2.28E-24	2.54E-25	M-BMDM
GO:0030695	GTPase regulator activity	550	1.60	1.68E-22	1.68E-23	M-BMDM

8.2. Chapter 4 – supplementary tables

8.2.1. mRNA-seq hierarchical clustering – cluster gene ontology

Term	Overlap	Adjusted.P.value	Z.score	Combined.Score	Cluster
inflammatory response (GO:0006954)	43/209	1.66E-20	-4.197133464	221.4158847	1
cytokine activity (GO:0005125)	21/103	1.53E-09	-3.592771335	94.2692837	1
chemokine activity (GO:0008009)	14/45	6.73E-09	-3.032177528	72.95814802	1
cellular response to lipopolysaccharide (GO:0071222)	15/55	3.94E-08	-2.445852101	57.63624494	1
chemokine-mediated signaling pathway (GO:0070098)	14/48	4.24E-08	-2.496082423	57.62010741	1
cellular response to interleukin-1 (GO:0071347)	12/53	1.64E-05	-2.378637018	40.05460666	1
positive regulation of transcription from RNA polymerase II promoter (GO:0045944)	49/712	2.63E-05	-6.361222626	102.6878939	1
positive regulation of NF-kappaB transcription factor activity (GO:0051092)	17/120	2.69E-05	-3.122589646	49.33376939	1
monocyte chemotaxis (GO:0002548)	10/38	2.69E-05	-2.284621301	36.06486811	1
negative regulation of viral genome replication (GO:0045071)	10/40	3.99E-05	-2.515559659	38.37963365	1
growth factor activity (GO:0008083)	11/67	0.000493821	-3.341543501	40.64847217	1
CCR1 chemokine receptor binding (GO:0031726)	4/5	0.000493821	-1.187020519	14.70874273	1
protease binding (GO:0002020)	11/78	0.001767065	-3.182946968	33.95101029	1
ribosome binding (GO:0043022)	7/34	0.003893649	-3.444946869	33.39595352	1
GDP binding (GO:0019003)	8/49	0.005725275	-2.946358845	26.97241492	1
CXCR3 chemokine receptor binding (GO:0048248)	3/5	0.012713928	0.491750465	-4.043738744	1
type I interferon signaling pathway (GO:0060337)	15/62	1.58E-08	-3.216796086	79.86639022	2
response to virus (GO:0009615)	15/100	9.20E-06	-2.799677231	49.74085209	2
interferon-gamma-mediated signaling pathway (GO:0060333)	11/65	0.000138989	-2.494812171	36.53978379	2
double-stranded RNA binding (GO:0003725)	9/50	0.000856489	-3.230223076	41.20602168	2
negative regulation of type I interferon production (GO:0032480)	7/33	0.002869598	-2.433383909	27.57289747	2
protein polyubiquitination (GO:0000209)	17/211	0.003317412	-3.609056919	39.56585946	2
negative regulation of viral genome replication (GO:0045071)	7/40	0.006176307	-2.547568371	25.48823806	2
positive regulation of defense response to virus by host (GO:0002230)	5/17	0.006176307	-2.149291684	21.7263635	2
defense response to virus (GO:0051607)	9/71	0.00652417	-2.674196314	26.25152447	2
ubiquitin-protein transferase activity (GO:0004842)	19/318	0.047443156	-5.372863043	43.2451428	2
single-stranded RNA binding (GO:0003727)	5/31	0.083582196	-3.566042315	25.2370405	2
SUMO binding (GO:0032183)	3/10	0.112530437	-2.269156267	14.73129287	2
cysteine-type endopeptidase activity involved in execution phase of apoptosis (GO:0097200)	3/13	0.203193601	-2.797822132	15.8857271	2
interleukin-12 receptor binding (GO:0005143)	2/5	0.239106321	-0.254668751	1.318845157	2
endopeptidase activator activity (GO:0061133)	2/5	0.239106321	0.256413628	-1.327881296	2
insulin receptor binding (GO:0005158)	3/18	0.294286312	-2.298551658	10.84849655	2
neutrophil degranulation (GO:0043312)	49/479	2.59E-05	-5.190194708	92.93527222	3
proteolysis (GO:0006508)	22/175	0.003156462	-3.195655703	38.36196242	3
NIK/NF-kappaB signaling (GO:0038061)	12/64	0.004620019	-2.426252752	26.96206774	3
negative regulation of G2/M transition of mitotic cell cycle (GO:0010972)	11/56	0.00550038	-2.410346303	25.92543837	3
transmembrane transport (GO:0055085)	18/140	0.005543431	-3.123309874	32.43611577	3
tumor necrosis factor-mediated signaling pathway (GO:0033209)	16/113	0.005543431	-2.787377299	29.49285982	3
lysophospholipase activity (GO:0004622)	5/17	0.07715077	-2.848386839	21.25582685	3
phosphatidylcholine 1-acylhydrolase activity (GO:0008970)	4/9	0.07715077	-2.627691872	20.87367871	3
amyloid-beta binding (GO:0001540)	6/25	0.07715077	-2.544451997	19.16915123	3
interleukin-10 receptor activity (GO:0004920)	3/5	0.07715077	-1.052343147	7.593659822	3
cadherin binding (GO:0045296)	23/272	0.108722987	-4.798505716	31.03408274	3
translation regulator activity (GO:0045182)	3/6	0.108722987	-1.625366766	10.65463181	3
3',5'-cyclic-AMP phosphodiesterase activity (GO:0004115)	4/14	0.14245711	-2.870135833	17.34439981	3
heparin binding (GO:0008201)	9/77	0.191275202	-3.291636167	17.09486782	3
peptidyl-serine phosphorylation (GO:0018105)	17/134	0.096352153	-3.091748042	28.99201036	4
tRNA modification (GO:0006400)	7/27	0.096352153	-2.660371394	23.83289595	4
protein autophosphorylation (GO:0046777)	17/145	0.111870495	-3.212829282	26.99961248	4
actin cytoskeleton organization (GO:0030036)	12/86	0.135789795	-2.898756444	22.85477163	4
apoptotic cell clearance (GO:0043277)	4/10	0.135789795	-2.779682058	20.46575169	4
cellular response to hypoxia (GO:0071456)	9/55	0.135789795	-2.635287333	19.48269273	4
positive regulation of mesenchymal cell proliferation (GO:0002053)	4/10	0.135789795	-2.060558773	15.17111789	4
neural tube closure (GO:0001843)	6/27	0.143743653	-2.624318124	18.23645179	4
protein serine/threonine kinase activity (GO:0004674)	24/296	0.489796798	-5.120883445	29.58071176	4
Rab GTPase binding (GO:0017137)	13/118	0.489796798	-4.499857078	27.75789182	4
GTPase activator activity (GO:0005096)	19/224	0.489796798	-4.833745106	25.66086034	4
protein serine/threonine kinase inhibitor activity (GO:0030291)	3/8	0.489796798	-3.240066046	17.85876737	4
guanyl-nucleotide exchange factor activity (GO:0005085)	10/95	0.489796798	-3.542910892	16.69134167	4
mRNA 3'-UTR AU-rich region binding (GO:0035925)	3/10	0.489796798	-2.498121286	12.03053115	4
non-membrane spanning protein tyrosine kinase activity (GO:0004715)	6/43	0.489796798	-2.641613931	11.94122336	4
WW domain binding (GO:0050699)	4/17	0.489796798	-2.280135092	11.81430098	4
protein kinase binding (GO:0019901)	34/292	2.38E-05	-5.541440908	92.73184253	5
ATP binding (GO:0005524)	28/243	0.000217918	-5.041630005	69.71207539	5
mitotic cell cycle (GO:0000278)	16/86	0.000298519	-2.845549666	41.92359827	5
sister chromatid cohesion (GO:0007062)	17/97	0.000298519	-2.736018789	40.13125569	5
protein phosphorylation (GO:0006468)	32/309	0.000630617	-4.401624371	58.15295815	5
protein autophosphorylation (GO:0046777)	20/145	0.000630617	-3.191527036	41.53312334	5
regulation of attachment of spindle microtubules to kinetochore (GO:0051988)	5/7	0.000630617	-2.68734957	34.85806176	5
mitotic sister chromatid segregation (GO:0000070)	7/17	0.000630617	-2.258309557	28.95441791	5
positive regulation of cytokinesis (GO:0032467)	9/33	0.001055888	-2.575993812	31.30268007	5
microtubule-based movement (GO:0007018)	12/62	0.001281575	-2.343119173	27.70609905	5
magnesium ion binding (GO:0000287)	17/124	0.002019635	-3.929998307	43.99739575	5
microtubule motor activity (GO:0003777)	10/52	0.004930353	-3.036248071	30.40831349	5
ATPase activity (GO:0016887)	16/134	0.011711526	-4.088691677	36.49888673	5
microtubule binding (GO:0008017)	15/125	0.012972247	-4.101820129	34.90355142	5
ADP binding (GO:0043531)	6/22	0.012972247	-2.596734341	22.04128306	5
protein serine/threonine kinase activity (GO:0004674)	26/296	0.014176337	-4.817646098	39.82162407	5

8.2.2. Average TPMs of genes in clusters

Cluster 1

Gene_Name	*IRF5ko_0hr*	*IRF5ko_1hr*	*IRF5ko_2hr*	*IRF5ko_4hr*	*IRF5ko_8hr*	*IRF5wt_0hr*	*IRF5wt_1hr*	*IRF5wt_2hr*	*IRF5wt_4hr*	*IRF5wt_8hr*
Ccl17	1056.12	1903.85	2672.64	2680.12	2444.34	1268.78	1977.46	2266.99	3253.22	2612.13
Ccl5	251.63	623.67	1097.21	1957.80	3107.24	244.20	529.42	1096.57	2146.66	3931.55
Il1b	5.83	636.91	431.37	359.54	333.59	12.20	1322.07	1088.81	1163.07	1275.95
Anxa1	350.39	414.98	640.16	703.31	573.01	415.53	633.21	895.05	919.30	981.33
Ccl3	69.75	688.84	492.57	474.74	307.61	94.71	846.04	732.71	1012.96	695.35
Bcl2a1b	149.81	419.82	572.45	521.00	449.77	201.72	509.75	661.38	595.35	664.61
Ccl4	48.32	719.86	562.16	323.72	159.72	49.40	583.32	646.11	613.82	218.69
Anxa2	138.18	185.47	342.93	402.38	403.23	167.29	237.85	372.16	402.09	456.64
Tnf	9.24	716.51	263.13	173.59	72.17	10.88	959.59	400.86	361.57	138.12
Srgn	76.58	312.86	401.49	454.67	377.89	55.01	210.96	302.77	351.48	380.69
Cxcl10	0.56	104.90	301.52	465.01	208.70	0.52	97.50	407.16	880.32	444.56
Il12b	5.09	327.84	238.17	324.06	140.34	4.69	426.73	437.79	575.19	419.44
Cxcl2	4.66	541.04	199.53	108.35	69.04	5.07	797.78	356.72	300.20	227.75
Calm1	118.37	193.56	270.01	339.09	357.42	135.66	213.36	275.25	297.08	397.62
Tagln2	130.92	232.48	282.46	362.05	385.47	114.79	180.34	231.66	335.33	319.98
Il1rn	47.91	173.23	244.13	226.18	205.97	58.74	314.06	425.38	419.25	432.40
Cxcl3	22.14	104.38	158.21	113.30	114.47	48.09	296.28	473.21	485.38	667.46
Cd40	9.58	178.99	304.88	400.60	366.99	4.71	125.95	225.70	446.64	395.63
Bcl2a1d	78.61	207.79	290.80	261.37	225.87	100.95	258.82	359.37	327.66	345.59
Il6	1.27	144.24	186.51	264.70	117.37	0.73	233.09	426.91	608.87	382.87
Isg15	1.96	114.74	316.83	427.61	374.95	1.36	77.79	225.95	430.01	381.11
Il1a	2.00	148.76	122.35	115.87	112.79	5.09	450.50	339.90	378.97	438.64
Acod1	5.47	88.36	162.64	159.06	141.19	13.67	229.31	393.63	428.36	412.58
Marcksl1	25.90	200.30	296.17	292.32	169.19	25.68	157.35	252.78	262.97	196.88
Slfn2	31.52	118.67	221.51	212.38	209.99	37.66	199.93	277.14	248.60	301.72
Bcl2a1a	54.29	159.36	232.58	181.94	125.83	83.25	234.75	299.15	237.63	233.20
Clic4	34.10	156.18	262.08	260.37	175.98	33.53	149.54	251.79	284.89	212.98
Rsad2	0.56	22.00	199.38	258.66	150.89	0.47	17.12	257.02	433.74	437.73
Ccl2	50.52	262.97	179.42	155.94	192.82	42.93	257.84	157.72	169.55	282.44
Rgs1	21.85	192.36	162.26	173.58	169.21	20.98	261.35	202.74	195.06	225.10
Abracl	69.13	114.28	187.06	189.70	159.43	84.82	144.21	214.31	222.14	234.47
Psma6	54.43	107.88	195.98	229.27	164.09	67.43	118.53	186.81	220.47	221.68
Nxf1	51.45	100.58	238.81	230.89	114.89	63.17	112.09	215.07	196.87	118.19
Apol7c	14.65	115.65	236.00	291.37	184.10	10.30	98.90	161.74	179.67	122.37
Nfkbia	26.16	281.98	205.67	154.48	114.98	19.20	177.52	158.71	147.33	109.72
Slc3a2	66.78	131.95	171.28	125.44	109.57	73.78	146.96	191.33	174.75	200.96
Sp140	12.53	51.13	167.51	218.56	186.46	16.55	61.70	181.82	224.03	231.38
Ptx3	6.17	76.41	77.87	55.33	31.81	20.27	265.65	284.81	262.39	228.46
Tnfaip2	22.62	253.55	222.43	110.04	80.64	22.16	194.42	180.11	114.66	62.75
Atf3	36.22	189.05	107.73	94.66	115.54	47.70	180.94	123.05	161.80	166.60
Oasl1	0.89	42.08	168.40	203.00	160.33	0.55	27.34	140.90	261.49	204.10
Tmem39a	31.42	181.49	157.63	144.05	119.14	29.80	159.79	144.95	121.05	117.44
Gnb1	73.82	88.38	123.36	132.78	147.25	81.37	105.16	125.23	147.64	168.56
Gbp2	10.07	13.64	45.10	147.20	187.12	19.24	26.00	90.03	240.75	403.01
Plek	24.66	129.35	161.11	98.50	51.73	21.36	209.00	248.51	144.41	79.84
Tcirg1	62.25	94.46	125.93	110.50	120.03	72.95	111.49	144.37	169.22	150.81
Rap1b	39.15	84.71	136.70	133.22	111.84	46.20	96.62	144.41	138.89	154.67
Prdx5	43.83	78.42	70.29	89.76	129.88	58.76	92.75	111.17	197.50	194.37
Msn	54.05	76.97	103.08	119.28	138.66	57.29	85.89	115.43	130.21	161.91
Hspa5	46.07	91.29	120.69	111.72	69.08	60.75	126.75	161.34	140.32	104.78

Cluster 2

Gene_Name	*IRF5ko_0hr*	*IRF5ko_1hr*	*IRF5ko_2hr*	*IRF5ko_4hr*	*IRF5ko_8hr*	*IRF5wt_0hr*	*IRF5wt_1hr*	*IRF5wt_2hr*	*IRF5wt_4hr*	*IRF5wt_8hr*
Ccl22	483.23	1406.79	2620.01	3899.09	4831.38	376.13	1216.43	2221.53	3542.71	4688.11
B2m	535.55	710.58	910.07	1168.31	1409.91	586.49	656.80	978.38	1081.93	1722.91
Psme2	261.22	298.95	598.87	820.71	1106.70	209.64	278.03	476.78	763.87	1165.19
Samhd1	90.16	93.71	186.94	424.68	410.14	122.78	132.41	240.17	472.53	609.62
Psme1	99.13	130.56	186.65	256.35	334.26	101.95	124.39	189.06	236.06	386.38
Pfkp	72.56	113.74	198.96	234.75	246.61	74.58	134.75	220.20	287.92	274.44
Mx1	24.86	21.83	163.15	263.79	236.79	32.90	29.38	229.69	354.53	386.15
Pnp	27.09	46.40	127.04	233.60	249.23	26.96	60.32	181.42	325.14	327.70
Ifitm3	9.98	21.08	86.57	209.54	312.18	9.75	20.09	100.84	285.60	413.26
Rnaset2b	71.88	86.15	126.47	145.28	145.72	60.32	84.65	140.33	184.87	219.98
Wnk1	39.94	87.50	166.43	156.98	143.54	25.71	56.17	103.45	94.29	109.21
Psma3	48.18	64.28	93.49	106.75	109.40	69.17	83.19	117.15	125.02	162.33
Cd86	21.97	61.74	137.44	132.58	124.38	16.07	53.32	112.38	98.52	118.28
Irf7	1.12	1.95	24.24	116.95	254.48	0.66	1.67	30.81	121.12	267.38
Inpp5b	16.15	30.81	90.31	137.19	119.11	16.48	34.54	100.97	135.35	137.08
Oasl2	2.77	5.49	47.16	147.04	145.31	2.21	4.53	68.45	180.01	192.15
Tapbp	23.58	38.55	73.78	135.32	153.43	19.35	27.93	58.11	122.59	133.85
Ptms	57.17	79.94	89.67	111.20	122.85	41.71	51.13	65.56	83.77	82.68
H2afy	39.41	57.22	86.45	109.08	115.09	34.08	49.39	69.83	103.67	106.55
Psmb9	35.18	36.77	66.76	114.94	162.67	25.05	25.35	50.05	105.49	139.23
Actn1	33.53	49.88	83.36	101.80	86.57	37.53	62.92	86.78	102.14	81.71
Rnf213	3.45	5.43	62.48	142.32	108.28	4.48	5.61	75.79	157.11	156.09
Cct3	32.24	37.99	71.71	106.22	81.22	37.95	49.76	77.46	111.46	98.10
Usp18	3.84	6.16	71.48	143.20	124.75	2.08	2.84	57.45	125.09	138.55
Eif6	35.05	50.06	72.50	80.40	79.23	31.40	47.27	63.78	93.00	76.88
Sp100	13.04	16.19	37.92	110.62	120.00	11.68	14.51	45.69	111.65	145.03
Slamf7	18.87	32.36	62.95	99.59	85.90	16.32	31.26	68.52	97.86	107.48
Sp110	9.91	25.56	61.24	91.95	101.95	11.00	28.31	68.50	101.41	116.86
Lgals9	9.85	11.10	32.28	86.51	127.29	13.12	16.83	44.38	102.44	164.31
Ifi47	1.90	2.66	59.48	141.74	86.73	1.78	2.45	66.36	135.21	109.80
Ifi209	3.68	8.96	64.38	116.89	79.73	2.81	8.38	85.77	121.51	114.76
Nt5c3	2.99	8.94	67.04	117.77	74.84	3.53	10.87	82.05	123.72	106.11
Ifi204	1.71	5.84	40.21	108.77	90.97	1.63	7.88	57.64	120.74	143.22
Tap1	19.18	19.40	59.96	109.78	112.70	9.88	8.58	44.49	106.39	82.35
Nono	28.16	34.58	55.13	90.10	96.89	22.13	28.47	44.95	85.39	64.01
Tor1aip2	9.51	12.72	68.25	98.02	82.14	8.64	13.61	69.14	89.21	90.91
Ifit3	0.44	2.97	41.00	112.92	104.39	0.38	1.53	27.63	93.31	138.14
Xaf1	3.43	3.80	43.91	87.90	92.38	3.00	3.65	53.31	94.56	124.18
Mbd2	29.78	36.25	55.39	70.78	70.47	27.16	34.50	47.03	65.03	68.17
Trafd1	16.26	16.93	47.14	87.75	86.42	14.07	15.13	47.59	90.29	81.29
Tap2	25.62	26.04	39.82	87.94	84.47	21.25	22.04	38.82	74.09	80.20
Irgm1	3.18	4.16	71.16	86.82	63.12	3.38	4.29	82.98	92.70	85.42
Il15	6.07	8.30	42.03	110.59	78.90	5.03	6.43	48.16	95.57	86.98
Slfn5	4.01	6.66	47.56	91.20	65.12	2.89	6.17	61.46	95.39	83.24
Cd200	6.66	17.21	38.04	68.66	96.76	4.70	16.16	35.62	72.17	105.62
Vwa5a	23.66	28.33	48.06	67.01	67.28	17.95	29.47	52.91	60.24	64.62
Trim30a	5.16	6.04	36.28	86.60	67.70	6.23	6.87	52.98	96.45	87.42
Alcam	16.74	20.28	40.03	70.73	66.58	16.49	21.29	46.76	63.79	82.68
Chmp2a	29.64	39.03	49.15	55.71	62.78	24.73	30.92	38.69	52.50	58.10
Phf11b	1.77	1.80	19.18	71.65	88.05	2.60	2.78	28.34	82.44	137.72

Cluster 3

Gene_Name	*IRF5ko_0hr*	*IRF5ko_1hr*	*IRF5ko_2hr*	*IRF5ko_4hr*	*IRF5ko_8hr*	*IRF5wt_0hr*	*IRF5wt_1hr*	*IRF5wt_2hr*	*IRF5wt_4hr*	*IRF5wt_8hr*
Tmsb4x	2401.25	3068.60	3852.13	3712.13	4381.48	3172.27	3935.40	4703.28	4317.83	6075.54
Fth1	1734.32	2229.06	2644.80	2202.13	2233.97	1963.43	2445.13	3045.08	2981.37	3797.49
Prdx1	684.32	867.54	1278.93	1171.62	1035.53	967.15	1324.01	1906.84	1645.76	2534.80
Lyz2	628.98	631.10	702.98	618.47	492.03	1988.93	2077.19	2176.26	1879.60	1526.75
Ccl9	438.46	745.95	1071.13	996.00	931.98	775.03	1402.30	1789.22	1656.26	1999.44
mt-Atp8	770.23	877.06	1080.83	972.11	837.48	1016.15	1333.52	1589.48	1384.90	1550.03
mt-Nd1	529.12	643.49	805.23	698.99	598.15	895.00	1071.51	1291.22	1113.51	1118.18
mt-Nd6	431.24	527.56	627.50	583.75	494.34	673.36	771.16	953.42	831.63	904.13
Ubc	406.92	749.24	440.00	807.93	971.81	266.21	450.73	266.01	774.98	692.22
Cd52	359.19	465.81	558.30	548.44	525.14	451.52	596.08	654.72	726.01	667.92
Akr1a1	277.71	323.21	445.49	504.37	561.34	350.61	419.18	554.44	617.58	1047.54
Rps24	289.51	355.88	463.57	456.50	464.21	326.22	404.85	510.32	458.61	639.89
Ctss	274.42	298.09	340.78	331.52	346.94	423.76	492.96	532.21	553.33	630.63
Esd	223.55	259.37	356.83	324.58	322.49	284.38	388.61	454.46	434.35	551.96
AA467197	40.35	73.45	128.99	178.54	251.45	97.84	185.45	308.50	418.05	776.81
Fcer1g	110.69	120.53	173.96	224.90	233.22	159.23	179.15	255.23	309.55	428.49
Rps27l	86.37	136.52	208.03	230.75	256.82	113.46	177.02	241.16	268.19	403.22
Wfdc17	119.46	143.83	185.11	168.93	151.61	180.02	236.19	287.58	255.22	326.92
Ctsz	117.45	147.99	156.25	159.57	248.56	142.30	176.77	189.09	227.83	292.77
H2-M2	64.54	104.69	139.16	146.45	128.33	115.24	225.53	272.06	297.69	282.96
Actr3	115.57	156.64	171.20	157.07	174.72	142.25	202.22	224.04	195.65	235.86
Anxa4	104.36	115.07	137.55	161.97	204.35	138.99	169.55	192.71	194.32	266.71
Anxa5	94.02	132.86	163.28	180.09	194.04	90.72	142.50	168.34	188.03	228.18
Txn1	54.15	90.08	139.99	197.90	241.79	71.26	94.75	153.24	206.41	296.07
Rpl24	92.62	119.39	162.73	139.06	114.41	131.00	154.07	210.87	179.92	226.86
Ccr7	80.00	141.10	89.41	229.42	274.81	56.36	104.29	68.35	175.50	241.55
Cstb	86.04	113.89	141.76	111.35	111.94	152.06	163.61	205.23	158.13	211.94
Cdc42	95.49	117.63	153.54	146.82	152.53	110.66	145.37	170.60	153.51	196.48
Rpl34	69.32	97.97	112.23	110.10	112.36	127.32	175.08	179.14	236.64	175.99
Uqcrh	76.60	94.17	124.44	135.80	136.74	116.64	133.99	165.11	153.22	189.09
Pla2g7	74.78	87.80	98.66	82.65	75.00	146.46	169.44	207.44	179.40	190.26
Grn	82.02	83.32	102.07	117.98	153.73	101.25	107.84	120.78	172.51	182.99
Ly6e	80.61	86.17	98.31	116.09	129.84	95.21	87.45	115.55	147.81	198.31
Tmsb10	63.96	74.69	92.06	88.89	95.57	85.12	129.70	139.83	150.19	197.77
Axl	65.88	74.30	89.98	130.02	134.92	77.12	91.15	111.26	170.36	162.12
Fkbp1a	69.42	79.05	110.13	100.59	139.23	77.73	98.57	110.69	117.36	162.72
Alas1	61.29	82.78	91.72	79.13	67.11	99.76	159.59	154.77	147.69	119.48
Btg1	45.71	136.10	83.24	92.73	104.60	60.83	162.80	97.66	112.44	141.93
Mtpn	38.37	60.87	83.18	95.58	74.89	65.53	113.83	158.61	168.14	174.94
Cxcl16	47.26	93.97	80.95	96.42	159.12	49.69	80.66	71.60	121.26	176.47
C3	18.15	19.96	36.38	67.85	80.95	64.47	82.53	128.10	196.36	266.00
Capza2	59.54	66.31	83.19	109.90	95.98	74.89	88.61	107.48	114.30	147.15
Ube2d3	58.73	72.91	92.66	100.26	93.65	67.78	98.77	112.55	120.28	128.74
Ywhae	55.44	68.33	87.27	95.70	106.79	60.08	81.33	104.40	101.71	138.51
Atp6v1e1	46.70	69.45	81.15	90.79	83.13	51.79	90.07	110.21	121.99	145.06
Glipr2	48.85	59.62	70.09	111.98	200.81	36.02	40.92	53.34	83.82	174.01
Rab11a	54.47	66.72	78.73	83.75	103.26	68.37	81.43	96.10	87.05	150.22
Pgk1	56.69	61.39	75.87	69.18	70.09	82.22	99.35	113.03	96.86	119.16
Itm2b	56.66	58.56	68.20	90.07	112.17	70.85	70.62	84.71	94.25	131.53
Txndc17	39.75	43.39	63.86	98.10	154.77	41.82	46.55	61.69	82.12	163.43

Cluster 4

Gene_Name	*IRF5ko_0hr*	*IRF5ko_1hr*	*IRF5ko_2hr*	*IRF5ko_4hr*	*IRF5ko_8hr*	*IRF5wt_0hr*	*IRF5wt_1hr*	*IRF5wt_2hr*	*IRF5wt_4hr*	*IRF5wt_8hr*
Hspa8	313.69	418.82	419.49	252.92	471.99	225.45	321.49	268.15	138.67	340.93
Rpl18	302.48	391.66	394.25	352.24	314.45	169.40	189.23	192.24	301.15	158.45
Rplp0	205.55	310.10	275.67	254.43	237.96	106.86	142.79	147.73	189.39	120.11
Cotl1	183.19	278.48	197.06	134.63	120.98	104.78	128.56	123.05	147.95	58.97
Hmox1	255.68	338.40	269.67	147.44	238.44	27.23	35.91	27.41	20.57	63.58
Coro1a	120.68	154.12	139.57	84.65	93.27	78.75	97.34	91.31	68.95	54.09
Irf5	125.18	132.76	125.86	111.91	162.10	38.44	45.07	33.37	56.46	62.90
Eef2	105.04	132.64	115.52	99.06	88.18	53.39	71.27	70.03	93.25	50.03
Rpl3	78.26	93.22	98.17	82.88	72.44	76.59	89.59	95.45	89.82	71.84
H2-DMa	74.19	77.18	69.91	52.37	45.01	61.72	63.22	58.55	55.52	34.29
Mfge8	65.83	85.48	72.88	49.23	25.04	28.10	35.13	33.01	29.42	13.97
Napsa	50.60	62.82	59.12	47.03	46.44	32.45	33.31	37.60	30.92	27.05
Zfp36l1	54.61	83.89	11.79	43.38	73.28	29.25	39.40	5.12	14.81	33.23
Etfb	41.38	54.71	48.21	32.87	21.90	25.16	29.68	29.13	31.36	12.67
Rogdi	48.43	48.50	40.59	26.39	42.87	28.25	25.01	21.40	17.74	23.16
Aes	38.40	41.03	39.92	31.35	26.99	29.98	30.27	29.15	33.68	18.73
Mbnl1	37.95	42.63	28.97	24.66	18.58	29.35	37.98	28.45	22.84	16.32
Aldh2	28.71	33.62	31.34	23.24	16.31	20.88	24.88	26.10	25.71	15.28
Slc48a1	32.34	29.08	28.04	17.61	15.03	28.51	25.55	22.41	14.65	13.31
Dap	19.88	25.21	22.37	20.49	15.06	16.36	19.01	20.11	17.52	15.71
Mt2	16.74	59.42	29.04	16.29	7.53	4.60	16.19	16.57	20.56	4.13
H2-DMb2	22.00	25.96	24.32	21.40	26.64	14.26	14.56	14.71	13.32	13.30
Tulp4	18.85	23.98	25.51	17.56	14.43	16.41	22.37	21.26	16.09	12.55
Uap1l1	22.78	25.12	21.11	12.85	12.17	16.96	18.74	17.10	15.00	8.73
Mt1	21.74	45.08	23.80	14.50	6.66	8.17	15.25	13.69	15.30	4.82
Vopp1	22.54	21.09	13.63	11.17	17.21	19.37	19.09	12.66	11.08	13.55
Cat	22.66	25.31	20.56	11.89	14.33	14.33	16.65	14.50	8.46	10.92
Slc25a39	15.72	18.83	19.06	14.36	12.69	16.14	15.27	16.91	16.52	11.08
Gpsm3	17.63	16.57	16.38	11.76	12.81	15.29	16.22	15.20	12.48	14.29
Kctd12	13.79	19.40	14.26	4.29	3.40	23.22	32.85	24.30	6.77	5.95
Asl	17.99	21.24	19.38	12.06	13.34	12.54	14.67	13.56	11.41	8.88
Dok2	30.32	27.04	11.39	6.47	9.85	19.90	14.06	8.49	5.62	6.38
Gng10	15.25	16.15	15.66	11.39	6.29	16.19	15.91	16.59	11.49	9.81
Higd2a	14.39	19.83	17.11	12.22	11.53	11.95	12.74	12.66	12.04	10.13
Slc35a4	15.65	15.65	15.32	11.14	12.69	11.65	13.12	12.37	12.49	7.85
Mt3	20.86	23.32	25.24	18.87	9.40	2.99	4.00	3.73	5.18	2.14
Bcat2	12.92	12.65	13.77	10.86	8.62	12.49	11.99	12.24	12.02	7.42
Adam23	15.46	17.22	16.88	9.00	6.62	10.78	13.64	12.26	4.97	4.20
Slc40a1	35.18	22.74	27.82	11.23	5.14	0.97	1.21	2.35	1.74	0.67
Mical1	17.73	13.78	8.77	4.69	10.75	18.43	11.09	7.00	4.00	7.63
Ezr	13.63	19.35	14.06	7.26	5.47	7.97	11.24	10.22	5.53	3.55
Ppp1r12c	12.11	9.83	7.96	7.59	9.86	13.14	10.06	7.65	8.26	10.23
Smim14	9.21	12.85	11.81	8.56	6.96	9.29	9.91	10.27	7.75	7.46
Rps6ka1	15.55	10.87	8.14	5.58	6.75	15.22	11.13	8.75	4.65	5.75
Jup	7.96	19.10	18.95	5.86	3.74	4.47	10.68	10.62	4.24	2.22
Mroh1	9.94	10.88	11.20	6.69	6.39	9.43	8.92	9.09	8.01	5.75
Dtx3	11.63	12.99	11.39	5.61	5.42	10.02	9.78	7.35	5.76	4.66
Ppm1m	13.57	10.98	9.56	6.25	9.40	8.81	6.87	5.35	5.66	5.79
Pip5k1c	12.87	13.96	8.00	4.55	8.16	8.82	8.96	6.06	5.20	5.64
Cd37	10.46	14.68	11.90	8.33	4.89	5.77	7.60	6.98	6.79	2.56

Cluster 5

Gene_Name	*IRF5ko_0hr*	*IRF5ko_1hr*	*IRF5ko_2hr*	*IRF5ko_4hr*	*IRF5ko_8hr*	*IRF5wt_0hr*	*IRF5wt_1hr*	*IRF5wt_2hr*	*IRF5wt_4hr*	*IRF5wt_8hr*
Clec4n	1419.51	1456.96	2012.63	1207.33	705.98	1170.59	1643.55	1639.01	926.48	584.64
Plet1	218.86	269.39	228.45	95.02	49.78	178.93	301.61	273.48	115.86	36.17
Laptm5	213.52	208.92	202.57	128.64	103.15	181.42	214.29	184.25	158.76	85.05
Glipr1	102.98	207.59	195.55	80.18	34.40	117.46	207.87	185.91	82.99	40.02
Alox5ap	120.00	130.71	132.16	70.74	30.20	154.54	149.41	148.87	96.46	36.88
Mgl2	169.15	162.40	159.90	94.27	30.18	113.36	115.56	105.40	70.07	23.58
Naaa	108.09	90.44	75.62	32.92	24.23	101.73	97.79	85.86	41.24	20.00
Gclm	90.67	86.43	85.74	43.28	33.42	52.70	58.17	53.59	25.78	30.05
Clec4a2	43.93	45.31	45.44	29.25	18.18	75.47	79.62	75.95	35.21	20.92
Cd24a	44.55	45.87	37.86	15.72	8.36	32.42	36.20	30.21	12.45	7.36
Csf1r	29.53	29.32	21.33	8.49	8.51	43.39	45.98	35.67	17.66	15.47
Asgr2	43.32	42.17	40.45	18.74	5.77	24.40	25.06	22.26	14.58	4.30
Hddc3	6.33	23.11	36.18	24.81	23.93	7.04	21.52	32.92	22.64	31.55
Il1r2	11.60	46.66	55.39	17.06	3.01	5.38	34.63	35.50	11.36	2.75
Gusb	24.25	21.74	21.59	11.86	9.04	32.78	31.26	29.17	20.67	13.56
Herpud1	28.15	42.11	15.09	12.69	13.11	24.37	32.33	15.07	12.40	10.22
Tbxas1	21.06	19.86	19.36	7.09	3.46	30.38	37.93	29.92	12.61	6.61
Prkcb	15.35	17.13	18.55	11.61	6.99	25.23	29.69	30.69	18.50	12.22
Nop58	14.95	27.83	24.31	10.34	6.95	19.51	35.19	29.50	10.35	6.98
Colgalt1	25.44	22.64	16.10	7.45	7.52	30.32	29.71	20.93	10.92	8.74
Gsn	22.72	25.71	24.82	16.80	10.06	16.72	19.17	18.39	16.25	7.32
Cdk4	21.79	24.90	21.71	11.93	10.53	21.18	22.52	19.17	12.35	8.08
Dnase2a	19.66	18.54	16.65	7.10	4.79	31.14	30.17	23.66	11.72	8.20
Dpp7	20.22	15.94	17.34	11.56	7.74	22.74	20.22	18.25	15.13	9.72
Plau	25.91	24.73	7.29	6.81	10.76	19.51	40.39	7.29	4.36	5.22
Haus8	18.08	18.58	16.68	6.40	7.22	23.14	23.08	17.83	7.75	7.65
Prcp	19.22	20.21	15.15	7.42	7.79	20.09	22.15	17.08	8.45	7.66
Slc1a5	20.61	21.22	16.57	9.22	5.86	18.77	20.56	16.87	11.19	4.10
Sept9	21.61	19.98	13.56	6.39	11.19	22.19	21.80	14.15	6.51	7.57
Uck2	22.73	25.62	20.47	6.84	5.12	16.29	22.89	16.36	5.57	2.70
Lta4h	17.26	16.97	14.48	6.70	4.88	22.93	22.14	19.99	8.37	6.39
Scd2	23.18	14.89	6.71	2.56	2.67	41.26	26.68	12.06	2.86	4.25
Eif4b	16.00	15.56	13.72	10.74	9.63	15.76	15.38	13.94	10.89	8.67
Ppbp	14.16	16.78	16.86	12.89	5.95	11.76	16.25	14.77	9.88	6.21
Tm6sf1	16.66	17.03	13.01	5.24	2.72	20.55	21.36	16.34	6.71	3.88
Fh1	15.14	15.29	13.01	6.41	6.93	17.11	17.18	15.13	9.02	6.89
Pygl	13.11	13.30	12.99	5.44	4.38	18.02	19.01	19.13	9.62	5.51
Lrmp	15.19	17.40	13.09	7.55	7.10	14.49	17.44	12.88	6.12	5.66
Cdc42se2	14.39	15.55	11.09	6.62	9.19	12.72	14.46	11.63	7.52	8.91
Acox3	17.08	13.70	8.61	5.08	9.70	13.56	14.17	8.88	6.53	8.63
Ivd	14.01	15.34	13.94	8.04	7.26	10.95	11.78	9.12	7.02	5.96
Nudcd2	11.25	11.65	10.73	6.86	3.51	16.37	14.67	14.15	8.04	5.06
Elovl5	13.32	14.72	11.86	4.23	5.92	11.75	16.39	11.83	4.63	4.99
Naga	16.13	16.77	12.04	7.49	6.14	10.13	10.59	8.70	6.73	4.48
Gnpda1	16.71	15.33	11.20	4.78	7.01	13.10	12.95	7.27	5.44	4.61
Mink1	15.48	14.52	9.63	6.52	10.07	11.62	10.96	6.99	5.02	6.71
Prkar2a	15.66	14.12	9.77	3.39	4.66	15.54	14.13	9.71	3.09	3.55
Sh3pxd2b	11.19	12.31	5.95	3.83	8.01	12.70	15.67	7.88	5.93	9.42
Irak1	12.02	12.77	9.98	7.95	7.77	10.01	9.73	8.75	7.56	5.32
Aldoc	9.79	12.27	11.35	7.42	3.95	10.48	11.00	10.72	10.39	4.29

8.2.3. IRF5 dependency of genes in clusters – DESeq2 results

Cluster 1

Gene_Name	FDR_0hr	baseMean_0hr	log2FC_0hr	FDR_1hr	baseMean_1hr	log2FC_1hr	FDR_2hr	baseMean_2hr	log2FC_2hr	FDR_4hr	baseMean_4hr	log2FC_4hr	FDR_8hr	baseMean_8hr	log2FC_8hr
Ccl17	2.25E-06	72848.94	0.70	4.59E-03	72848.94	0.45	3.25E-01	72848.94	0.19	4.77E-04	72848.94	0.55	5.25E-05	72848.94	0.60
Il1b	1.26E-04	55202.55	1.15	5.80E-04	55202.55	1.02	4.94E-06	55202.55	1.30	3.39E-09	55202.55	1.63	9.39E-14	55202.55	1.97
Anxa1	2.85E-01	49311.04	0.32	2.90E-02	49311.04	0.58	9.29E-02	49311.04	0.49	4.55E-01	49311.04	0.33	1.59E-03	49311.04	0.79
Acod1	1.15E-17	46044.10	1.46	1.02E-12	46044.10	1.22	5.24E-12	46044.10	1.19	1.57E-16	46044.10	1.39	6.17E-17	46044.10	1.40
Il12b	7.23E-01	42866.91	-0.11	1.13E-01	42866.91	0.37	1.87E-04	42866.91	0.81	4.21E-04	42866.91	0.78	2.05E-15	42866.91	1.53
Anxa2	1.18E-01	39200.17	0.32	7.81E-02	39200.17	0.33	8.39E-01	39200.17	0.05	9.64E-01	39200.17	-0.03	3.43E-01	39200.17	0.20
Helz2	1.64E-16	33335.29	-1.61	7.76E-08	33335.29	-1.10	2.85E-02	33335.29	-0.53	5.60E-01	33335.29	-0.25	5.29E-02	33335.29	-0.46
Slfn2	2.46E-01	31853.45	0.34	6.74E-04	31853.45	0.83	1.77E-01	31853.45	0.40	7.65E-01	31853.45	0.19	7.12E-03	31853.45	0.67
Ccl5	1.93E-01	30197.93	-0.47	3.25E-02	30197.93	-0.70	5.32E-01	30197.93	-0.26	9.94E-01	30197.93	-0.01	8.52E-01	30197.93	0.08
Gbp2	1.39E-01	28074.47	0.88	1.19E-01	28074.47	0.87	1.38E-01	28074.47	0.91	5.30E-01	28074.47	0.62	6.57E-02	28074.47	1.03
Hspa5	2.26E-02	25005.94	0.48	2.11E-02	25005.94	0.46	6.30E-02	25005.94	0.41	3.63E-01	25005.94	0.28	3.30E-05	25005.94	0.76
Ccl3	1.85E-02	24410.61	0.63	5.90E-03	24410.61	0.70	4.82E-03	24410.61	0.73	6.22E-07	24410.61	1.16	1.66E-09	24410.61	1.35
Il1a	3.98E-04	24295.82	1.16	5.68E-08	24295.82	1.62	2.17E-06	24295.82	1.44	1.03E-07	24295.82	1.59	1.52E-10	24295.82	1.85
Rsad2	7.19E-01	23400.18	-0.15	2.89E-01	23400.18	-0.33	4.30E-01	23400.18	0.28	8.08E-02	23400.18	0.60	3.71E-07	23400.18	1.30
Tnf	6.29E-01	23127.25	-0.12	8.85E-01	23127.25	0.03	1.34E-01	23127.25	0.32	1.58E-08	23127.25	0.93	2.12E-03	23127.25	0.55
Cd40	7.27E-14	21808.92	-0.98	9.93E-06	21808.92	-0.57	8.66E-04	21808.92	-0.45	7.76E-01	21808.92	0.10	3.05E-01	21808.92	0.16
Rnf19b	2.87E-01	21119.32	-0.14	1.18E-02	21119.32	-0.29	2.13E-05	21119.32	-0.46	3.86E-01	21119.32	-0.16	7.60E-01	21119.32	0.04
Msn	4.28E-01	21097.54	-0.17	5.87E-01	21097.54	-0.11	9.06E-01	21097.54	-0.03	9.89E-01	21097.54	0.01	6.46E-01	21097.54	-0.10
Ifih1	8.68E-01	19164.89	-0.05	3.65E-03	19164.89	0.64	8.74E-02	19164.89	0.43	7.22E-01	19164.89	0.19	1.53E-02	19164.89	0.55
Tagln2	6.21E-01	19085.13	-0.12	9.04E-02	19085.13	-0.33	1.26E-01	19085.13	-0.33	6.79E-01	19085.13	-0.17	2.63E-01	19085.13	-0.23
Plek	3.02E-01	18820.88	-0.27	8.36E-04	18820.88	0.73	1.45E-02	18820.88	0.58	7.53E-02	18820.88	0.48	1.45E-02	18820.88	0.56
Il6	9.04E-02	18414.78	-0.71	4.24E-02	18414.78	0.73	4.64E-04	18414.78	1.19	1.19E-03	18414.78	1.13	2.88E-08	18414.78	1.73
Ifit2	8.05E-01	18101.27	0.12	6.35E-02	18101.27	-0.64	9.54E-01	18101.27	-0.03	7.48E-01	18101.27	0.27	1.04E-02	18101.27	0.86
Gbp5	9.17E-03	17982.48	-0.51	6.18E-02	17982.48	0.36	2.01E-02	17982.48	0.46	8.07E-01	17982.48	0.12	6.62E-02	17982.48	0.36
Isg15	3.72E-02	17723.74	-0.55	9.90E-03	17723.74	-0.54	3.12E-02	17723.74	-0.48	9.77E-01	17723.74	-0.03	7.33E-01	17723.74	0.09
Nfkb1	6.29E-05	17454.63	-0.36	1.34E-01	17454.63	-0.15	8.47E-01	17454.63	-0.03	3.16E-01	17454.63	0.14	9.71E-01	17454.63	0.00
Tnfaip3	5.75E-01	17406.64	0.10	8.25E-01	17406.64	-0.04	6.80E-01	17406.64	0.07	2.05E-01	17406.64	0.24	1.27E-01	17406.64	0.22
Serpinb9	9.84E-01	16543.50	-0.01	6.40E-01	16543.50	-0.13	4.50E-01	16543.50	-0.21	3.28E-01	16543.50	-0.34	2.27E-01	16543.50	0.30
Ifit1	7.54E-01	16521.69	-0.14	3.63E-01	16521.69	-0.31	9.05E-01	16521.69	0.05	6.35E-01	16521.69	0.30	1.27E-02	16521.69	0.76
Tnfaip2	2.82E-01	16197.06	0.23	3.74E-01	16197.06	-0.18	7.73E-01	16197.06	-0.07	8.84E-01	16197.06	0.08	8.72E-01	16197.06	-0.04
Ccl4	7.90E-02	15741.03	0.33	8.52E-01	15741.03	-0.04	1.34E-02	15741.03	0.44	1.16E-05	15741.03	0.70	1.66E-08	15741.03	0.86
Calm1	4.79E-01	15457.01	0.20	6.12E-01	15457.01	0.14	9.79E-01	15457.01	0.01	7.20E-01	15457.01	-0.20	5.12E-01	15457.01	0.18
Plk2	4.60E-01	15103.53	-0.20	9.09E-02	15103.53	0.38	6.81E-01	15103.53	0.12	3.81E-01	15103.53	0.31	1.15E-02	15103.53	0.56
Ptx3	1.53E-39	14656.56	1.59	2.51E-41	14656.56	1.55	3.19E-51	14656.56	1.72	5.91E-80	14656.56	2.16	3.83E-119	14656.56	2.63
Il1rn	1.63E-01	14541.88	0.37	5.37E-05	14541.88	0.89	2.48E-04	14541.88	0.83	3.13E-05	14541.88	0.93	5.19E-08	14541.88	1.15
Srgn	2.40E-03	14507.14	-0.85	4.27E-04	14507.14	-0.94	3.01E-02	14507.14	-0.64	3.81E-01	14507.14	-0.39	1.56E-01	14507.14	-0.42
Apol7c	2.88E-03	14205.95	-0.45	6.60E-01	14205.95	-0.08	3.03E-03	14205.95	-0.43	4.24E-08	14205.95	-0.72	2.47E-03	14205.95	-0.43
Brd2	5.39E-02	14103.11	0.22	8.54E-05	14103.11	0.38	3.71E-01	14103.11	0.11	3.53E-01	14103.11	0.15	4.56E-03	14103.11	0.29
Mmp13	3.46E-01	13279.67	-0.30	3.50E-01	13279.67	0.28	2.78E-03	13279.67	0.81	8.65E-05	13279.67	1.02	4.20E-07	13279.67	1.23
Nfkbia	2.93E-01	13189.11	-0.37	4.05E-02	13189.11	-0.64	2.50E-01	13189.11	-0.41	9.69E-01	13189.11	-0.05	7.12E-01	13189.11	-0.14
Oasl1	2.64E-05	13119.40	-1.08	1.40E-04	13119.40	-0.77	1.48E-02	13119.40	-0.54	4.98E-01	13119.40	0.26	8.52E-01	13119.40	0.05
Ehd1	1.06E-01	13103.88	-0.42	2.93E-02	13103.88	-0.52	6.96E-02	13103.88	-0.47	9.53E-01	13103.88	0.06	6.17E-01	13103.88	-0.14
Clic4	7.58E-01	12696.73	0.10	6.17E-01	12696.73	0.15	6.35E-01	12696.73	0.16	9.68E-01	12696.73	0.04	1.76E-01	12696.73	0.37
Psma6	1.70E-01	12547.00	0.40	5.78E-01	12547.00	0.17	9.37E-01	12547.00	-0.03	9.31E-01	12547.00	-0.08	2.97E-02	12547.00	0.58
Cxcl10	7.21E-01	12225.05	-0.15	5.96E-01	12225.05	-0.10	3.54E-02	12225.05	0.37	2.16E-09	12225.05	0.87	9.60E-15	12225.05	1.09
Slc7a2	8.56E-03	12113.31	0.74	1.53E-04	12113.31	0.98	5.93E-04	12113.31	0.91	7.83E-05	12113.31	1.03	1.15E-08	12113.31	1.38
Cd274	3.40E-01	11247.27	-0.29	8.61E-01	11247.27	0.06	7.29E-01	11247.27	0.12	9.85E-01	11247.27	0.02	5.90E-01	11247.27	0.17
Malt1	9.55E-01	11219.00	0.02	6.38E-02	11219.00	0.44	1.18E-01	11219.00	0.41	3.18E-01	11219.00	0.35	2.83E-03	11219.00	0.67
Ccl2	3.10E-01	11187.12	-0.24	6.01E-01	11187.12	-0.12	3.81E-01	11187.12	-0.22	9.07E-01	11187.12	0.08	9.65E-03	11187.12	0.52
Hcls1	1.23E-01	11066.40	0.21	5.02E-02	11066.40	0.25	6.33E-01	11066.40	0.08	6.83E-01	11066.40	0.11	9.06E-01	11066.40	0.02

Cluster 2

Gene_Name	FDR_0hr	baseMean_0hr	log2FC_0hr	FDR_1hr	baseMean_1hr	log2FC_1hr	FDR_2hr	baseMean_2hr	log2FC_2hr	FDR_4hr	baseMean_4hr	log2FC_4hr	FDR_8hr	baseMean_8hr	log2FC_8hr
Ccl22	3.75E-01	87986.11	-0.24	9.58E-01	87986.11	-0.02	8.75E-01	87986.11	-0.05	7.72E-01	87986.11	-0.17	4.12E-01	87986.11	0.21
B2m	8.10E-01	52992.00	0.04	7.61E-01	52992.00	-0.05	8.47E-01	52992.00	0.04	7.01E-01	52992.00	-0.12	3.65E-02	52992.00	0.29
Samhd1	4.04E-02	37384.87	0.41	4.99E-02	37384.87	0.37	1.04E-01	37384.87	0.34	8.45E-01	37384.87	0.10	3.84E-03	37384.87	0.53
Rnf213	4.50E-01	32149.31	-0.24	6.29E-01	32149.31	-0.15	5.69E-01	32149.31	0.19	8.26E-01	32149.31	-0.16	7.51E-01	32149.31	0.11
Mx1	1.85E-01	28726.33	0.41	1.56E-01	28726.33	0.41	1.03E-01	28726.33	0.50	3.79E-01	28726.33	0.38	1.08E-02	28726.33	0.70
Pfkp	9.08E-01	27781.25	-0.01	3.46E-01	27781.25	0.09	5.80E-01	27781.25	0.06	5.15E-02	27781.25	0.20	6.74E-01	27781.25	0.04
Parp14	8.86E-01	23875.09	-0.05	5.62E-01	23875.09	0.18	2.52E-01	23875.09	0.36	9.81E-01	23875.09	-0.03	2.69E-01	23875.09	0.32
Actn1	7.40E-01	20649.60	0.08	6.85E-01	20649.60	0.08	8.17E-01	20649.60	-0.06	9.60E-01	20649.60	-0.04	4.72E-01	20649.60	-0.14
Wnk1	2.45E-02	16200.79	-0.73	3.29E-02	16200.79	-0.67	6.01E-02	16200.79	-0.63	1.43E-02	16200.79	-0.81	1.43E-01	16200.79	-0.48
Sifn5	8.58E-02	15957.94	-0.55	8.41E-01	15957.94	-0.07	2.61E-01	15957.94	0.39	9.90E-01	15957.94	-0.01	5.74E-01	15957.94	0.19
Znfx1	1.66E-01	14502.86	-0.21	7.28E-02	14502.86	-0.25	5.26E-01	14502.86	0.11	8.22E-01	14502.86	0.08	7.51E-01	14502.86	0.05
Pnp	9.11E-01	10642.49	0.03	1.18E-02	10642.49	0.42	9.46E-04	10642.49	0.54	1.15E-02	10642.49	0.45	1.13E-03	10642.49	0.52
Ifi47	9.15E-01	10494.92	-0.04	9.04E-01	10494.92	-0.04	4.80E-01	10494.92	0.20	8.68E-01	10494.92	-0.11	6.87E-02	10494.92	0.43
Usp18	1.09E-11	10235.73	-1.09	1.01E-14	10235.73	-1.22	2.70E-02	10235.73	-0.39	3.66E-01	10235.73	-0.24	4.57E-01	10235.73	0.14
Cd86	7.50E-02	10031.11	-0.49	2.41E-01	10031.11	-0.31	1.06E-01	10031.11	-0.46	1.38E-02	10031.11	-0.67	6.64E-01	10031.11	-0.13
Samd9l	6.94E-01	9934.37	0.14	4.70E-01	9934.37	0.23	4.50E-01	9934.37	0.26	9.43E-01	9934.37	-0.08	1.18E-01	9934.37	0.46
Irgm1	7.07E-01	9802.34	0.13	7.42E-01	9802.34	0.11	5.64E-01	9802.34	0.20	9.49E-01	9802.34	0.07	1.07E-01	9802.34	0.46
Gbp3	5.45E-03	9557.86	0.66	6.86E-03	9557.86	0.63	1.00E-05	9557.86	0.95	1.97E-03	9557.86	0.72	3.28E-07	9557.86	1.05
H2afy	8.26E-02	9505.93	-0.27	8.18E-02	9505.93	-0.25	6.62E-03	9505.93	-0.39	6.36E-01	9505.93	-0.14	3.50E-01	9505.93	-0.15
Vwa5a	2.67E-01	9365.51	-0.32	9.50E-01	9365.51	-0.02	9.80E-01	9365.51	0.01	5.15E-01	9365.51	-0.30	8.94E-01	9365.51	-0.04
Anxa7	5.19E-01	9301.96	0.09	8.22E-01	9301.96	0.03	7.53E-01	9301.96	-0.05	4.53E-01	9301.96	-0.15	5.69E-02	9301.96	0.23
Parp9	8.86E-01	9265.67	0.05	8.00E-01	9265.67	0.08	1.48E-01	9265.67	0.40	9.45E-01	9265.67	0.06	7.80E-02	9265.67	0.44
Ifi204	8.82E-01	9231.84	-0.06	2.14E-01	9231.84	0.36	4.12E-02	9231.84	0.59	9.13E-01	9231.84	0.10	3.28E-03	9231.84	0.76
Ly75	9.64E-02	8927.37	-0.44	7.16E-01	8927.37	-0.10	7.47E-01	8927.37	0.10	9.00E-01	8927.37	0.10	1.36E-01	8927.37	0.38
Lgals9	8.80E-02	8197.92	0.44	7.86E-03	8197.92	0.63	6.29E-02	8197.92	0.48	7.13E-01	8197.92	0.20	8.11E-02	8197.92	0.43
Usp25	9.77E-01	8196.44	0.01	6.29E-01	8196.44	0.11	2.83E-01	8196.44	0.26	8.79E-01	8196.44	-0.09	1.26E-01	8196.44	0.33
Oasl2	3.15E-01	8160.30	-0.23	3.10E-01	8160.30	-0.22	7.15E-02	8160.30	0.38	6.93E-01	8160.30	0.17	1.08E-01	8160.30	0.32
Nub1	3.71E-01	8101.40	-0.17	5.54E-01	8101.40	-0.11	6.30E-01	8101.40	-0.10	5.39E-01	8101.40	-0.19	8.94E-01	8101.40	-0.03
Ubr4	4.82E-03	8043.81	-0.44	2.60E-02	8043.81	-0.35	2.69E-01	8043.81	-0.20	1.02E-01	8043.81	-0.31	7.27E-02	8043.81	-0.29
Trafd1	1.04E-01	7883.96	-0.39	5.29E-02	7883.96	-0.43	5.14E-01	7883.96	-0.18	8.53E-01	7883.96	-0.11	2.42E-01	7883.96	-0.27
Psme2b	2.76E-01	7868.68	-0.19	3.49E-01	7868.68	-0.15	1.44E-01	7868.68	-0.25	6.51E-01	7868.68	-0.14	2.63E-01	7868.68	0.18
Stat2	3.44E-03	7820.40	-0.51	9.50E-01	7820.40	-0.01	3.92E-01	7820.40	0.18	9.90E-01	7820.40	0.01	9.83E-01	7820.40	-0.01
Herc6	9.62E-01	7527.85	0.01	4.91E-01	7527.85	0.16	9.75E-02	7527.85	0.39	8.75E-01	7527.85	0.10	6.47E-03	7527.85	0.56
Fgl2	3.09E-02	7522.05	-0.57	3.34E-05	7522.05	-0.95	6.84E-03	7522.05	-0.67	1.53E-01	7522.05	-0.45	3.25E-01	7522.05	0.27
Ifit1bl1	7.67E-01	7481.39	-0.13	4.61E-01	7481.39	-0.26	2.69E-03	7481.39	-0.85	2.99E-04	7481.39	-0.99	7.94E-01	7481.39	0.09
Cct3	6.86E-02	7316.46	0.36	2.73E-03	7316.46	0.53	3.78E-01	7316.46	0.19	9.65E-01	7316.46	-0.03	1.92E-02	7316.46	0.43
Slamf7	6.41E-01	7257.97	-0.15	9.11E-01	7257.97	0.04	6.59E-01	7257.97	0.14	9.72E-01	7257.97	-0.04	1.30E-01	7257.97	0.40
Ifi209	4.08E-01	7181.36	-0.29	9.88E-01	7181.36	0.01	1.74E-01	7181.36	0.45	9.72E-01	7181.36	0.04	3.21E-02	7181.36	0.63
Irf7	2.86E-02	7068.87	-0.87	4.36E-01	7068.87	-0.31	8.26E-01	7068.87	0.10	9.73E-01	7068.87	-0.05	6.65E-01	7068.87	-0.18
Sp100	9.01E-01	7037.55	-0.05	6.65E-01	7037.55	-0.14	3.32E-01	7037.55	0.31	9.63E-01	7037.55	-0.05	1.84E-01	7037.55	0.39
Alcam	8.52E-01	6905.52	-0.05	9.82E-01	6905.52	0.01	3.72E-01	6905.52	0.23	6.56E-01	6905.52	-0.20	9.88E-02	6905.52	0.36
Psme1	8.50E-01	6883.41	0.05	8.77E-01	6883.41	-0.03	9.88E-01	6883.41	0.00	7.01E-01	6883.41	-0.16	1.70E-01	6883.41	0.26
Tor1aip1	5.75E-01	6695.92	0.12	3.65E-01	6695.92	0.18	3.04E-01	6695.92	0.21	8.83E-01	6695.92	0.08	2.09E-01	6695.92	0.24
Inpp5b	9.01E-01	6694.37	0.03	5.07E-01	6694.37	0.12	5.83E-01	6694.37	0.11	8.64E-01	6694.37	-0.08	3.86E-01	6694.37	0.15
Ifitm3	9.36E-01	6576.81	-0.02	8.75E-01	6576.81	-0.04	2.24E-01	6576.81	0.25	3.59E-02	6576.81	0.41	1.13E-03	6576.81	0.54
Tap1	7.94E-05	6529.48	-0.95	3.89E-08	6529.48	-1.25	1.47E-01	6529.48	-0.42	8.75E-01	6529.48	-0.12	1.18E-01	6529.48	-0.42
Snx2	1.11E-02	6383.31	0.47	1.25E-02	6383.31	0.45	1.11E-02	6383.31	0.46	9.31E-01	6383.31	-0.06	1.13E-01	6383.31	0.30
Parp12	7.88E-01	6261.21	-0.06	3.53E-01	6261.21	-0.16	2.12E-01	6261.21	0.21	9.68E-01	6261.21	-0.02	5.40E-01	6261.21	0.10
Fndc3a	8.10E-01	5888.00	-0.09	8.11E-01	5888.00	0.08	4.27E-01	5888.00	0.26	8.57E-01	5888.00	-0.14	6.21E-01	5888.00	0.16
Ddx58	2.90E-01	5596.27	0.29	4.77E-01	5596.27	0.19	4.51E-02	5596.27	0.49	7.62E-01	5596.27	0.17	1.83E-02	5596.27	0.54

Cluster 3

Gene_Name	FDR_0hr	baseMean_0hr	log2FC_0hr	FDR_1hr	baseMean_1hr	log2FC_1hr	FDR_2hr	baseMean_2hr	log2FC_2hr	FDR_4hr	baseMean_4hr	log2FC_4hr	FDR_8hr	baseMean_8hr	log2FC_8hr
Fth1	1.64E-01	162853.24	0.21	3.75E-01	162853.24	0.13	2.15E-01	162853.24	0.20	4.66E-03	162853.24	0.40	4.16E-11	162853.24	0.78
mt-Nd1	5.56E-05	100731.86	0.81	1.24E-04	100731.86	0.77	6.97E-04	100731.86	0.70	3.75E-03	100731.86	0.63	1.77E-07	100731.86	0.99
Tmsb4x	7.31E-02	75400.79	0.35	1.17E-01	75400.79	0.29	4.33E-01	75400.79	0.18	7.16E-01	75400.79	0.15	9.82E-03	75400.79	0.47
Ctss	9.36E-04	60486.39	0.64	6.17E-05	60486.39	0.74	1.28E-03	60486.39	0.63	2.21E-04	60486.39	0.71	1.08E-06	60486.39	0.87
Lyz2	1.19E-30	50296.79	1.71	7.80E-33	50296.79	1.77	2.75E-34	50296.79	1.81	5.55E-27	50296.79	1.61	2.68E-30	50296.79	1.70
Akr1a1	9.95E-01	45487.31	0.00	9.45E-01	45487.31	0.01	9.22E-01	45487.31	-0.02	3.82E-01	45487.31	0.19	1.03E-04	45487.31	0.50
Prdx1	8.30E-02	35308.11	0.53	2.48E-02	35308.11	0.64	5.42E-02	35308.11	0.59	2.48E-01	35308.11	0.46	2.76E-08	35308.11	1.38
Ccl9	2.55E-03	34922.48	0.83	3.01E-04	34922.48	0.94	7.49E-03	34922.48	0.75	2.15E-02	34922.48	0.69	9.68E-07	34922.48	1.21
mt-Nd6	8.48E-03	31945.58	0.71	2.93E-02	31945.58	0.59	2.56E-02	31945.58	0.63	1.70E-01	31945.58	0.48	6.64E-05	31945.58	0.98
Ctsz	1.38E-04	25680.11	0.42	1.19E-03	25680.11	0.36	5.39E-03	25680.11	0.33	3.63E-06	25680.11	0.49	1.52E-03	25680.11	0.35
Pla2g7	3.55E-05	25379.80	1.05	1.03E-05	25379.80	1.10	7.85E-06	25379.80	1.12	3.13E-05	25379.80	1.06	1.61E-11	25379.80	1.58
H2-M2	1.72E-02	24652.02	0.83	5.15E-04	24652.02	1.12	5.26E-03	24652.02	0.94	5.45E-03	24652.02	0.96	2.43E-04	24652.02	1.16
C3	3.45E-25	21438.09	1.64	1.29E-27	21438.09	1.72	5.99E-26	21438.09	1.66	2.47E-19	21438.09	1.43	1.77E-20	21438.09	1.47
Mpeg1	3.79E-02	20439.36	0.64	4.88E-03	20439.36	0.79	2.93E-03	20439.36	0.85	2.80E-01	20439.36	0.45	6.60E-03	20439.36	0.77
AA467197	2.57E-04	19736.06	1.31	4.25E-04	19736.06	1.26	8.88E-04	19736.06	1.21	3.15E-03	19736.06	1.12	1.82E-07	19736.06	1.74
Ccr7	4.39E-03	18528.14	-0.51	4.82E-03	18528.14	-0.50	4.19E-02	18528.14	-0.39	2.12E-02	18528.14	-0.45	3.28E-01	18528.14	-0.19
Grn	3.51E-03	18361.22	0.44	8.70E-03	18361.22	0.39	2.13E-02	18361.22	0.36	2.98E-04	18361.22	0.52	1.07E-02	18361.22	0.38
Anxa5	2.28E-01	17953.48	0.23	6.89E-02	17953.48	0.31	3.06E-01	17953.48	0.20	9.51E-01	17953.48	0.04	5.49E-03	17953.48	0.45
Cd52	1.72E-02	17439.98	0.63	9.45E-04	17439.98	0.81	4.94E-02	17439.98	0.54	3.52E-01	17439.98	0.37	1.36E-04	17439.98	0.91
Anxa4	5.56E-02	17219.77	0.34	6.13E-03	17219.77	0.45	2.62E-02	17219.77	0.39	4.48E-01	17219.77	0.22	6.01E-02	17219.77	0.32
Axl	6.15E-01	16476.72	0.12	8.88E-01	16476.72	0.03	6.35E-01	16476.72	0.11	4.59E-01	16476.72	0.23	4.50E-01	16476.72	0.16
Fn1	7.16E-51	16004.54	3.12	1.00E-60	16004.54	3.40	2.91E-61	16004.54	3.42	1.41E-55	16004.54	3.25	6.55E-49	16004.54	3.06
Cybb	3.41E-03	15660.54	0.90	1.17E-04	15660.54	1.11	6.01E-04	15660.54	1.02	7.40E-02	15660.54	0.65	3.84E-03	15660.54	0.87
Alas1	1.91E-19	14558.83	0.87	1.47E-25	14558.83	1.00	1.22E-21	14558.83	0.92	9.09E-19	14558.83	0.86	2.68E-30	14558.83	1.09
Slc15a3	1.79E-02	14506.65	0.25	7.15E-02	14506.65	0.19	1.32E-01	14506.65	0.18	1.97E-10	14506.65	0.57	1.14E-20	14506.65	0.79
Itm2b	9.87E-04	13961.08	0.35	2.95E-02	13961.08	0.24	8.16E-03	13961.08	0.29	9.10E-01	13961.08	0.04	3.79E-02	13961.08	0.23
F10	1.29E-01	13491.47	0.23	1.59E-05	13491.47	0.54	2.59E-10	13491.47	0.75	4.18E-19	13491.47	1.01	2.38E-20	13491.47	1.04
Nfe2l2	3.83E-07	12855.22	0.94	3.66E-10	12855.22	1.12	2.56E-13	12855.22	1.29	2.12E-10	12855.22	1.14	1.09E-09	12855.22	1.09
Actr2	6.04E-01	11592.35	0.16	3.53E-01	11592.35	0.26	3.63E-01	11592.35	0.28	9.93E-01	11592.35	0.01	1.29E-01	11592.35	0.41
Stat1	4.64E-01	11540.60	-0.14	5.21E-01	11540.60	-0.12	2.85E-01	11540.60	0.21	9.61E-01	11540.60	0.03	1.87E-01	11540.60	0.23
Txn1	1.27E-01	11475.71	0.34	9.19E-01	11475.71	-0.03	8.87E-01	11475.71	0.04	9.92E-01	11475.71	0.01	2.26E-01	11475.71	0.26
Cxcl16	8.32E-01	11399.24	-0.04	7.40E-02	11399.24	-0.26	5.24E-02	11399.24	-0.30	1.30E-01	11399.24	0.28	8.11E-01	11399.24	0.04
Uba1	6.64E-02	11395.16	0.22	4.22E-05	11395.16	0.43	1.42E-02	11395.16	0.29	3.15E-03	11395.16	0.34	7.17E-05	11395.16	0.41
Lamp2	7.23E-02	10754.34	0.44	1.19E-02	10754.34	0.57	3.60E-02	10754.34	0.50	2.30E-01	10754.34	0.38	2.81E-06	10754.34	0.95
Cdc42	3.85E-01	9954.09	0.23	1.03E-01	9954.09	0.37	4.32E-01	9954.09	0.21	9.17E-01	9954.09	0.08	5.25E-02	9954.09	0.44
Lgals3bp	6.94E-01	9770.51	-0.08	5.30E-01	9770.51	-0.11	2.32E-01	9770.51	0.21	6.80E-01	9770.51	0.13	3.39E-01	9770.51	0.16
Esd	1.65E-01	9742.94	0.46	5.50E-02	9742.94	0.58	1.13E-01	9742.94	0.53	5.04E-01	9742.94	0.35	1.87E-04	9742.94	1.03
Actr3	7.93E-02	9425.64	0.44	5.82E-02	9425.64	0.44	1.22E-01	9425.64	0.40	4.58E-01	9425.64	0.29	1.41E-02	9425.64	0.56
Capza2	2.48E-01	8997.08	0.42	1.94E-01	8997.08	0.43	2.81E-01	8997.08	0.40	9.60E-01	8997.08	0.07	2.71E-02	8997.08	0.72
Ctsc	1.67E-01	8983.73	0.42	2.61E-02	8983.73	0.62	4.93E-02	8983.73	0.59	4.62E-01	8983.73	0.35	4.40E-02	8983.73	0.57
Psmb8	3.19E-02	8512.78	-0.31	7.18E-03	8512.78	-0.37	2.23E-03	8512.78	-0.42	8.95E-01	8512.78	-0.06	9.38E-02	8512.78	-0.24
Mmp14	1.22E-18	8208.01	1.06	1.20E-15	8208.01	0.97	8.16E-16	8208.01	0.97	2.06E-25	8208.01	1.22	1.10E-20	8208.01	1.10
Acsl1	3.62E-05	7974.98	1.02	2.64E-14	7974.98	1.70	9.65E-14	7974.98	1.66	1.18E-12	7974.98	1.60	3.63E-16	7974.98	1.79
Npc2	4.68E-01	7683.98	-0.18	2.01E-01	7683.98	-0.28	6.33E-01	7683.98	-0.13	8.53E-01	7683.98	0.11	9.28E-01	7683.98	-0.03
Sh3glb1	6.13E-01	7591.58	0.17	4.79E-01	7591.58	0.22	5.92E-01	7591.58	0.19	9.95E-01	7591.58	0.01	6.77E-02	7591.58	0.52
Fcer1g	1.67E-04	7581.88	0.49	4.50E-06	7581.88	0.57	6.81E-04	7581.88	0.45	9.89E-03	7581.88	0.37	7.94E-14	7581.88	0.86
Sdcbp	2.70E-01	7392.58	0.29	2.01E-02	7392.58	0.54	4.60E-02	7392.58	0.50	2.67E-01	7392.58	0.37	1.64E-03	7392.58	0.70
Ywhae	2.08E-01	7386.16	0.23	5.24E-02	7386.16	0.32	2.09E-01	7386.16	0.24	8.62E-01	7386.16	0.08	1.76E-03	7386.16	0.49
Tlr2	7.45E-06	7004.73	1.23	3.36E-05	7004.73	1.14	3.06E-02	7004.73	0.68	2.69E-01	7004.73	0.47	3.00E-02	7004.73	0.66
Psmd8	1.06E-01	6981.93	0.31	8.50E-04	6981.93	0.57	1.44E-01	6981.93	0.30	4.21E-01	6981.93	0.24	2.10E-05	6981.93	0.69

Cluster 4

Gene_Name	FDR_0hr	baseMean_0hr	log2FC_0hr	FDR_1hr	baseMean_1hr	log2FC_1hr	FDR_2hr	baseMean_2hr	log2FC_2hr	FDR_4hr	baseMean_4hr	log2FC_4hr	FDR_8hr	baseMean_8hr	log2FC_8hr
Eef2	2.69E-02	19150.19	-0.75	1.81E-02	19150.19	-0.76	1.83E-01	19150.19	-0.50	8.43E-01	19150.19	-0.18	7.78E-02	19150.19	-0.59
Hmox1	1.05E-95	15559.80	-3.37	3.54E-97	15559.80	-3.40	7.77E-96	15559.80	-3.39	3.11E-70	15559.80	-2.91	6.11E-36	15559.80	-2.08
Irf5	3.21E-05	11088.93	-1.55	2.22E-06	11088.93	-1.72	1.43E-06	11088.93	-1.75	9.54E-03	11088.93	-1.09	1.99E-03	11088.93	-1.19
Mfge8	2.99E-07	8415.12	-1.24	1.15E-07	8415.12	-1.27	8.33E-06	8415.12	-1.10	8.08E-03	8415.12	-0.75	2.82E-03	8415.12	-0.78
Napsa	3.66E-05	7816.05	-0.70	1.30E-08	7816.05	-0.92	1.31E-06	7816.05	-0.80	2.98E-04	7816.05	-0.64	4.31E-06	7816.05	-0.75
Coro1a	1.10E-01	6985.73	-0.66	1.85E-02	6985.73	-0.88	1.40E-01	6985.73	-0.63	6.79E-01	6985.73	-0.34	6.28E-02	6985.73	-0.72
Rplp0	2.22E-02	6078.89	-1.23	4.66E-03	6078.89	-1.42	4.12E-02	6078.89	-1.12	6.40E-01	6078.89	-0.50	9.23E-03	6078.89	-1.33
H2-DMa	7.08E-01	6023.21	-0.15	5.63E-01	6023.21	-0.20	5.61E-01	6023.21	-0.23	9.73E-01	6023.21	0.05	3.74E-01	6023.21	-0.31
Cotl1	3.39E-01	5299.51	-0.42	1.15E-01	5299.51	-0.62	4.09E-01	5299.51	-0.38	9.02E-01	5299.51	0.15	2.19E-01	5299.51	-0.51
Emilin2	1.12E-22	3489.38	-1.79	8.03E-23	3489.38	-1.80	3.06E-18	3489.38	-1.62	4.07E-08	3489.38	-1.09	2.22E-26	3489.38	-2.03
Cat	1.83E-06	3369.61	-0.59	1.64E-04	3369.61	-0.48	5.63E-04	3369.61	-0.46	6.41E-04	3369.61	-0.47	9.05E-03	3369.61	-0.36
Wdfy4	7.81E-15	3352.75	-1.04	2.98E-13	3352.75	-0.98	6.62E-09	3352.75	-0.81	5.26E-04	3352.75	-0.55	2.16E-06	3352.75	-0.70
Arhgap45	1.13E-02	3050.78	-1.12	1.03E-03	3050.78	-1.35	2.52E-02	3050.78	-1.02	2.03E-01	3050.78	-0.74	1.24E-03	3050.78	-1.33
Srebf2	5.63E-02	2531.30	-0.67	6.08E-03	2531.30	-0.89	7.03E-02	2531.30	-0.65	6.84E-01	2531.30	-0.30	1.81E-02	2531.30	-0.78
Adam23	1.00E-03	2419.36	-0.63	1.04E-02	2419.36	-0.50	1.29E-03	2419.36	-0.61	8.81E-07	2419.36	-0.89	1.12E-07	2419.36	-0.95
Ezr	4.51E-04	2401.95	-0.82	4.59E-05	2401.95	-0.91	1.06E-02	2401.95	-0.63	1.23E-01	2401.95	-0.47	3.95E-04	2401.95	-0.82
Mbnl1	1.43E-03	2382.88	-0.85	2.42E-02	2382.88	-0.61	1.06E-01	2382.88	-0.49	6.60E-01	2382.88	-0.26	2.39E-04	2382.88	-0.94
Pik3cg	4.39E-03	2262.05	-0.64	4.22E-02	2262.05	-0.46	8.41E-02	2262.05	-0.44	6.01E-04	2262.05	-0.77	6.12E-07	2262.05	-1.01
Hspa8	1.10E-36	2209.53	-1.42	2.65E-55	2209.53	-1.74	1.72E-56	2209.53	-1.79	7.37E-53	2209.53	-1.80	3.19E-43	2209.53	-1.54
Zmiz2	3.41E-03	1988.28	-1.08	6.60E-05	1988.28	-1.37	2.23E-03	1988.28	-1.11	3.19E-01	1988.28	-0.55	1.72E-03	1988.28	-1.11
Rogdi	4.06E-02	1951.08	-0.76	6.88E-03	1951.08	-0.93	1.50E-02	1951.08	-0.88	2.31E-01	1951.08	-0.58	3.83E-02	1951.08	-0.74
Aldh2	1.81E-01	1881.29	-0.55	1.08E-01	1881.29	-0.62	4.72E-01	1881.29	-0.33	9.95E-01	1881.29	0.01	7.42E-01	1881.29	-0.15
Mical1	1.15E-01	1654.86	-0.47	4.44E-03	1654.86	-0.76	2.26E-02	1654.86	-0.66	3.71E-01	1654.86	-0.39	2.54E-03	1654.86	-0.80
Inf2	7.47E-02	1621.01	-0.79	1.68E-02	1621.01	-0.98	6.31E-02	1621.01	-0.83	2.64E-01	1621.01	-0.66	1.26E-02	1621.01	-1.03
Vrk1	4.45E-07	1559.97	-0.91	1.21E-06	1559.97	-0.88	8.40E-04	1559.97	-0.66	4.46E-01	1559.97	-0.26	9.20E-01	1559.97	0.03
Rps6ka1	1.31E-01	1456.36	-0.44	1.40E-01	1456.36	-0.40	2.89E-01	1456.36	-0.33	5.23E-01	1456.36	-0.31	1.15E-01	1456.36	-0.44
Adam15	4.01E-01	1354.80	-0.42	2.01E-01	1354.80	-0.57	6.07E-01	1354.80	-0.28	9.22E-01	1354.80	0.15	5.72E-01	1354.80	-0.28
Slc40a1	4.91E-100	1339.00	-4.80	3.03E-80	1339.00	-4.43	6.98E-55	1339.00	-3.53	4.11E-26	1339.00	-2.48	5.10E-22	1339.00	-2.41
Pip5k1c	4.25E-02	1324.08	-0.71	1.46E-02	1324.08	-0.80	1.80E-01	1324.08	-0.51	9.40E-01	1324.08	0.09	6.35E-02	1324.08	-0.64
Asl	2.00E-02	1247.91	-0.54	3.01E-03	1247.91	-0.65	1.71E-02	1247.91	-0.56	8.13E-01	1247.91	-0.14	2.09E-02	1247.91	-0.53
Cux1	2.36E-20	1160.96	-0.94	3.60E-13	1160.96	-0.76	7.91E-09	1160.96	-0.63	4.24E-08	1160.96	-0.61	1.30E-04	1160.96	-0.46
Aes	3.47E-01	1131.04	-0.26	1.29E-01	1131.04	-0.37	1.17E-01	1131.04	-0.42	9.57E-01	1131.04	0.05	1.95E-01	1131.04	-0.33
Fasn	1.18E-01	1130.07	-0.73	6.03E-02	1130.07	-0.81	6.04E-01	1130.07	-0.28	5.80E-01	1130.07	-0.46	1.29E-02	1130.07	-1.08
Cpsf1	2.20E-01	1126.75	-0.38	2.60E-01	1126.75	-0.34	4.39E-01	1126.75	-0.27	9.82E-01	1126.75	0.03	1.95E-01	1126.75	-0.39
Uap1l1	3.49E-01	1123.32	-0.26	1.28E-01	1123.32	-0.38	4.37E-01	1123.32	-0.23	7.81E-01	1123.32	0.17	2.05E-01	1123.32	-0.34
Ilf3st	1.11E-01	1113.06	-0.37	6.12E-01	1113.06	-0.13	8.69E-01	1113.06	0.05	8.95E-02	1113.06	-0.46	8.44E-03	1113.06	-0.57
Nedd4	7.54E-08	1099.89	-1.14	2.38E-05	1099.89	-0.93	1.86E-06	1099.89	-1.05	6.22E-13	1099.89	-1.52	5.08E-17	1099.89	-1.73
Map3k14	8.34E-04	1098.53	-1.29	8.81E-05	1098.53	-1.47	2.27E-03	1098.53	-1.24	6.91E-03	1098.53	-1.12	3.87E-03	1098.53	-1.12
Mroh1	1.13E-01	1062.36	-0.61	1.49E-02	1062.36	-0.85	2.06E-01	1062.36	-0.52	9.42E-01	1062.36	0.10	2.53E-01	1062.36	-0.44
Rpl18	7.23E-02	1054.95	-0.71	4.48E-03	1054.95	-1.02	3.21E-03	1054.95	-1.07	8.05E-01	1054.95	-0.24	5.74E-03	1054.95	-0.99
Rptor	2.96E-02	1051.13	-0.60	7.41E-02	1051.13	-0.48	1.58E-01	1051.13	-0.42	6.24E-01	1051.13	-0.27	1.52E-01	1051.13	-0.40
Dok2	2.28E-01	1020.63	-0.82	1.19E-01	1020.63	-0.97	4.64E-01	1020.63	-0.55	9.99E-01	1020.63	0.00	3.01E-01	1020.63	-0.69
Tmem8	1.21E-03	999.20	-0.65	3.69E-05	999.20	-0.79	5.52E-06	999.20	-0.87	9.13E-03	999.20	-0.58	4.28E-04	999.20	-0.71
Rfx7	3.47E-01	999.16	-0.28	7.00E-01	999.16	-0.12	8.28E-01	999.16	0.08	5.07E-01	999.16	-0.31	1.63E-01	999.16	-0.38
Bcat2	3.22E-01	958.36	-0.32	2.68E-01	958.36	-0.34	3.77E-01	958.36	-0.30	9.26E-01	958.36	0.09	3.19E-01	958.36	-0.32
Ppp2r5d	3.17E-01	934.87	-0.19	7.58E-01	934.87	-0.06	1.21E-03	934.87	-0.55	4.78E-03	934.87	-0.51	1.78E-03	934.87	-0.53
Zfp36l1	1.70E-02	926.26	-1.06	4.31E-03	926.26	-1.20	8.29E-03	926.26	-1.19	1.48E-04	926.26	-1.57	3.87E-03	926.26	-1.21
Man2b2	9.63E-02	924.38	-0.66	4.82E-02	924.38	-0.73	3.85E-01	924.38	-0.38	9.60E-01	924.38	0.07	3.30E-01	924.38	-0.40
Pkd1	5.02E-02	911.78	-0.65	2.64E-02	911.78	-0.70	4.11E-02	911.78	-0.68	6.00E-01	911.78	-0.33	1.68E-02	911.78	-0.76
Slc25a39	2.25E-01	911.69	-0.56	5.10E-02	911.69	-0.82	1.94E-01	911.69	-0.62	9.92E-01	911.69	-0.02	2.03E-01	911.69	-0.57

Cluster 5

Gene_Name	FDR_0hr	baseMean_0hr	log2FC_0hr	FDR_1hr	baseMean_1hr	log2FC_1hr	FDR_2hr	baseMean_2hr	log2FC_2hr	FDR_4hr	baseMean_4hr	log2FC_4hr	FDR_8hr	baseMean_8hr	log2FC_8hr
Clec4n	5.13E-01	49839.04	-0.17	7.09E-01	49839.04	0.09	4.07E-01	49839.04	-0.22	1.53E-01	49839.04	-0.39	7.07E-01	49839.04	-0.10
Plet1	1.85E-02	20620.62	-0.37	8.67E-01	20620.62	0.03	5.07E-01	20620.62	0.13	1.85E-01	20620.62	0.27	6.34E-06	20620.62	-0.62
Mgl2	5.28E-05	11974.35	-0.47	1.61E-03	11974.35	-0.38	1.29E-06	11974.35	-0.54	9.23E-05	11974.35	-0.46	9.12E-02	11974.35	-0.23
Csf1r	7.98E-11	11759.27	0.59	6.66E-15	11759.27	0.69	1.46E-17	11759.27	0.75	8.96E-32	11759.27	1.02	8.70E-25	11759.27	0.90
Laptm5	5.78E-01	10784.99	-0.16	8.47E-01	10784.99	-0.06	8.70E-01	10784.99	-0.06	6.66E-01	10784.99	0.22	2.71E-01	10784.99	-0.29
Glipr1	3.81E-01	7880.79	0.26	7.74E-01	7880.79	0.09	9.57E-01	7880.79	-0.02	9.71E-01	7880.79	0.04	1.88E-01	7880.79	0.36
Naaa	6.67E-01	5352.62	-0.06	4.49E-01	5352.62	0.10	2.67E-01	5352.62	0.15	3.97E-02	5352.62	0.27	5.20E-02	5352.62	-0.24
Gusb	1.33E-02	5271.16	0.39	8.50E-04	5271.16	0.49	1.09E-02	5271.16	0.40	6.87E-09	5271.16	0.79	1.23E-03	5271.16	0.48
Gsn	3.99E-02	4397.31	-0.49	5.38E-03	4397.31	-0.61	4.05E-02	4397.31	-0.49	8.67E-01	4397.31	-0.11	7.34E-02	4397.31	-0.42
Colgalt1	7.94E-01	3765.16	0.07	3.85E-01	3765.16	0.19	4.84E-01	3765.16	0.18	2.21E-02	3765.16	0.51	9.83E-01	3765.16	0.01
Clec4a2	5.33E-03	3742.31	0.83	1.89E-03	3742.31	0.90	2.67E-02	3742.31	0.70	6.13E-01	3742.31	0.30	1.69E-01	3742.31	0.44
Mink1	4.03E-02	3488.77	-0.34	1.59E-02	3488.77	-0.37	1.82E-04	3488.77	-0.56	4.04E-01	3488.77	-0.22	4.56E-02	3488.77	-0.32
Il1r2	5.16E-05	3387.19	-0.95	1.32E-01	3387.19	-0.38	5.61E-03	3387.19	-0.68	3.09E-02	3387.19	-0.60	7.46E-01	3387.19	-0.10
Gclm	1.13E-02	3214.79	-0.52	6.32E-02	3214.79	-0.38	1.06E-02	3214.79	-0.52	3.99E-04	3214.79	-0.69	9.43E-01	3214.79	0.02
Prcp	4.64E-01	3107.78	0.16	1.00E-01	3107.78	0.32	1.68E-01	3107.78	0.30	6.79E-01	3107.78	0.17	6.35E-01	3107.78	0.11
Eif4b	3.14E-01	3102.22	-0.18	2.50E-01	3102.22	-0.19	8.02E-01	3102.22	-0.05	9.30E-01	3102.22	-0.05	4.58E-02	3102.22	-0.33
Alox5ap	1.97E-01	3038.91	0.25	4.46E-01	3038.91	0.15	5.74E-01	3038.91	0.13	1.01E-01	3038.91	0.36	1.26E-01	3038.91	0.30
Tbxas1	3.24E-09	2946.01	0.60	1.95E-12	2946.01	0.70	5.54E-06	2946.01	0.48	2.43E-13	2946.01	0.77	4.47E-13	2946.01	0.80
Plau	2.14E-02	2863.06	-0.34	1.48E-09	2863.06	0.76	9.24E-01	2863.06	0.02	7.67E-06	2863.06	-0.63	3.99E-16	2863.06	-1.03
Hsd17b4	2.89E-01	2730.05	-0.17	6.85E-01	2730.05	-0.07	3.01E-01	2730.05	-0.17	6.00E-01	2730.05	0.15	5.24E-01	2730.05	0.11
Mrc1	1.81E-07	2601.84	1.03	2.45E-11	2601.84	1.27	1.67E-08	2601.84	1.10	9.83E-05	2601.84	0.82	1.71E-02	2601.84	0.56
Ivns1abp	4.66E-02	2373.58	0.42	2.12E-02	2373.58	0.46	8.98E-02	2373.58	0.37	9.82E-01	2373.58	-0.02	3.45E-01	2373.58	0.21
Lta4h	6.49E-02	2356.37	0.31	2.78E-02	2356.37	0.35	9.29E-02	2356.37	0.30	9.93E-02	2356.37	0.33	4.27E-02	2356.37	0.35
Pygl	3.67E-01	2196.40	0.16	2.08E-01	2196.40	0.21	1.13E-01	2196.40	0.28	4.80E-06	2196.40	0.67	6.20E-02	2196.40	0.32
Naga	1.01E-01	2194.31	-0.48	5.88E-02	2194.31	-0.52	2.44E-01	2194.31	-0.37	8.55E-01	2194.31	-0.14	3.44E-01	2194.31	-0.29
Sept9	4.62E-01	2163.90	0.12	4.05E-01	2163.90	0.13	5.55E-01	2163.90	0.11	9.84E-01	2163.90	0.01	1.09E-02	2163.90	-0.37
Herpud1	6.26E-01	2053.62	-0.10	1.19E-02	2053.62	-0.41	6.49E-01	2053.62	-0.10	8.68E-01	2053.62	0.08	1.03E-01	2053.62	-0.29
Ap1b1	2.55E-02	1970.35	-0.39	6.08E-02	1970.35	-0.32	5.77E-02	1970.35	-0.35	8.17E-01	1970.35	-0.10	6.48E-03	1970.35	-0.45
Asgr2	1.82E-03	1919.81	-0.69	2.73E-03	1919.81	-0.66	4.25E-04	1919.81	-0.77	2.25E-01	1919.81	-0.38	2.91E-01	1919.81	-0.28
Atp8b4	8.36E-01	1897.60	0.06	4.05E-01	1897.60	0.21	8.40E-01	1897.60	0.06	1.12E-01	1897.60	-0.46	1.54E-04	1897.60	-0.84
Inpp5d	4.51E-02	1893.73	-0.25	5.26E-01	1893.73	-0.08	3.38E-02	1893.73	-0.29	7.60E-01	1893.73	-0.11	2.07E-01	1893.73	-0.17
Plcb2	9.31E-02	1878.67	0.27	4.87E-02	1878.67	0.30	1.80E-01	1878.67	0.23	8.91E-01	1878.67	0.07	4.63E-01	1878.67	0.14
Trio	8.50E-03	1851.11	-0.51	1.44E-01	1851.11	-0.29	1.15E-01	1851.11	-0.34	6.74E-01	1851.11	-0.18	4.05E-01	1851.11	-0.18
Vps13b	3.36E-01	1782.92	-0.31	7.15E-01	1782.92	0.12	7.80E-01	1782.92	0.11	9.16E-01	1782.92	-0.10	8.40E-01	1782.92	-0.07
Aldh9a1	4.51E-04	1654.72	-0.45	7.44E-06	1654.72	-0.55	6.81E-04	1654.72	-0.44	1.53E-01	1654.72	-0.26	3.79E-07	1654.72	-0.64
Fh1	1.98E-01	1651.75	0.22	1.27E-01	1651.75	0.25	1.08E-01	1651.75	0.28	7.88E-04	1651.75	0.54	4.07E-01	1651.75	-0.15
Sh3pxd2b	1.25E-01	1649.59	-0.48	2.14E-01	1649.59	-0.37	8.41E-01	1649.59	-0.08	7.82E-01	1649.59	0.21	1.48E-01	1649.59	-0.44
Arhgap9	6.46E-01	1629.70	-0.11	4.17E-01	1629.70	-0.17	4.33E-01	1629.70	-0.19	9.69E-01	1629.70	-0.03	6.65E-01	1629.70	-0.10
Fgr	5.69E-02	1619.81	0.32	1.63E-02	1619.81	0.38	7.42E-01	1619.81	0.07	7.32E-02	1619.81	0.34	5.82E-02	1619.81	0.35
Dapk1	4.93E-01	1602.96	-0.12	9.80E-01	1602.96	0.00	4.18E-01	1602.96	0.14	9.63E-01	1602.96	0.03	1.71E-02	1602.96	-0.36
Acat1	6.83E-01	1561.94	-0.12	8.02E-01	1561.94	-0.07	4.27E-01	1561.94	-0.22	8.45E-01	1561.94	-0.13	1.20E-01	1561.94	-0.39
Adcy7	3.69E-01	1525.55	-0.27	1.63E-01	1525.55	-0.37	9.01E-01	1525.55	-0.05	7.83E-01	1525.55	0.18	2.53E-01	1525.55	-0.32
Tm6sf1	6.92E-02	1515.60	0.32	4.14E-02	1515.60	0.34	7.20E-02	1515.60	0.33	2.86E-01	1515.60	0.27	4.83E-03	1515.60	0.50
Hipk1	8.71E-02	1507.28	-0.45	9.42E-01	1507.28	-0.02	3.09E-01	1507.28	0.30	2.49E-01	1507.28	0.40	6.12E-01	1507.28	0.15
Lrmp	4.92E-01	1487.07	-0.22	2.81E-01	1487.07	-0.31	6.14E-01	1487.07	-0.17	3.62E-01	1487.07	-0.39	1.42E-01	1487.07	-0.42
Prkcb	3.38E-01	1478.30	0.21	9.25E-03	1478.30	0.49	1.01E-03	1478.30	0.61	2.70E-02	1478.30	0.48	1.59E-01	1478.30	0.30
Dmxl2	1.44E-01	1470.23	0.45	1.81E-02	1470.23	0.66	2.11E-01	1470.23	0.41	9.60E-01	1470.23	0.06	8.45E-01	1470.23	-0.07
Dpp7	8.12E-01	1434.76	-0.07	9.54E-01	1434.76	0.02	5.01E-01	1434.76	-0.19	5.80E-01	1434.76	0.25	8.21E-01	1434.76	0.07
Acox3	9.92E-02	1376.75	-0.42	5.72E-01	1376.75	-0.15	9.96E-01	1376.75	0.00	5.88E-01	1376.75	0.25	3.27E-01	1376.75	-0.26
Kmt2c	3.14E-01	1335.24	-0.31	7.90E-01	1335.24	-0.09	8.66E-01	1335.24	-0.07	9.94E-01	1335.24	-0.01	5.78E-01	1335.24	-0.18

8.2.4. Number of differentially expressed genes (WT vs IRF5$^{-/-}$) in each cluster

	Time	***0hr***		***1hr***		***2hr***		***4hr***		***8hr***	
	IRF5_reg	***down***	***up***	***down***	***up***	***down***	***up***	***down***	***up***	***down***	***up***
Cluster	***1***	41	45	49	81	40	78	22	79	12	141
	2	35	8	46	12	10	26	9	8	6	51
	3	13	128	18	174	5	165	8	149	1	297
	4	253	0	343	0	190	1	97	0	221	0
	5	38	48	38	80	25	50	17	27	40	10

8.2.5. IRF5 regulated clusters - gene set enrichment results

Term	Overlap	Adjusted.P.value	Z.score	Combined.Score	Genes	Cluster
inflammatory response (GO:0006954)	29/209	4.66E-06	-4.197133464	79.67683301	CD40;CXCL9;FPR1;CXCL1;MEFV;CXCL3;TNF;CXCL2;PRDX5;CCL7;CCL5;CCR12;CCL4;BLNK;CCL3;NLRP3;TNFRSF8;CCL1;CCL17;ANXA1;CD180;NFKB2;IL1A;CXCL10;IL6;ADORA2A;IL1B;IL2RA;PTX3	1
cytokine activity (GO:0005125)	13/103	0.000895367	-3.592771335	44.25070485	IL1RN;CXCL9;IFNB1;LIF;INHBA;TNF;IL1A;IL6;IL1B;CCL4;IL12B;IL12A;TIMP1	1
chemokine activity (GO:0008009)	11/45	0.001618629	-3.032177528	33.44899903	CXCL10;CXCL9;CCL7;CCL5;CCL4;CCL3;CXCL1;CCL1;CXCL13;CXCL2;CCL17	1
positive regulation of NF-kappaB import into nucleus (GO:0042346)	5/14	0.006451034	-2.737188233	29.75207884	IL23A;IL1B;IL12B;TLR7;TNF	1
chemokine-mediated signaling pathway (GO:0070098)	11/48	0.006451034	-2.496082423	26.58768332	CXCL10;CXCL9;CCL7;CCL5;CCL4;CCL3;CXCL1;CCL1;CXCL13;CXCL2;CCL17	1
cellular response to organic cyclic compound (GO:0071407)	5/12	0.049919257	-3.855928246	30.62827627	TIPARP;IL1B;CCL5;CCL3;TNF	1
response to lipopolysaccharide (GO:0032496)	10/78	0.049919257	-2.679519548	21.20156796	CXCL9;CD40;SLPI;GCH1;LY96;TNFRSF8;CXCL1;IL12A;CXCL3;CXCL2	1
positive regulation of interferon-gamma production (GO:0032729)	6/27	0.049919257	-2.368726056	19.25577288	IL23A;IL1B;TNFSF4;IL12B;IL12A;CD14	1
growth factor activity (GO:0008083)	8/67	0.056937487	-3.384614546	22.47791501	IL6;JAG1;LIF;IL12B;IL12A;OSGIN2;INHBA;EREG	1
CCR1 chemokine receptor binding (GO:0031726)	4/5	0.056937487	-0.915701544	6.002131309	CCL7;CCL5;CCL4;CCL3	1
interleukin-12 receptor binding (GO:0005143)	2/5	0.056937487	-0.563358147	3.69263282	IL12B;IL12A	1
response to virus (GO:0009615)	11/100	0.083169401	-2.632986032	17.37173948	IFIH1;RSAD2;IFNB1;TNFSF4;CCL5;CCL4;IFI44;IL12A;IFIT1;TNF;IFIT2	1
positive regulation of inflammatory response (GO:0050729)	7/38	0.083169401	-2.390560359	16.24816816	NFKBIA;IL23A;TNFSF4;SERPINE1;CCL3;IL12B;TLR7	1
positive regulation of T cell proliferation (GO:0042102)	7/36	0.083169401	-2.226561224	15.59380485	IL6;ANXA1;IL23A;IL1B;TNFSF4;CCL5;IL12B	1
monocyte chemotaxis (GO:0002548)	8/38	0.083169401	-2.224799546	15.12152455	IL6;ANXA1;CCL7;CCL5;CCL4;CCL3;CCL1;CCL17	1
CXCR chemokine receptor binding (GO:0045236)	3/9	0.165434567	-2.474824417	13.13076853	CXCL1;CXCL3;CXCL2	1
single-stranded RNA binding (GO:0003727)	3/31	0.431692099	-3.261785806	9.527281454	IFIH1;TLR7;RBM7	1
N-formyl peptide receptor activity (GO:0004982)	1/5	0.431692099	0.821772746	-2.324970735	FPR1	1
thioredoxin peroxidase activity (GO:0008379)	1/5	0.431692099	1.009204564	-2.855255409	PRDX5	1
positive regulation of natural killer cell mediated cytotoxicity (GO:0045954)	5/13	0.899156248	-3.164736704	20.46869301	CADM1;CRTAM;CD226;SLAMF6;RASGRP1	3
neutrophil degranulation (GO:0043312)	28/479	0.899156248	-4.937942286	13.74450226	CSTB;ORM1;GMFG;HP;FPR2;CTSS;C3;SDCBP;PRDX4;FTH1;LAMP2;C3AR1;OLR1;CTSC;FCER1G;TMEM30A;ARG1;CYBB;RHOA;VAMP8;RAB10;BST1;VAPA;PSMA2;TARM1;ACPP;GLA;TLR2	3
heterophilic cell-cell adhesion via plasma membrane cell adhesion molecules (GO:0007157)	4/39	0.899156248	-3.000103552	10.06617192	CADM1;CRTAM;CD226;CBLN1	3
protein import (GO:0017038)	3/5	0.899156248	-1.577171043	9.025099924	LAMP2;APOE;CLU	3
blood coagulation, extrinsic pathway (GO:0007598)	3/5	0.899156248	-1.139049258	7.956863356	F9;F10;F3	3
release of cytochrome c from mitochondria (GO:0001836)	3/16	0.899156248	-2.333825759	7.867730391	GGCT;SOD2;CLU	3
extracellular matrix disassembly (GO:0022617)	6/76	0.899156248	-2.533775237	7.505562251	MMP14;MMP2;CTSK;FN1;HTRA1;CTSS	3
triglyceride homeostasis (GO:0070328)	3/22	0.899156248	-2.611030419	7.280118242	IL18;NR1H3;APOE	3
toll-like receptor signaling pathway (GO:0002224)	6/44	0.899156248	-2.359264964	7.197870411	TLR1;CTSK;TLR8;TLR6;CTSS;TLR2	3
triglyceride catabolic process (GO:0019433)	3/21	0.899156248	-2.138167098	6.139919161	FABP4;GPD2;APOE	3
amyloid-beta binding (GO:0001540)	5/25	0.929811334	-2.593593066	11.791963	TM2D1;GSAP;APBB2;APOE;CLU	3
heparin binding (GO:0008201)	8/77	0.929811334	-3.660537726	10.68219723	SERPINE2;FN1;APOE;THBS1;THBS4;VEGFA;PAFAH1B1;HBEGF	3
lysophospholipase activity (GO:0004622)	4/17	0.929811334	-2.848386839	9.280196461	PLA2G4F;ENPP2;PLA2G4A;LYPLAL1	3
low-density lipoprotein particle receptor binding (GO:0050750)	3/17	0.929811334	-2.669084098	8.696018553	DNAJA1;APOE;CLU	3
serine-type endopeptidase activity (GO:0004252)	10/185	0.929811334	-3.102734463	6.371078751	C3;MMP14;F9;F10;MMP2;CTSK;HTRA1;F3;CFB;CTSS	3
endopeptidase inhibitor activity (GO:0004866)	3/28	0.929811334	-2.29478965	5.431774641	CAST;CSTB;SPINK2	3
integrin binding (GO:0005178)	5/75	0.929811334	-2.098619265	3.834000778	ADAM17;FN1;CD226;THBS1;THBS4	3
cholesterol binding (GO:0015485)	4/39	0.929811334	-1.280930723	2.334727122	STARD5;OSBPL3;NR1H3;APOE	3
amino acid transmembrane transporter activity (GO:0015171)	3/41	0.929811334	-1.018536773	1.776866762	SLC7A8;SLC1A2;SLC6A12	3
phosphoric diester hydrolase activity (GO:0008081)	1/5	0.929811334	-0.529820792	1.282195223	SMPDL3B	3
substrate adhesion-dependent cell spreading (GO:0034446)	6/30	0.430858329	-2.8050364	21.29290408	LAMA5;PEAK1;ITGB3;TYRO3;RADIL;ITGB7	4
protein kinase B signaling (GO:0043491)	5/20	0.430858329	-2.914872452	20.37731625	TYRO3;GAS6;MT3;ZFP36L1;EPHA2	4
apoptotic cell clearance (GO:0043277)	4/10	0.430858329	-3.003136111	20.18020895	ALOX15;TYRO3;RARA;GAS6	4
regulation of cell proliferation (GO:0042127)	11/124	0.479130933	-3.100579839	15.37261371	JAG2;JUP;GRAP2;TNK2;TNFRSF18;CDCA7;MZB1;PTK6;RELT;TNFRSF4;TGFBR2	4
cytoskeleton organization (GO:0007010)	9/91	0.479130933	-2.663507467	14.42250057	LAMA5;MAST3;MICAL1;MICAL3;ARAP3;TNIK;SIPA1L3;SYNE3;FGD2	4
platelet aggregation (GO:0070527)	5/30	0.479130933	-2.500208688	13.58937648	ITGB3;TYRO3;GAS6;GATA1;PIK3CG	4
negative regulation of autophagy (GO:0010507)	5/31	0.479130933	-2.528710601	13.43957779	RUBCN;DAP;WDR6;BMF;MT3	4
single organismal cell-cell adhesion (GO:0016337)	7/54	0.479130933	-2.336294521	11.52166523	CYFIP2;JUP;CD93;SCRIB;PIP5K1C;CD34;NECTIN1	4
viral entry into host cell (GO:0046718)	4/17	0.479130933	-2.223573495	11.34495278	ITGB3;HYAL2;GAS6;NECTIN1	4
protein serine/threonine kinase inhibitor activity (GO:0030291)	2/8	0.530859928	-3.643590755	15.84346451	RPTOR;SPRED2	4
protein kinase activity (GO:0004672)	11/177	0.530859928	-4.073418502	12.42772395	PINK1;DYRK3;EEF2K;MAP3K10;VRK1;PRKD2;PRKCQ;TNIK;TRIB1;MAP3K14;PIK3CG	4
protein kinase B binding (GO:0043422)	2/8	0.530859928	-2.708579156	11.77774361	PINK1;RARA	4
oxidoreductase activity, acting on paired donors, with incorporation or reduction of molecular oxygen, NAD(P)H as one donor, and incorporation of one atom of oxygen (GO:0016709)	2/8	0.530859928	-2.608773323	11.34375684	MICAL1;MICAL3	4
protein serine/threonine kinase activity (GO:0004674)	15/296	0.530859928	-4.31225052	11.32490334	MAP4K2;DYRK3;DMPK;MAST3;VRK1;MAPK13;STK10;PINK1;GRK5;MAP3K10;PRKD2;PRKCQ;TNIK;MAP3K14;CSNK1G2	4
Rho guanyl-nucleotide exchange factor activity (GO:0005089)	5/52	0.530859928	-3.143068827	11.09421224	MCF2L;PLEKHG5;ARHGEF17;ARHGEF18;FGD2	4
phosphatidylinositol binding (GO:0035091)	5/51	0.530859928	-2.899689836	10.41699173	MCF2L;HIP1R;TULP4;SNX8;C2CD2L	4
RNA polymerase II core promoter sequence-specific DNA binding (GO:0000979)	4/24	0.530859928	-2.459077463	10.14969114	RUVBL2;FOS;GATA1;RREB1	4
acylglycerol lipase activity (GO:0047372)	2/9	0.530859928	-2.406251673	9.894202142	ABHD2;MGLL	4
transforming growth factor beta binding (GO:0050431)	2/17	0.530859928	-3.224098014	9.352186402	HYAL2;TGFBR2	4

8.3. Chapter 5 – supplementary tables

8.3.1. IRF5 gene ontology

ID	name	Binom_Observed_Region_Hits	Binom_Fold_Enrichment	AdjustedBinomPValue	FDR
GO:0046817	chemokine receptor antagonist activity	7	199.60	4.33E-11	7.10E-12
GO:0031726	CCR1 chemokine receptor binding	8	113.24	4.97E-11	7.10E-12
GO:0031730	CCR5 chemokine receptor binding	7	63.40	1.24E-07	8.88E-09
GO:0008121	ubiquinol-cytochrome-c reductase activity	6	23.05	1.20E-03	3.06E-05
GO:0016679	oxidoreductase activity, acting on diphenols and related substances as donors	6	22.17	1.50E-03	3.41E-05
GO:0019957	C-C chemokine binding	6	21.64	1.72E-03	3.83E-05
GO:0016004	phospholipase activator activity	9	19.10	7.07E-06	4.72E-07
GO:0060229	lipase activator activity	9	16.66	2.28E-05	1.20E-06
GO:0016493	C-C chemokine receptor activity	9	13.26	1.57E-04	5.82E-06
GO:0048019	receptor antagonist activity	9	10.36	1.22E-03	3.06E-05
GO:0043426	MRF binding	10	10.04	3.69E-04	1.12E-05
GO:0048020	CCR chemokine receptor binding	10	9.18	8.24E-04	2.17E-05
GO:0008009	chemokine activity	22	7.47	3.57E-09	2.98E-10
GO:0042379	chemokine receptor binding	24	7.31	5.40E-10	6.75E-11
GO:0005164	tumor necrosis factor receptor binding	17	6.20	1.98E-05	1.10E-06
GO:0004950	chemokine receptor activity	14	6.06	5.54E-04	1.51E-05
GO:1902107	positive regulation of leukocyte differentiation	94	4.38	2.16E-27	9.39E-29
GO:0043021	ribonucleoprotein complex binding	18	4.37	1.26E-03	3.08E-05
GO:0071219	cellular response to molecule of bacterial origin	74	4.27	2.38E-20	5.81E-22
GO:0002699	positive regulation of immune effector process	72	4.23	1.65E-19	3.50E-21

8.3.2. Super enhancer and traditional enhancer gene ontology

ID	Name	Binom_Observed_Region_Hits	Binom_Fold_Enrichment	AdjustedBinomPValue	FDR	Enhancer
GO:0005488	binding	9495	1.15	1.08E-140	1.08E-140	Traditional Enhancer
GO:0019222	regulation of metabolic process	5680	1.30	2.82E-132	2.82E-132	Traditional Enhancer
GO:0050789	regulation of biological process	8239	1.19	1.33E-130	6.64E-131	Traditional Enhancer
GO:0080090	regulation of primary metabolic process	5263	1.32	5.80E-130	1.93E-130	Traditional Enhancer
GO:0044237	cellular metabolic process	6807	1.24	6.58E-128	1.64E-128	Traditional Enhancer
GO:0031323	regulation of cellular metabolic process	5287	1.32	8.70E-127	1.74E-127	Traditional Enhancer
GO:0065007	biological regulation	8415	1.18	4.65E-126	7.75E-127	Traditional Enhancer
GO:0008152	metabolic process	7419	1.21	1.72E-125	2.46E-126	Traditional Enhancer
GO:0060255	regulation of macromolecule metabolic process	4975	1.34	3.73E-125	4.66E-126	Traditional Enhancer
GO:0050794	regulation of cellular process	8010	1.19	6.80E-125	7.55E-126	Traditional Enhancer
GO:0009987	cellular process	9870	1.12	4.59E-122	4.59E-123	Traditional Enhancer
GO:0005515	protein binding	6672	1.19	1.00E-79	5.00E-80	Traditional Enhancer
GO:1901363	heterocyclic compound binding	5233	1.24	3.66E-76	1.22E-76	Traditional Enhancer
GO:0097159	organic cyclic compound binding	5280	1.23	6.63E-76	1.66E-76	Traditional Enhancer
GO:0003676	nucleic acid binding	3551	1.27	5.01E-52	1.00E-52	Traditional Enhancer
GO:0003677	DNA binding	2583	1.34	7.76E-51	1.29E-51	Traditional Enhancer
GO:0003824	catalytic activity	5025	1.16	1.69E-37	2.42E-38	Traditional Enhancer
GO:0008134	transcription factor binding	706	1.69	9.10E-36	1.14E-36	Traditional Enhancer
GO:0019899	enzyme binding	1352	1.40	2.70E-31	3.00E-32	Traditional Enhancer
GO:0043167	ion binding	5698	1.13	4.78E-31	4.78E-32	Traditional Enhancer
GO:0002376	immune system process	196	2.42	7.14E-27	7.14E-27	Super Enhancer
GO:0065007	biological regulation	733	1.29	7.78E-26	3.89E-26	Super Enhancer
GO:0050789	regulation of biological process	710	1.28	5.44E-23	1.81E-23	Super Enhancer
GO:0001775	cell activation	108	3.23	5.54E-22	1.38E-22	Super Enhancer
GO:0019222	regulation of metabolic process	502	1.45	8.03E-21	1.61E-21	Super Enhancer
GO:0080090	regulation of primary metabolic process	468	1.48	1.93E-20	3.22E-21	Super Enhancer
GO:0045321	leukocyte activation	95	3.28	2.35E-19	3.36E-20	Super Enhancer
GO:0050794	regulation of cellular process	683	1.27	2.81E-19	3.51E-20	Super Enhancer
GO:0060255	regulation of macromolecule metabolic process	442	1.49	4.12E-19	4.58E-20	Super Enhancer
GO:0031323	regulation of cellular metabolic process	466	1.46	6.18E-19	6.18E-20	Super Enhancer
GO:0046649	lymphocyte activation	87	3.43	1.06E-18	9.65E-20	Super Enhancer
GO:0048523	negative regulation of cellular process	363	1.57	1.65E-17	1.38E-18	Super Enhancer
GO:0005488	binding	776	1.18	5.40E-15	5.40E-15	Super Enhancer
GO:0005515	protein binding	558	1.24	1.53E-09	7.65E-10	Super Enhancer
GO:0005126	cytokine receptor binding	44	3.23	1.11E-07	3.55E-08	Super Enhancer
GO:0097159	organic cyclic compound binding	439	1.29	1.42E-07	3.55E-08	Super Enhancer
GO:1901363	heterocyclic compound binding	434	1.29	2.29E-07	4.58E-08	Super Enhancer
GO:0003677	DNA binding	220	1.43	6.97E-05	1.16E-05	Super Enhancer
GO:0003676	nucleic acid binding	293	1.31	5.27E-04	7.53E-05	Super Enhancer
GO:0004896	cytokine receptor activity	20	4.07	8.07E-04	1.01E-04	Super Enhancer

8.3.3. RUNX1 gene ontology

ID	name	Binom_Observed_Region_Hits	Binom_Fold_Enrichment	AdjustedBinomPValue	FDR
GO:0016493	C-C chemokine receptor activity	20	12.71	2.67E-12	1.16E-13
GO:0005149	interleukin-1 receptor binding	20	9.79	3.19E-10	9.37E-12
GO:0008009	chemokine activity	43	6.30	4.77E-17	2.98E-18
GO:0042379	chemokine receptor binding	47	6.17	1.81E-18	1.39E-19
GO:0071219	cellular response to molecule of bacterial origin	228	5.67	2.43E-90	7.60E-92
GO:0071222	cellular response to lipopolysaccharide	216	5.60	2.36E-84	6.73E-86
GO:0071216	cellular response to biotic stimulus	238	5.48	1.40E-91	4.65E-93
GO:0002237	response to molecule of bacterial origin	391	4.97	3.88E-140	6.47E-141
GO:0032496	response to lipopolysaccharide	365	4.83	8.29E-127	9.21E-128
GO:0050727	regulation of inflammatory response	266	4.32	9.50E-81	2.43E-82
GO:0009617	response to bacterium	457	4.22	4.88E-139	6.98E-140
GO:0051707	response to other organism	555	3.83	4.19E-153	2.09E-153
GO:0006954	inflammatory response	354	3.79	1.68E-93	6.22E-95
GO:0031347	regulation of defense response	351	3.77	5.73E-92	1.97E-93
GO:0004715	non-membrane spanning protein tyrosine kinase activity	56	3.74	1.11E-12	5.30E-14
GO:0009607	response to biotic stimulus	563	3.73	1.25E-150	4.17E-151
GO:0043130	ubiquitin binding	58	3.60	1.64E-12	7.45E-14
GO:0005125	cytokine activity	186	3.60	1.19E-44	3.97E-45
GO:0050660	flavin adenine dinucleotide binding	47	3.53	1.85E-09	4.51E-11
GO:0001817	regulation of cytokine production	411	3.53	3.46E-100	1.82E-101